Republic of Iraq
Ministry of Higher Education &Scientific Research
University of Babylon
College of Materials Engineering
Department of Metallurgical Engineering

Oxidation and Corrosion Characterization of Copper-Based Alloys Used in Heat Exchanger

A thesis
Submitted to The Council of The College of Materials Engineering/ University of Babylon in Partial Fulfillment of The Requirements for the Degree of Doctor of Philosophy in Materials Engineering/Metallurgical

By
Roaa Jameel Abbas Farhod

B.Sc. In Materials Engineering (2013)
M.Sc. In Metallurgical Engineering (2016)

Supervised by

Prof.
Ekbal Mohammed Saeed(Ph.D.)

Prof.
Haider A. H. Al-Jubori (Ph. D.)

2022 A.D. **1443 A.H.**

﴿نَرْفَعُ دَرَجَاتٍ مَنْ نَشَاءُ وَفَوْقَ كُلِّ ذِي عِلْمٍ عَلِيمٌ﴾

سورة يوسف : الاية (٧٦)

Supervisors certificate

We certify this thesis entitled , " ***Oxidation and Corrosion Characterization of Copper-Based Alloys Used in Heat Exchanger*** " prepared by (Roaa Jameel Abbas) under our supervision at the department of Metallurgical Engineering / College of Materials Engineering / university of Babylon in partial fulfillment of the requirements for the Degree of Philosophy-Doctorate in Materials Engineering

Signature:
Dr. Ekbal Mohammed Saeed
/ / 2022

Signature:
Dr. Haider A. H. AL-Jubori
/ / 2022

Examination Committeee Certification

We certify that we had read this thesis entitled (***Oxidation and Corrosion Characterization of Copper-Based Alloys Used in Heat Exchanger***) and as an Examination Committee examined the student (Roaa Jameel Abbas) in its contents and that in our opinion it meets the standard of a thesis and is adequate for the award of the Degree of Doctor of Philosophy in Material´s Engineering/ Metallurgical Engineering.

Signature:
Prof. Dr. Saad Hameed Al-Shafaie
University of Babylon
Date: / / 2022
(Chairman)

Signature
Prof. Dr. Abdul Raheem. K. Abid Ali
University of Babylon
Date: / /2022
(Member)

Signature
Asst. Prof.Dr.Israa Abd Alkadir Aziz
University of Technology
Date: / /2022
(Member)

Signature
Asst. Prof.Dr.Zaineb Fadhil Kadhim
University of Technology
Date: / /2021
(Member)

Signature
Asst. Prof.Dr.Firas Farhan Sayyid
University of Technology
Date: / /2021
(Member)

Signature
Prof. Dr. Ekbal Mohammed Saeed
University of Babylon
Date : / / 2022
(Supervisor)

Signature
Prof. Dr. Haider A. H. Al-Jubori
University of Babylon
Date: / /2022
(supervisor)

Approval of Metallurgical
Engineering Department
Head of the Department

Signature

Prof. Dr. Saad Hameed Al-Shafaie

Date : / / 2022

Approval of Material´s
Engineering College
Dean of the College

Signature

Prof. Dr. Imad Ali Disher

Date : / / 2022

Abstract

Recycling is the most important factor in ensuring that most metallic elements continue to progress and develop, particularly recycling copper, recycling aluminum, and recycling iron. Recently, recycling aluminum, copper and iron have been the focus of most research as there is an increased demand to use the green industry and as well as to reduce the emissions to the environments. The recycled Aluminum, copper and iron can be converted to different forms to be used in different purposes, like using in the preparation of alloys used for tube heat exchangers.

The main alloy used in this research is the (90%Cu-10%Ni) alloy used in the electric power plant (South Baghdad station). Where two types of alloys were prepared: first remove nickel from the base alloy as it was replaced by other elements. These alloys are A2 (69.33%Cu+27.4%Zn+3.05%Al) ,A3 (66.01%Cu-27.94% Zn-3.10% Al-2.67%Sn),A4 (66.46%Cu-29.21%Zn-3.60%Al-0.3%Ge) andA5 (6.28%Cu-28.7%Zn-3.50%Al-0.23%Y)

Secondly, alloys in which the percentage of nickel has been reduced from the base alloy and the replacement for nickel with other elements. these alloys are A6(79.44%Cu-8.21%Ni-10.66%Al), A7(78.38%Cu-8.34%Ni-10.58%Al-2.33%Fe),A8(80.26%Cu-8.53%Ni-9.55%Zn) and A9(78.76%Cu-8.28%Ni-10.12% Zn-2.6%Fe)

Traditional mold casting and heat treatment elements were used, and casting was carried out in such a way as to ensure the smoothing of the grains to improve the properties. A number of tests have been carried out, including oxidation, thermal shock testing at high temperatures (25 C°, 250 C°, 350 C°, 450 C°, 550 C° , 650 C° , 750 C°, and 850 C°). As well as the

test for hardness, mechanical wear, corrosive wear, simple immersion and Tafel test.

The alloy with better properties among the nickel-free alloys is (A4) and the alloy with the best properties among the alloys in which the nickel percentage has been reduced is (A7).

Results showed remarkable superiority of free nickel alloys in various tests, i.e. the improvement of corrosion resistance in salt solution (simple immersion test), for instance the reduction in corrosion rate of alloy (A4), compared to base alloy (A1), has led to improve reaches to 27.30 %). While the corrosion rate of the alloy containing nickel was reduced compared to the base alloy, the corrosion rate of alloy(A7) was 53.8%.

On the other hand, the reduction of current density of alloys (A4)and (A5) compared to base alloy (A1), has led to improve reaches to in order (96.5%) and (99.92%) respectively, while improvement in the reduction of current density of alloy(A7) compared to base alloy (A1) was (99.99%).

In oxidation test the reduction in specific weight change for A4 at 850C° was 17.07%, while improvement in the reduction in specific weight change for(A7) at 850C° was 23.21%.

While the improvement for free nickel alloys and alloys with nickel during mechanical tests, for instance the increasing in hardness of alloys A4 and A7 compared to base alloy (A1) were in order (89.2%) and (97.98%) respectively, in addition, the reduction in erosion rate has led to improvement to (89.28%) and (92.85%) respectively . Besides, the improvement in wear resistance at (load 20N and speed 250rpm) has reached(57.2%) and (70.15%)respectively.

The concept of optimization is used to find the best sample in terms of properties by dealing with the concept of Particle Swarm algorithms and that depends on the principle of its work. The program is designed depending on 75 samples with referring to the papered nine samples. It has used of the principle of selection as a function of a better validity as the relationship between this measure and authority is an inverse relationship. Then, the optimum samples resulted from the PSO were convergence the properties of sample A4 (Cu-Ni-Al-Ge).

DEDICATION

To my Mother

With my love and

respect

ROAA

2021

Acknowledgment

First of all, I would like to express my gratitude to ALLAH for show me the path.

I would like to thank my supervisors, **Dr. Ekbal M.S. Salih** and **Dr. Haider A. H. AL-Jubori** for their unwavering support and guidance in this research.

I would like also to extend my gratitude to the Dean of the Materials Engineering College, Head Metallurgy Engineering Department and all the staff for their great efforts.

I wish to express my deepest thanks to the staff and laboratories of the Metallurgical Department of the Materials Engineering College/University of Babylon.

I greatly thankful to all our well-wishers, classmates, friends and family for their inspiration and help.

Roaa

2021

CONTENTS

List of Greek Symbols

List of Greek Symbols Symbol	Meaning	Units
α	Alpha phase	-
β	Beta phase	-
γ	Gamma phase	-
ρ	Density	g/cm^3 or Kg/m^3

List of Subscripts & Superscripts

Symbol	Meaning	Units
ECor.	Corrosion Potential	mV
ICor.	Total Anodic Current	µA
iCor.	Corrosion Current Density	$\mu A/mm^2$

List of Abbreviations

Symbol	Meaning
ASTM	American Society For Testing And Materials
BCC	Body Center Cubic
FCC	Faced Center Cubic
EDS	Energy-Dispersive Spectrometry
EW	Equivalent Weight
HCP	Hexagonal Close Packed
mpy	Mils per year
mV	Millivolt
LOM	Light Optical Microscope
OCP	Open-Circuit Potential
SEM	Scanning Electron Microscopy
XRD	X-Ray Diffraction
XRF	X-Ray Fluorescent
$\Delta W/A$	The Change in Weight per Specimen Surface Area
wt. %	Weight Percentage
CR	Corrosion Rate
rpm speed	Revolutions per minute
HTC	High Temperature Corrosion
CTE	Coefficient of Thermal Expansion

INTRODUCTION

1.1 General View

Recycling of industrial waste has existed in nature since ancient times; however it has practiced human waste retrieval process since the Bronze Age, where the metal material was dissolved to be converted into new tools. It is intended for recycling the reuse of waste; to produce other products of quality lower than that of original product. In recent years, waste production acquired a great importance in modern societies as a result of the change in consumption habits and patterns of consumers lives. The development of societies all over the world led to the phenomena of mass consumption, leading to increased amounts of the produced waste which result from such waste environmental impact [1].

Metals play an important role in modern societies and have traditionally been known with technological advancement and higher living standards. Metal resources can be found in the Earth's crust as well as metal that has been discarded after being used in the economy. Inefficient metal recovery from the economy increases reliance on primary resources and has the potential to harm the environment by increasing metal dispersion in ecosystems. Although the practice of recovering metals for their value can be traced back to ancient civilizations, it would still be currently practiced[2].

Metals can be recycled nearly indefinitely. Unlike polymer plastics, the properties of metals can be restored fully, although not always easily, regardless of their chemical or physical form. Nevertheless, the ability to recover metals economically after use is largely a function of their chemical reactivity and how they are initially used in the economy. The success of secondary metals markets depends on the cost of retrieving and processing metals embedded in abandoned structures, discarded products, and other waste streams, relative to the prices of primary metals[3,4].

Many of the technologically important metals and alloys are partially or completely damaged while being attacked by different mediums, whether at high or low temperatures. As for the amount of damage, it depends on the type of engineering material and the nature of the medium of use.The current study aims to increase the effective life of alloys of heat exchangers and compressors used in electric power plants in Iraq, as it was found that these tubes suffer from early failure.

The danger of early damage lies in the possibility of leakage of coolant into the exchanger. If the exchanger is part of a complex system, the possibility of getting rid of the liquid and its immediate and future effects becomes difficult, in addition to high-cost downtime for the purpose of maintenance.

Heat exchangers represent means of exchange between one medium and another. Perhaps the radiator in the car is one of the most common examples. The exchangers are of various types that vary in their designs and properties and may be used for cooling or heating. In modern aircraft, the exchanger is

used to heat the air entering the combustion chamber with the exhaust gas to increase efficiency.

For the exchanger to be effective, it must be integrated between its design and the alloy used. The design should provide more space than the limited space, reduce weight and damage from gaps, and enable the use of high operating speeds. As for the alloy, perhaps its most important features: resistance to erosion and erosion, damage to gaps, in addition to durability, high thermal conductivity, and low cost.

Since the 1930s, various materials such as brass, bronze, cupronickel alloys, stainless steel and even cast iron have been used in certain parts. Its problems ranged from selective dissolution, high price, pitting and galvanic corrosion, in addition to the limited flow rate in some of them.

Copper-nickel alloys are commonly used in seawater-cooled heat exchangers due to their inherent properties, which include a low corrosion rate, antifouling properties, and erosion-corrosion resistance compared to other alloys. The formation of a "protective film" on the underlying metal is critical to the corrosion behavior of these alloys. Furthermore, when compared to pure copper, alloying copper with nickel increases the tendency toward passivity and improves erosion-corrosion resistance. The addition of iron and manganese improves erosion-corrosion.

Because of their superior electrical and thermal conductivities, corrosion resistance, and ease of production, copper-nickel alloys are widely utilized in marine applications. The 90/10 copper-nickel alloy is a popular choice for condensers and heat exchangers in desalination plants and other applications where saltwater is utilized as a coolant. This alloy offers good resistance to

biofouling due to the release of copper ions and is resistant to stress corrosion cracking by ammonia and sulphide ions. In calm seawater, this alloy is also resistant to pitting and crevice corrosion. Thousands of tons of copper-nickel alloy (UNS C70600, CuNi 90/10) have been placed in various maritime engineering structures in the shipbuilding, offshore, power, and desalination industries over the last few decades, mostly as pipe for seawater handling and heat exchangers[5]. This alloy, which has been adopted by a number of standards (Table 1-1).

Table 1.1: Chemical composition of cupronickel 90/10 used as tube material compared to various requirements[6].

Standard	DIN/EN	ASTM	ISO	EEMUA	KME
Designation	CuNi10Fe1Mn		CuNi10Fe1Mn		CuNi10Fe1,6Mn
Ref. No.	2.0872/ CW352H	UNS C70600		UNS 7060X	Osna10 ®
Copper	Rem.	Rem.	Rem.	Rem.	Rem.
Nickel	9.0-11.0	9.0-11.0	9.0-11.0	10.0-11.0	10.0-11.0
Iron	1.0-2.0	1.0-1.8	1.0-2.0	1.5-2.00	1.50-1.8
Manganese	0.5-1.0	1.0	0.5-1.0	0.5-1.0	0.6-1.0
Tin	0.03	-	0.03	-	0.03
Carbon	0.05	0.05	0.05	0.05	0.02
Lead	0.02	0.02	0.02	0.01	0.01
Phosphorus	0.02	0.2	0.02	0.02	0.02
Sulphur	0.05	0.02	0.02	0.02	0.005
Zinc	0.05	0.5	0.5	0.2	0.05
Cobalt	0.1	-	0.05	-	0.1
Total other impurities	0.2	-	0.1	0.3	0.02
Single values represent the maximum content.					

1.2 Heat Exchanger

A heat exchanger is a device that is used to transfer thermal energy (enthalpy) between two or more environments using a working fluid and a working surface having different temperatures. Heat transfer can occur

between a solid surface and a liquid, between solid particles and a liquid, etc. The heat-exchange (or heat-utilizing) apparatus is one of the most common and important elements of power, utility and technological installations. Any conversion of energy from one type to another, as well as the transfer of energy from one device to another, is accompanied by the transition of a certain part of the energy to heat. Therefore, in almost all machines and apparatuses, heat transfer is important. Heat exchangers play an important role in technological processes, energy, oil refining, manufacturing, transportation, air conditioning, cryogenic and recovery systems. They also serve as key components of many industrial products available on the market. All heat exchangers can be classified according to various criteria[7].

1.2.1 Fields of applications of heat exchangers:

Heat exchangers are used in many different technological processes. The following roster lists some types of heat exchangers and their main purpose[8].

1. Chiller: a heat exchanger that uses refrigerant to cool a liquid through a vapor compression or absorption refrigeration cycle.
2. Condenser: condenses steam or a mixture of vapors with or in the presence of non-condensing gases.
3.Cooler: cools a liquid or gas, usually using water.
4. Heat exchanger: cools one liquid while heating another.
5. Heater: transfers heat to a liquid or gas by contact with a heated surface.
6. Reboiler: generates steam through fractional distillation. Heating occurs

with the help of a heating element, as a result of which condensation of steam occurs.

7. Thermosiphonreboiler: the natural circulation of boiling liquid is maintained by sufficient pressure.
8. Forced circulation reboiler: A pump is used to circulate the fluid in the reboiler.
9. Superheater: Heats the steam to a temperature above its boiling point.
10. Evaporator: a heat exchanger that evaporates part or all of the liquid flow.

1.2.2 Classification of Heat Exchangers:

1. Pipe-in-pipe heat exchangers

Equipment consisting of two pipes with different diameters inserted one into the other. With the help of clutch couplings, all parts of the pipes are assembled into a coil, which provides the necessary space for the heating and cooling medium. Sections are placed one above the other. The flows are directed counter-currently (towards each other). The cooling agent comes from below, and after heating rises up. The heated steam accumulates from above. After condensation, it goes to the bottom of the heat exchanger. This heat exchange equipment is used in the food industry. Heat exchangers of this design are characterized by a significant heat transfer coefficient and can operate at high pressure. The pipes are cleaned mechanically on level areas. The flow inside the two-pipe heat exchangers can be parallel or counter-current[9].

2. Shell-and-tube heat exchangers:

The shell-and-tube heat exchanger includes a tubular tank and an integrated tubing section. The heat carriers in the heat exchanger are directed

both parallel and towards each other. Shell-and-tube heat exchangers are used in the chemical, food, oil and gas and other fields. They are used as evaporatorsand condensers. Depending on the operating conditions of the equipment, it is installed in a vertical or horizontal position [10].

In multi-way devices, it is necessary to firmly fix the base and pipe sections. Such modules function even with a small difference in temperature of the working environment. When choosing the material of the heat exchanger, it is necessary to take into account the aggressiveness of the environment. Due to the inaccessibility of the heat exchanger tubes, the formation of corrosion is highly undesirable. Cleaning is carried out exclusively by a chemical method [11].

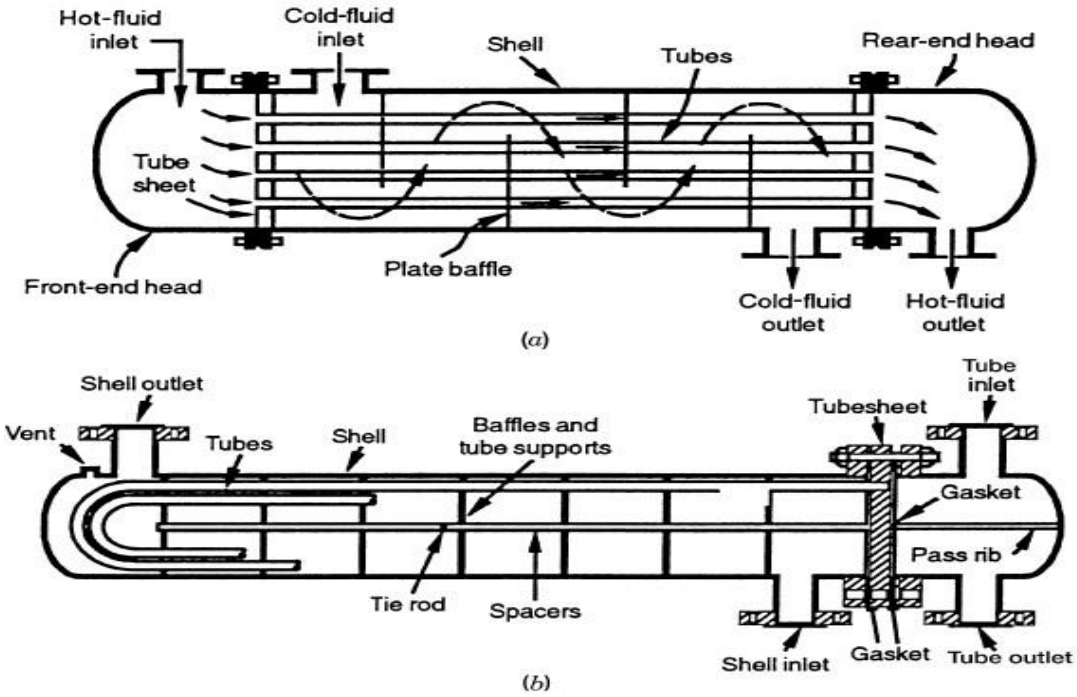

Figure(1.1): a) shell-and-tube heat exchanger with one outer shell and one pipe passage; b) shell-and-tube heat exchanger with one outer shell and two pipe passages.[12]

3. Plate Heat Exchangers

They consist of a large number of corrugated plates made of stainless steel. They are separated by seals that are installed without the use of adhesive mixtures, but allow tight fit to each other. Gaskets provide absolute tightness and do not allow mixing of media. The direction of flow is counter-current. The power of the heat exchanger is determined by the number of plates installed inside. Service, cleaning and repair of the device is done by disassembling it. Areas of use: housing and public utilities, shipbuilding, metallurgy, oil and gas, pharmaceutical industries and so on. The choice of material of the heat exchanger must be carried out depending on the technological process, the type of coolants in the system, temperature load and pressure. The most universal in application: plate heat exchangers made of stainless steel with copper pipes [13].

Figure (1.2) :Plate heat exchanger

4. Spiral plate heat exchangers:

Spiral plate heat exchangers are made of two metal plates that are wound on each other. One stream of process fluid enters the heat exchanger through

the center and flows from the outside, while the second stream enters from the outside and flows inward. This creates a close to natural backflow [14].

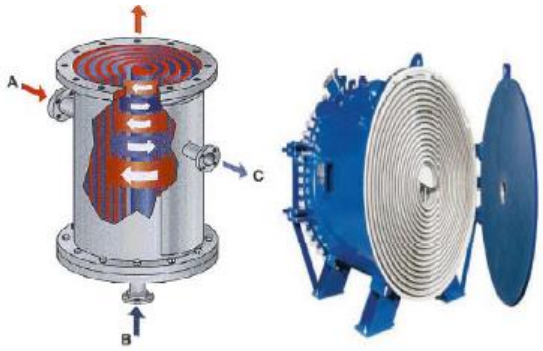

Figure (1.3):Spiral plate heat exchanger

1.3 Objectives of the Present Study

The current study aims to reduce the percentage of nickel in the alloys used in heat exchangers in electric power plants, as the alloy that was studied in the current research taken from the southern Baghdad power station contains 10% nickel and 90% copper. Where two groups of alloys were prepared, the first was completely replaced by nickel with elements such as (zinc, aluminum, tin, germanium and yttrium). In the second group, the proportion of nickel was reduced by adding elements such as (aluminum, zinc and iron). It should be noted that some of the elements used in the preparation of alloys were from recycling, such as (copper, aluminum and iron). Then, the corrosion and oxidation properties of the prepared alloys were studied.

One of the optimization methods was used to reach the optimal solution, and this method was the swarm of particles optimization(PSO), as this method is characterized as being easy to apply and implement.

Chapter Two

Theoretical Part

Introduction 2.1

This chapter dealt with a number of topics: including metal recycling and usually focus on the recycling of metals, copper and its alloys, Cu-Zn alloys, Cu- Ni alloys, corrosion of copper alloys, wear of copper alloys, oxidation of copper alloys and particle swarm optimization.

:Metals scrap recycling 2.2

Metals play an important part in modern societies and have historically been linked with industrial development and improved living standards. Society can draw on metal resources from Earth's crust as well as from metal discarded after use in the economy. Inefficient recovery of metals from the economy increases reliance on primary resources and can impact nature by increasing the dispersion of metals in ecosystems. Although the practice of recovering metals for their value dates back to ancient civilizations [15], today the protection of Earth's resource endowments and ecosystems adds to the incentive for recovering metals after use. Industrial society values metals for their many useful properties. Their strength makes them the preferred material to provide structure, as girders for buildings, rails for trains, chassis for automobiles, and containers for liquids. Metals are also uniquely suited to conduct heat (heat exchangers) and electricity (wires), functions that are indispensable to industrial economies. Finally, metals and their compounds are used for their chemical properties as catalysts for chemical reactions, additives to glass, electrodes in batteries, and many other applications. The basic and unique properties of metals,

including the ability to work them into complex shapes (i.e. ductility), .ensure that long-term demand for metals will certainly grow [16]

.Table (2-1): Primary metal resource consumption and reserve base[16]

Resource (MMT)[a]	World mine production 1996 (MMT/year)	Reserve base[b] (MMT)	Reserve base/annual mine production (years)
Ores			
Iron ore	1,000	232,000	232
Bauxite	111	28,000	252
Metals			
Copper	10	610	61
Lead	2.8	120	43
Zinc	7.2	330	46
Magnesium	0.347	Recovered from natural brines and dolomite	
Nickel	1.1	110	100
Tin	0.190	10	53
Tungsten	0.030	3.3	110
Cobalt	0.024	9	375
Mercury	0.003	0.24	80

Metal scrap recycling, also called secondary metal processing, is a large industry that processes, in the U.S. alone, 56 million tons of scrap iron and steel (including 10 million tons of scrap automobiles), 1.5 million tons of scrap copper, 2.5 million tons of scrap aluminum, 1.3 million tons of scrap lead, 300,000 tons of scrap zinc and 800,000 tons of scrap stainless steel, and smaller quantities of other metals, on a yearly basis.

2.2.1 The Process of Metal Recycling

The process of metal recycling involves four stages. Metal is collected by scrap yards, where it is sorted into bins. Any nonferrous metal items that have a component of steel or iron is treated as scrap steel. Scrap metal centres then sell the scrap to larger super collectors where it is shredded and then melted in furnaces at high temperatures to produce blocks, ingots or sheets to be sold to manufacturers of metal products.

Below is the metal recycling process in detail[17]:

1. Collection and sorting

The first step in metal recycling is the collection of all metal products. Adelaide residents bring in a variety of metallic items. Examples of items brought in for scrap metal recycling include whitegoods, radiators, steel or alloy wheels, roller shutters, bicycles and batteries, even the stainless steel kitchen sink can be recycled. Metal items are sorted into rubbish skips, ready to be transported to scrap metal super collectors for processing.

Scrap metal prices are high due to the demand for scrap metal that has been recycled.

2. Crushing and Shredding

Scrap metal processing plants first crush the metal in compactors so it can be handled on conveyor belts easier. Hammer mills then shred the metal into pieces the size of your hand.

3. Separation

Shredded metal is then placed into magnetic drums that separates ferrous and non ferrous metals. Non metallic materials such as paint or plastic is removed by blowing hot air (550°C) through the shredded metal, sucking up the impurities much like a vacuum.

4. Melting and Purification

The next step is to melt the different scrap metals in large furnaces. Each metal has a specially designed furnace depending on its properties. The furnaces have fuel-efficient regenerative burners to reduce the amount of energy used and the impact on the environment. They are also equipped with jet stirrers, ensuring an even temperature and composition by promoting metal circulation within the furnaces. The stirring process ensures the highest quality end product.

While in a molten state, the metals are purified further by 'Eddy current' electrolysis before being poured into different moulds; depending on the metal, and cooled. Large aluminium ingots, weighing up to 18 tons and containing around 1.5 million used cans, are sent to mills where they are rolled into sheets, then bought by aluminium can manufacturers to make into new cans. Despite the energy costs used in scrap metal recycling, the energy required is less in this case as compared with the making from raw material.
Making steel from recycled cans for example uses 75% less energy than when producing steel from raw materials. Australia has around 90% recycle rate for steel products consumed, with every tonne of recycled steel saving 1130kg of iron ore, over 630kg of coal and 54kg of limestone from being mined[18].

2.2.2 Environmental Impacts of Metal Production

One of the most striking environmental benefits of secondary metals production is the reduction in energy needed to produce a ton of metal. The primary reason for this phenomenon is that melting metal requires less energy than that needed for reducing naturally occurring oxides and sulfides. Fig.2.1 compares the energy requirement for producing a ton of aluminum, copper, and steel starting from ore or scrap. Steel produced from primary ore uses three and one half times more energy than steel from melted scrap. Copper from ore requires five to seven times more energy than that required for processing recycled[19].

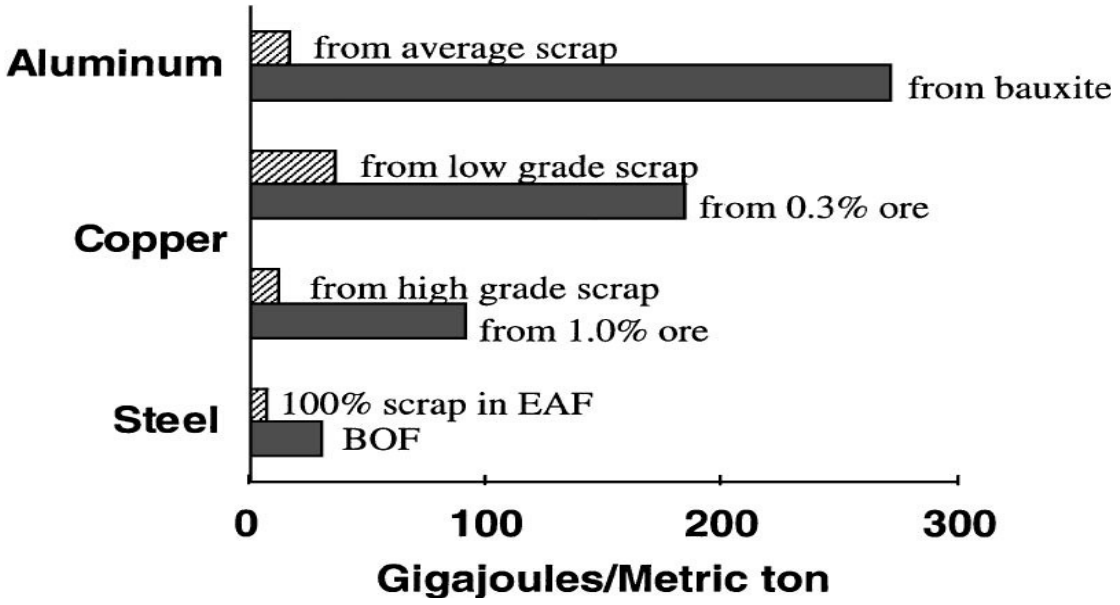

.Figure (2.1): comparison of energy inputs for various metals

Besides conserving energy resources, metals recycling also reduces mining and beneficiation activities that disturb ecosystems. Although land used for the extraction of primary metals represents under 0.1% of Earth's terrestrial surface [20], exploration and mining activity can affect surrounding ecosystems owing to necessary infrastructure and by dispersing metal compounds into the environment, either as airborne particles or as ions in aqueous solutions. Developing newly discovered resource deposits can also damage sensitive ecosystems, especially in less developed regions where the need for foreign exchange from mineral rents overshadows domestic environmental concerns [21].

2.3.Copper and Copper-Base Alloys

Copper was undoubtedly the first useful metal to be employed by Man. In many countries it is found in small quantities in the metallic state and, being soft, it was readily shaped into ornaments and utensils. Moreover, many of the ores of copper can easily be reduced to the metal, and since these ores often contain other minerals, it is very probable that copper alloys were produced as the direct result of smelting[22].

2.3.1 Properties and Uses of Copper

A very large part of the world's production of metallic copper is used in the unalloyed form, mainly in the electrical industries. Copper has a very high specific conductivity, in this respect, second only to silver, to which it is but little inferior. When relative costs are considered, copper is naturally the metal used for industrial purposes demanding high electrical conductivity[22].

2.3.2. Copper-Base Alloys

The ever-present demand by the electrical industries for the World's diminishing resources of copper has led industry to look for cheaper materials to replace the now expensive copper alloys. Whilst the metallurgist has been perfecting more ductile mild steel, the engineer has been developing more efficient methods of forming metals so that copper alloys are now only used where high electrical conductivity or suitable formability coupled with good corrosion resistance are required [22].

For application requiring good resistance to corrosion, it is possible to move towards copper-base alloys and stainless steel. The cheapest copper-base are the brasses, because zinc is one-third the cost of copper, high temperature brazing is effected above 800ºC, usually with 60/40 brass filler.

Copper and its alloys are available as duplex tubing (inside one metal, outside another) in combination with steel, aluminum, and stainless steel. This construction solves many heat- exchanger materials problems. For example, tubing with ammonia on one side (steel) and brackish water on the side (Admiralty Metal). Copper and copper alloys find extensive application as water piping, valves, heat-exchanger, tubes, tube sheets, hardware, wire, screens, shafts, roofing, bearings, stills, tanks, and other vessels [23].

2.3.3.The Brasses Alloys:

The brasses comprise the useful alloys of copper and zinc containing up to 45% zinc, and constitute one of the most important groups of non-ferrous engineering alloys. As shown by the constitutional diagram Fig.(2.1), copper will dissolve up to 32.5% zinc at the solidus temperature of 902°C, the proportion increasing to 39.0% at 454°C. With extremely slow rates of

cooling, which allow the alloy to reach structural equilibrium, the solubility of zinc in copper will again decrease to 35.2% at 250°C. Diffusion is very sluggish, however, at temperatures below 450°C, and with ordinary industrial rates of cooling the amount of zinc which can remain in solid solution in copper at room temperature is about 39%. The solid solution so formed is represented by the symbol (α). Since this solid solution is of the disordered type, it is prone to the phenomenon of coring, though this is not extensive, indicated by the narrow range between liquids and solidus. If the amount of zinc is increased beyond 39% an intermediate phase, β', equivalent to CuZn, will appear in the microstructure of the slowly cooled brass. [24,25]. Fig. (2.3) shows copper-zinc partial phase diagram.

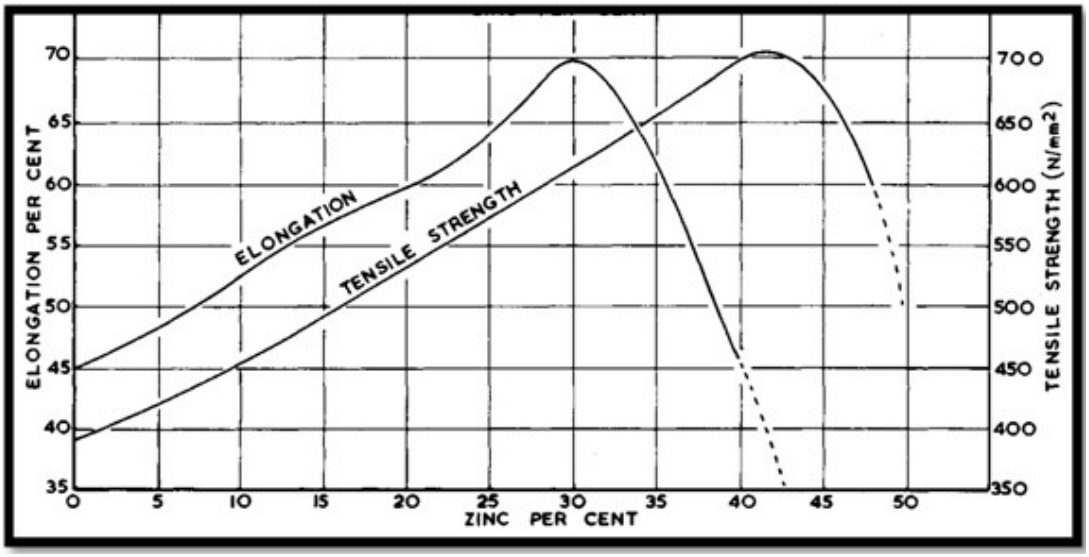

Figure (2.2): The Copper-Zinc Constitutional Diagram Indicates the Relationship Between Composition and Mechanical Properties[26].

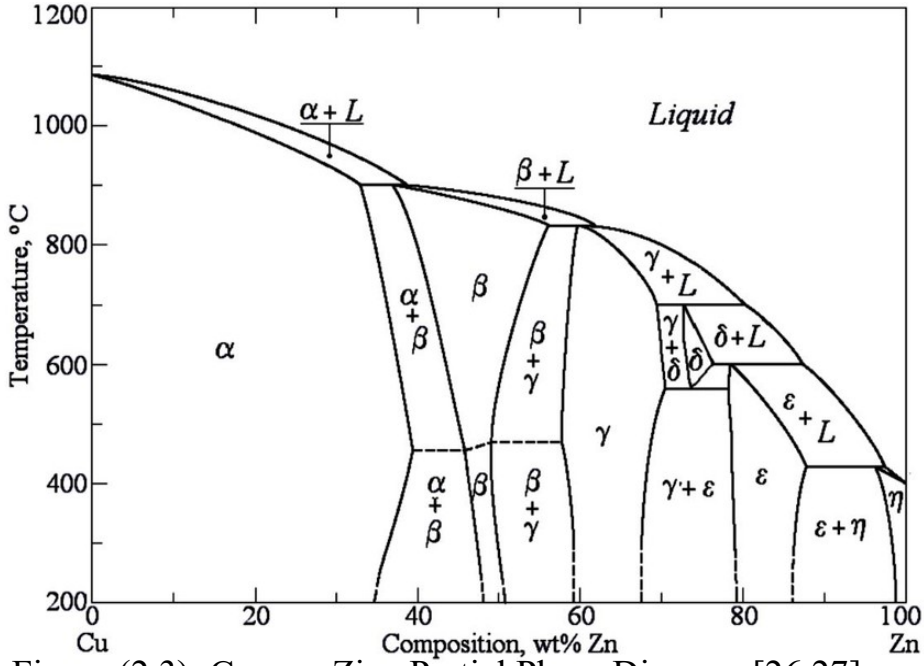

Figure (2.3): Copper-Zinc Partial Phase Diagram [26,27].

2.3.4 Bronze Alloys

Bronze is an alloy consisting primarily of copper, commonly with about 12–12.5% tin and often with the addition of other metals (such as aluminium, manganese, nickel or zinc) and sometimes non-metals or metalloids such as arsenic, phosphorus or silicon. These additions produce a range of alloys that may be harder than copper alone, or have other useful properties, such as strength, ductility, or machinability[28].

Bronze is not a pure metal, but rather, a metal alloy. This is because it contains various metals and alloys. It is mostly comprised of copper, but also retains a few other common metal constituents. Generally, tin is added in, but alloys like aluminum, arsenic, manganese, phosphorous, and silicon are

sometimes used as well. This means there are various versions of bronze alloys, all of which retaining separate attributes and properties. But the collective property among them all is strength. When these metal constituents are added to copper, it makes it much stronger. This is why bronze is a common metal used in the construction of musical instruments, sculptures, medals, and several industrial applications (i.e. bearings, bushings, etc.) [29]

2.3.5 Copper- Nickel alloy

Copper and nickel have similar atomic radii and lattice parameters and so the phase diagram is relatively simple Fig.(2.7), At all temperatures, Cu-Ni alloys are represented by a single phase face centered cubic structure. The absence of phase transformation during thermal cycles reduces the effect of welding on mechanical characteristics and the corrosion resistance of the material. This crystallographic structure reveals very good ductility and impact strength even at temperatures well below freezing point. The slow diffusion rate for nickel in copper leads to concentration gradients in the melt and consequently in-creases a segregation tendency in the cast structure at normal cooling rates Fig.2.8. Thus, to provide a uniform establishment of protective oxide layers, the homogenization of the segregated structure is required by hot forging or cold working with a subsequent recrystallisation anneal[30].

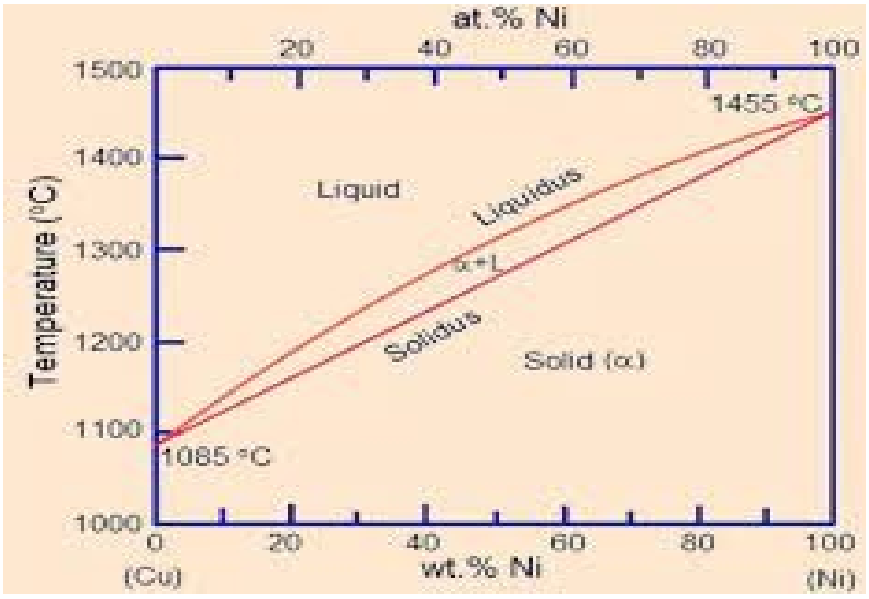

Figure (2.4): Phase diagram for Cu-Ni alloys[31].

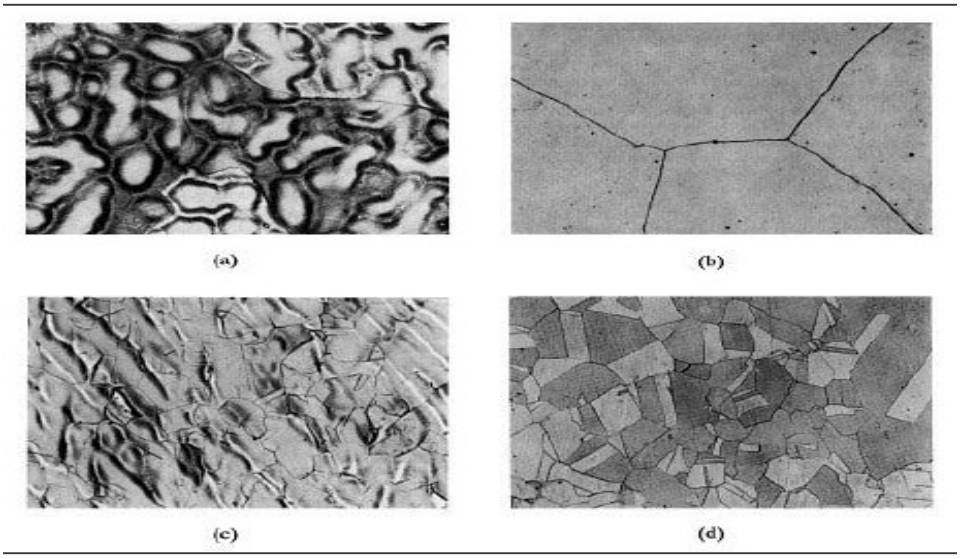

Figure (2.5) : The matrix of UNS C71500 etched with FeCl3, (a) cast, (b) cast and annealed at 1100°C/ 30 min, (c) cast, 50% cold worked, and annealed at 850°C/ 4 h, (d) cast, 50% cold worked, and annealed at 850°C/25 h[32].

Some specifications monitor more strictly the iron content which is an essential alloying element and responsible for the improvement in corrosion resistance of the alloy. To provide the appropriate quality of cupro-nickel

products, the cooling rate from the solution annealing temperature must keep the precipitation of iron containing particles to a minimum. The quality of the piping can be easily assessed by measurement of the relative magnetic permeability, which should be lower than 1.5. As for all metallic materials, if the CuNi 90/10 has to be welded, the maximum limits for some impurities such as lead, sulfur, carbon, and phosphorus should be carefully controlled[33, 34, 35].

Corrosion of Copper Alloys 2.4

Copper and copper alloys are widely used in many environments and applications because of their excellent corrosion resistance, which is coupled with combinations of other desirable properties, such as superior electrical and thermal conductivity, ease of fabricating and joining, wide range of attainable mechanical properties, and resistance to biofouling.

When copper and its alloys are immersed in water and form a film of cuprous oxide (Cu_2O), it is usually protective, and corrosion rates are low. However, if this film breaks down locally, or a non-protective film forms, particularly in localized areas, then rapid local attack can occur. Once this develops, the pits can be very narrow and may propagate rapidly. Failures by pitting attack may occur in a few months or only after 10 or more years [36,37]. Fig.(2.9) showed Cross section of a tube damaged by pitting corrosion.

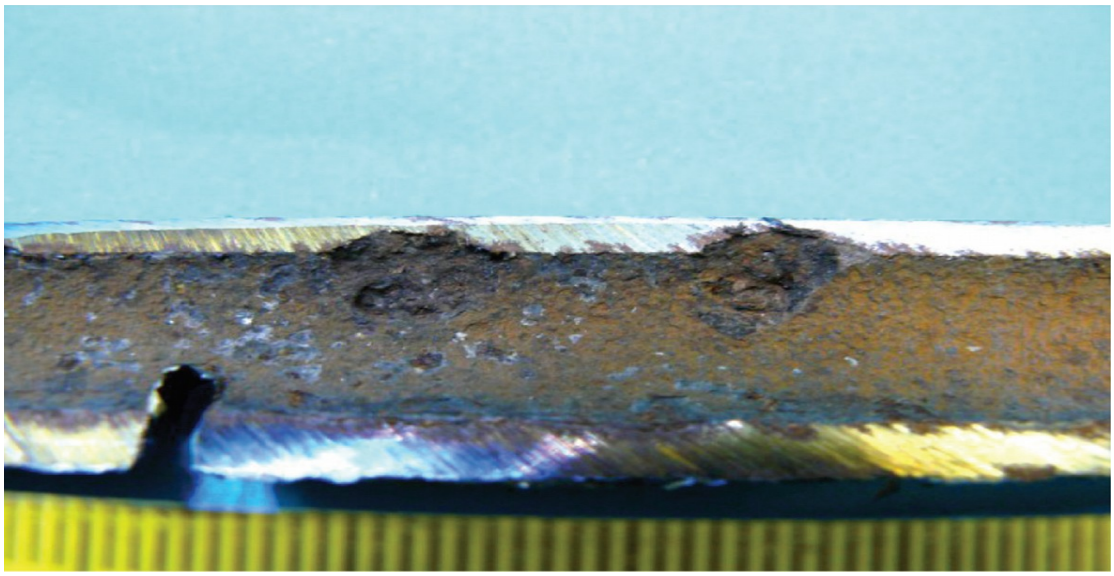

Figure (2.6): Cross section of a tube damaged by pitting corrosion [38].

2.5 Corrosion resistance of copper –nickel

Copper-nickel alloys are generally known for their good corrosion resistance, excellent machinability, and outstanding thermal and electrical conductivity in marine environments [39–40]. The 90/10 copper-nickel alloy has been widely applied in various fields, such as seawater piping, heat exchangers and condensers in ships, desalination plants, power plants, and ship hulls [41–42]. The excellent corrosion resistance of Cu-Ni alloy is mainly due to two reasons. First, the ionization of copper is difficult as a result of the positive equilibrium potential and the high thermodynamic stability of Cu. Second, nickel was incorporated into Cu_2O film and increases the corrosion resistance in two ways: (i) Ni^{2+} occupies the vacant position of Cu+ and increase the ionic resistance, which makes two Cu^{+} ions disappear and thus increases the ion resistance of the film; (ii) Ni^{2+} replaces Cu+ directly, while the ionic resistance does not change and each substitution results in the disappearance of one Cu+ and increases the electronic resistance [43]. Moreover, it is relevant to the formation of a

duplex oxide layer on the surface of copper alloy, which is mainly composed of CuxO and Cu-hydroxide/oxide layer and protects the copper matrix. Corrosion products often deposit on the film and play a protective role [44,45]. Therefore, copper and copper alloys are more corrosion-resistant than other metal alloys . In marine exposure conditions, Cu2O rapidly forms on the surface of the matrix in the initial stage and reacts with chlorides, leading to the formation of CuCl, which usually converts to $Cu_2(OH)_3Cl$ as end corrosion products [46,47]. The above components have already been confirmed on bare copper at atmospheric exposures by Fuente ,and also observed after exposure in laboratory conditions with humidified air and pre-deposited NaCl [48,49]. However, the failure mainly happens on the Cu alloys surface in marine environments and severely disrupts the safe operation of ship and marine engineering [50]. Table 2.3 explained Corrosion rate of a Cu-Ni alloy containing 30% nickel and different iron contents in seawater at various flow rates; temperature 30 C, test duration 60 days.

Table 2.2.: Corrosion rate of a Cu-Ni alloy containing 30% nickel and different iron .contents in seawater at various flow rates; temperature 30 C, test duration 60 days [51]

		Corrosion rate in g/m^{2}at a flow rate in m/s of			
Iron content %	Semi-fabricated form	3	4.12	6.1	8.23
0.04	Tube	27.5		35.5	
0.49		2.2		2.7	
0.03	Bar		24.7		22.9
0.48			2.5		3.2

Since copper and nickel form a continuous series of solid solutions, no heterogeneous structure can occur in these alloys. Alloys containing 10% and 30% Ni have good resistance even to hot seawater and at high flow

rates. Thus these alloys are stable up to moderate flow rates of 6 m/s. It is necessary to maintain a minimum flow rate of 0.6 m/s to avoid corrosion problems. Rates are guide values[51].

The 90/10 and 70/30 alloys have excellent resistance to seawater corrosion and biofouling. If water velocity is accelerated above 1 m/sec, any slight biofouling on metal with good fouling resistance will be easily detached and swept away. On a material that does not have this good fouling resistance, strongly adherent, marine organisms would continue to thrive and multiply[51,52,53].

2.6 Erosion-Corrosion

Erosion-corrosion is the acceleration or increase in rate of deterioration or attack on a metal because of relative movement between corrosive fluid and the metal surface. Generally this movement is quite rapid, and mechanical wear effects or abrasion are involved. Metal is removed from the surface as dissolved ions, or it forms solid corrosion products that are mechanically swept from the metal surface. Sometimes movement of the environment decreases corrosion, particularly when localized attack occurs under stagnant conditions, but this is not erosion corrosion because deterioration is not increased [54].

Erosion corrosion is characterized in appearance by grooves, gullies, waves, rounded holes, and valleys and usually exhibits a directional pattern, Fig.(2.13) a sketch representing erosion-corrosion of a heat-exchanger tube handling water [54].

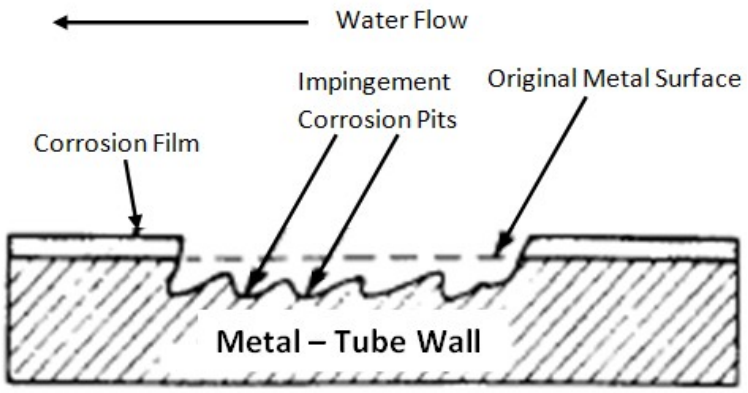

.Figure (2.7): Erosion /Corrosion of Condenser Tube Wall [25]

Most metal and alloys are susceptible to erosion-corrosion damage. Many depend upon the development of a surface film of some sort (passivity) for resistance to corrosion. Erosion–corrosion results when the protective surfaces are damaged or worn and the metal or alloy are attacked at rapid rate. Metals that are soft and readily damaged or worm mechanically, such as copper and lead, are quite susceptible to erosion-corrosion.

The nature and properties of the protective films that form on some metals or alloys are very important from the standpoint of resistance to erosion – corrosion. The ability of these films to protect the metal depends on the speed or ease with which they form when originally exposed to the environment, their resistance to mechanical damage or wear, and their rate of the re-forming when destroyed or damaged. A hard, dense, adherent, and continuous film would provide better protection than one that is easily removed by mechanical means or worn off. A brittle film that cracks or spalls under stress may not be protective. Sometimes the nature of the protective film that forms on a given metal depends upon the specific

environment to which it is exposed, and this determines its resistance to erosion corrosion by that fluid[54].

One of the central problems in the use of copper base alloys with sea water is the limiting flow velocity for which these can be used without the onset of erosion corrosion. It is important, however, to recognize that, in wear, material is removed from surfaces. The form of that removal can take place in different manners according to the mechanisms operating in the system. It is quite clear that the formation and growth of the Cu_2O layer in copper base alloy in sea water accompany with a decrease in the rate of ionic migration in the oxide films should lead to a better resistance to erosion-corrosion[55].

Previously, Thiruvengadam suggested model scaling laws for non-corrosive systems, based on model testing to aid in predicting prototype performance. The basis of time-scale model law is the relation between the relative erosion rates and relative exposure periods for several materials. The purpose of our program was to see how corrosive environment affects this relation and to explore the reasons for these effects.

As shown in Fig.(2.14), cavitation erosion is known to be time dependent From previous investigations. Four distinct periods are described, namely, incubation, acceleration, deceleration, and steady state, both Heyman and Thriuvengadam have proposed theories of erosions to explain the time-dependent nature of erosion[56,57].

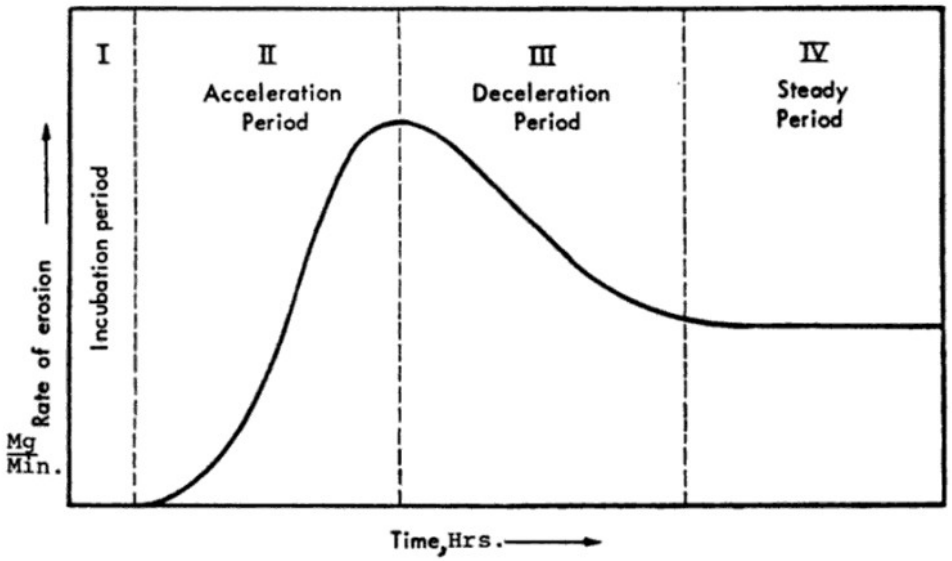

Figure (2.8): Rate of Erosion Versus Time[57].

2.7 Wear of Metals

When two solid surfaces are placed in solid-state contact, it is difficult to envision the absence of some wear even in the most efficiently lubricated systems because of asperity contact. Wear is the removal of material from one or both of two solid surfaces in solid-state contact. It occurs when solid surfaces are in sliding, rolling, or rubbing motion relative to one another. Wear can occur on an extremely fine scale as might be the case in lightly loaded, well-lubricated systems where penetration of the boundary lubricating film is only intermittent and where solid-state contact occurs infrequently[58].

On the other hand, the wear process can be extremely gross and thus result in the bulk removal of material from one surface or both in sliding rubbing, or rolling contact with the result that the

removed material is visible to the naked eye. Wear can take place gradually over a prolonged period of time with small amounts of material removed, or wear can take place rather drastically with the instantaneous loss of material from a surface[58].

The material-intrinsic surface properties, such as hardness, strength, ductility, and work hardening, are very important factors for wear resistance. High wear resistance are related to the role of grain boundaries as effective obstacles for lattice dislocation slip. The quality of most metal products depends on the condition of their surfaces and on surface deterioration due to use. Surface deterioration is also important in engineering practice; it is often the major factor limiting the life and the performance of machine components.

Substantial wear may be defined as unintentional deterioration resulting from use or environment. It may be considered essentially a surface phenomenon. Wear is one of the most destructive influences to which metals are exposed, and the importance of wear resistance needs no amplification. The displacement and detachment of metallic particles from a metallic surface may be caused by contact with (1) another metal (adhesive or metallic wear), (2) a metallic or a nonmetallic abrasive (abrasion), or (3) moving liquids or gases (erosion). Erosion is usually accompanied by some form of corrosion. The above three types of wear may be subdivided into wear under rolling friction or sliding friction and, further, according to whether lubrication can or cannot be used[59].

Wear involving a single type is rare, and in most cases both abrasive and adhesive wear occur. Each form of wear is affected by a variety of

conditions, including environment, type of loading, relative speeds of mating parts, lubricant, temperature, hardness, surface finish, presence of foreign particles, and composition and compatibility of the mating parts involved. Since in most machinery applications wear can rarely be avoided completely even with the best lubrication, it is common practice to use a hard metal and a relatively soft one together. The softer material is used(as bearing) for the part which is most economical to replace[60].

2.8 Oxidation

When any metal combines with an atom or with a molecular group and loses electrons, then an oxidation reaction has taken place. A metal is also oxidized and loses electrons when it goes from one valency to a higher one. The term oxidation, therefore, describes the transfer of electrons, and reactions involving oxygen combining with metals form only a small section under the general heading.

When a metal is oxidized, other species taking part in the reaction is reduced, i.e. it gains electrons. Some common examples can be cited[65]:

Reduced species		Oxidized species
$2Cu_2O$ ……..…..(2.1)	⇄	Cu + O_2 4
4CuO ……..…(2.2)	⇄	$2Cu_2O$ + O_2

Oxides are composed of grains that exhibit behavior similar to that of a metal. An oxide can recrystallize, exhibit grain growth and it may deform plastically, particularly at high temperatures. Diffusion rates will be higher along the intercrysttaline paths than within oxide crystals. Similarly, diffusion rates on the surfaces of crystals will be greater than within the bulk [66].

Most metals are thermodynamically less stable than their oxides and they will; react with the environment to reduce their Gibbs energy. This reaction normally leads to the formation of solid oxide layer on the surface which separate the metal from the environment. If the diffusion of the reacting species through the oxide layer is slow, then the reaction will also be slow and the metal will appear to be unaffected by the environment. If the materials is then heated, the diffusion rate through this layer thin oxide layer would increase. The composition and microstructure of this thin oxide layer would control the diffusion of metal ions and oxygen and thus would affect the scale's development. It is also possible that the layer may affect the diffusion of different metal ions to different extents, so as to favor the development of one type of oxide scale. In general there are three oxidations stages[67]:

(1) The transient stage.
(2) The steady state stage.
(3) The breakaway stage.

Oxidation is an important (HTC) phenomenon. Metals or alloys are oxidized when heated to elevated temperatures in air or in highly oxidizing environments, such as combustion atmospheres with excess air or oxygen. Many metallic components are subject to oxidation in engineering applications[68,69].

2.8.1 Mechanism of Oxide Film Growth

When the surface of the metal is exposed to oxygen, a single layer of oxygen will quickly cover it with a process called chemical adsorption. Thus, nuclei of the oxide are formed on the surface of the metal, and these nuclei grow to cover the surface of the metal or alloy with a thin layer of oxide[70].

The oxide scale forms and grows on the surface of the metal when the surface of the clean metal is exposed to oxygen, so a thin oxide scale will cover the surface of metal quickly at first. The metals which are covered by stable oxides generally exhibit two types of behavior, such as sodium, potassium and magnesium, which are porous oxides, while the thin oxide scale, which covers iron, copper, and nickel, is more dense[71].

The thickness, growth rate, adhesion of the oxide layer and its other properties, determine the potential of oxide to protect the metal, which covered it, whether the oxide layer is porous or dense, its protective ability can be known to a certain extent from the (Pilling-Bedworth Ratio)[72].

The mechanisms in which the oxide layer grows are summed up as follows:

1. If the oxide layer is porous, the oxygen molecules can pass through their pores to interact with the metal or alloy at the interface (metal / oxide) as in Figure (2. 6a).
2. If the oxide layer is non-porous, the oxidation reaction occurs at the interface (air / oxide) where the metal ions diffuse from the surface separating the metal and the oxide towards the outer surface (air / oxide). The electrons also migrate in the same direction for the purpose of completing the reaction as in figure (2.6b)
3. Oxidation reaction may also occur at the interface (metal / oxide)

when the oxide layer is porous. The oxygen ions diffuse into the oxide layer to interact with the metal at the indicated interface, and the electrons are free to move towards the interface (air / oxide) as in figure (2-6c).

4. This case is a combination of the (2) and (3) cases mentioned above, where the oxygen ions diffuse into the interior. The ions of the metal and the electrons are moving outward, and the reaction will occur anywhere where the ions meet in the oxide layer as in Fig.(2-6d) [73]

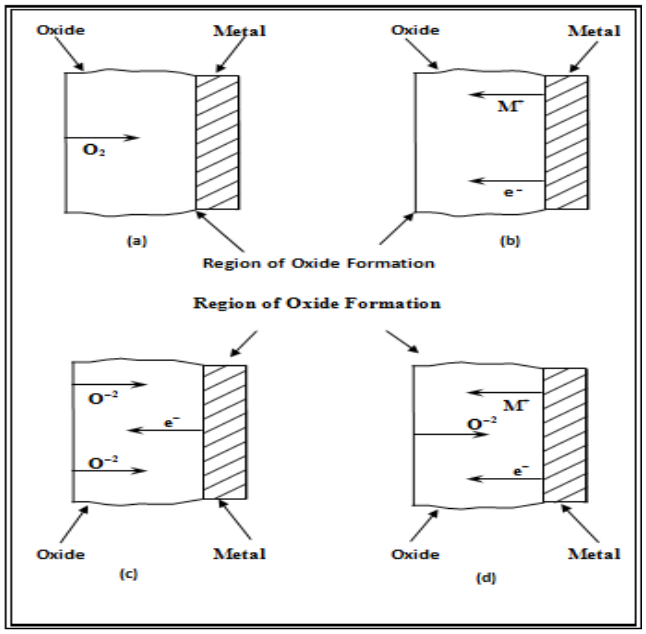

Figure (2.9): Mechanism of Oxide Film Growth[71].

2.8.2 Pilling-Bedworth Ratio for Oxidation of Alloys

The resistance of a metal to high temperature oxidation requires the development of an oxide barrier, while continuous resistance requires maintenance of this protective barrier. Stress generation in an oxide scale may cause scale cracking and spallation, directly affecting the maintenance of the protective oxide scale. There are generally two types of stresses in oxide scales: growth stress, which develops during the oxidation process, and thermal stress, which develops due to the differential thermal expansion between the oxide scale and metal substrate. When an oxide forms at the metal/oxide interface, the volume change due to the formation of the oxide can be expressed with the Pilling-Bedworth ratio (PBR) [74].

$$\text{latem} = \frac{\text{emuloV}}{\text{emuloV}} \quad \text{...3,2} \quad (\text{...})$$

When an alloy is exposed to an oxidizing atmosphere at high temperature, one or more elements in the alloy will be oxidized. In the case of metal Al oxidation, the formation of a mole Al_2O_3 consumes two moles metal Al based on the chemical reaction:

$$\text{'A} + \frac{3}{2}\text{O} \rightarrow \text{lA Q}_3 \quad \text{.....4,2} \quad (\text{.....})$$

When an oxide forms at the metal/oxide interface, the volume change due to the formation of the oxide can be expressed with the Pilling-Bedworth ratio (PBR), The Pilling-Bedworth ratio is expressed as[75].

$$PBR_{Alloy} = \frac{Volume\ of\ a\ mole\ of\ B_x O_y}{Volume\ of\ x\ moles\ of\ B \in alloy} \quad \text{.....} (2.5)$$

2.8.3 Oxidation Kinetics

The most important parameter of metal oxidation from an engineering view-point is the reaction rate. Since the oxide reaction product is generally retained on the metal surface. The rate of oxidation is usually measured and expressed as weight gain per unit area. The various empirical rate laws sometimes observed during oxidation for various metals under various conditions are illustrated in Fig. (2.8). In which a plot of weight gain per unit area versus time is shown. The simplest empirical relationship is the linear law

$$W = k_L.t \text{ …… ..(2.6)}$$

Where W is weight gain per unit area, t is time, and k_L is the linear rate constant. Linear oxidation is characteristic of metals for which a porous or cracked scale is formed so that the scale does not represent a diffusion barrier between the two reactants. Metals which oxidize linearly, such as Sodium and potassium.

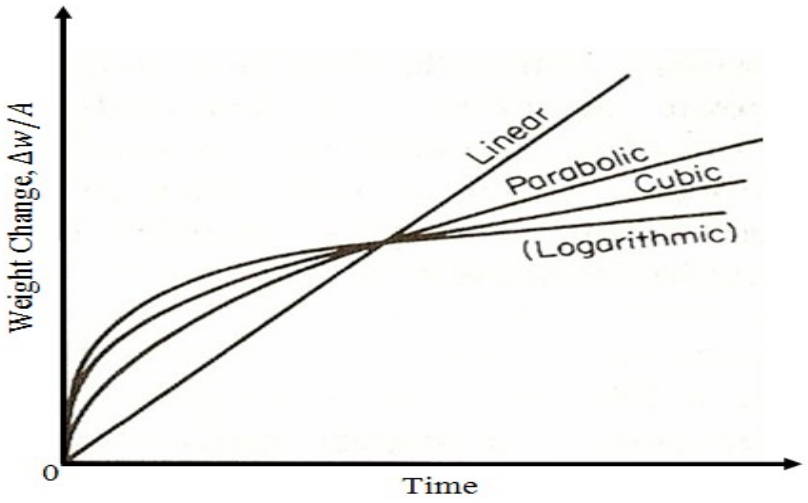

Figure(2.10): Oxidation Rate Laws[76].

The ideal ionic diffusion- controlled oxidation of pure metals have been showed should follow a parabolic oxidation rate law,

$$W^2=k_p.t+C \text{ ……..…(2.7)}$$

Where W is weight gain per unit area, t is time, k_P is the parabolic rate constant, and C is a constant. Metals demonstrating a parabolic oxidation rate yield a straight line when the data are plotted as W^2 versus time.

The logarithmic empirical reaction rate law

$$W = k_e \log(Ct + A)\text{……....(2.8)}$$

Where k_e, C, and A are constants, and the related inverse logarithmic oxidation rate law. Logarithmic oxidation behavior is generally observed with thin oxide layers (e.g. less than 1000Å) at low temperatures. Aluminum, copper, iron, and some other metals oxidize in this manner at ambient or slightly elevated temperatures.

Under specific conditions, some metals appear to oxidize to a cubic law

$$W^3 = k_c.t + C\text{……..……(2.9)}$$

Where k_c, and C are constants[77,78].

2.8.4Oxidation of Copper Alloys

Copper oxidizes according to a logarithmic law up to around 200°C. Above that temperature there appears to be a cubic law which is operative over a small range and then a parabolic law is found. It was pointed out that the value of activation energy, 158 kJ/mole (37.7 kcal/mole), found from the variation of the rate constant above 550°C, corresponds to the activation energy for the diffusion of cuprous ions in Cu_2O, below this temperature the value is much less, 83.6 kJ/mole (20 kcal/mole), and is thought to be associated with a reaction in CuO. The proportion Cu_2O/ CuO found

experimentally is shown in Fig. (2.9). This is pressure sensitive and the amount of CuO decreases with decreasing oxygen pressure.

The addition of aluminum, beryllium, and magnesium increase the oxidation resistance of copper considerably, mainly by preferential oxidation. Many binary alloys oxidize at a similar rate to copper and grow a double scale consisting of outermost CuO and innermost mainly alloy oxide.

Copper-zinc alloys have an oxide consisting of Cu_2O matrix with ZnO particles, which form a continuous outermost film when the zinc content is 20%. At low temperatures the presences of zinc cations lowers the growth rate of Cu_2O, while at high temperatures zinc evaporates away when it has permeated the cuprous oxide film. Many dilute copper alloys suffer from internal oxidation [78,79].

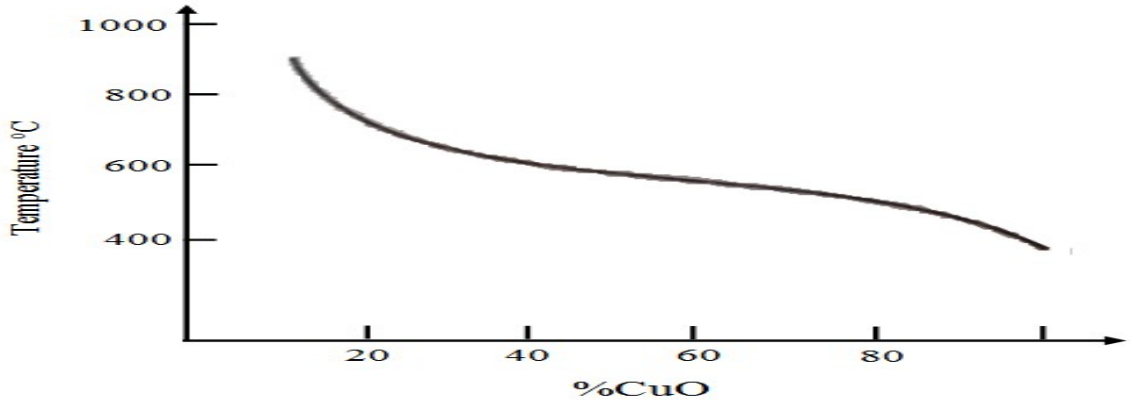

Figure(2.11): Approximate Variation of Cu_2O/CuO Ratio with Temperature for the Oxidation of Copper[80].

2.8.5 Oxide Adhesion

Practical adhesion may be defined as the physical strength of an interface between two regions of a material system. Interfaces may be formed by a

variety of processes and techniques each of which will form interfaces having differing properties. The failure strength of the interface by fracture or deformation will depend on a number of factors including:-

(1) The nature of the stresses at the interface.

(2) The deformation and fracture properties of the interracial material.

The loss of adhesion under mechanical stress (tensile, compressive or shear) occurs by deformation and fracture of material at or near the interface, loss of adhesion may also occur because of non-mechanical stresses such as corrosion or solution of interfacial material, generation of flaws, diffusion to or away from the interface of species which can influence adhesion. Adhesion of the oxide on the surface of the alloy will be poor with increasing its thickness, due to increasing the defects in the oxide scale[81,82,83].

2.8.6 Thermal stresses.

Even when no stress exists at the oxidation temperature cyclic, stresses will be generated during heating and cooling because of the difference in thermal-expansion coefficient of the metal and oxide. The oxides on most engineering alloys are in compression because the growth stresses tend to be compressive and, particularly, the thermal stresses, when they develop on cooling, are compressive because of the sign of the thermal expansion mismatch between the alloy and oxide Table (2.3) [84].

These cyclic stresses (Growth stress, Thermal stress) are generally assumed to arise from coefficient of thermal expansion (CTE) mismatch between oxide and metal[36]. The difference between the coefficient of

expansion of Cu_2O (4.3×10^{-6}/ºC) and that of CuO (9.3×10^{-6}/ºC) could be a source of stress. This difference is even greater than between most other oxides and their metals and stress relief is less likely between oxides than between oxide and metal.

Table (2.3) Linear coefficients of thermal expansion of metals and oxides [84,85].

Ratio	Metal coefficient×10^{-6}/ ºC	Oxide coefficient×10^{-6}/ºC	System
1.25	15.3	12.2	Fe–FeO
1.03	15.3	14.9	Fe–Fe_2O_3
1.03	17.6	17.1	Ni–NiO
0.93	14.0	15.0	Co–CoO
1.30	9.5	7.3	Cr–Cr_2O_3
4.32	18.6	4.3	Cu–Cu_2O
2.00	18.6	9.3	Cu–CuO

2.8.7 Improvement of Scale Adhesion

The basic properties for oxide scale are of adhesion on alloy surface, ability to resist exerted stresses, reduce the rate of oxidation, and self rebuild (self healing protective oxide on its surface) immediately in case of fracture[86].

Most of protective oxides which cover surfaces of alloys are of the high temperatures resistance lack of perfect adhesive and suffer from spalling under influence of stresses. The adhesion between scale and alloy is

markedly improved and this increase the alloy's resistance to thermal cycling exposure, in some but not all cases the actual growth rate of the oxide is also reduced[87].

The improvement in oxidation resistance of high temperatures alloys as results of [88]:-

- Additions of rare earth elements, other reactive metals, or dispersions of stable oxides.
- Yttrium (Y) and hafnium (Hf) improve the adherence of the oxide scale to the substrate by reducing the amount of the oxide that spalls off during a thermal cycle.
- Addition elements such as Al and Cr, their oxides Al_2O_3 and Cr_2O_3 are generally regarded as the best protective oxides under various environment.
- Addition of noble elements such as platinum (Pt), it also improves the adherence of oxide scale, but the needing of much amount from this expensive noble element, make its using in limitation application.

The Particle Swarm Algorithm 2.9

Introduction .2.9.1

Maximizing earns or minimizing losses has always been a concern in engineering problems. For diverse fields of knowledge, the complexity of optimization problems increases as science and technology develop. Often, examples of engineering problems that might require an optimization approach are in energy conversion and distribution, in mechanical design, in logistics, and in the reload of nuclear reactors. To maximize or minimize a function in order to find the optimum, there are several approaches that one could perform. In spite of a wide range of optimization algorithms that could be used, there is not a main one that is considered to be the best for any case. One optimization method that is suitable for a problem might not be so for another one; it depends on several features, for example, whether the function is differentiable and its concavity (convex or concave). In order to solve a problem, one must understand different optimization methods so this person is able to select the algorithm that best fits on the features' problem. The particle swarm optimization (PSO) algorithm, proposed by Kennedy and Eberhart [89], is a metaheuristic algorithm based on the concept of swarm intelligence capable of solving complex mathematics problems existing in engineering [90]. It is of great importance noting that dealing with PSO has some advantage swhen compared with other optimization algorithms, once it has fewer parameters to adjust, and the ones that must be set are widely discussed in the literature [91].

2.9.2 Overview Particle Swarm Optimization

In the early of 1990s, several studies regarding the social behavior of animal groups were developed. These studies showed that some animals

belonging to a certain group, that is, birds and fishes, are able to share information among their group , and such capability confers these animals a great survival advantage [92]. Inspired by these works, Kennedy and Eberhart proposed in 1995 the PSO algorithm [89], a metaheuristic algorithm that is appropriate to optimize nonlinear continuous functions. The author derived the algorithm inspired by the concept of swarm intelligence, often seen in animal groups, such as flocks and shoals. In order to explain how the PSO had inspired the formulation of an optimization algorithm to solve complex mathematical problems, a discussion on the behavior of a flock is presented. A swarm of birds flying over a place must find a point to land and, in this case, the definition of which point the whole swarm should land is a complex problem, since it depends on several issues, that is, maximizing the availability of food and minimizing the risk of existence of predators. In this context, one can understand the movement of the birds as a choreography; the birds synchronically move for a period until the best place to land is defined and all the flock lands at once.

In the given example, the movement of the flock only happens as described once all the swarm members are able to share information among themselves; otherwise, each animal would most likely land at a different point and at a different time. The studies regarding the social behavior of animals from the early 1990s stated before in this text pointed out that all birds of a swarm searching for a good point to land are able to know the best point until it is found by one of the swarm's members. By means of that, each member of the swarm balances its individual and its swarm knowledge experience, known as social knowledge. One may notice that the criteria

to assess whether a point is good or not in this case is the survival conditions found at a possible landing point, such as those mentioned earlier in this text.

The problem to find the best point to land described features an optimization problem. The flock must identify the best point, for example, the latitude and the longitude, in order to maximize the survival conditions of its members. To do so, each bird flies searching and assessing different points using several surviving criteria at the same time. Each one of those has the advantage to know where the best location point is found until known by the whole swarm. Kennedy and Eberhart inspired by the social behavior of birds, which grants them great surviving advantages when solving the problem of finding a safe point to land, proposed an algorithm called PSO that could mimic this behavior. The inertial version, also known as classical version, of the algorithm was proposed in 1995 [89]. Since then, other versions have been proposed as variations of the classical formulation, that is, the linear-decreasing inertia weight [93], the constriction factor weight [94], besides hybrid models [95] or even quantum inspired approach optimization techniques that can be applied to PSO [96]. This chapter will only present the inertial model of PSO, as it is the state-of-the-art algorithm, and to understand better the derivations of PSO, one should firstly understand its classical version.

The goal of an optimization problem is to determine a variable represented by a vector $X = [x_1 x_2 x_3 \ldots x_n]$ that minimizes or maximizes depending on the proposed optimization formulation of the function f(X). The variable vector X is known as position vector; this vector represents a variable model and it is n dimensions vector, where n represents the number of variables that may be determined in a problem, that is, the latitude and the longitude in the

problem of determining a point to land by a flock. On the other hand, the function f(X) is called fitness function or objective function, which is a function that may assess how good or bad a position X is, that is, how good a certain landing point a bird thinks it is after this animal finds it, and such evaluation in this case is performed through several survival criteria.

Considering a swarm with P particles, there is a position vector $X_t^i = [x_{i1}x_{i2}x_{i3} \ldots x_{in}]^T$ and a velocity vector $V_t^i = [\ v_{i1}v_{i2}v_{i3} \ldots v_{in}]^T$ at a t iteration for each one of the i particle that composes it. These vectors are updated through the dimension j according to the following equations:

$$V^{t+1}_{ij} = \omega\, V^t_{ij} + c1\ r1\ (pbest_{ij} - X^t_{ij}) + c2\ r2\ (gbest_j - X^t_{ij}) \qquad (2\text{-}10)$$

and

$$X^{t+1}_{ij} = X^t_{ij} + V^{t+1}_{ij} \qquad (2\text{-}11)$$

where i = 1,2,…,P and j = 1,2,…,n.

Eq. (1) denotes that there are three different contributions to a particle's movement in an iteration, so there are three terms in it that are going to be further discussed. Meanwhile, Eq. (2) updates the particle's positions. The parameter w is the inertia weight constant, and for the classical PSO version, it is a positive constant value. This parameter is important for balancing the global search, also known as exploration (when higher values are set), and local search, known as exploitation (when lower values are set). In terms of this parameter, one may notice that it is one of the main differences between classical version of PSO and other versions derived from it.

Lastly, Figure 1 shows the PSO algorithm flowchart, and one may notice that the optimization logic in it searches for minimums and all position vectors are assessed by the function f(X), known as fitness function. Besides that, Figures 2 and 3 present the update in a particle's velocity and in its position at a t iteration, regarding a bi-dimensional problem with variables x_1 and x_2.

1. Initialization
    1.1. For each particle i in a swarm population size P:
        1.1.1. Initialize X_i randomly
        1.1.2. Initialize V_i randomly
        1.1.3. Evaluete the fitness $f(X_i)$
        1.1.4. Initialize $\boldsymbol{pbest}_i$ with a copy of X_i
    1.2. Initialize $\boldsymbol{gbest}$ with a copy of $X_i$with the best fitness
2. Repeat until a stopping criterion is satisfied:
    2.1. For each particle i:
        2.1.1. Update V_i^t and X_i^t according to Eqs. (1) and (2)
        2.1.2. Evaluete the fitness $f(X_i^t)$
        2.1.3. $\boldsymbol{pbest}_i \longleftarrow X_i^t$ if $f(\boldsymbol{pbest}_i) < f(X_i^t)$
        2.1.4. $\boldsymbol{gbest} \longleftarrow X_i^t$ if $f(\boldsymbol{gbest}) < f(X_i^t)$

Figure (2.16): The PSO algorithm[94].

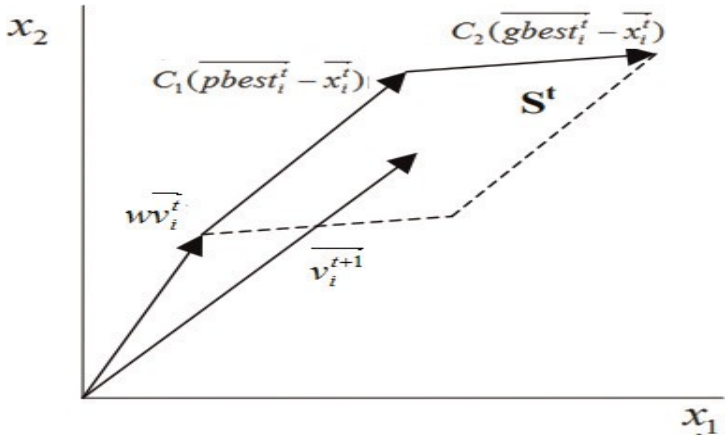

Figure (2.12): The velocity vector at a t iteration as being composed by two components regarding a bi-dimensional problem[92].

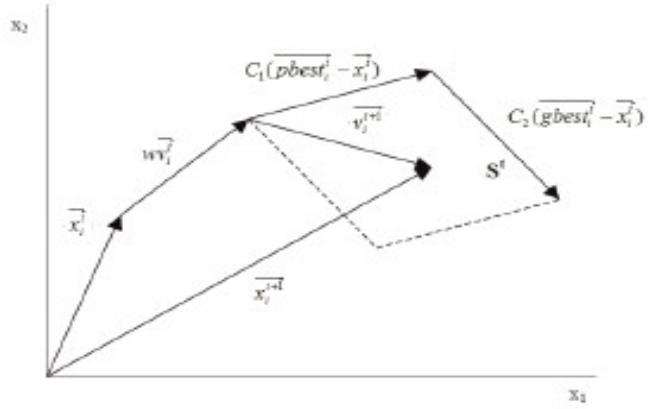

Figure (2.13): The position vector being updated at a t iteration as being composed by two components regarding a bi-dimensional problem[92].

2.9.3 Recent applications and challenges

PSO can be applied to many types of problems in the most diverse areas of science. As an example, PSO has been used in healthcare in diagnosing problems of a type of leukemia through microscopic imaging [97]. In the economic sciences, PSO has been used to test restricted and unrestricted risk investment portfolios to achieve optimal risk portfolios [98]. In the engineering field, the applications are as diverse as possible. Optimization problems involving PSO can be found in the literature in order to increase the heat transfer of systems [99] or even in algorithms to predict the heat transfer coefficient [100]. In the field of thermodynamics, one can find

papers involving the optimization of thermal systems such as diesel engine–organic Rankine cycle [101], hybrid diesel-ORC/photovoltaic system [102], and integrated solar combined cycle power plants (ISCCs) [103].

PSO has also been used for geometric optimization problems in order to find the best system configurations that best fit the design constraints. In this context, we can mention studies involving optical-geometric optimization of solar concentrators [104] and geometric optimization of radiative enclosures that satisfy temperature distribution and heat flow [105]. After having numerous versions of PSO algorithm such as those mentioned in the first section, PSO is able to deal with a broad range of problems, from problems with a few numbers of goals and continuum variables to others with challenging multipurpose problems with many discreet and/or continuum variables. Besides its potential, the user must be aware that the PSO will only achieve appreciated results if one implements an objective function capable of reflecting all goals at once. To derive such a function may be a challenging task that should require a good understanding of the physical problem to be solved and the ability to abstract ideas into a mathematical equation as well. The problems presented in the fourth section of this work provide examples of objective functions capable of playing this role. Another challenge for one using PSO is how to handle the bounds of the search domain whenever a particle moves beyond it [106].

Literature Review 2.10

2:10:1 Recent Studies Related to Copper-Zinc alloys:

Jamal Al-Deen 1998: studied the addition of (Ge, Te, and Al) to (70/30) brass alloy for improvement erosion-corrosion resistance, it was found that the erosion rate increase with increasing sand concentration but the erosion efficiency decreases. The maximum erosion rate was found at (20^{o}) and decreases with increasing the angle up to (90^{o}), at the ($53\mu m$) sand particle size and concentration of (0.1%). Erosion rate at $52^{o}C$ was smaller than that at $13^{o}C$. The optimization sequence of elements which led to the improvement of erosion resistance at room temperature ($13^{o}C$) (Te, Al, and Ge) i.e. Te is the best and so on, and that at $52^{o}C$ was (Ge,Te, and Al) [107].

Gaoyong, et.al 2011: studied the corrosion behaviors of Al-brass in stagnant and flowing marine water as a function of combinative rare earths (Ce and La) addition were investigated by electrochemical techniques, X-ray diffraction (XRD) and scanning electron microscopy (SEM). It was demonstrated that RE elements could make the corrosion product layer more protective and strengthen the cohesion between the film and matrix in stagnant seawater. The electrochemical impedance spectroscopy (EIS) and scanning electron microscopy (SEM) analysis confirmed that a duplex layer, which was mainly composed of an inner Al_2O_3 with trace amounts of RE compounds and an outer basic chloride of copper or zinc layer was formed on RE-contained Al-brass surface and that the inner layer was responsible for the good corrosion resistance of the alloy. While only a porous and non-protective corrosion product layer was formed on the Al-brass alloy without RE addition, which made small

values of the corrosion resistance. Additionally, in flowing marine water with velocity about 2 m/s, pitting corrosion occurred on the Al-brass surface and RE addition could availably decrease pitting sensitivity of the alloy [108].

Haleem, et.al 2011: have studied the adding of Aluminum to brass alloy (α) for improving the oxidation resistance. In this work, pure Aluminum (1- 2% wt.) has been added to brass alloy (α). These alloys have been prepared by melting and casting in a metallic mold. Tests of cyclic oxidation have been conducted on the alpha brass alloy including Aluminum and no including, at a wide range of temperatures (500 – 900)°C in still air for (52 hours) at (4 hours) cycle. The oxidation kinetics follows breakaway behavior for alpha brass alloy at 800°C and 900°C. This indicates that the oxidation behavior of this alloy is non-protective. The phases presents on the cyclic oxidation of alpha brass alloy including Aluminum addition as revealed by X-Ray Diffraction (XRD) analysis are: Cu_2O, CuO, and ZnO. Alpha brass alloy (α) alloys containing Al demonstrates high oxidation resistance. This is attributed to the formation of protective alumina (Al_2O_3). Oxide morphology was examined using light optical microscope (LOM) [109].

2:10:2 Recent Studies Related to Copper-Nickel alloys:

Badawy, et.al. 2014: described copper alloys are important materials for many industrial applications. The addition ofAl, Ni and Zn to Cu either as single alloying element in binary alloys like brasses and bronzes or the well-known Cu-Ni alloys or as couples in ternary alloys leads to specific properties important for different applications.. It is important to compare the corrosion behavior and the stability of each alloy in these media. For this

reason they have used Cu-10Al-10Ni, Cu-10Al-10Zn and Cu-10Ni-10Zn, in which the ratio of Cu is kept constant and the two alloying elements of equal percentage[110].

Nady, et.al. 2016: studied copper-based alloys are widely used in the consumer electronics industry for components such as connector contacts, shielding gaskets, and terminals. Nickel silver is a general term for alloys that contain copper, nickel, and zinc. Nickel silver first became popular as a base metal for silver-plated cutlery and other silverware, notably electro-plated nickel silver, jewelery and coins. The electrochemical stability of Cu–10Ni–10Zn alloy was compared with that of pure copper and two of copper ternary alloys, namely Cu–10Al–10Zn and Cu–10Al–10Ni in synthetic sweat solution, Hank's solution and in Ringer physiological solution[111].

Shi, el.at. 2017 : studied corrosion behaviors of pure Cu and Cu-Ni-Zn alloy were investigated in 3.5% NaCl solution and artificial seawater by electrochemical impedance spectroscopy and potentiodynamic polarization technologies, and the corrosion morphologies were observed by field emission scanning electron microscopy. The results revealed that Cu-Ni-Zn alloy possessed better corrosion resistance than that of pure Cu in both 3.5% NaCl solution and artificial seawater. The corrosion morphology displayed the corrosion product films on Cu-Ni-Zn alloy were more compact and uniform than that on the pure Cu in both 3.5% NaCl and artificial seawater media[112].

Tandon, et. al. 2017: studied Cu-10Ni alloy has an outstanding resistance to corrosion in seawater due to formation of protective Cu2O film. However, in presence of S2 − ions, it suffers accelerated corrosion. The

present paper investigates the corrosion behaviour of Cu-10Ni, Cu-10Ni-6Zn and Cu-10Ni-12Zn alloys using weight loss, electrochemical impedance spectroscopy and potentiodynamic polarization technique. The experiments were performed in clean seawater and sulphide contaminate seawater. The Cu-10Ni-6Zn and Cu-10Ni-12Zn alloys were found to exhibit lower corrosion rat than Cu-10Ni alloy in clean and sulphide contaminated seawater. Lower corrosion rate of Zn containing alloys in clean seawater is attributed to the incorporation of Zn^{2+} ions in Cu_2O lattice. Lower corrosion rate of Zn containing alloys sulphide contaminated seawater is attributed to formation of ZnS in the film[1113].

2:10:3 Recent Studies Related to particle swarm

Pol, et.al. 2007: described particle swarm optimization (PSO) has undergone many changes since its introduction in 1995. As researchers have learned about the technique, they have derived new versions, developed new applications, and published theoretical studies of the effects of the various parameters and aspects of the algorithm [114].

Wang, et. al. 2013: studied three different variations of PSO algorithms, i.e. Canonical, Gaussian Bare -bone and Lévy Bare-bone PSO, are tested to optimize the ultimate oil recovery of a large heavy oil reservoir. The performance of these algorithms was compared in terms of convergence behaviour and the final optimization results. It is found that, in general, all three types of PSO methods are able to improve the objective function. The best objective function is found by using the Canonical PSO, while the other two methods give similar results. The Gaussian Bare -bone PSO may picks positions that are far away from the optimal solution. The Lévy Bare-bone

PSO has similar convergence behavior as the Canonical PSO. For the specific optimization problem investigated in this study, it is found that the temperature of the injection steam, CO_2 composition in the injection gas, and the gas injection rates have bigger impact on the objective function, while steam injection rate and the liquid production rate ha ve less impact on the objective function[115].

Alam 2016: discussed an algorithm for classical particle swarm optimization (PSO). Also, its codes in MATLAB environment have been included. The effectiveness of the algorithm has been analyzed with the help of an example of three variable optimization problem. Also, the convergence characteristic of the algorithm has been discussed[116].

Aje. et. al. 2020: Studied particle Swarm Optimization (PSO) is one of the concepts of swarm intelligence inspired by studies in neurosciences, cognitive psychology, social ethology and behavioral sciences, introduced in the domain of computing and artificial intelligence as an innovative collective and distributed intelligent paradigm for solving problems, mostly in the domain of optimization, without centralized control or the provision of a global model. The PSO method has roots in genetic algorithms and evolution strategies and shares many similarities with evolutionary computing such as random generation of populations at system initialization or updating generations at optima search. This paper presents an extensive literature review on the concept of PSO, its application to different systems including electric power systems, modifications of the basic PSO to improve its premature convergence, and its combination with other intelligent algorithms to improve search capacity and reduce the time spent to come out of local optimums[117].

Chapter Three

Experimental Part

3.1 Introduction

A general overview of the experimental work steps is given in this chapter and also includes all the circumstances under which the study took place. It takes up the specifics of the experimental component by describing the main materials, instruments used and measurements in the current work, and all physical, chemical and mechanical test of base alloy (Cu-Ni), nickel and free nickel samples including: chemical composition analysis (XRF), optical microscope analysis, scanning electron microscope (SEM), energy dispersive spectroscopy (EDS) and X-ray diffraction (X-ray diffraction) (XRD. Chemical tests include open circuit potential, potentiostatic polarization, simple immersion and erosion-corrosion. Wear rate tests have been studied in addition to evaluating specific mechanical properties such as micro-hardness. Thermal shock and oxidation test was also conducted for all samples.

3.2 Experiments Program of Present Study:

Figure (3.1) displays the experimental program of the present study.

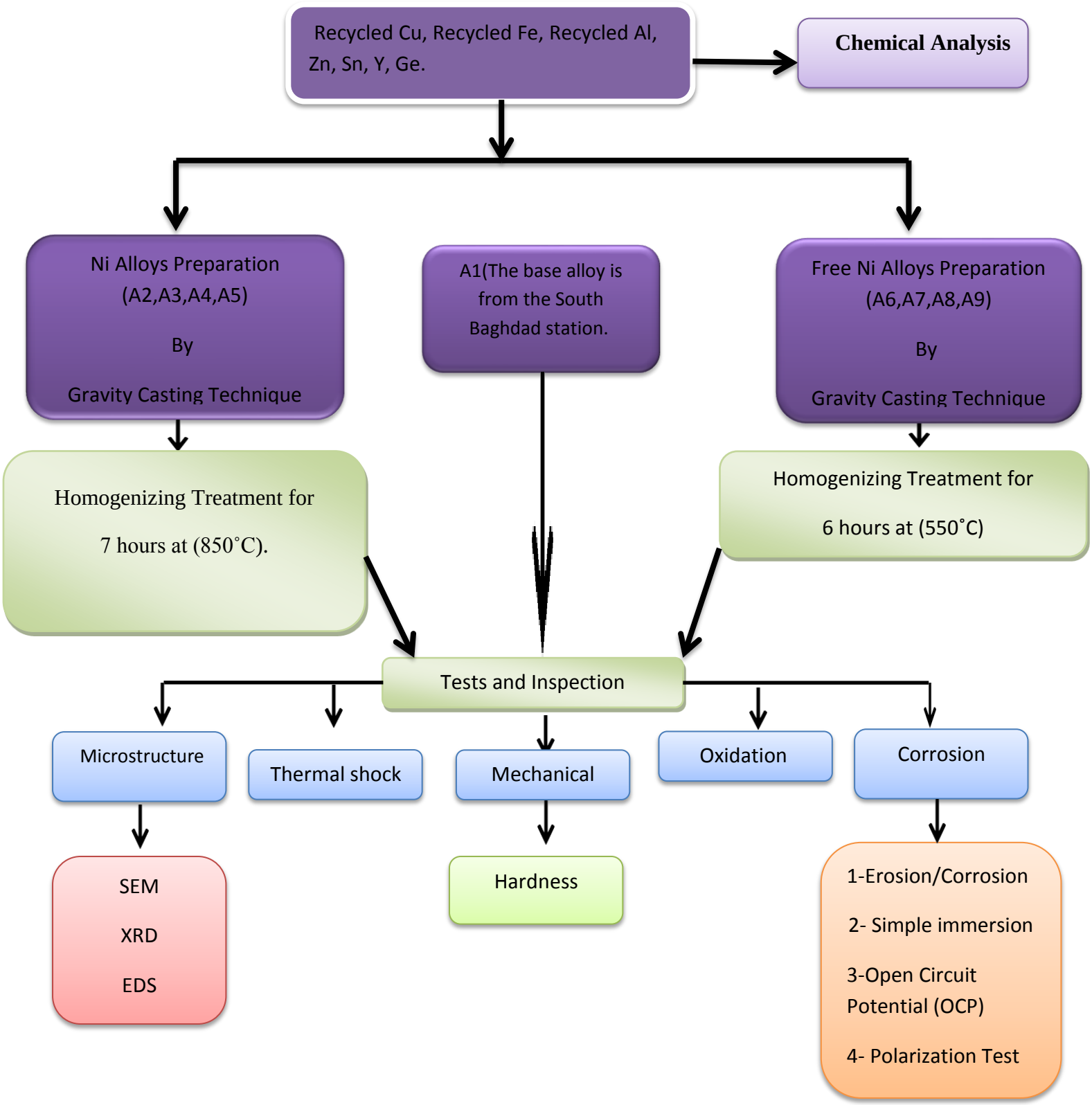

Figure (3.1): Shows the Block Diagram of the Experimental Procedures.

3.3Preparation of Recycled Materials:

Preparation of the main metals included in the preparation of alloys in this study, the recycling technique was used for the purpose of preparing the main metals used in the manufacture of these alloys, namely (copper, iron, aluminum), where soft drink bottles were collected as a source for preparing the aluminum element and the spent cupper-coils as a source for preparing copper and iron scrap as a source for preparing iron shows in figures (3.2, 3.3, and 3.4), where those consumables were cleaned, washed and dried and then weighed, and the prepared weights were: 250 g of aluminum, 250 g of iron and 1 kg of copper .These materials were cut into small pieces using a cutter and melted in a ceramic crucible, it has a capacity of 1 kg and using an electric furnace. Borax was used to purify metals from slag and impurities suspended in them. This suspended slag was pulled from the surface of the molten before the casting process, which was done in pre-heated metal molds with a range of 200-300 C°, and after cooling, aluminum and copper were obtained. , iron and its purity reached 93.44%, 96.5%, 95.6%, respectively. Table (3.1) shows the chemical composition of the metals used in preparing the alloys under study.

Table (3.1) shows the purity of the used materials

Material	**Purity**
copper	**96.5**
zinc	**99.99**
aluminum	**94.86**
nickel	**99.99**
Tin	**99.99**
Iron	**93.40**
Germanium	**99.99**
Yttrium	**99.99**

Figure(3.2); Aluminum soft drinks cans that prepared.

Figure(3.3): Copper coils scrap that prepared.

Fig.(3.4): Iron scrap that prepared.

3.4 Preparation of Specimens

3.4.1 Melting and Casting

In order to prepare the samples (A2, A3, A4, A5, A6, A7, A8and A9), melting and casting processes have been used. Using electric furnace as showed in Figure (3.5).

The melting temperature of copper (Cu) is 1083°C, zinc (Zn) is 419.6°C, aluminum (Al) is 660^{o}C, tin (Sn) is 231.9^{o}C, germanium (Ge) is 938.2^{o}C,yterium is 1526 C°, nickel is 1455 C°, and Iron is 1538 C° . The melted alloy (mixture) was mixed with a homogeneous melting alloy using a ceramic rod.

The metals are poured into the cylindrical metallic mold (with 30, 22, and 150mm) outer diameter, inner diameter, and height respectively, The die was heated and graphite was used as lubricant before casting process, they were added in small quantities to ensure sample eject from the die.

Figure (3.5): The electric furnace used for Casting.

To avoid thermal shock, the mold should be preheated at approximately, then cooled gradually, then the molten metal was poured into a metal mold and allowed to solidify to room temperature. Copper and aluminum foil paper were used during the melting process to preserve the proportion of alloying elements (Zn, Al, Sn, Ni, Y, Fe and Ge) added to copper, and borax was added to the surface of the liquid metal during melting to prevent zinc evaporation, while argon gas atmosphere was used in the electric furnace during melting to prevent material oxidation.

3.4.2 Heat Treatment

The homogeneous process is carried out at a temperature (850 C°) to homogenize the composition in order to ensure that the elements and inclusions are regularly distributed in the alloy. Residence in time is (7hrs.) The alloys would obtain homogeneous ductility and mechanical properties through this process for (A2, A3, A4 and A5) at this temperature, and leave them cooling slowly in the furnace. While the ingots (A6, A7, A8, and A9) were annealed for 6 h at 550 °C to solve the cast structure. Figure (3.6) The electric heat treatment furnace, shown, was used.

Figure (3.6) The electric heat treatment furnace.

3.4.3 Preparation of Specimens

The samples were cut by a turning machine to prepare the specimens (A1, A2, A3, A4, A5, A6, A7, A8 and A9) into disks shape (22 diameter, 5mm thickness). The samples were prepared in accordance with normal metallographic methods and conducted on a cross-section of the sample. On the successively finer grades of emery sheets, rough polishing was done. Different silicon carbide papers range from silicon carbide grid papers (80, 120, 180, 220, 400, 600, 800, 1000, 1200, 2000, 2500, and 3000). By using diamond past, polishing was done by the polishing cloths.

Diamond polishing with a particle size of 1μm was carried out. In order to facilitate hand grinding, water was used as a coolant and lubricant. They washed these samples with distilled water and alcohol. The samples are kept in polyethylene bags after drying in hot air.

3.4.2 Analysis of Chemical Composition

X-ray fluorescence (XRF) was examined for chemical composition analysis of alloys (A1, A2, A3, A4, A5, A6, A7, A8 and A9) using metal analysis by SPECTROMAX (Germany), as shown in Figure (3.7). This inspection (Razi Metallurgical Research Centre/Iran) has been completed.

Figure (3.7): SPECTROMAX Analyzer Device.

3.5 The Tests

3.5.1 Hardness Test

According to ASTM E92-17, the micro-hardness test was carried out using the Digital Vickers hardness tester type (HVS-1000) presented at the Metals Laboratory at the College of Materials Engineering at the University of Babylon. The Vickers rigidity tester is shown in Fig (3.8). It was used with a square-based diamond pyramid to measure the sample hardness (A1, , A2, A3,A4, A5,A6,A7,A8 & A9) at a load of 500 grams and to hold for 15 seconds.

Three readings were taken for each sample and the average value was used. By the following equation below, the Vickers hardness was determined:

$$HV = 1.854\frac{P}{d^2} \dots\dots\dots\dots\dots\dots (3.1)$$

Where:

(HV): Vickers Hardness (kgf/mm^2).

(P): Applied load (Kg).

(d): The average diameter of the indentation (mm).

Figure (3.8): Micro-Hardness ((HV) Measuring.

3.5.2 Dry Sliding Wear Test

Using (pin-on-disc) MT 4003 version 10, concept using (950 r.p.m) and constant radius (6.5mm) with a different sliding distance, the dry sliding wear is investigated and the loads are loaded (20N). The specimen is weighed using a sensitive balance (±0.0001 g) before starting the test. The specimen test is weighted after a period of time (5, 10, 15, 20, 25 and 30 min.) and the volume loss is calculated according to the equation (3.2).

The test method is covered in accordance with (ASTM G9). The wear device used in this work was located in the laboratories University of Technology, Department of Materials, as shown in Figure (3.9).

$$\textbf{Volume Loss}, \textbf{mm}^3 = \frac{\textbf{mass loss}, \ \textbf{g}}{\textbf{density}, \ \ \textbf{g/cm}^3} \times \textbf{1000} \ldots\ldots\ldots (\textbf{3.2})$$

Figure (3.9): Pin-on-Disc Wear Instrument.

3.6 Density Measurement

Using the responsive balance (±0.0001 g) to measure the alloy and the electronic weight meter to measure the density in a realistic way in order to determine the density of the alloys. 'Mastu HaKu HGH PRECISION DENSITY TESTER GP-120S' was used to measure the density of the specimen, as shown in Figure (3.10).

The measurement of density was based on the Archimedes way, based on a measured specimen weight in the air and then in the water. The reading is based on the linear potentiometer Where (±0.02) is used to calculate sample dimensions for the size calculation density equation (3.3).

$$\rho = \frac{w_{Air}}{w_{Air-}\, w_{Water}} \times \rho_{Water} \dots\dots\dots\dots (3.3)$$

Where:

(ρ) refer to the alloy density (g/cm^3).

(w_{Water}) refer to alloy weight in the water (g).

(w_{Air}) refers to alloy net weight in the air (g).

(ρ_{Water}) refer to density of water (g/cm^3).

Figure(3.10): Density measurement instrument.

3.7 Oxidation Tests

3.7.1 Cyclic Oxidation

In order to study the oxidation resistance of the specimens, cyclic oxidation was carried out at high temperatures in the furnace. The oxidation resistance assessments of the specimens were conducted by heating the specimens in a furnace at test temperatures and weighing them every 5 hours.

The specimens were weighed accurately and then put into a ceramic crucible. In a furnace with a temperature range of (250-850)oC in air at (1 atm.) pressure, cyclic oxidation tests were carried out. Heating in the furnace for (5 hours) at the test temperature and cooling inside the furnace are included in each heating cycle. Specimens of changes in weight were measured before and after each oxidation cycle. Usually, at least 10 weight measurements have been made.

3.7.2 Thermal Shock Test

The testing was carried for all samples that were placed in an electrical furnace with a temperature range (50-850) C° for (30 min.), then quenched in water, and continued to heat by increasing the temperature for each time by (50C°) and using the same time period and cooling them with tap water until a temperature of 850 0C is reached.

The weight variation was calculated according to the unit area (w/A) and several records were taken and the changing relationship between the weight of the unit area and the temperature was recorded.

3.8 Corrosion Test

3.8.1 Simple Immersion Method

The test was carried out by immersing the samples (A1, A2, A3, A4, A6, A7, A8 and A9) in salt water (sea water) (3.5% NaCl), as shown in Figure (3.10). Each of the weight changes has been cached (3 days).

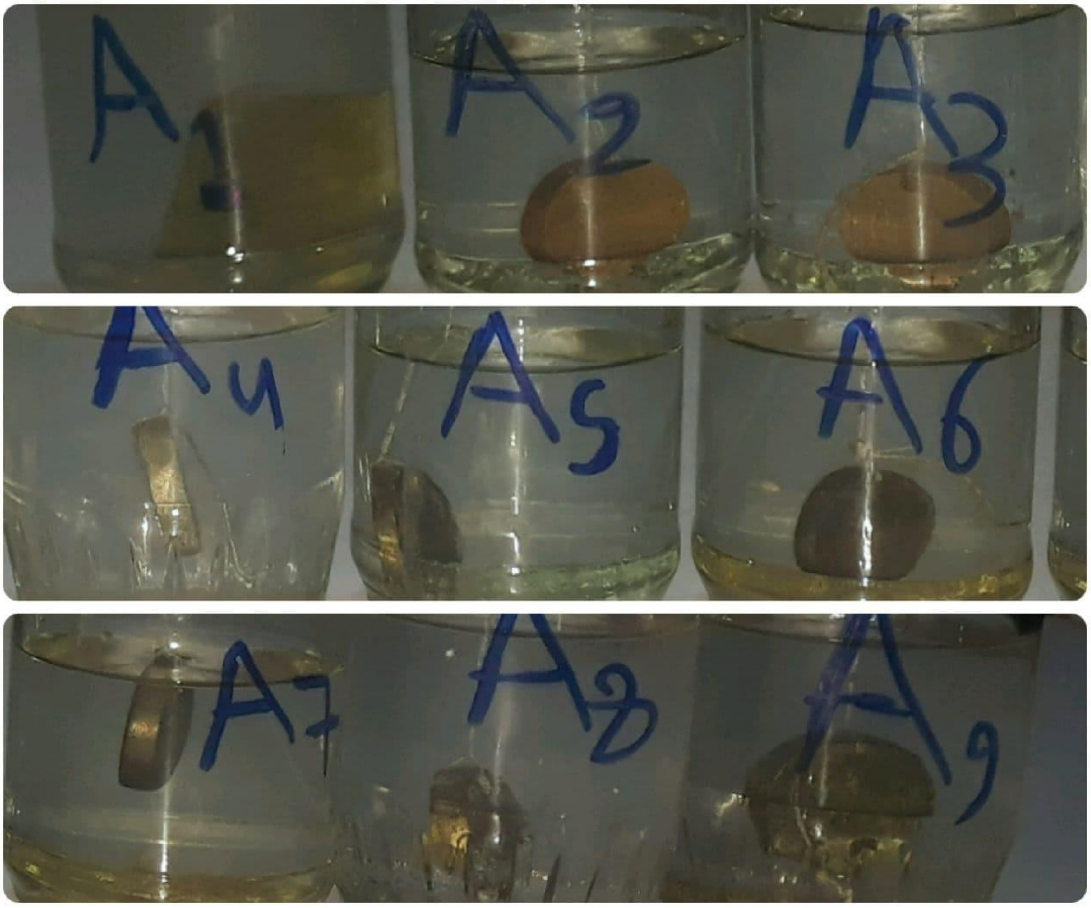

Fig. (3.11): Sample Immersion Inside Containers of Sea Water.

All samples were weighted with a sensitive weighting balance with an accuracy (±0.0001 g) prior to the immersion process and surface areas were measured for each sample. Samples were taken out after each immersion process to clean them by distilling water, drying with warm air, and then weighing them.

The change of weight was measured and reported for each experiment.

The rate of corrosion was defined by the following relationship[46]:

$$\textbf{Corrosion Rate}\left(\frac{\textbf{mg}}{\textbf{mm}^{\textbf{2}}\cdot\textbf{day}}\right)=\frac{\textbf{change in weight}\ (\Delta\textbf{w})}{\textbf{surface area}\times\textbf{time}}\ldots\ldots(\textbf{3.4})$$

3.8.2 Open Circuit Potential Test (O.C.P)

Open-Circuit Potential (O.C.P) The potential of an electrode determined with respect to a reference electrode in the absence of current is also known as equilibrium potential (under open-circuit conditions).It is simply a valuable technique which determines the potential difference between a reference electrode and the work (specimen). For a specimen in the corrosion solution, the O.C.P. (voltage versus time) was recorded every five minutes. Open circuit potential (O.C.P) was calculated as a function of time before steady-state potential.

At a scan rate of 0.4 mV/s from an open circuit potential of (200 mV) below the open circuit potential, the polarization curves were potentiostatcally determined and the scan was continued up to (200 mV) above the open circuit potential.

In Fig.(3.12), in which a schematic drawing explains the experimental situation, the experimental structure for the calculation of open circuit potential is shown.

Figure (3.12): Open Circuit Potential Measurement.

3.8.3 Polarization Test

Another corrosion measurement method used to observe anodic and cathodic behaviors is the potentiostatic technique (i.e. monitoring the corrosion reactions on specimen of desired metal). The corrosion current and corrosion potential are calculated using this process. The "polarization" was carried out in an electrochemical corrosion cell that includes a working electrode, a platinum electrode as a counter electrode and (SCE) saturated calomel .electrode .has (241) mV, the process has been programmed in the computer to draw potential (mV) and log current (μA) to obtain corrosion current density by an intersection of the tangents to the two polarization curves to determine .the potential .of the electrode.

This test was conducted in the Metallurgical Department of the University of Babylon - College of Materials Engineering. Both corrosion potential and corrosion current density were measured using Tafel extrapolation. The electrochemical method used is shown in Figure (3.13).

For the determination of corrosion rate by current density in the solution on the alloy during electrochemical reactions, the general equation applied is:

$$\textbf{Corrosion Rate(mpy)} = \frac{\mathbf{0.13\ I_{Cor}\ (EW)}}{\mathbf{A.\rho}} \ldots\ldots\ldots\ldots (\mathbf{3.5})$$

$$\mathbf{i_{Cor}} = \frac{\mathbf{I_{Cor}}}{\mathbf{A}}$$

Where:

0.13 = metric and time conversion factor.

i_{Cor}= corrosion current density, µA/ cm².

I_{Cor}= total anodic current, µA

E.W= equivalent weight (g/eq.).

A= exposed specimen area, cm²

ρ= density of alloy (g/cm³)

mpy = Corrosion rate (mils per year).

Figure (3.13): The Electrochemical System.

3.8.4 Erosion/Corrosion Test

Because of the collision or gases and liquid impact, erosion is a mechanical mechanism such as removing part of the material from the surfaces. During this study, the erosion-corrosion apparatus was designed to rely on ASTM (G 73), as shown in Figure (3.14). The erosion-corrosion system consists of the motor (Q max 53 l/min, H max = 38m, HP = 1hp, 2850 rpm, scale 1in-1in), the granite tank, the tubes on the specimen to drop the water by nozzle.Temperature (25-30oC) tested by all alloys, anywhere salt solution (sea water) induces erosion-corrosion and falls from the nozzle at angle=90 ° (the impact angle between the line of water and surface of specimen).

The nozzle has a diameter of (2mm) and is mounted at a fixed distance of (10 mm) from the specimen. The change in weight can be determined and then the erosion rate according to the equation (3.3) is obtained as follows.

$$\text{Change in weight}(\Delta w) = \text{original weight}(w_o) - \text{weight after a fixed time}\left(w_{1,2,\ldots.}\right)$$

$$\textbf{Erosion rate } (\textbf{gm/hr}) = \frac{\Delta \mathbf{w}}{\textbf{time of exposure}} \ldots\ldots\ldots\ldots\ldots (\mathbf{3.6})$$

Figure (3.14): erosion-Corrosion Apparatus Depend on (G73) ASTM.

3.9.X-Ray Diffraction (XRD)

For X-Ray diffraction study, specimens with a diameter of (20mm) and a thickness of (5mm) were prepared. (Lab. Razi Metallurgy Research Center/Iran) checked the study. The measurement conditions are (target: Cu, wave length 1.54060, voltage and current 30 KV and 15 mA respectively, scanning velocity 2 deg/min, scanning range 2 degrees = 0 to 100 degrees). In order to determine the phases produced after heat treatment, the X-Ray Diffraction was used and then compared with the standard charts. Figure (3.15) illustrates the XRD unit.

Figure(3.15) : The XRD Device.

3.10 Scanning Electron Microscopy

A scanning electron microscope SEM has been used to obtain a surface composition and its topography, it is considered one of the most widely used surface analysis techniques in that a large amount of levels and component is noted, where the specimen is imaged through a high pack of electrons. In (Lab. Razi Metallurgical Research Center/Iran), this testing was done using the SEM model (TESCAN S8000, USA) as shown in Figure (3.16).

Figure (3.16): Scanning Electron Microscopy Device (SEM).

3.11 Atomic Absorption Spectroscopy (AAS) Test

In the simple immersion test, Figure (3.10) and after the samples have been removed, washed and cleaned from the corrosive solution (salt solution), the solution in which the samples are submerged is tested to detect the concentration (Zn++) and (Ni) in the test solution .

This testing was carried with instrument type AA (Atomic Absorption Spectrophotometers), model AA7000-Serious, Rom version 1.01, lamb mode BGC-D2, SHIMADZU, as shown in Figure (3.17).

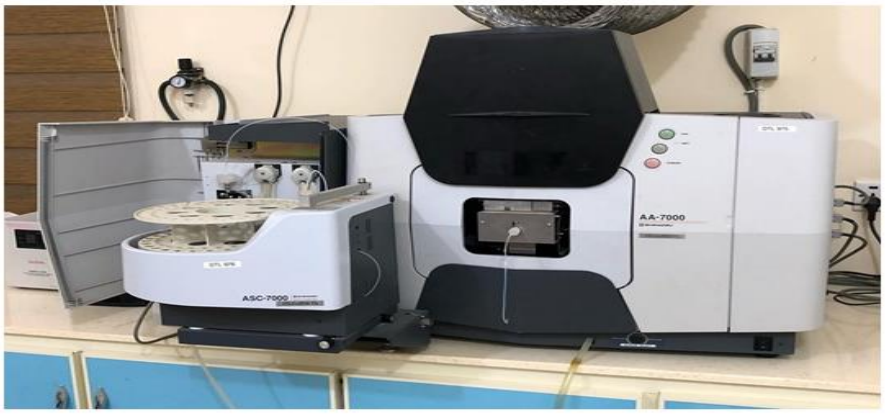

Figure (3.17): Atomic Absorption Spectroscopy Device (AAS).

Chapter Four

Results & Discussion

4.1 Introduction

This chapter deals with the section of experimental results that have been already obtained during practical work and discusses these results in several respects, these research results evaluated corrosion behavior using simple immersion test, erosion-corrosion, polarization curves, open circuit potential and calculated the corrosion rate at room temperature, microstructure examination, mechanical properties tests involving(hardness and wet sliding wear tests). Imaging topography of the specimens surface after corrosion by using scanning electron microscopy (SEM), XRD, and EDS.

4.2 Chemical Composition

Table (4.1) shows chemical composition of alloys used in this study. This inspection has been completed in (Razi Metallurgical Research Center/Iran).

Table (4.1) shows chemical composition of alloys used in this study.

Alloy Samples	Cu%	Zn%	Ni%	Al%	Sn%	Ge%	Y%	Fe%
A1	Bal.	-	9.72	-	-	-	-	-
A2	Bal.	27.4	-	3.05	-	-	-	-
A3	Bal.	27.92	-	3.10	2.67	-	-	-
A4	Bal.	29.21	-	3.6	-	0.3	-	-
A5	Bal.	28.7	-	3.5	-	-	0.23	-
A6	Bal.	-	8.21	10.66	-	-	-	-
A7	Bal.	-	8.34	10.58	-	-	-	2.36
A8	Bal.	9.55	8.53	-	-	-	-	-
A9	Bal.	10.12	8.28	-	-	-	-	2.52

4.3 X-Ray Diffraction Analysis

By the XRD pattern of alloy A1:(Cu-10%Ni) shown in Figure (4.1), it is found that the phases existing were α-Cu, Ni, Cu3.8Ni. Figures (4.2, 4.3, 4.4, and 4.5) show the results of XRD analysis for all free nickel specimens, where the results of XRD analysis for all samples , specimen reveal to exist peaks represent phases (α, Cu_3Zn) , (CuZn), (Cu5Zn8) and aluminum copper, intermetallic (Al_2Cu) phase (tetragonal crystal system) was showed also as Figure (4.2).

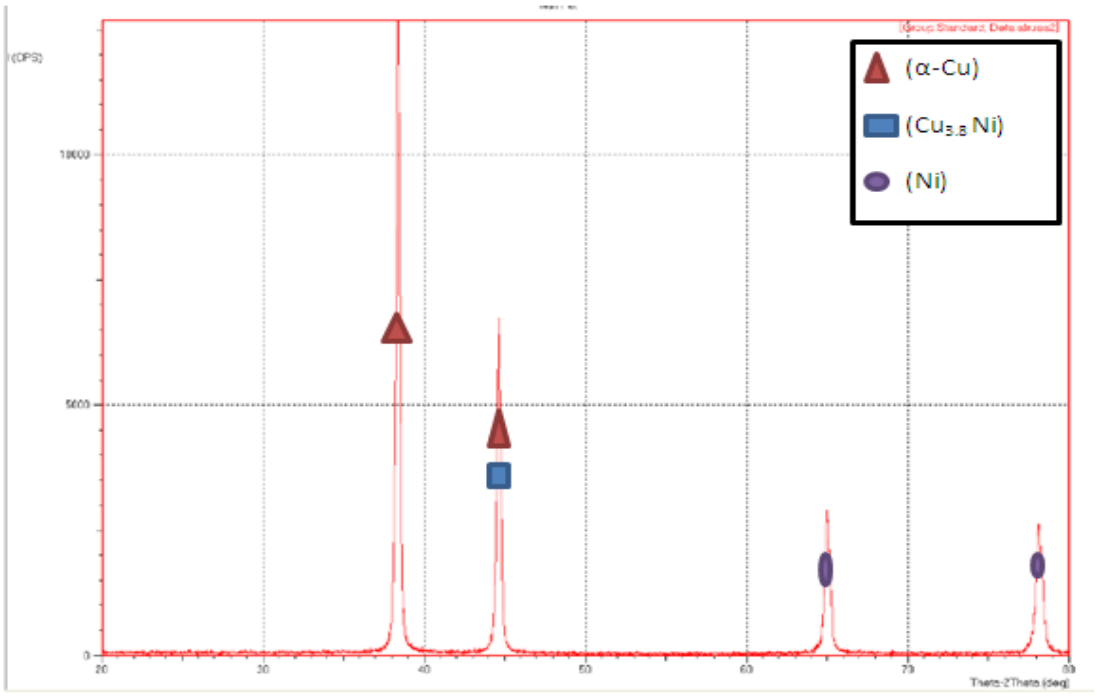

Figure (4.1): X-Ray diffraction analysis for A1, base alloy.

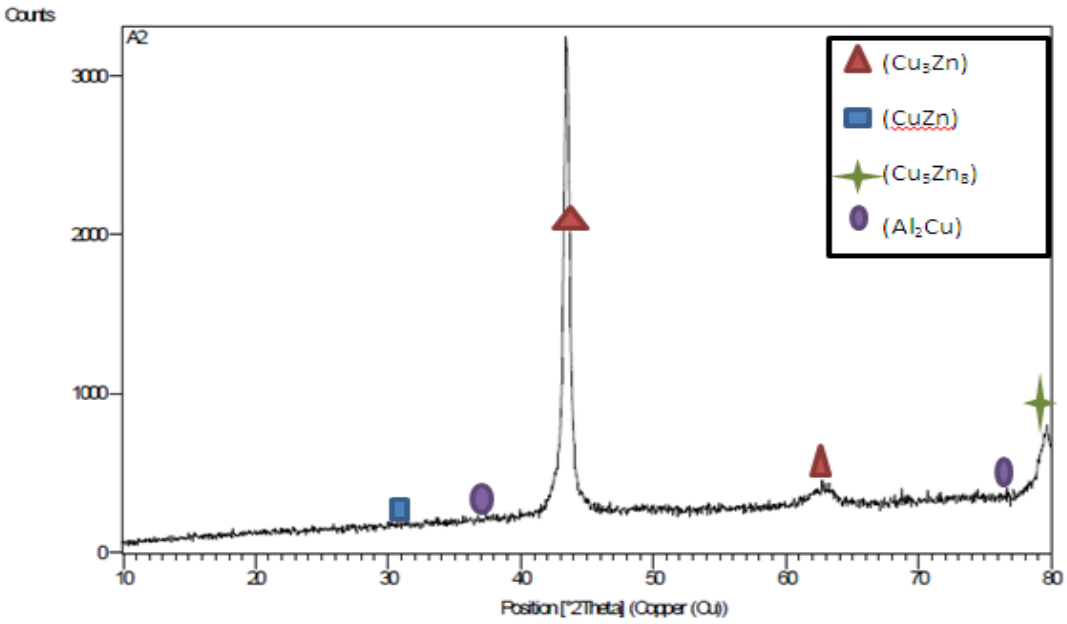

Figure (4.2): X-Ray diffraction analysis for A2

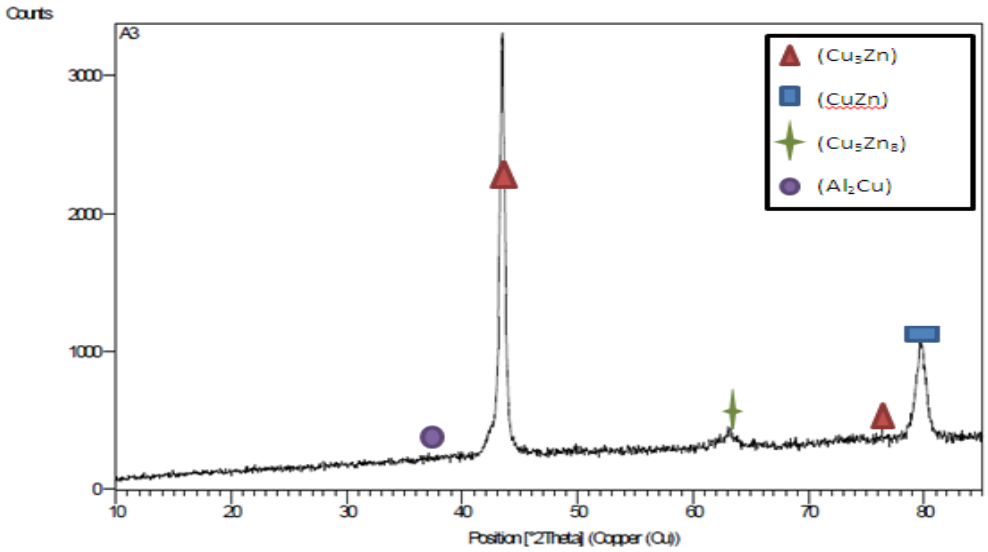

Figure (4.3): X-Ray diffraction analysis for A3

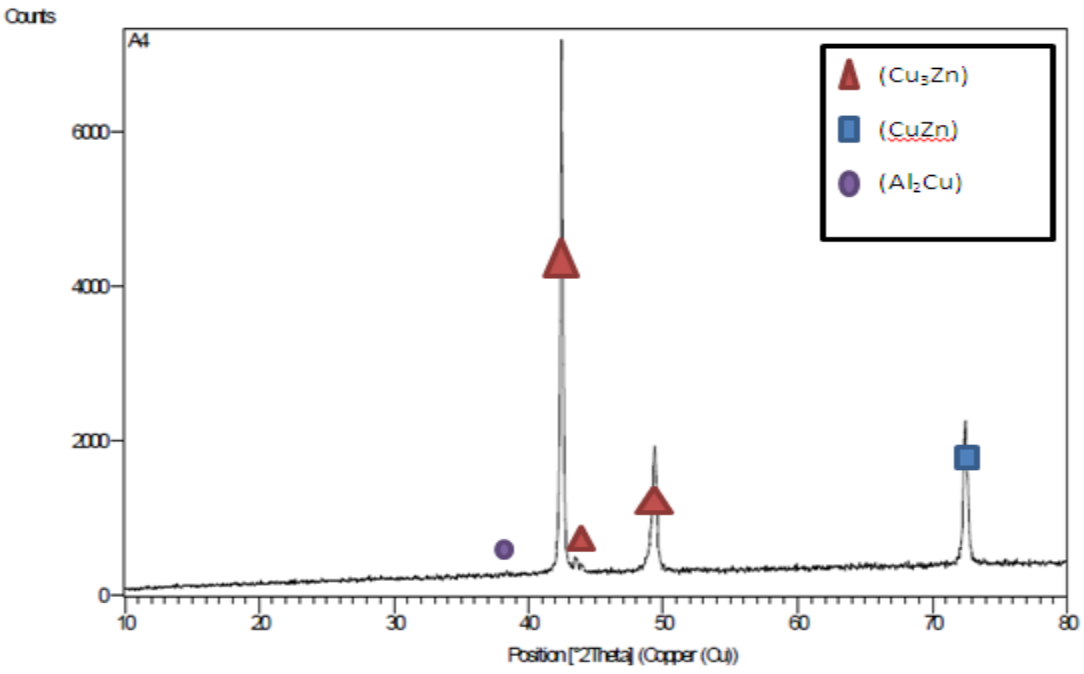

Figure (4.4): X-Ray diffraction analysis for A4.

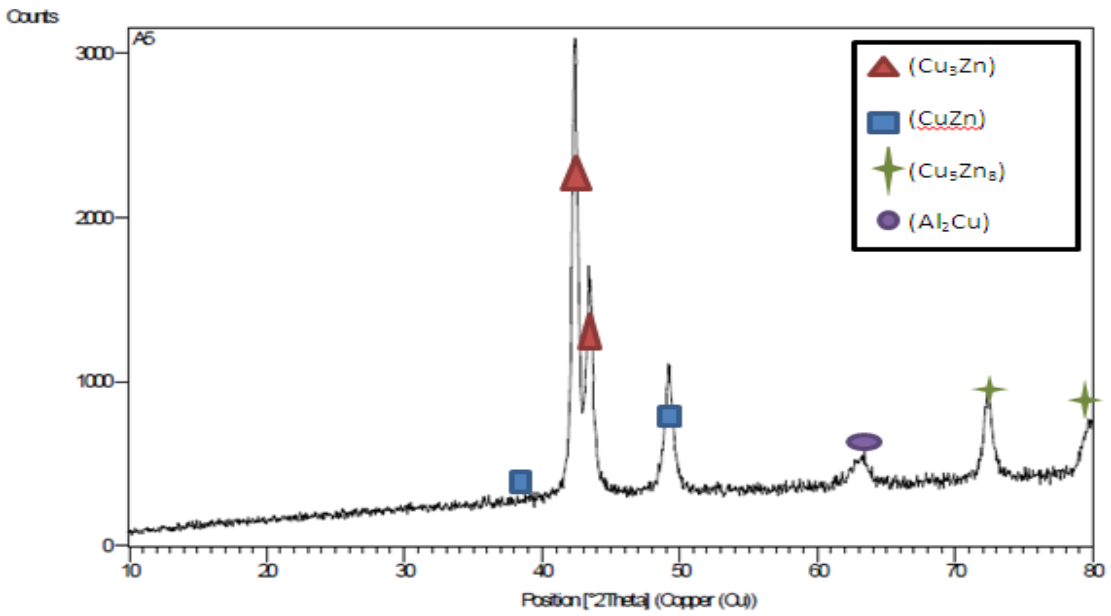

Figure (4.5): X-Ray diffraction analysis for A5.

In samples A6 and A7, it is found that the hominization heat treatment leads to precipitation in the intermetallic compound Al,γ2 AlCu3 and α phase. As for the other phases that can be formed between copper, aluminum, nickel, iron, which certainly have a great influence on the alloy's properties which did not appear in the x-ray diffraction pattern may be in proportions outside the limits of the XRD detection.

But the results of XRD analysis for A8 and A9 specimens reveal to exist peaks represent phases are (α-Cu) and (NiZn) Figures (4.8) and (4.9) .

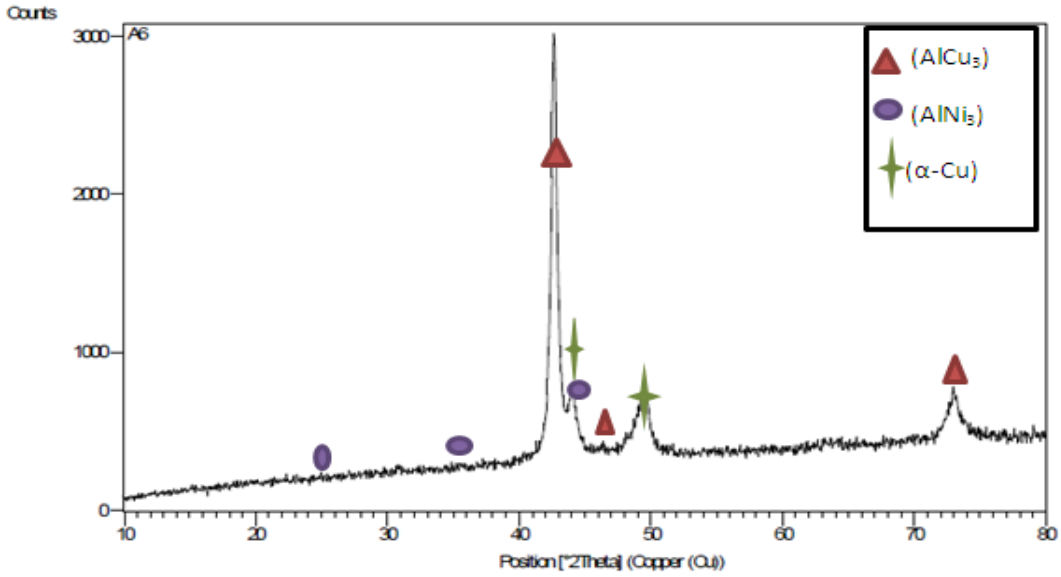

Figure (4.6): X-Ray diffraction analysis for A6.

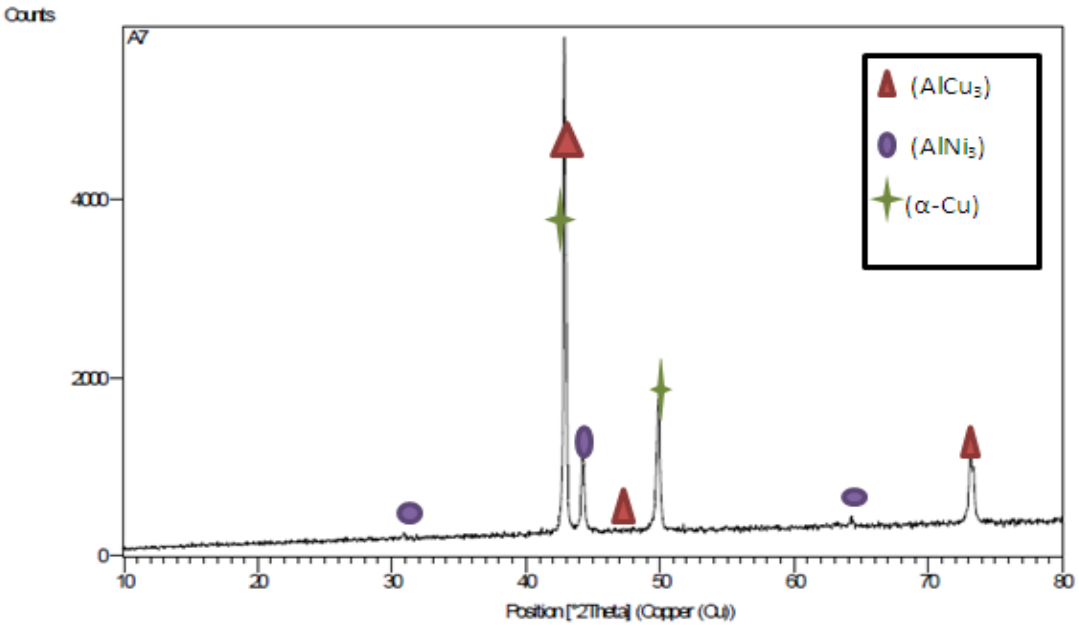

Figure (4.7): X-Ray diffraction analysis for A7.

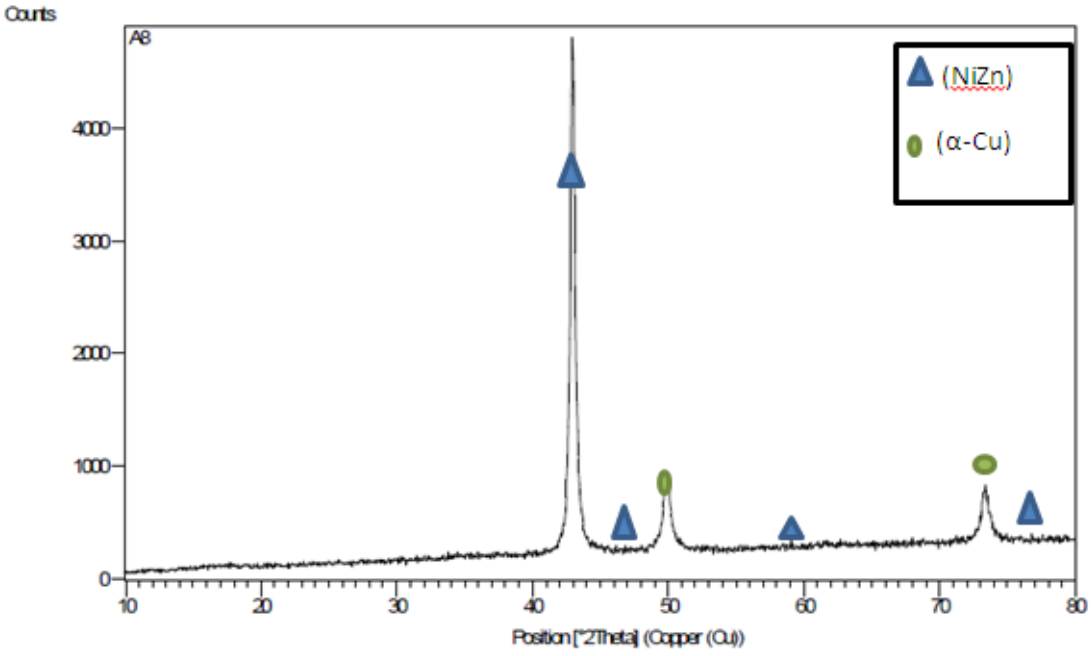

Figure (4.8): X-Ray diffraction analysis for A8.

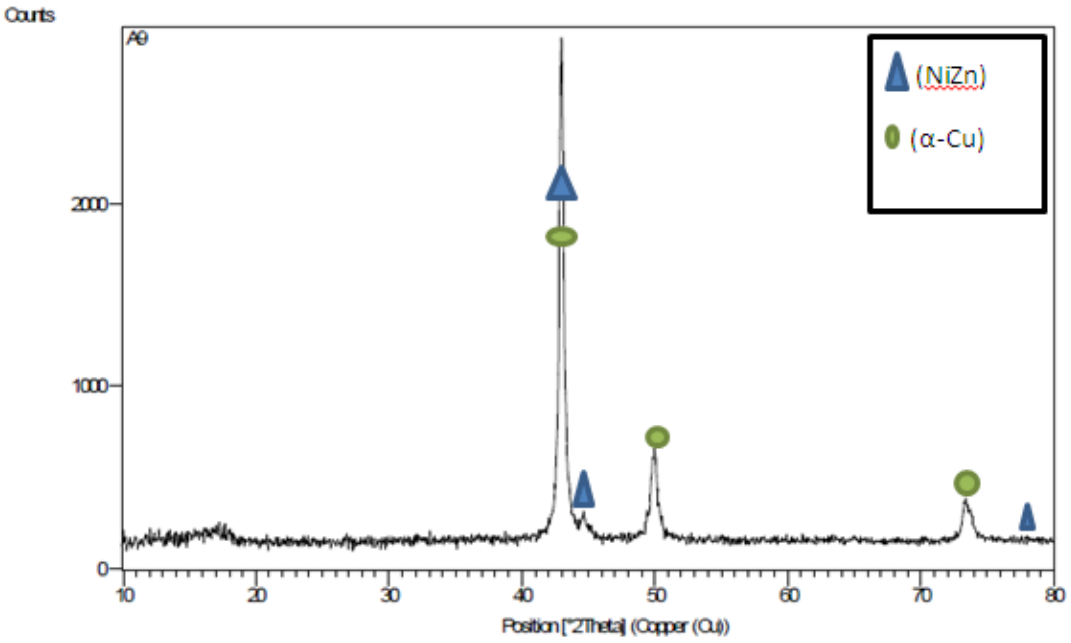

Figure (4.9): X-Ray diffraction analysis for A9.

4.4 Vickers Hardness

The hardness was calculated in the current study by Vickers micro-hardness method . The hardness of base alloy(cu-Ni) A1 is (105.324 Hv). Sample A1 has the lowest hardness value compared other samples, and this is expected because the relationship between copper and nickel is complete solubility and at any percentage of them are completely dissolving each other

Table (4-2) shows the hardness values for nickel-free alloys have increased. The hardness of the sample (A2) has been improved by (55.4%) and the hardness of the sample (A3) increased by (88.45%) relative to base alloy(A1). (A4) and (A5) hardness have improved by (89.27%) and (61.6%), respectively. The addition of Ge and Y has the same effect as the previous results as it is well known that the addition of germanium will be deposited freely, thereby, helping to refine the grains and thus, increasing hardness compared to alloys A1 this is in agreement with[118].

Table (4.2): Shown the Hardness of all Examined Specimens.

Alloy Specimens	Vickers hardness (HV) g/mm$_2$	Improving (%)
A1	**105.324**	**-**
A2	**163.74**	**55.4**
A3	**198.585**	**88.45**
A4	**199.35**	**89.27**
A5	**170.23**	**61.6**
A6	**208.525**	**97.98**
A7	**229.445**	**117.84**
A8	**110.245**	**4.677**
A9	**124.515**	**18.22**

According to Table (4.2), it was given the hardness values of each individual samples with Nickel, and we note that alloys A6, A7 have the highest hardness values compared to the other alloys. The solid solubility of aluminum in Cu-Ni alloy is lower, and nickel–aluminum intermetallic compounds compound (Ni3Al, NiAl or NiAl3) are produced in Cu-Ni-A1 alloy , which has obvious precipitation hardening effect. From this, it is speculated that, in this study, solid solution hardening and precipitation hardening of aluminum are the reasons for enhancing the hardness.

A8 and A9 hardness have improved by (4. 7%) and (18.22%), respectively. Add zinc alloys make more ductility this is in agreement with[119].

4.5Dry Sliding Wear Test

This test method describes a laboratory procedure for determining the wear of materials during sliding using a pin-on-disk apparatus. Wear results are usually obtained by conducting a test for a selected sliding distance and for selected values of load and speed.

The plots of cumulative wear rate (cm^3/cm) versus sliding time (min.) for A1, base alloys (*Cu-Ni*) and the other alloys free nickel (A2, A3, A4, and A5) under loads (20N) with different times (10, 15, 20, 25, and 30 minutes). Volume loss versus time at different normal forces have been calculated as in equation (6) according to ASTM G9.

Figure (4.10) shows the relationship between wear rate and time for free-nickel alloys. It is very clear that the wear rate of these alloys are lower than that of the base alloy. There are two important points can be gotten:

Firstly, Figure (4.20) and Table (4.3), show a great enhancing in wear rate behavior, for specimens A2, A3, A4, and A5 improving in wear rate was

equal to (57.2, 58.67, 23.98, 59.90)% respectively, with respect to reference sample.

Secondly, sample A5 shows higher improving in wear rate comparing with A2, A3, and A4, this is attributed to finger microstructure, so has higher hardness this is in agreement with[120].

Table (4.3): Shows Improving in Wear Rate at (Load 20N & Speed 250rpm) for free nickel alloys.

Sample	**Wear rate(cm^3/cm)$\times 10^{-4}$ at steady state**	**Improving (%)**
A1(Cu-Ni)	8.88	-
A2(Cu-Zn-Al)	3.8	57.2
A3(Cu-Zn-Al-Sn)	3.67	58.67
A4(Cu-Zn-Al-Ge)	6.75	23.98
A5(Cu-Zn-Al-Y)	3.56	59.90

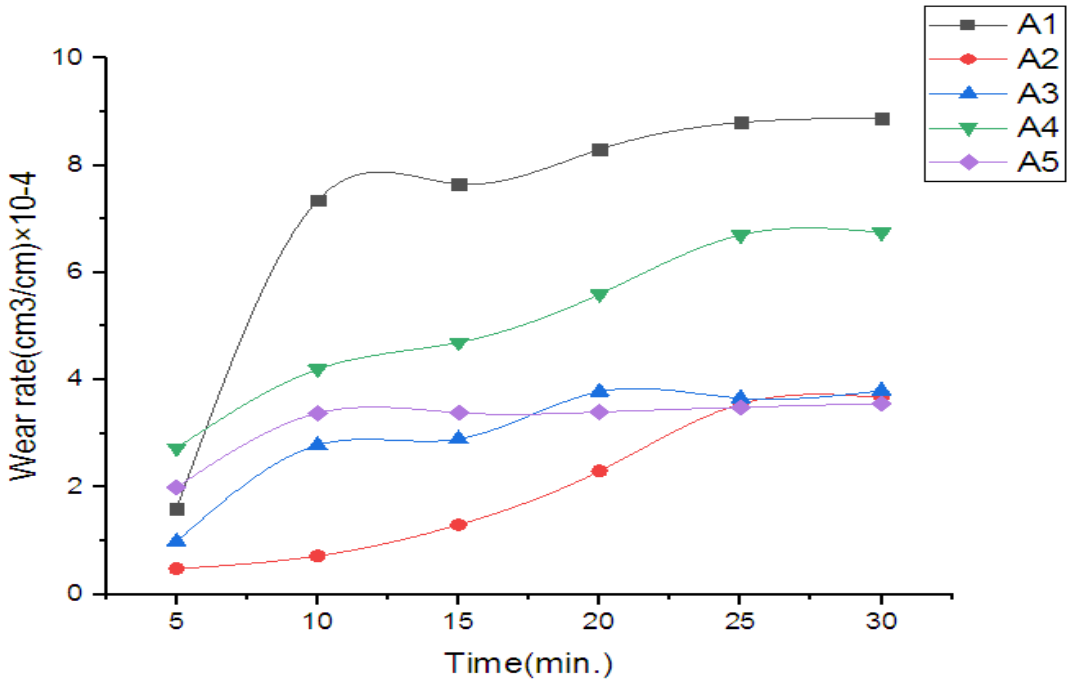

Figure (4.10): Wear behavior of free nickel Specimens at vertical load was (20N) and speed (250 rpm).

Figure (4.11) shows the relationship between the wear rate and time of nickel-containing alloys. It is very clear that the wear rate of these alloys are lower than that of the reference alloy.There are two significant points that can be obtained:

To begin, Figure (4.11) and Table 4.3 show a significant improvement in wear rate behavior, with specimens A6, A7, A8, and A9 improving by 57.2, 58.67, 23.98, and 59.90 percent, respectively, when compared to the reference sample.Second, as compared to samples A8 and A9, sample A6 shows a higher improvement in wear rate, which can be attributed to the finger microstructure, which has a higher hardness this is in agreement with[121] .

Table (4.4): Shows Improving in Wear Rate at (Load 20N & Speed 250rpm) for with nickel alloys.

Sample	Wear rate(cm^3/cm)×10^{-4} at steady state	Improving (%)
A1(Cu-Ni)	8.88	-
A6(Cu-Ni-Al)	3.25	63.4
A7(Cu-Ni-Al-Fe)	2.65	70.15
A8(Cu-Ni-Zn)	4.9	44.8
A9(Cu-Ni-Zn-Fe)	3.8	57.2

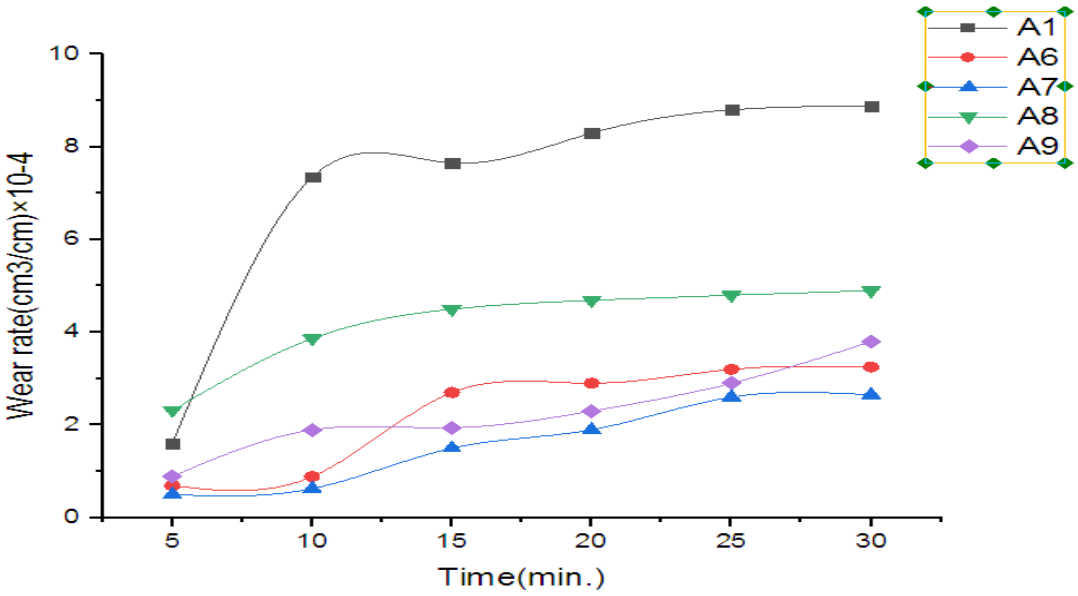

Figure (4.11): Wear behavior of specimens containing nickel at vertical load was (20N) and Speed (250 rpm).

Whereas Figures (4.12, 4.13, 4.14) which depicts topographic broken surfaces after sliding wear, it is clear that sliding wear area, and grooves,

can be clearly seen on the wear tracks in base alloy, while decrease in other specimens, which results from the penetration of the strong abrasive ball on the surface alloys.

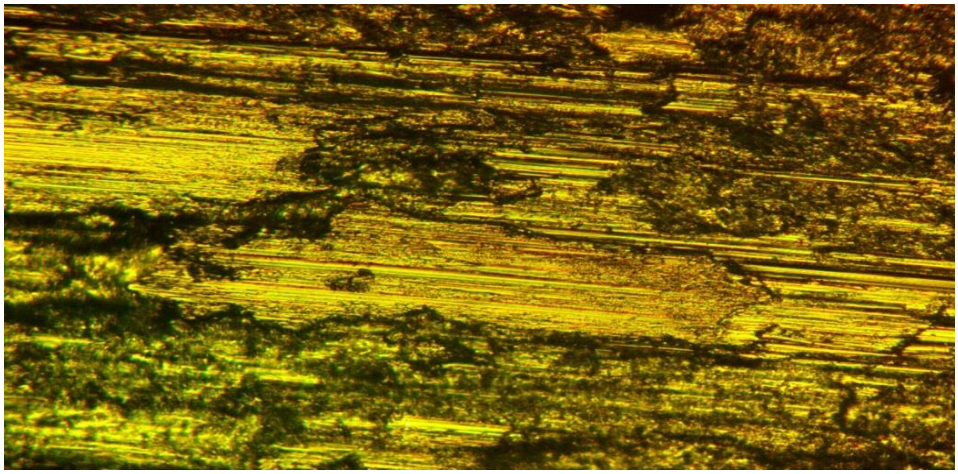

Figure (4.12): Topographic of worn surfaces for A1(Cu-Ni) alloy.

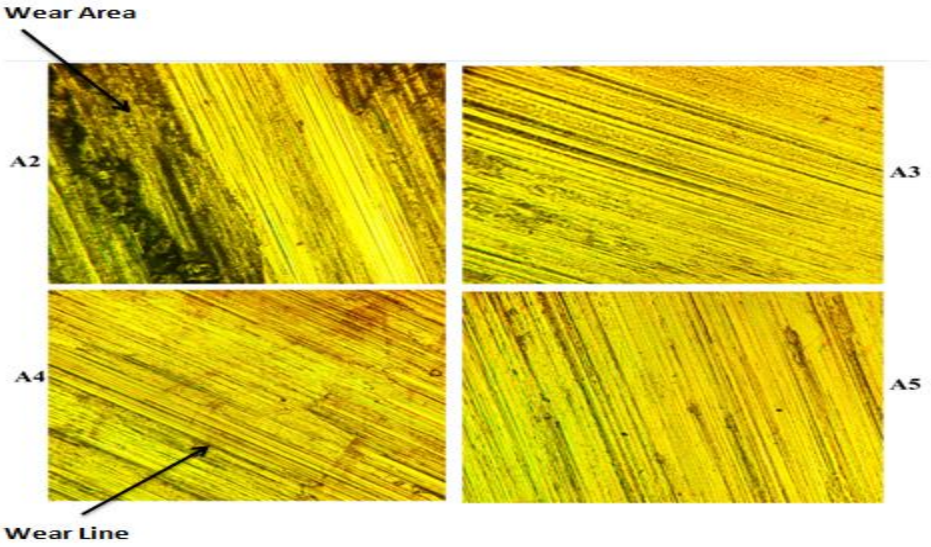

Figure (4.13): Topographic of worn surfaces aor all free nickel alloys.

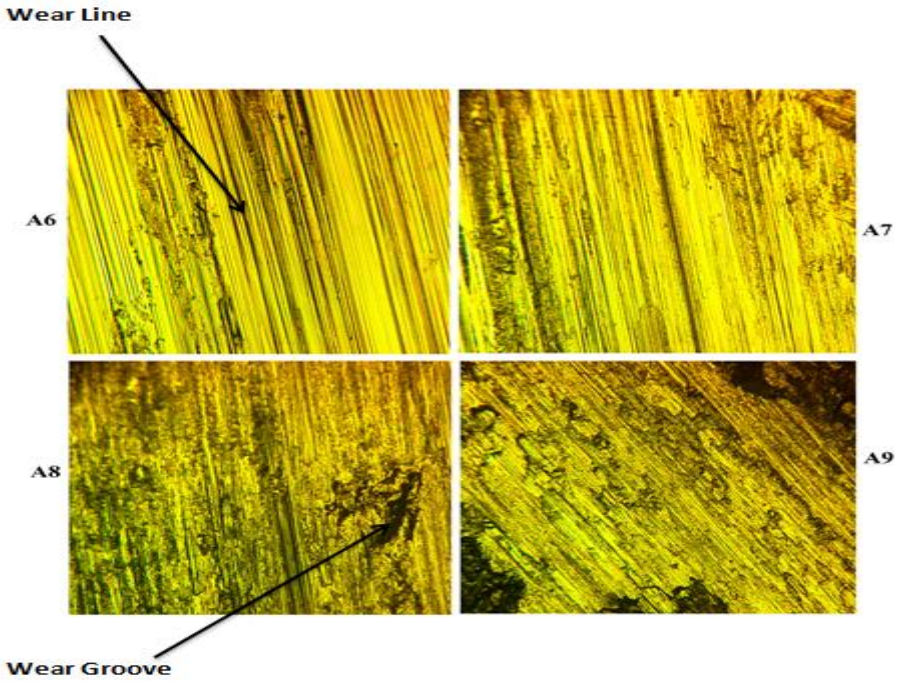

Figure (4.14): Topographic of worn surfaces for all alloys containing nickel.

4.6 Corrosion Tests

4.6.1Simple Immersion Test

To investigate the corrosion rate of specimens based on astm G3. After 3 days of immersion at room temperature, the specimens were fully immersed in salt solution (3.5 percent NaCl) and taken out to examine the loss in mass.

In case of dezincification of brass, zinc preferentially leached out of the copper-zinc alloy, leaving behind a copper-rich surface layer that is porous and brittle, due to different metals and alloys have electrochemical potential or (corrosion potential) in the same electrolyte.

Corrosion rate can be calculated according the following relationship:

$$\textbf{\textit{Corrosion Rate}}\ (\frac{mg}{cm^2.day}) = \frac{\textbf{\textit{Change in weight}}\ (\Delta w)}{\textbf{\textit{surface area}}\ (A) \times \textbf{\textit{immersion time}}\ (t)} \quad \ldots\ldots(4.1)$$

According to Figure (4.15), which represents the corrosion rate of free nickel Specimens, sample A4 shows lower corrosion rate after more than 90 days, then sample A2,A3,and A5, this is due to ability of these alloys to build a protective layers such as (Al_2O_3, ZnO, Ge_2O, & Y_2O_3) which improving the corrosion rate for specimens A2, A3,A4 & A5 where (46.8, 46, & 31.2) respectively, with respect to reference sample A1this agree with [122].

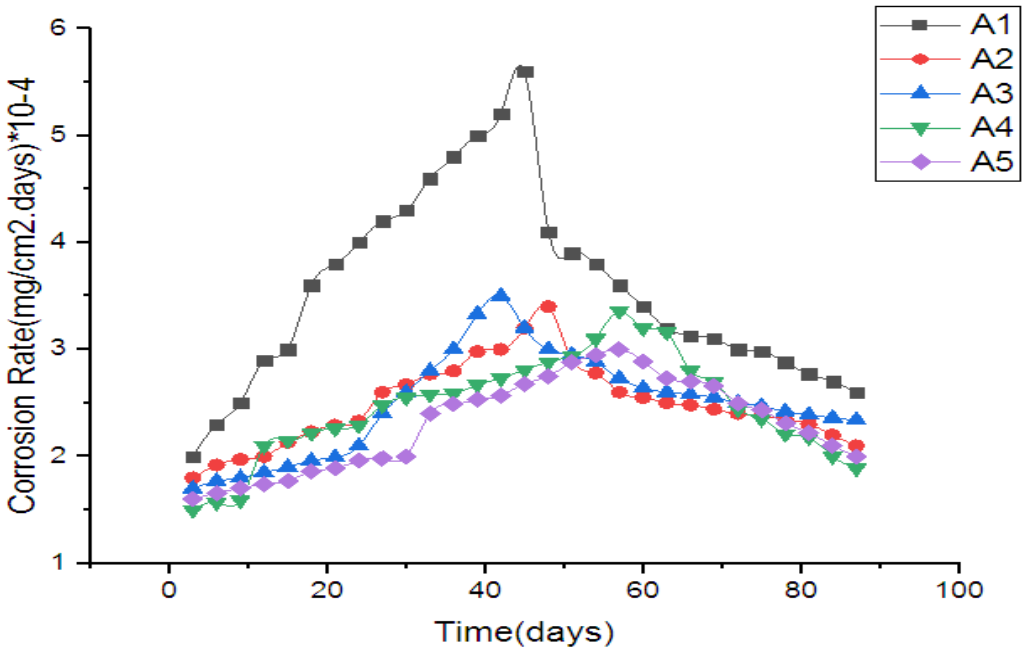

Figure (4.15): Curves of simple immersion test for free nickel specimens in salt solution for immersion period (90 days).

While the Figure (4.16) which represents the corrosion rate of free nickel Specimens, sample A7 shows lower corrosion rate after more than 90 days, then sample A6,A8,and A9, this is due to ability of these alloys to build a protective layers such as (NiO3, AL_2O3, & ZnO) which improving the corrosion rate for specimens A6, A7,A8 & A9 where (46.8, 46, & 31.2) respectively, with respect to reference sample A1 this agree with [123].

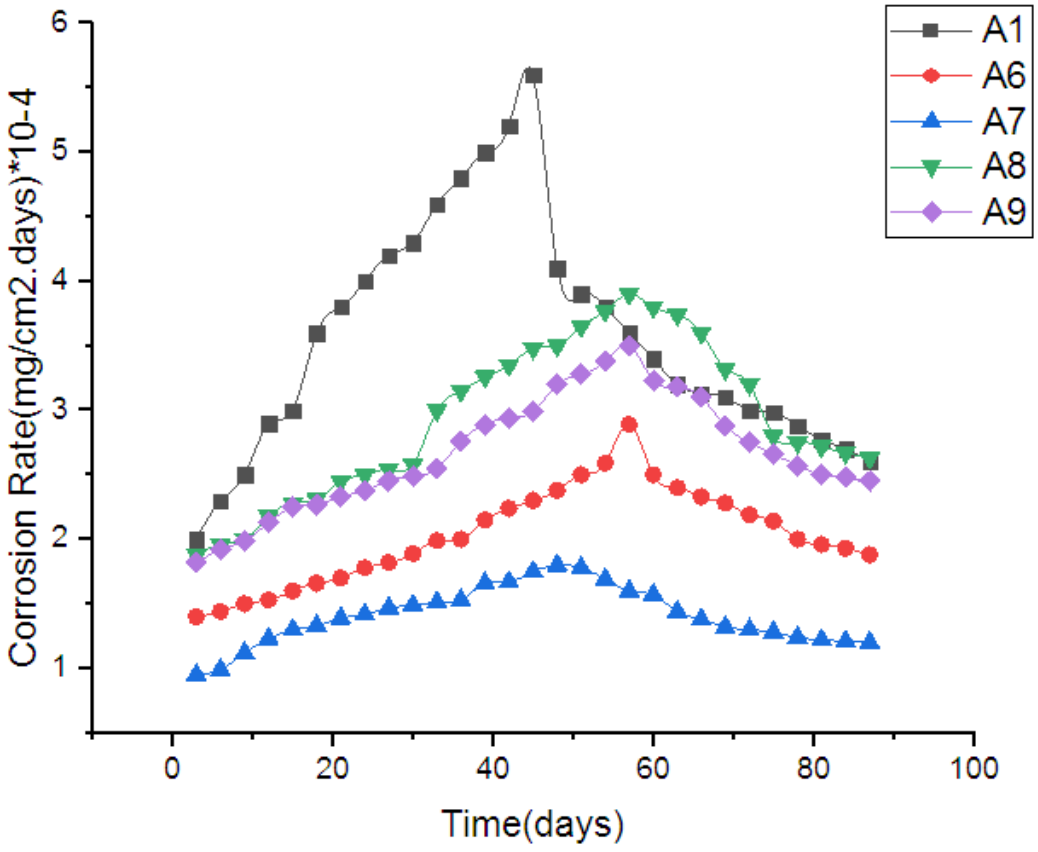

Figure (4.16): Curves of simple immersion test for specimens containing nickel in salt solution for immersion period (90 days).

4.6.2 Atomic Absorption Spectrophotometer Test:

This test has been conducted to detect the concentration of Zn^{++} and Ni^{++} in the (immersion solution test), to determine the solubility of Zn^{++} and Ni^{++} in test solution. Table (4.5) shows the release of zinc in brine for nickel-free alloys, while table (4.6) shows the release of nickel for nickel-free alloys.

Table (4.5): Shows concentration of Zinc Ion (Zn^{++}) in Salt Solutions (3.5% NaCl) for all free nickel Alloys

Immersion Solution	Zn: Flame Cont Actual Conc.
Test Sample	**Concentration of Zn ions/ppm**
A2	5.377
A3	4.979
A4	2.994
A5	3.574

Table (4.6): Shows concentration of Zinc Ion (Zn^{++}) in Salt Solutions (3.5% NaCl) for all containing nickel Alloys.

Immersion Solution	Ni: Flame Cont Actual Conc.
Test Sample	**Concentration of Ni ions/ppm**
A1	3.029
A6	.9331
A7	0.4383
A8	1.354
A9	1.349

4.6.3 Erosion /Corrosion Test

This test is a good measure of a metal's or alloy's resistance to erosion rate in a given setting. It's also a good indication of the adhesion of the oxides growing on the alloy's surface and their ability to repair itself. It's also a measure of the protective layer's ability to remain effective, coherent, and adhered to the alloy surface amid the movement of the liquid jetting and the possibility of the layer drifting.

It is clear that the curves representing the action of alloys exposed to salt solution jetting have fluctuated; the explanation for this fluctuation is repeated building and fracturing of the protective surface layer. As this coating forms on the surface of the alloy, the erosion rate decreases, while when it is broken down, the erosion rate increases. The impact force and the value of adhesion it has on the surface of alloys determine how quickly the protective surface layer breaks down.

A dark gray film of CuO was applied to brass in sodium chloride solution. Brass had more resistance due to the dark gray film's greater stability or protectiveness.

Just one face of the specimen will be impinged during the examination, leaving all other surfaces of the specimen unaffected by the environment.

According to Figure (4.17) which represent the erosion rate (mg/hr) and verses time (hrs.) for free nickel alloys(A2, A3, A4, & A5) compare to base alloy(A1) , there is a significant improvement in erosion-corrosion behavior, with weight loss per unit hour improving reach to (10.7, 57.14, 89.28 and 67.85) for A2, A3,A4 and A5 specimens, respectively this agree with [118].

While Figure (4.18) represent erosion rate of the specimens with nickel, there are a great improving in erosion- corrosion behavior, there are an enhancement in weight lose per unit hour improving reach to (82.14, 92.85, 21.42 & 50) for B1, B2, & B3 specimens respectively, with respect to base alloy Tables (4.8- 4.9) & Figures (4.19-4.20), this is due to two factors: first, high hardness; second, protective oxide layers formed on the surface; XRD and EDS show the presence of oxides with high properties capable of protecting the surface from corrosion and oxidation this agree with [124].

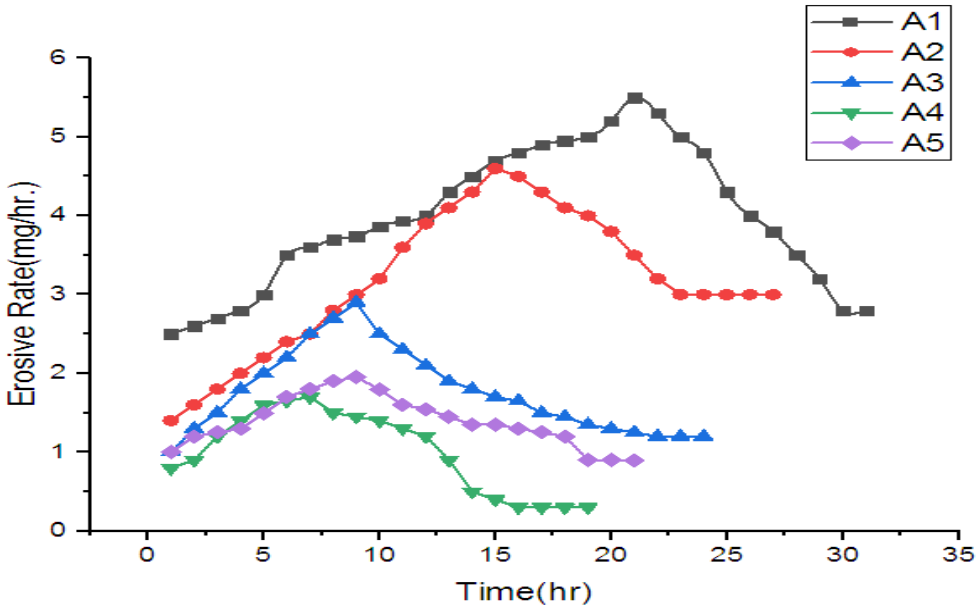

Figure (4.17): Erosion rate versus time for free nickel alloys.

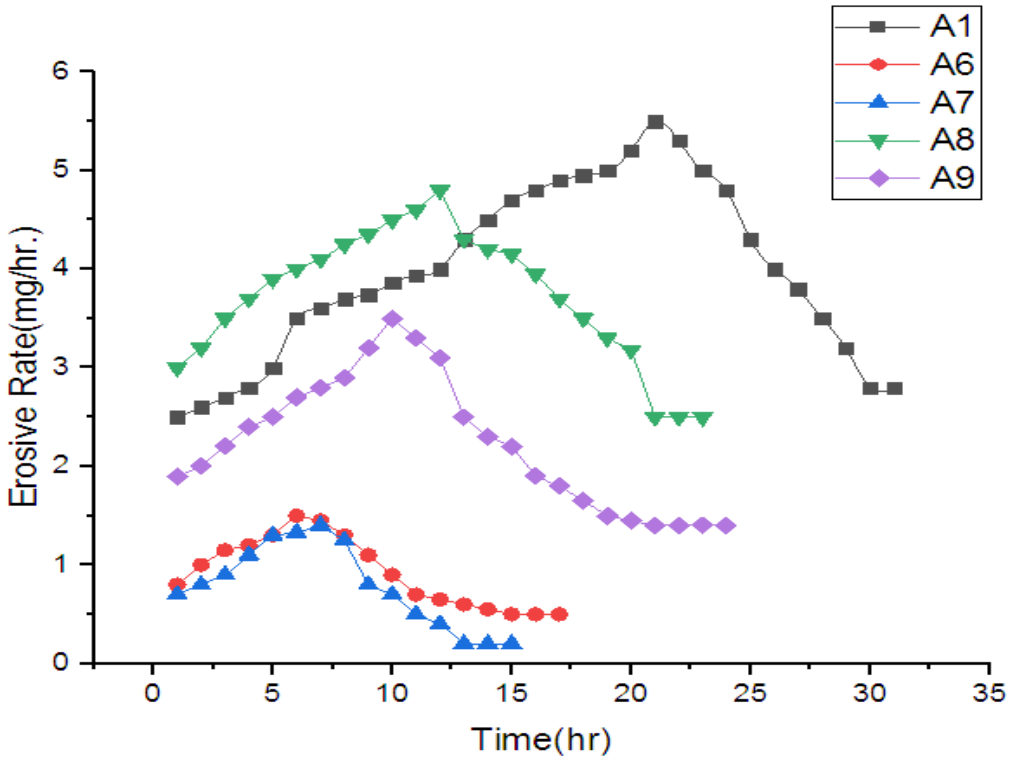

Figure (4.18): Erosion rate versus time for alloys containing nickel.

Table (4.7): Shows improving in erosive rate at steady state for free nickel alloys.

Sample	Erosive Rate(mg/hr.) at steady state	Improving (%)
A1(Cu-Ni)	2.8	-
A2(Cu-Zn-Al)	2.5	10.7
A3(Cu-Zn-Al-Sn)	1.2	57.14
A4(Cu-Zn-Al-Ge)	0.3	89.28
A5(Cu-Zn-Al-Y)	0.9	67.85

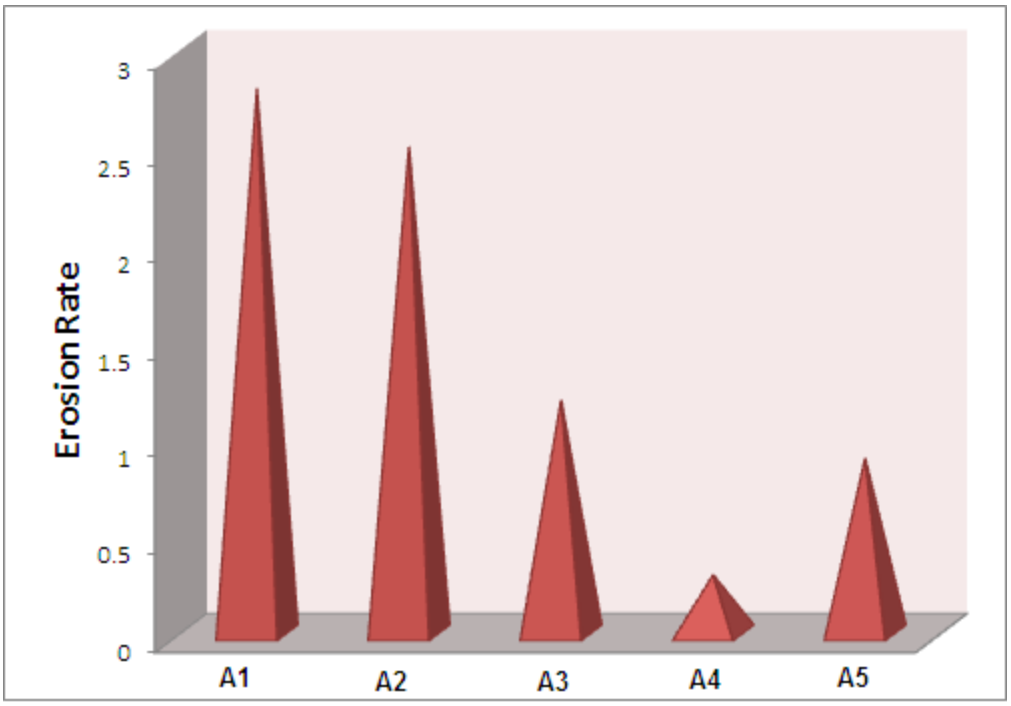

Figure (4.19): Comparative in corrosion rate for free nickel alloys with respect to base alloy.

Table (4.8): Shows improving in erosive rate at steady state for containing nickel alloys.

Sample	Erosive Rate(mg/hr.) at steady state	Improving (%)
A1(Cu-Ni)	2.8	-
A6(Cu-Ni-Al)	0.5	82.14
A7(Cu-Ni-Al-Fe)	0.2	92.85
A8(Cu-Ni-Zn	2.2	21.42
A9(Cu-Ni-Zn-Fe)	1.4	50

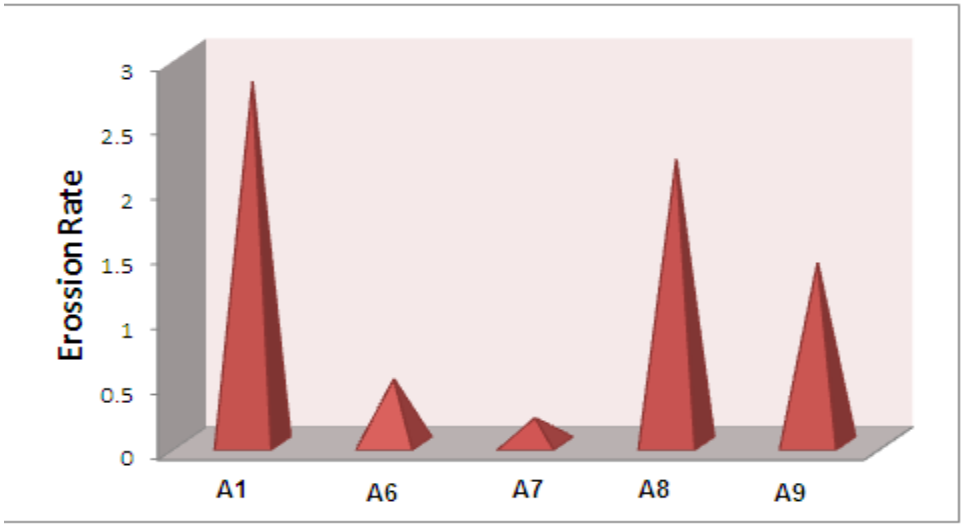

Figure (4.20): Comparative in corrosion rate for alloys containing nickel with respect to base alloy.

4.6.3.1 X-Ray Diffraction Analysis Sample A1 After Erosion-Corrosion Test.

The results of XRD analysis for A1, (base alloy with Cu- Ni) specimen reveal to exist peaks represent the main peaks NiO, Cu_2O and α-Cu, this alloy had appeared the highest loss weight rate during is exposing to impingement of water jetting (salt solution) comparing with other alloys, this has been due to the protective layer formed on the surface of the sample is weak, non-adherent and are subject to flake, Figure (4.21).

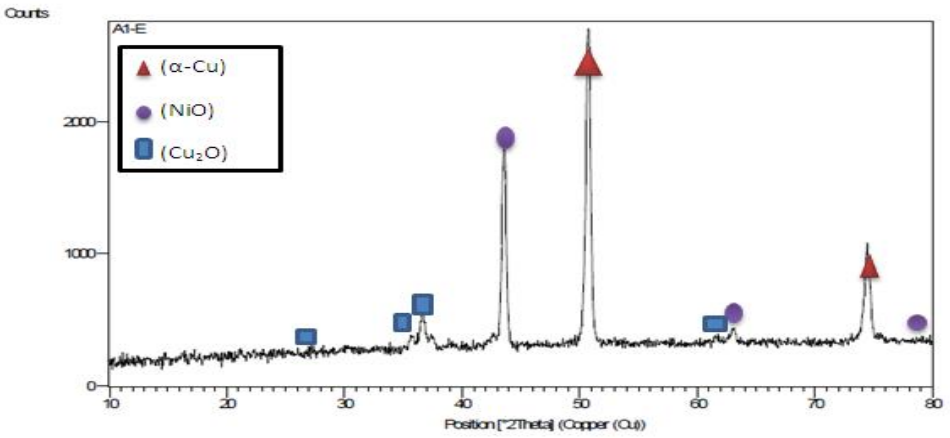

Figure (4.21): X-Ray diffraction analysis for sample A1.

4.6.3.2 X-Ray Diffraction Analysis for free Nickel Samples (After Erosion-Corrosion Test.

This test was conducted in the corrosive environment (laboratory-prepared seawater) specification. For samples A2,A3, A4, A5 we note that the weight loss of sample A2 is the biggest compared with A3,A4 and A5 in the steady state. This is expected because the aluminum oxide layer is weak in the sample (A2). The addition of elements such as tin, germanium and yttrium makes the aluminum oxide layer stronger and more adhesion, so the corrosion rate in these samples (A3,A4, and A5) is less than the samples (A2) , this has been attributed to exist protective layer of aluminum oxide on the surface of alloy and this oxide reduces selective leaching, beside the existence of Tin oxide, germanium oxide and yttrium oxide which improves the oxide plasticity and adhesion was noticed, Figures (4.22, 4.23,4.24, and 4.25).

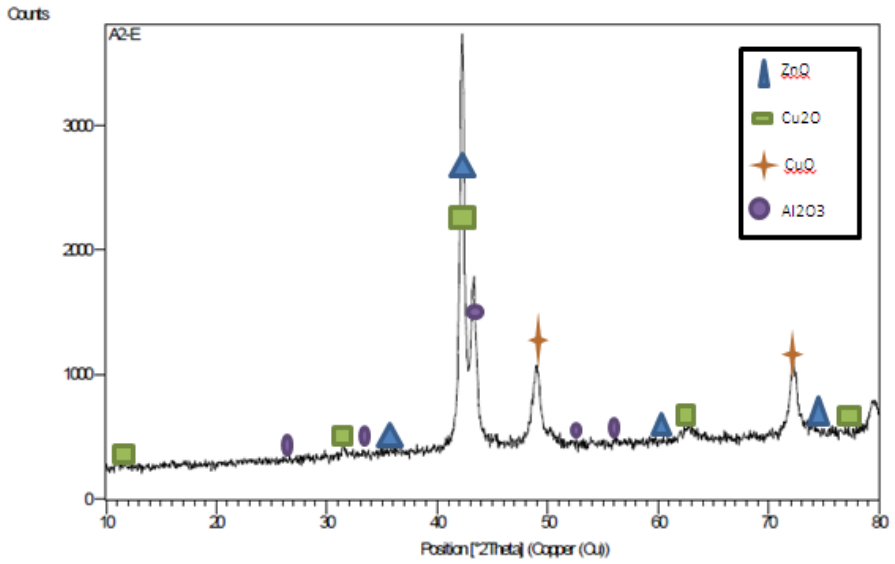

Figure (4.22): X-Ray diffraction analysis for sample A2.

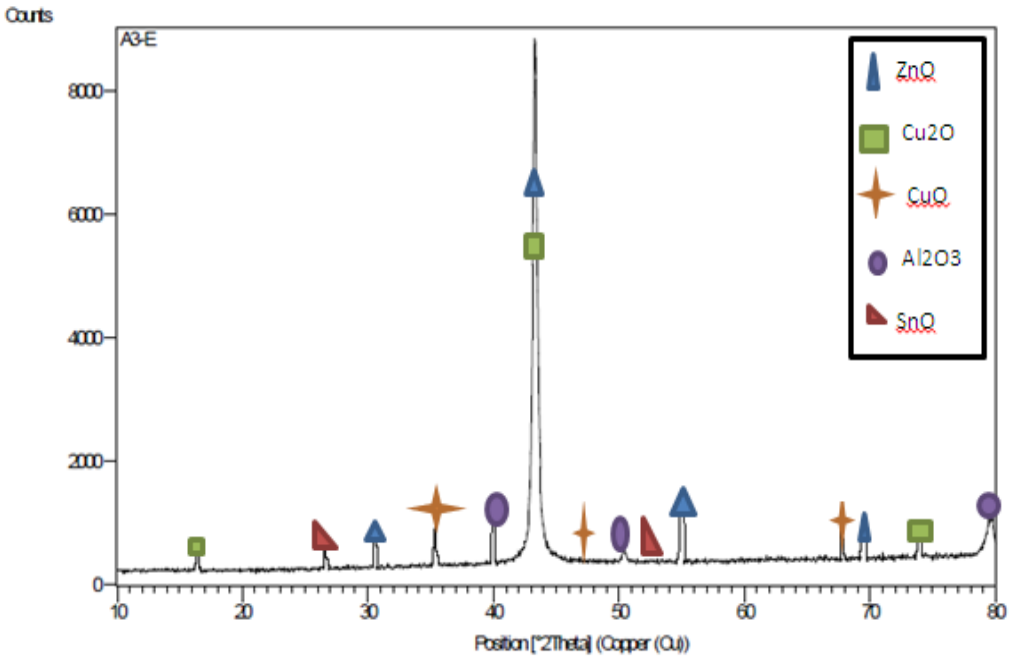

Figure (4.23): X-Ray diffraction analysis for sample A3.

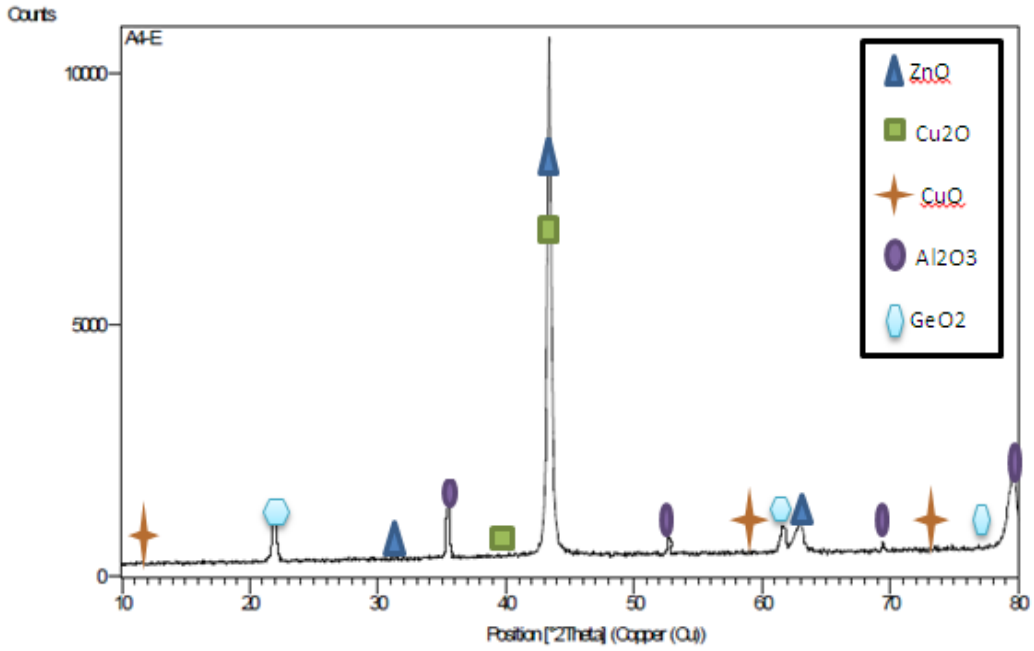

Figure (4.24): X-Ray diffraction analysis for sample A4.

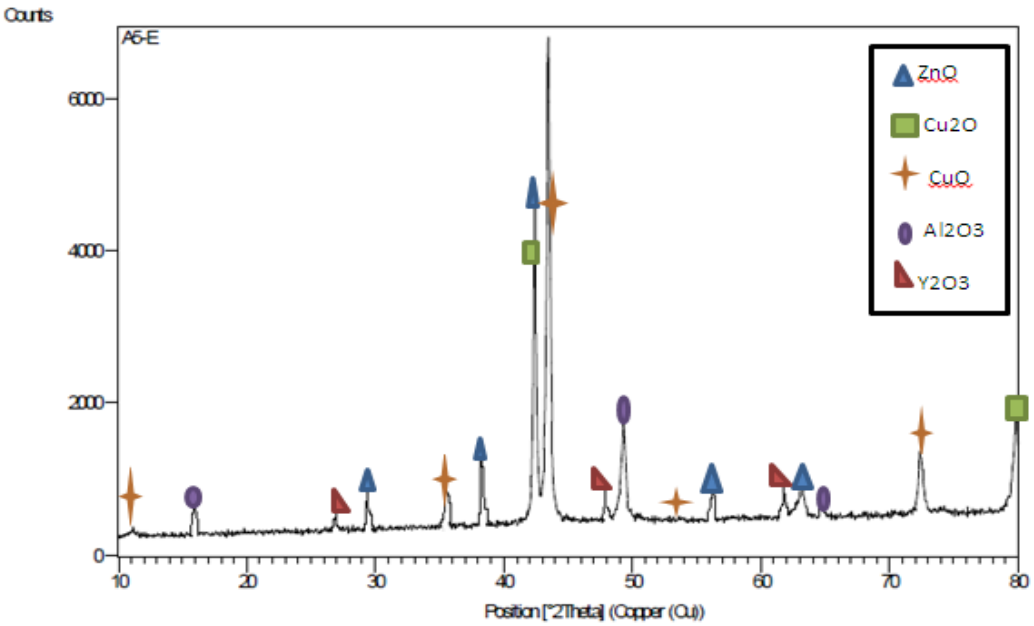

Figure (4.25): X-Ray diffraction analysis for sample A5.

4.6.3.3 X-Ray Diffraction Analysis For Samples Containing Nickel (After Erosion-Corrosion Test).

The compositions of erosion-corrosion product films on samples (A6&A7) appear to be similar**,** some characteristic peaks in sample A6 are marked to indicate the existence of Cu2O, α-Cu, NiO, Al2O3 while diffraction pattern characterized the corrosion products formed on the surface of sample A7. It shows the characteristic peaks and Fe2O3of Cu2O, α-Cu, Al2O3 and Fe_2O_3. Although there is a difference in the erosion-corrosion rate of the samples used, they all have good resistance to erosion-corrosion because the formation of Al2O3 greatly protects the surface against corrosion.

The diffraction pattern belongs to the corrosion products formed on the surface of samples A8 & A9 as a result of exposure to sea water which reveals the presence of Cu2O, α-Cu, NiO, ZnO, and Fe_2O_3, show in Figures (4.26-4.29).

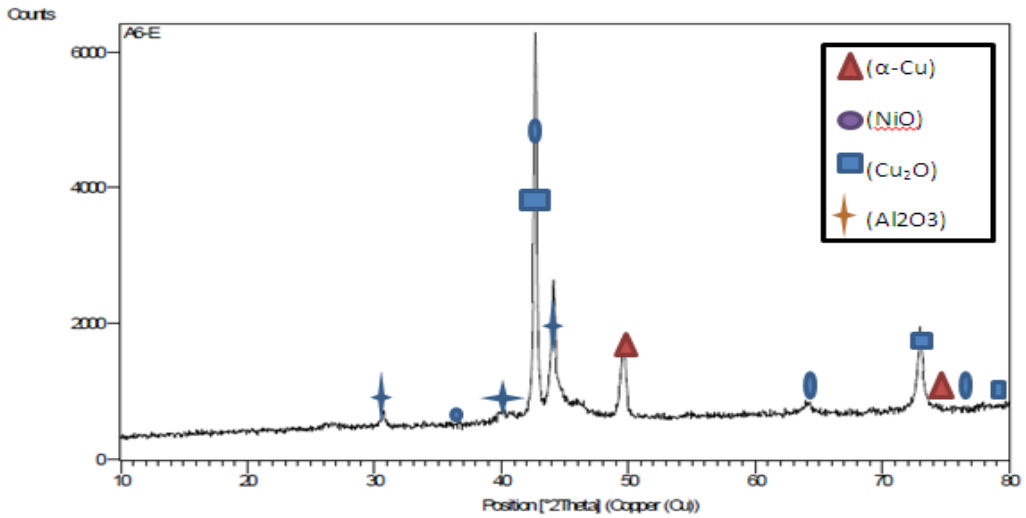

Figure (4.26): X-Ray diffraction analysis for sample A6.

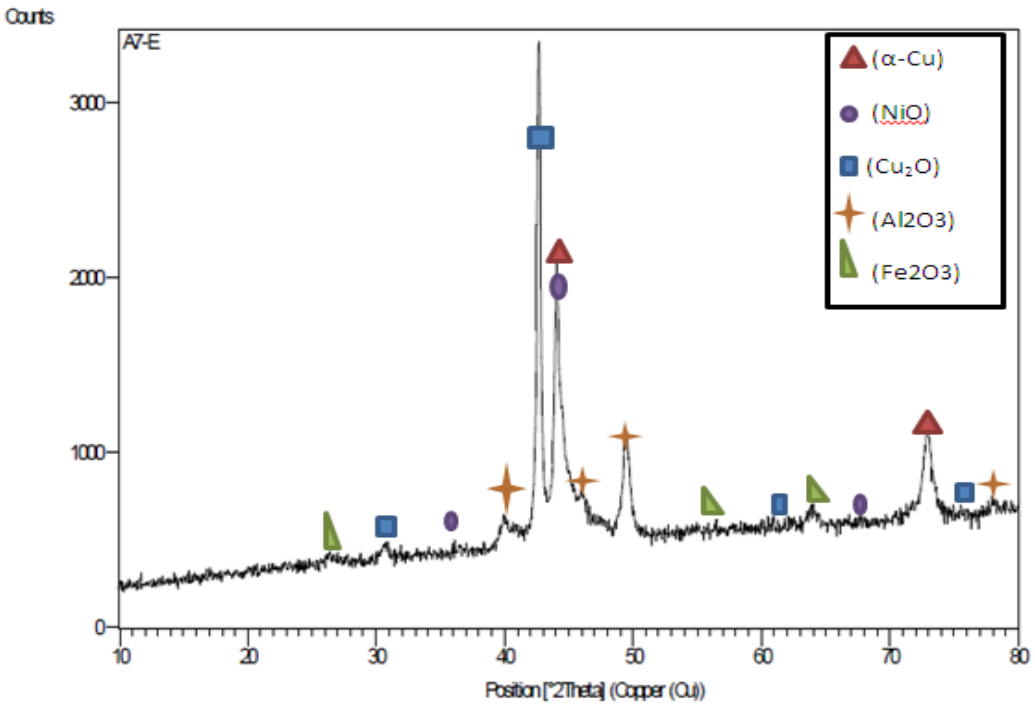

Figure (4.27): X-Ray diffraction analysis for sample A7.

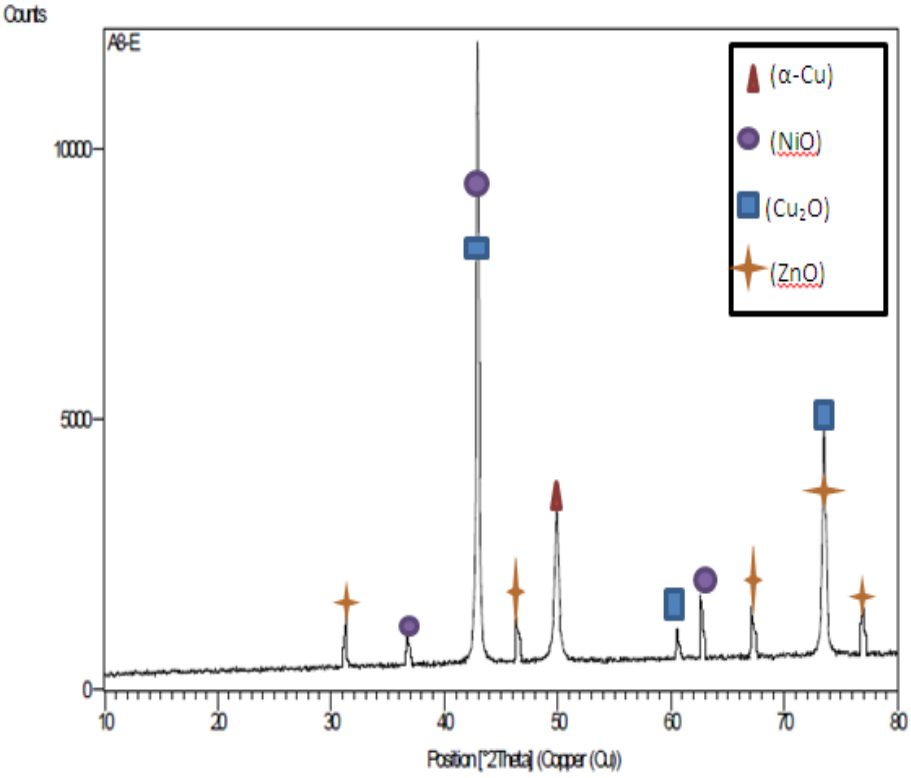

Figure (4.28): X-Ray diffraction analysis for sample A8.

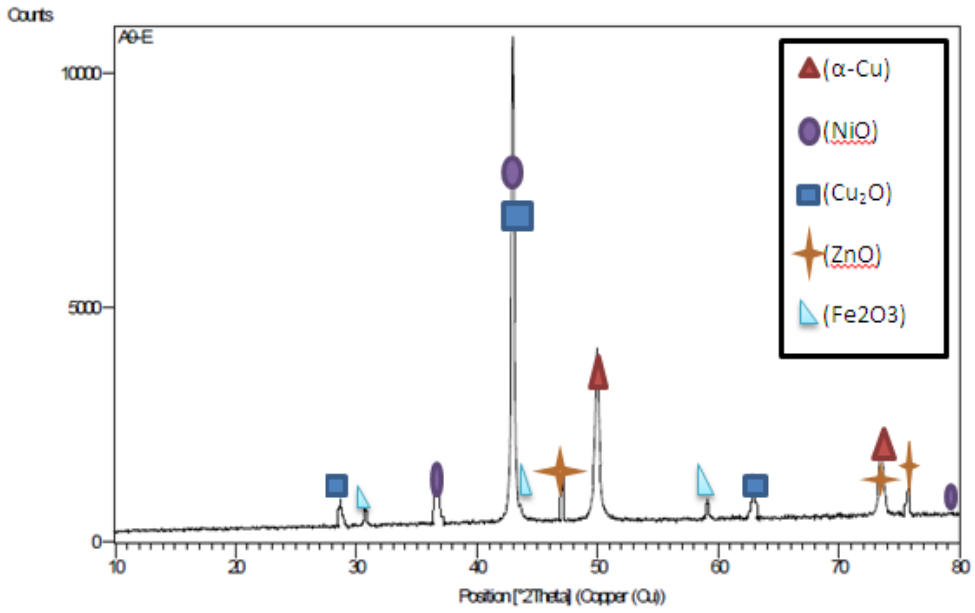

Figure (4.29): X-Ray diffraction analysis for sample A9.

4.6.4 Open Circuit Potential (O.C.P)

A method for deciding whether the corrosion system is active or passive, as well as a formation on the free corrosion potential, which can be used to apply electrochemical protection methods. The open circuit potential of the working electrode was calculated as a function of time before beginning polarization until saturation and semi-stability were achieved. In the seawater medium, open circuit potential (OCP) measurements were taken. After immersing the working electrode in the test solution, the corrosion potential E(V vs. Ag/AgCl) was monitored until the potential stabilized. Figure(4.30) & Figure(4.31) display plot curves of potential versus immersion time, which clearly show that the potential drops to a fairly steady value and that the curves' directions generally decrease with time.

These figures show that voltage is decreasing due to the formation of stable oxide films on specimen surfaces, and that at the corrosion potential (Ecorr), the anodic and cathodic rates are exactly equal; hence, there is no applied current density.

It is very noticed that sample A1 is recorded more active than the other specimens, this behavior is expected, because reference sample free from any protective layers (against corrosion), unlike specimens that alloying elements were added (Al, Sn, Ge, Y, Zn and Fe), they appear more noble because protective layers sch as Al_2O_3, ZnO, Ge_2O, Y_2O_3 and Fe_2O_3 which increase the potential in opposite direction.

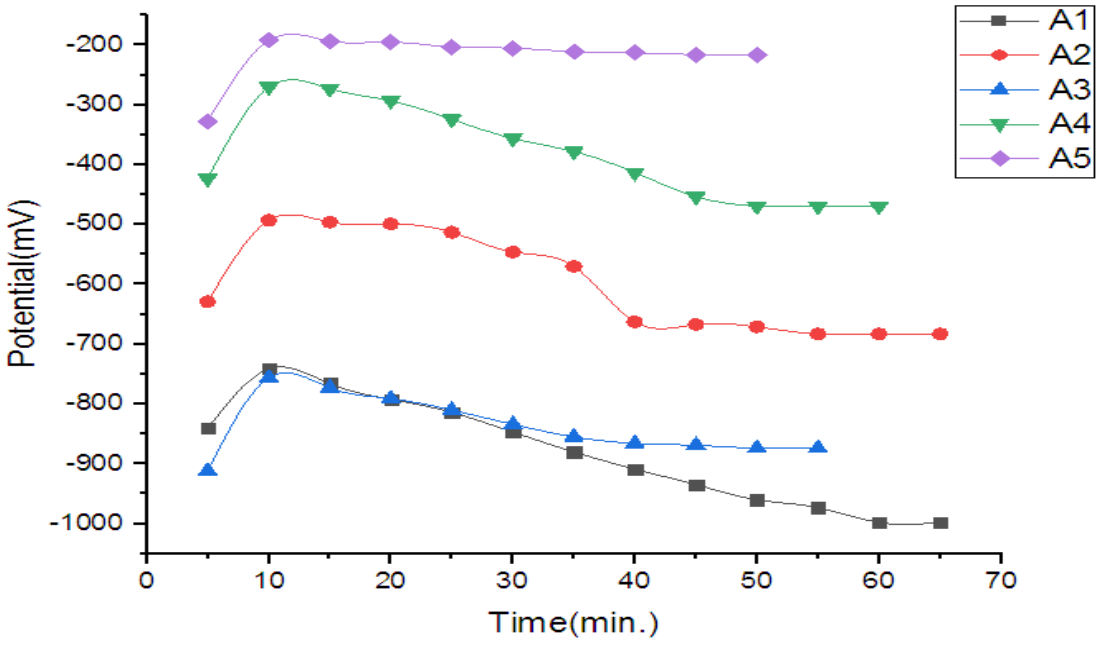

Figure (4.30): Open circuit potential curve for sample A1,in salt solution.

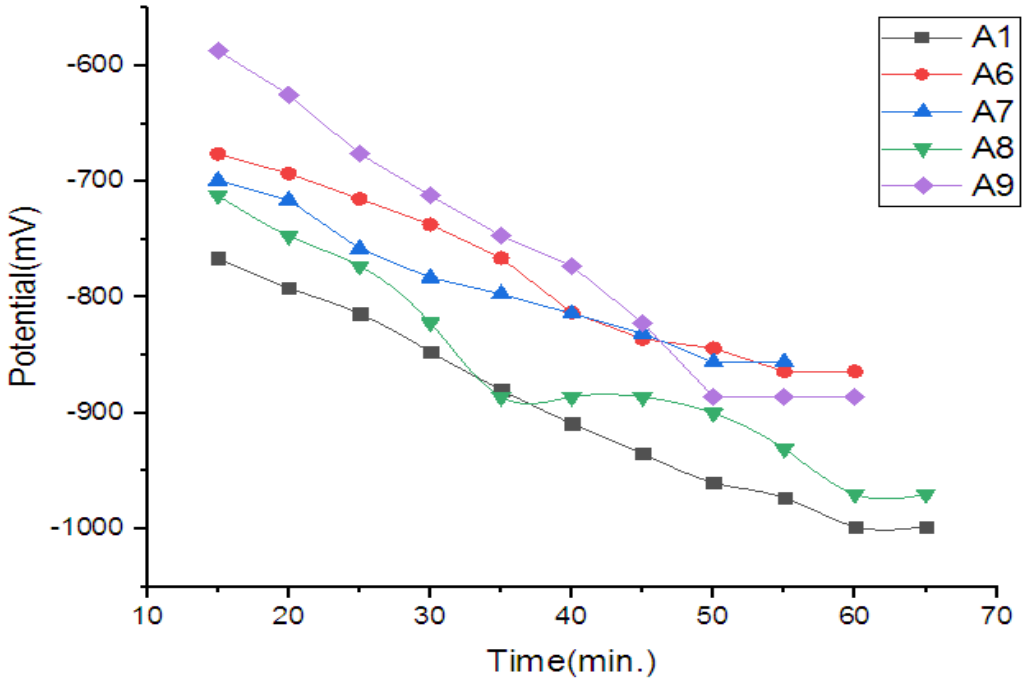

Figure (4.31): Open circuit potential curve for samples containing nickel ,in salt solution.

4.6.5 Potentionstatic Polarization Test

Tafel extrapolation, which is used to estimate corrosion current, was used to investigate the corrosion behavior of specimens. A saturated calomel electrode was used to test the potentials (SCE). As a counter-electrode, a platinum wire was used. The working electrodes are made up of cylindrical components. The open circuit potential (OCP) was measured for at least 30 minutes before each experiment. The linear potential sweep was performed at a (250) mV potential window around the measured OCP, from the cathodic to the anodic side, at scan rates of 1 mVs-1, to obtain polarization curves potentiodinamically.

According to Table (4.6), the improvement in corrosion rate was greater in sample A5(99.92%) than in the reference sample. This expected for several reasons: first, the non porous protective layer of Al_2O_3 and Y_2O_3,

as well as the adhesive, prevent any leaching of Zn2+; second, germanium particles precipitate as free particles on the grain boundary of (α) grains, obstructing any diffusion; third, germanium particles precipitate as free particles on the grain boundary of (A4) grains, This topic also refers to samples A2, A3, and A4.

Table (4.9): Corrosion Parameters for Polarization of Specimens in Salt Solution environment.

Specimens	Density (g/cm^3)	Exposed Surface Area (cm^2)	Equivalent Weight (E.W.)	E_{cor} (mV)	Current Density, i_{cor} ($\mu A/cm^2$)	Corrosion Rate (CR) mm/yr	Improving (%)
A1(Cu-Ni)	8.77	4.15	29.87	-710.7	8.022	186. 9 × 10 -3	-
A2(Cu-Zn-Al)	7.82	4.15	29.81	-447.6	7.5	91.4 × 10 -3	51
A3(Cu-Zn-Al-Sn)	7.96	4.10	29.79	-651.5	1.45	17.3× 10 -3	90.7
A4(Cu-Zn-Al-Ge)	7.98	4.10	30.78	-1028.3	0.0113	6.439 × 10 -3	96.5
A5(Cu-Zn-Al-Y)	7.74	4.15	30.24	-856	0.1176	.14128*10^{-3}	99.92

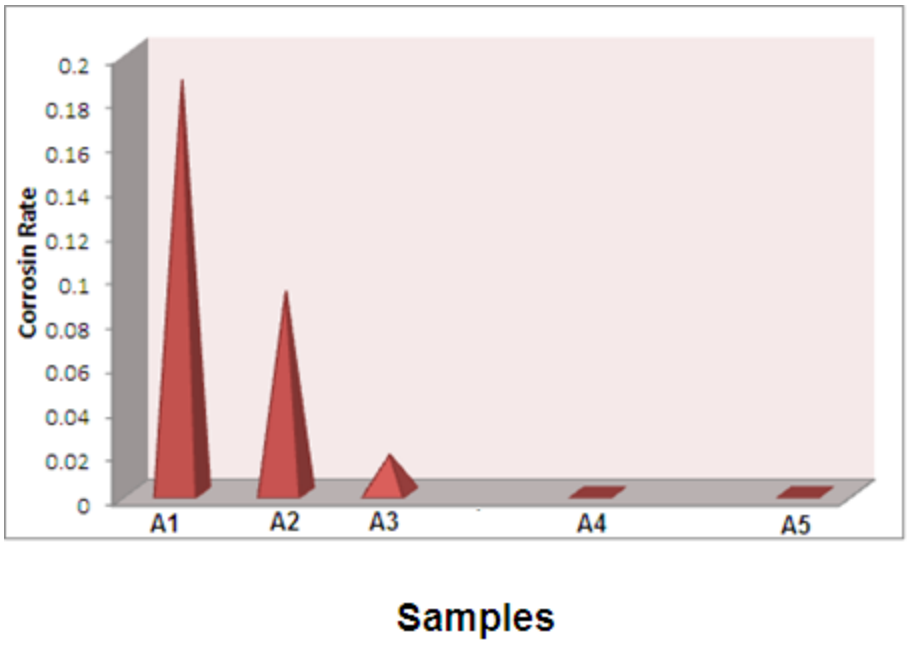

Figure (4.32): Comparative in corrosion rate with respect to base alloy(A1).

From Table (4.6), improving in corrosion rate was greater in sample A8, it was (99.3) with respect to reference sample, It seems that the presence of Ni and Zn together with Cu decreases the corrosion rate of the alloy. Generally, oxides of Ni, Zn and other corrosion products form a compact layer, which is tightly bound to the alloy substrate and improves its corrosion resistance.

Within ternary alloys, a further passivation process is carried out in neutral solutions where the surface dissolution of Al produces a layer of al-oxide [125] as follows:

$$Al+4Cl^{-}\rightarrow AlCl_4+3e^{-} \quad (4.2)$$

$$AlCl_4^{-}+3H_2O \rightarrow Al_2O_3 + 6H^{+} + 8Cl \quad (4.3)$$

Al2O3 is subject to continual dissolving in chloride solutions and the process of corrosion takes place as follows[126]:

Al_3+(inAl_2O_3.nH_2Ocrystallattice) + Cl−⟶ $Al(OH)_2Cl$ +2H^+ (4.4)

or

Al_3+(inAl_2O_3.nH2Ocrystalttice) +2Cl−⟶$Al(OH)_2Cl2^-$ +2H^+ (4.5)

Progress of these processes in some places leads to barrier film dilution. The process of hydrolysis creates acidity at local levels and rapid corrosion of recession [119]. In the Zn containing alloys a further passivation process occurs as a result of the creation, through dezinification, of Zn-oxide films [127,128]:

$Zn+H_2O \rightarrow ZnO+2H^+ +2e^-$ (4.6)

The dissolved nickel ions from the alloy dissolution are integrated into the Cu_2O crystal mesh, which in the presence of Ni has been formed as a barrier layer. In addition to the segregation of Ni into the Cu_2O layer, solid state reactions and mobile vacancies interact to loose the ionic conductivity and to enhance the electronic conductance and, so, raise the resistance to the corrosion of alloys[129]

Table (4.10): Corrosion Parameters for Polarization of Specimens in Salt Solution environment.

Specimens	Density (g/cm^3)	Exposed Surface Area (cm^2)	E_{cor} (mV)	Current Density, i_{cor} ($\mu A/cm^2$)	Corrosion Rate (CR) mm/yr($\times 10^{-3}$)	Improving (%)
A1(Cu-Ni)	8.77	4.15	-710.7	29.87	186.9	-
A6(Cu-Ni-Al)	7.2	4.15	-982	24.07	1.258	99.3
A7(Cu-Ni-Al-Fe)	7.099	4.15	-1046.7	23.35	0.00405	99.99
A8(Cu-Ni-Zn	8.6	4.15	-897.5	30.79	0.30607	99.83
A9(Cu-Ni-Zn-Fe)	8.3	4.15	-925.4	29.62	5.8191	96.8

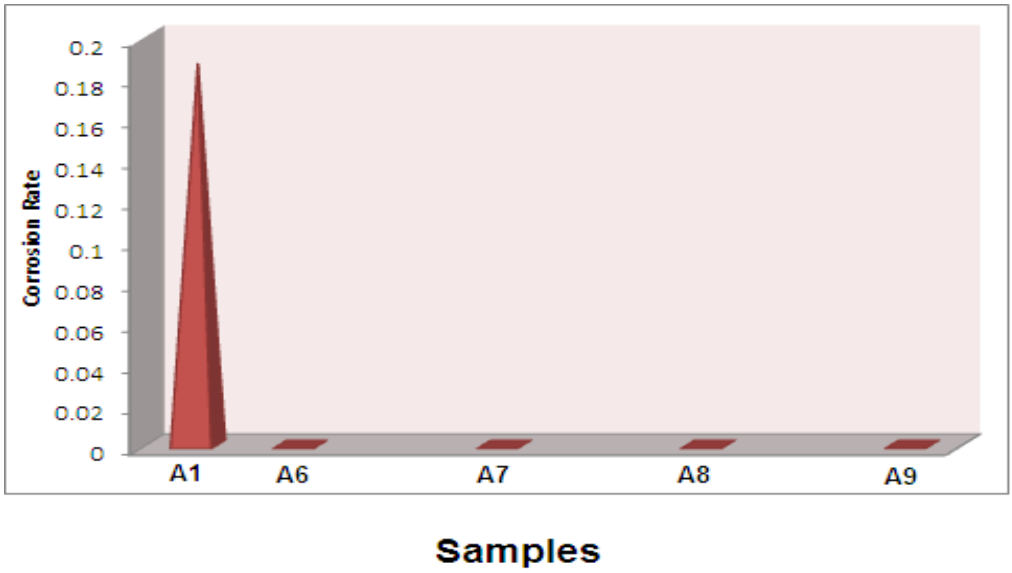

Figure (4.33): Comparative in Corrosion rate with respect to base alloy(A1).

4.7Oxidation Test

4.7.1 Cyclic oxidation

All alloys (A1, A2, A3, A4, A6, A7, A8, and A9) are subjected to cyclic oxidation tests at high temperatures and in an air environment. The resistance of the protective oxide layer was measured by heating the specimens in the furnace at the test temperature and weighing them every 5 hours. After allowing the samples to cool in the furnace, they were cleaned to extract the spalled oxide, and the weight change per unit surface area was calculated using the Martinengo et al. process. [130].

The oxidation behavior of reference sample A1 is shown in Figure(4.34)for various temperatures (450, 550, 650, 750, and 850) C°. This behavior is expected (stratified) due to the existence of the oxide film that forms on the alloy surface, which is porous, dense, and non-adhesive, as verified by XRD and EDS.

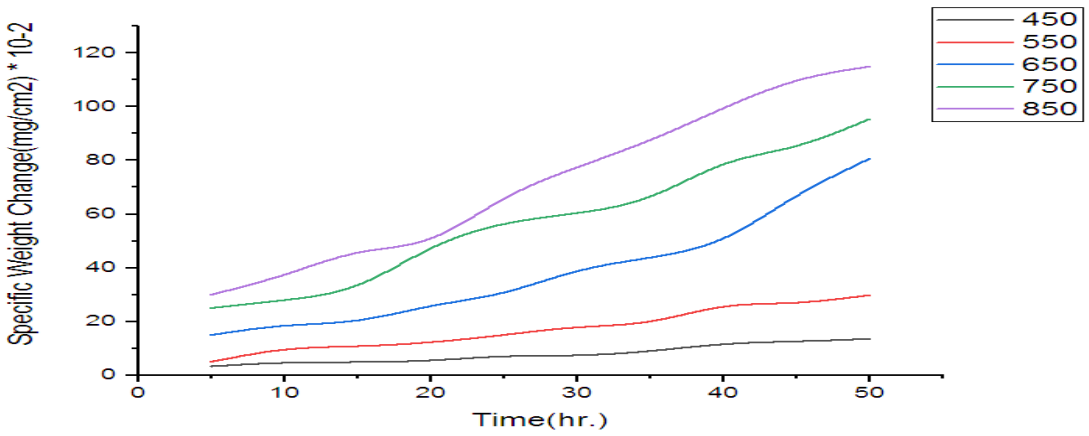

Figure(4.34): Effect temperatures of oxidation on specific weight change for A1, base alloy (*Cu- Ni*), at different temp. after 50 hrs. at 5 hrs. cycle.

There are two important points to note about free nickel specimens A2, A3, A4 and A5. First, the behavior of these specimens was different; this is due to protective layers that form on the alloy surface; these layers have a great ability to protect and prevent any Cu++ and Zn++ from diffusing through these layers; both XRD and EDS findings indicated the existence of Al_2O_3, ZnO, Ge_2O, and Y_2O_3. Secondly, in all oxidation temperatures studies, B3 serves as a best alloy in oxidation resistance, then B2 and B1 Figures(4.35, 4.36, 4.37, & 4.38).

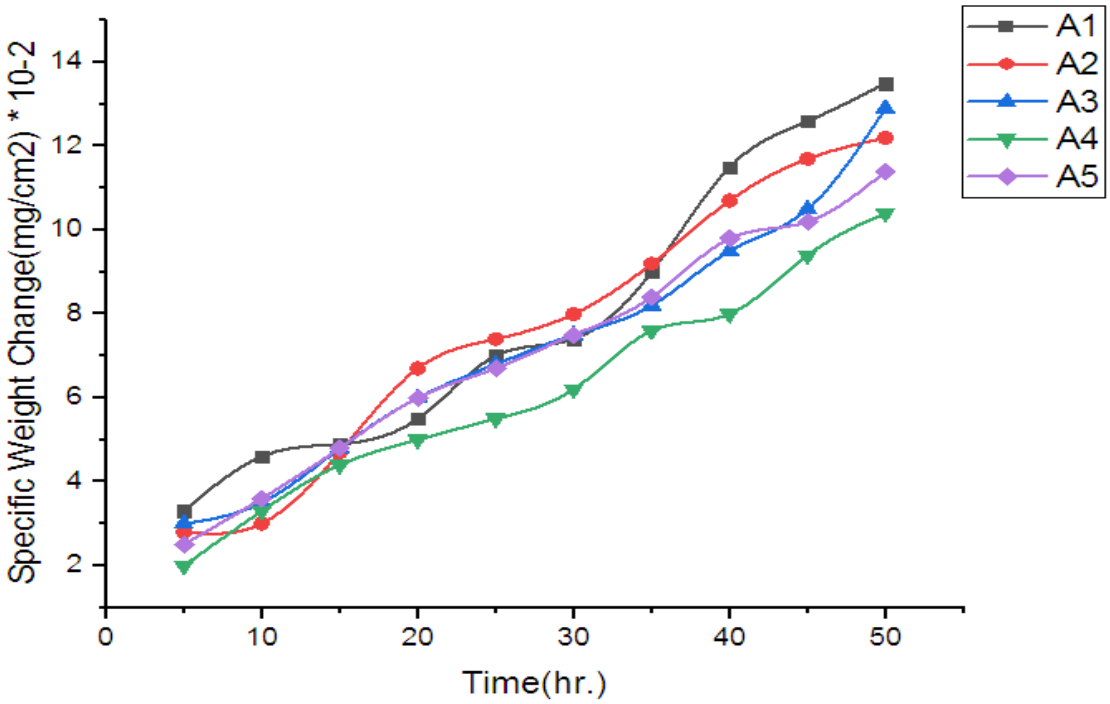

Figure (4.35): Effect of temperature of oxidation on specific weight change for alloys (A2, A3, A4 and A5) at 450^{o}C for 50 hrs. at 5 hrs. cycle.

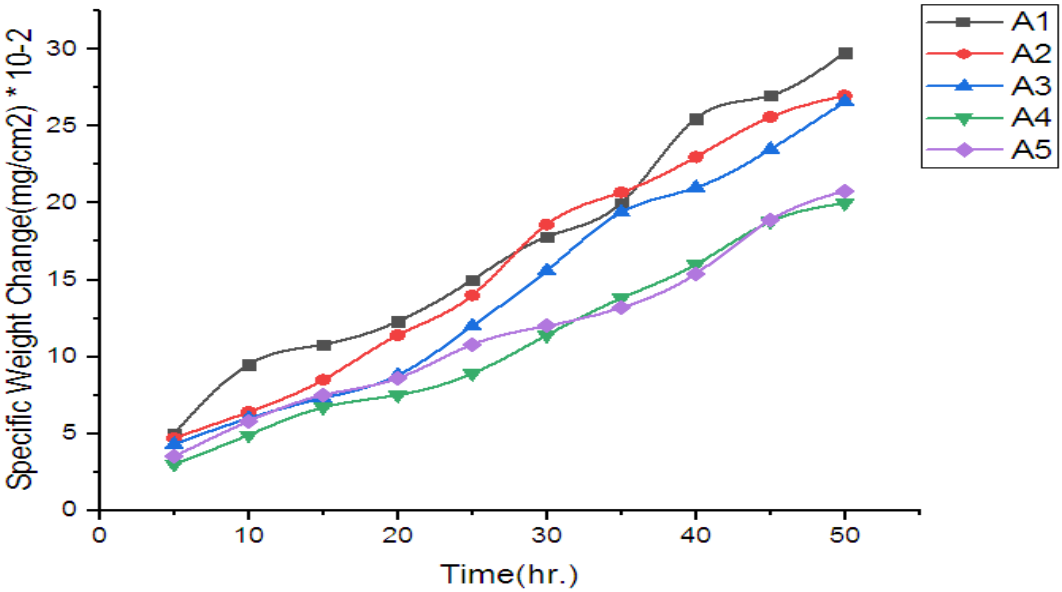

Figure (4.36): Effect of temperature of oxidation on specific weight change for alloys (A2, A3, A4 and A5) at 550^{o}C for 50 hrs. at 5 hrs. cycle.

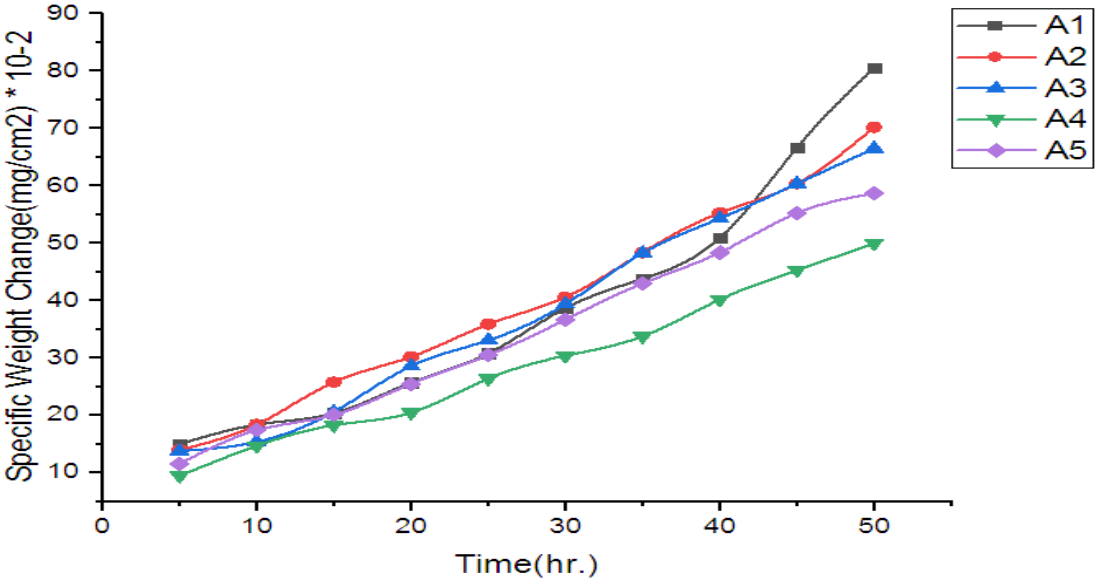

Figure (4.37): Effect of temperature of oxidation on specific weight change for alloys (A2, A3, A4 and A5) at 650^{o}C for 50 hrs. at 5 hrs. cycle.

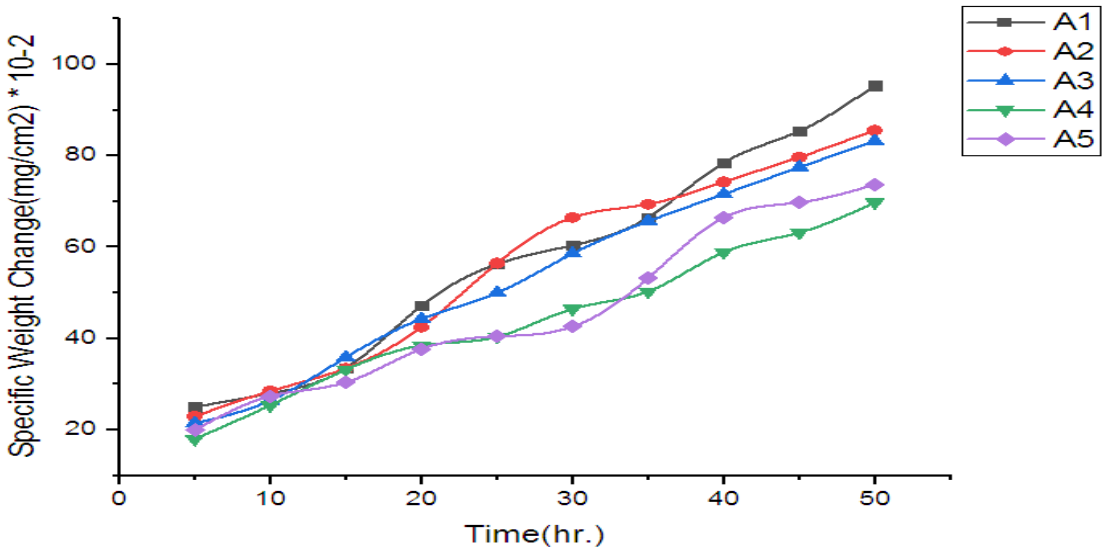

Figure(4.38): Effect of temperature of oxidation on specific weight change for alloys (A2, A3, A4 and A5) at 750^{o}C for 50 hrs. at 5 hrs. cycle.

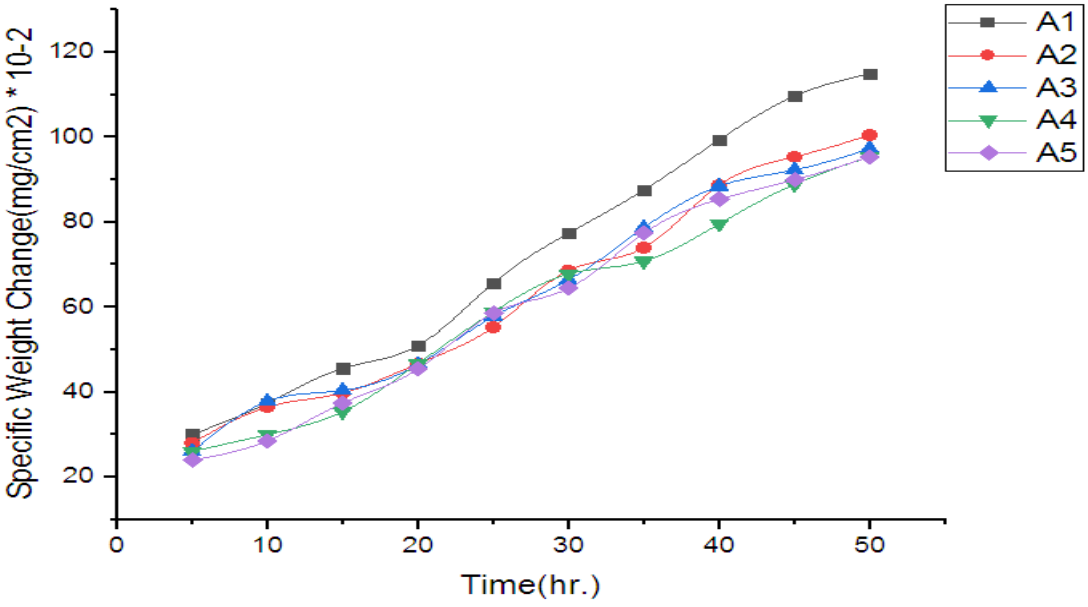

Figure (4.39): Effect of temperature of oxidation on specific weight change for alloys (A2, A3, A4 and A5) at 850^{o}C for 50 hrs. at 5 hrs. cycle.

In comparison to other alloys, the alloy A4 oxidation resistance improves as temperatures rise from (450 – 850) C°. This best behavior is due to the alloying element (Ge), which acts as an appropriate element against corrosion.

While the figures (4.40-4.44) represent the comparison of the sample (A1) with the samples containing nickel (A6, A7, A8, and A9). Sample A1: (Cu-Ni) has the highest weight gain, which according to research is likely due to Cu^{+2} in Cu_2O as seen in XRD study, which increases the amount of voids that influence the diffusion process and increases the oxidation rate [131].The oxidation rate of this sample is higher than the oxidation rate of other samples, this means that the layer is thick and, when exposed to a cyclic oxidation, it suffers a little spalling. Samples A6 α A7: (Cu-Ni-Al) α(Cu-Ni-Al-Fe) have low weight gain with compared with other samples ; this is expected due to aluminum, which has the ability to protect itself by creating a stable layer from aluminum oxide (Al2O3) as found in XRD pattern of cyclic oxidation test at 450℃.

However, it is brittle and it is not very adhesive due to which cracking and fracture occurs in the oxide layer when the sample is exposed to a cyclic oxidation. Then, it begins to build a protective layer again and thus, over time, the intensity of the process will increase when the temperature rises to 850℃ as shown in Figure (4.40) as the cyclic oxidation effect of 800℃ can be more severe than 450℃, it can be explained by the fact that thick oxide layers are more susceptible to breakage due to the many defects and to the value of high thermal stress placed on the oxide layer these result are in good agreement with those given by[132].

The weight gain of alloy A7 decreasing is clearly due to alloying elements Fe, and this indicates the importance of adding some elements to improve the general characteristics of the alloy including cyclic oxidation resistance as shown in the Figure (4.41) the tendency to reduce the weight gain after the samples were subjected to periodic oxidation at 450℃ and 850℃, note that the weight gain and the building of the protective layer for these alloys is much lower than the alloys of A1, A8 and A9 which contain elements that together affect the formation of a protective layer with the best possible adhesion.

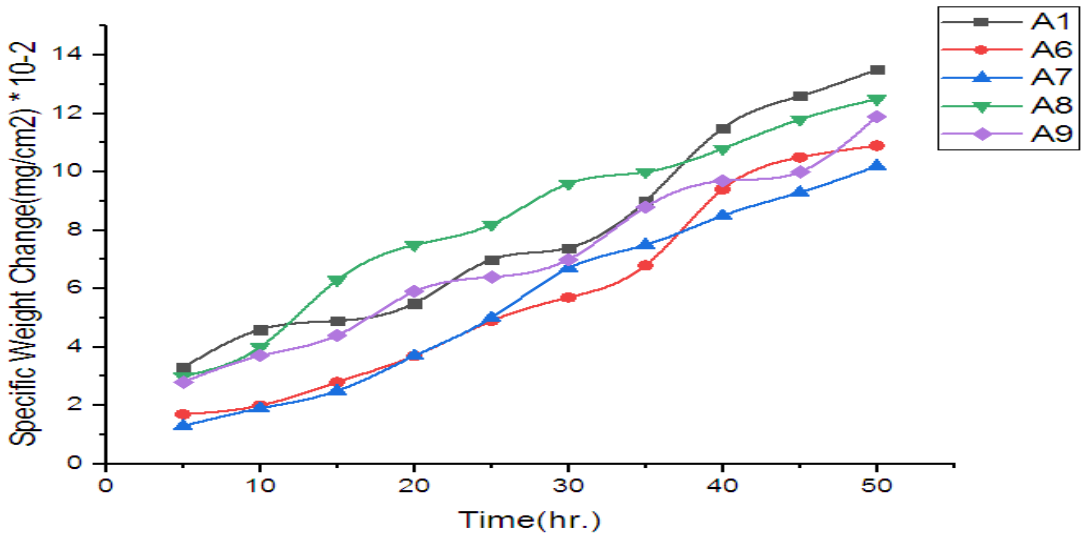

Figure (4.40): Effect of temperature of oxidation on specific weight change for alloys (A1, A6, A7, A8 and A9) at 450^{o}C for 50 hrs. at 5 hrs. cycle.

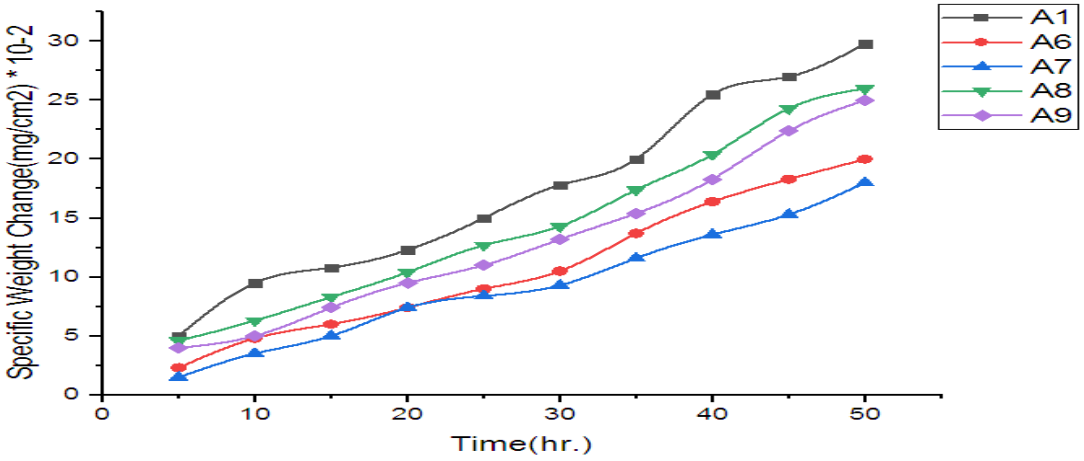

Figure (4.41): Effect of temperature of oxidation on specific weight change for alloys (A1, A6, A7, A8 and A9) at 550°C for 50 hrs. at 5 hrs. cycle.

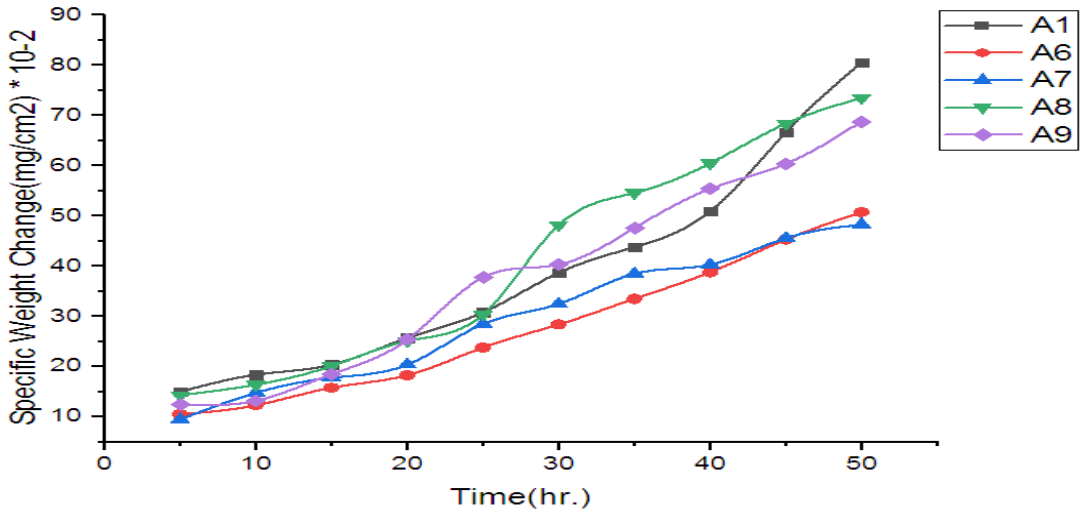

Figure (4.42): Effect of temperature of oxidation on specific weight change for alloys (A1, A6, A7, A8 and A9) at 650°C for 50 hrs. at 5 hrs. cycle.

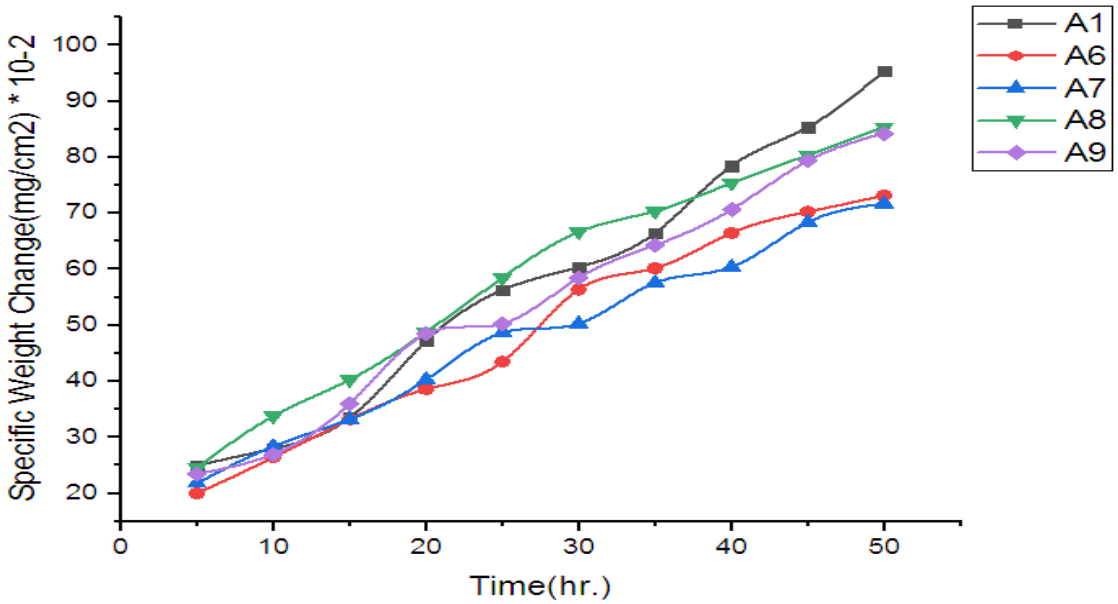

Figure (4.43): Effect of temperature of oxidation on specific weight change for alloys (A1, A6, A7, A8 and A9) at 750^{o}C for 50 hrs. at 5 hrs. cycle.

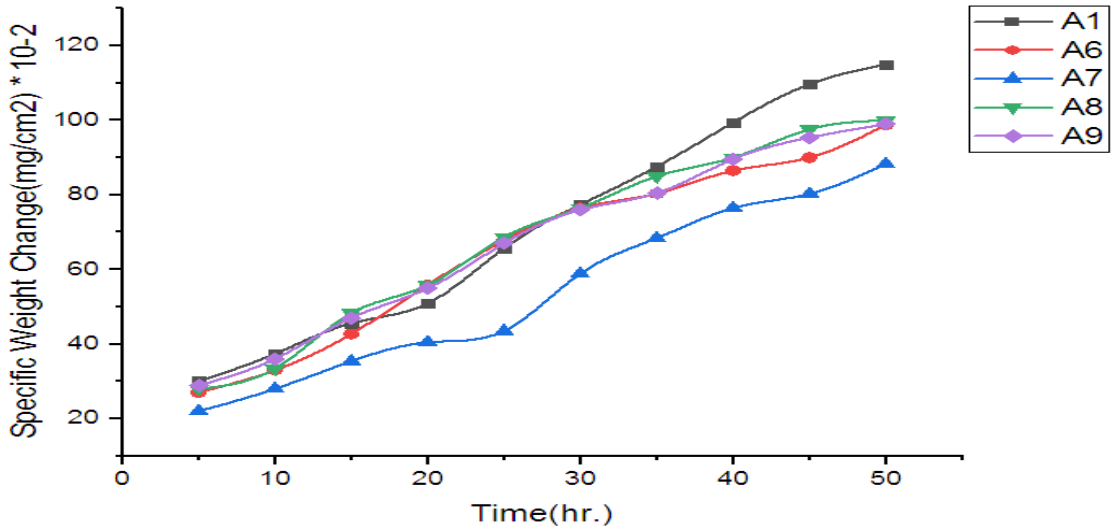

Figure (4.44): Effect of temperature of oxidation on specific weight change for alloys (A1, A6, A7, A8 and A9) at 850^{o}C for 50 hrs. at 5 hrs. cycle.

4.7.1.1 X-Ray Diffraction Analysis Patterns for A1, After Oxidation Process

The results of XRD analysis for A1(Cu-Ni) specimen reveal to exist peaks represent the main oxides NiO, Cu_2O and α-Cu, this alloy had appeared the higher loss weight rate during is exposing to high temperatures than other alloys, this has been attributed that, cupronickel oxidizes and grow a double scale consisting of outermost CuO and innermost mainly alloy oxide, and it has an oxide consisting Cu_2O matrix with NiO particles, which form a continuous outermost film, Figure (4.45).

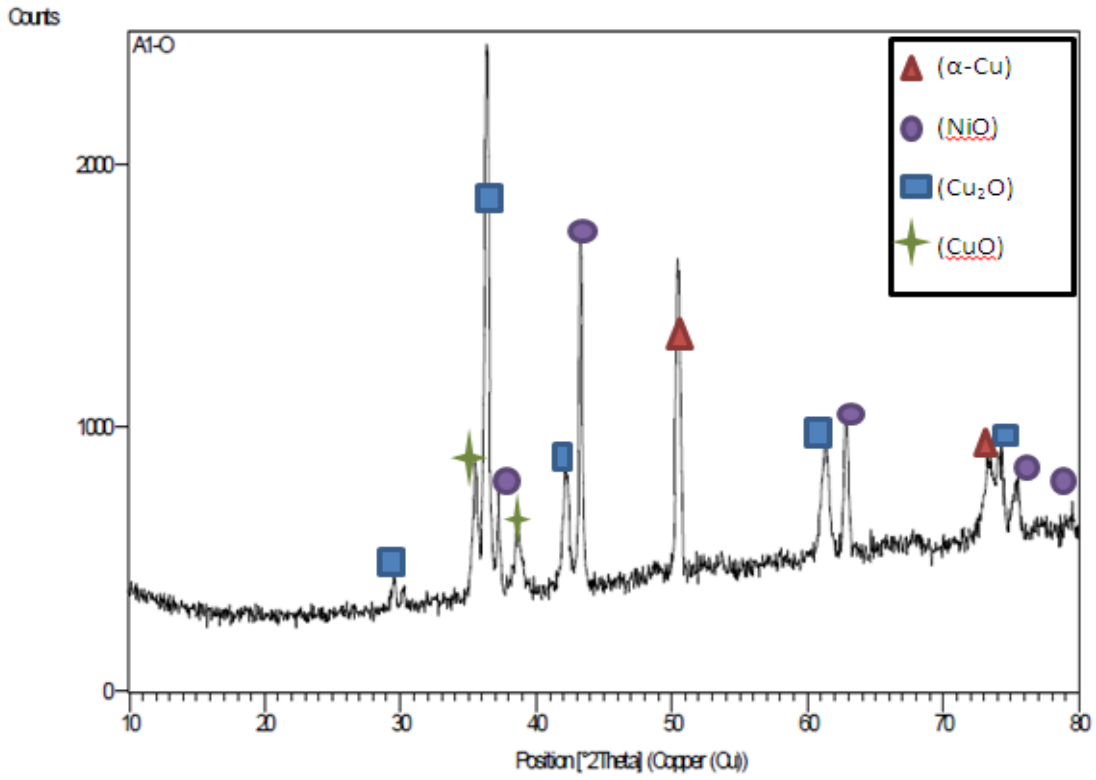

Figure (4.45): X-Ray diffraction analysis for A1.

4.7.1.2 X-Ray Diffraction Analysis Patterns For Free Nickel Samples After Oxidation Process

The results of XRD analysis for A2, A3, A4, and A5 specimens reveal to exist peaks represent the main oxides Al_2O_3 , SnO, GeO_2 , and Y2O3 , these alloys had appeared the least specific change weight during oxidation process compared to A1, this has been explained, that existence Aluminum oxide, it is the one and alone protective oxide layer in alloys that content Al, but it is exposed for cracking and spalling, due to its brittle and weak adhesion, so that the plasticity, adhesion and resistance for thermal shock and oxidation of that oxide have been improved by addition the tin, germanium, and yttrium elements. The surface chemical analysis has appeared existence the Sn, Ge,and Y within the scale is formed on surface of alloys Figures (4.46, 4.47, 4.48, and 4.49).

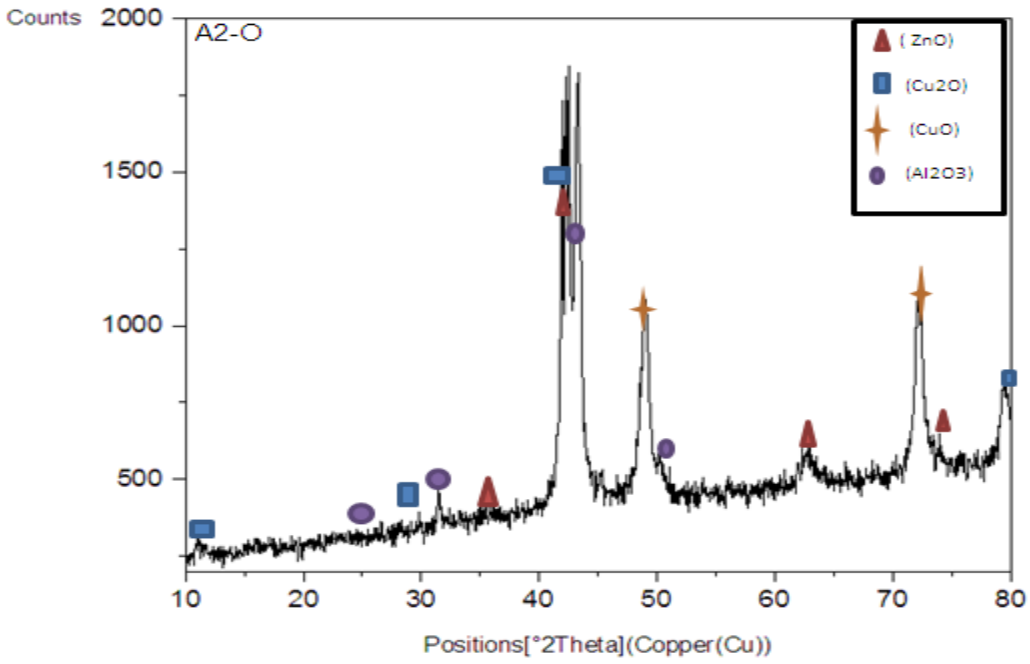

Figure (4.46): X-Ray diffraction analysis for A2.

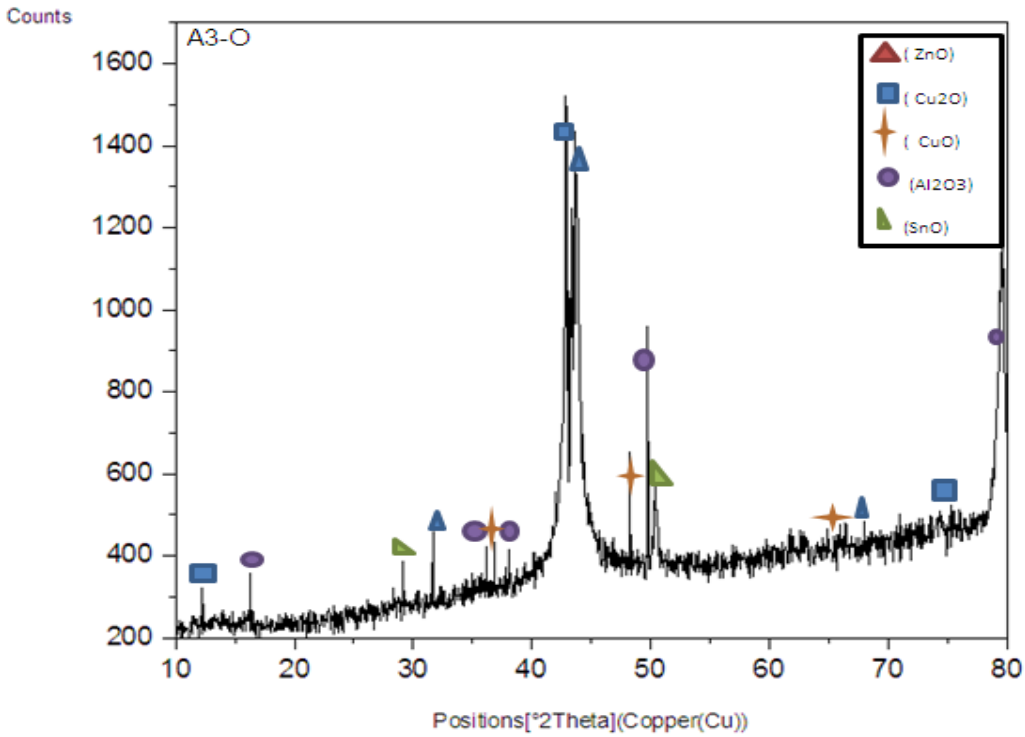

Figure (4.47): X-Ray diffraction analysis for A3.

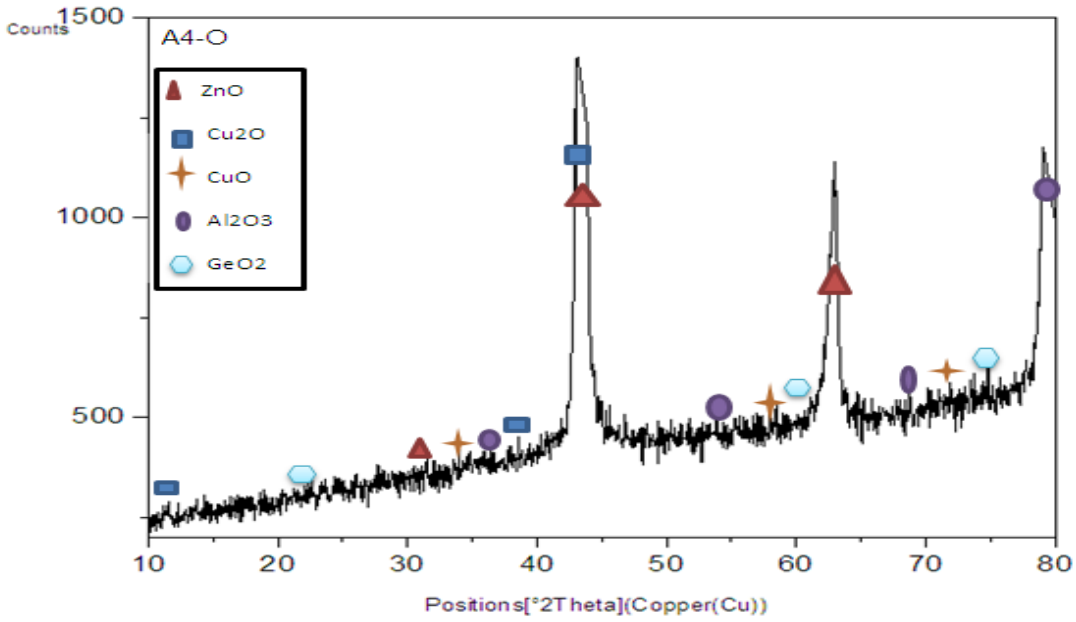

Figure (4.48): X-Ray diffraction analysis for A4.

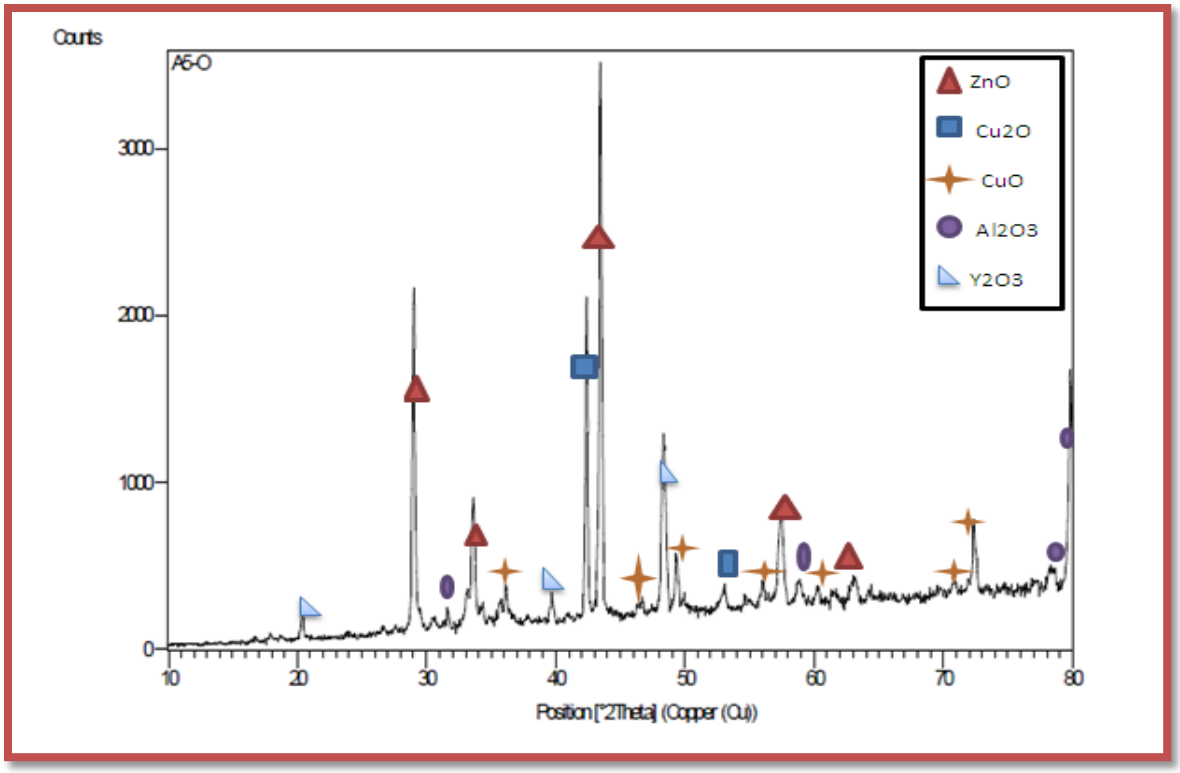

Figure (4.49): X-Ray diffraction analysis for A5.

4.7.1.3 X-Ray Diffraction Analysis Patterns For Samples Containing Nickel After Oxidation Process

In XRD pattern for samples A6& A7at 850℃ which has been showed in figsures (4.50) and (4.51) it is found α -Cu, Al2O3 peaks while some intermetallic compound.

While in the XRD pattern of samples A8 & A9, representing α - Cu, ZnO, CuO peaks. Therefore, Fe2O3 exists in XRD pattern for sample A9 Fig.(4.52) & (4.53).

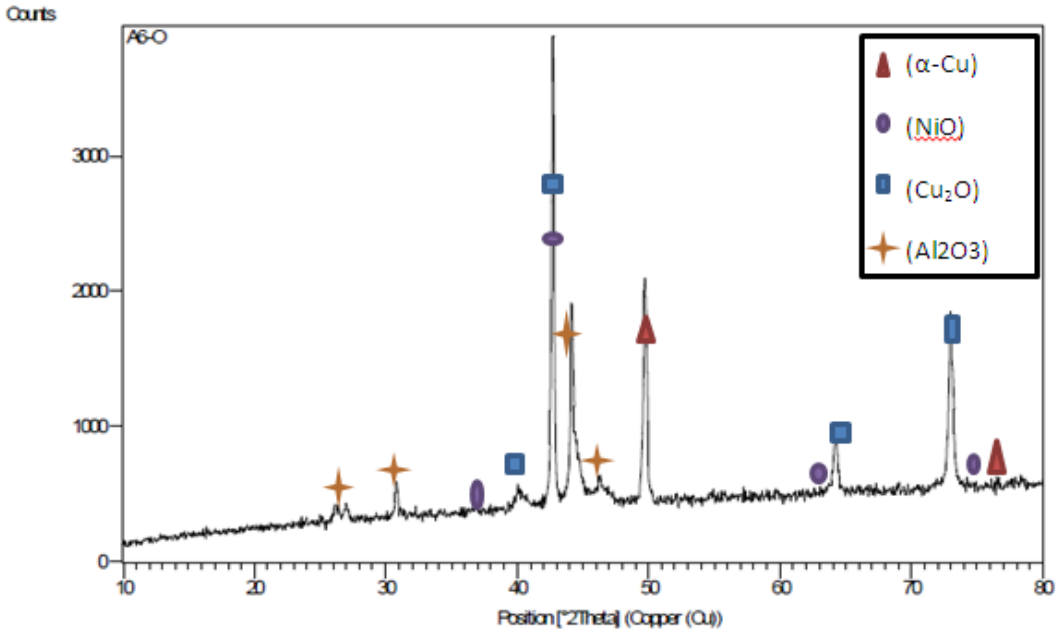

Figure (4.50): X-Ray diffraction analysis for A6.

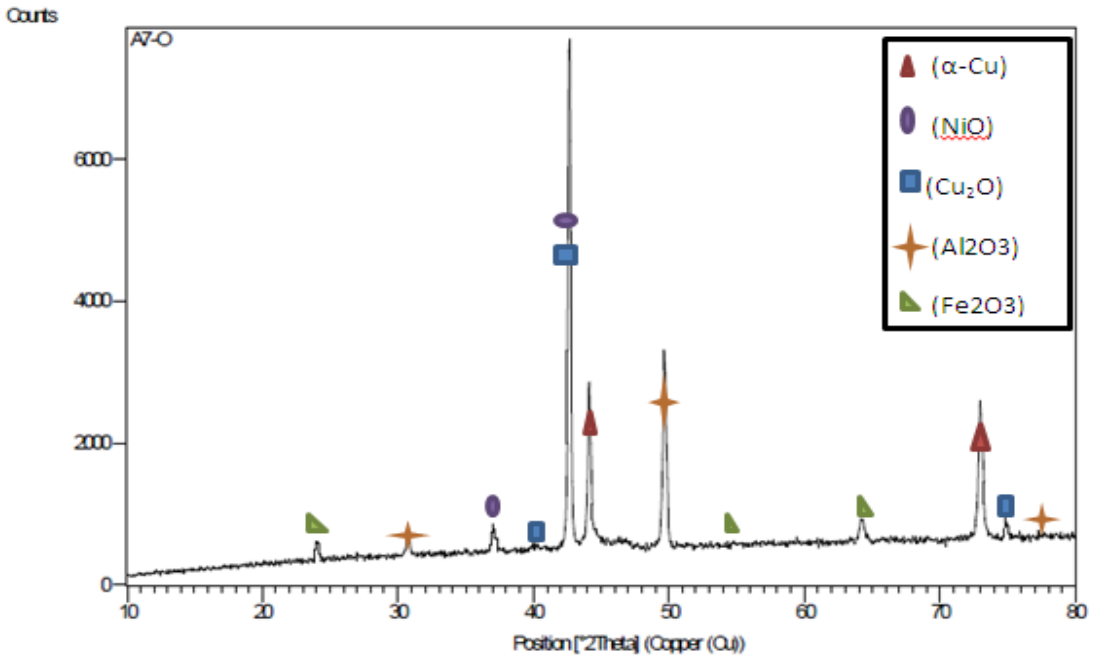

Figure (4.51): X-Ray diffraction analysis for A7.

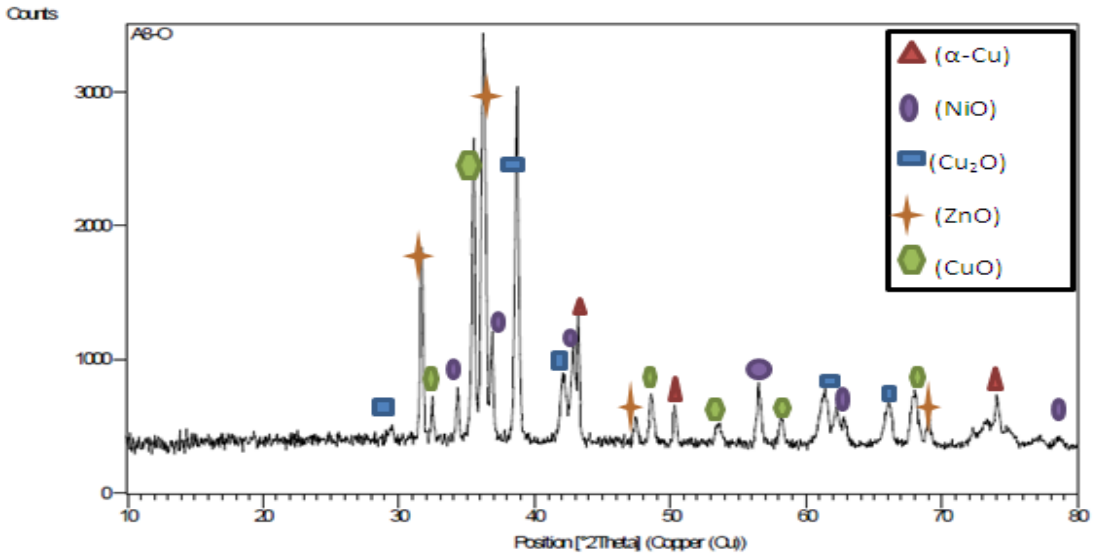

Figure (4.52): X-Ray diffraction analysis for A8.

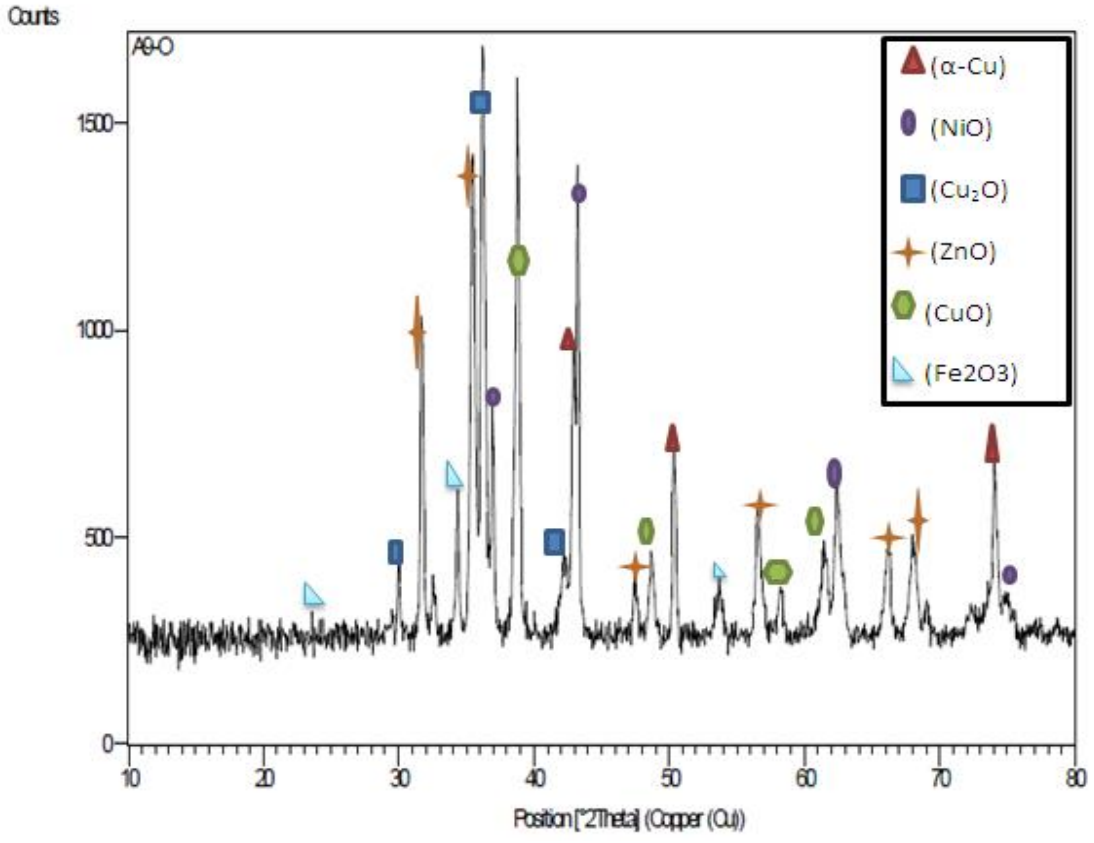

Figure (4.53): X-Ray diffraction analysis for A9.

4.7.2 Thermal Shock

Thermal shock is the term used to describe the thermal stresses that the body is exposed, due to sudden change in temperature. This test is considered as a criterion for the extent of adhesion force of oxide layer on base metal, and a measure for the extent of spalling or cracking of that oxide layer. The fact, if that the oxidation rate is lower does not necessarily mean that the growing oxide layer is the best, and to be so it must resist cracking and spalling by the impact of thermal stresses, in other meaning that it must have a good plasticity and adhesion.

The effect of thermal shock on the oxidation behavior has been studied for all samples that were placed in an electrical furnace with a temperature range (50-850) C° for (30 min.), then quenched in water, and continued to heat by increasing the temperature for each time by (50C°) and using the same time period and cooling them with tap water until a temperature of 850 0C is reached.

According to Figures (4.54& 4.55) which show the effect of thermal shock on the oxide layer formed on surface of A1, base alloy (*Cu-Ni*), which is very clearly suffering from large cracking and spelling, this is evident by the significant decreasing in the weight of the sample compared with other specimens specially in high temperatures, this is expected due to absence of protective layers. On the other hand, the change in weight of A2, A3, A4 & A5 decreases comparing with base alloy, but the change in weight for base alloy increases with time, (stratified) while for other specimens fixed

approximately at long time ,this is due to build protective layer of Al_2O_3, ZnO, Ge_2O, and Y2O3.

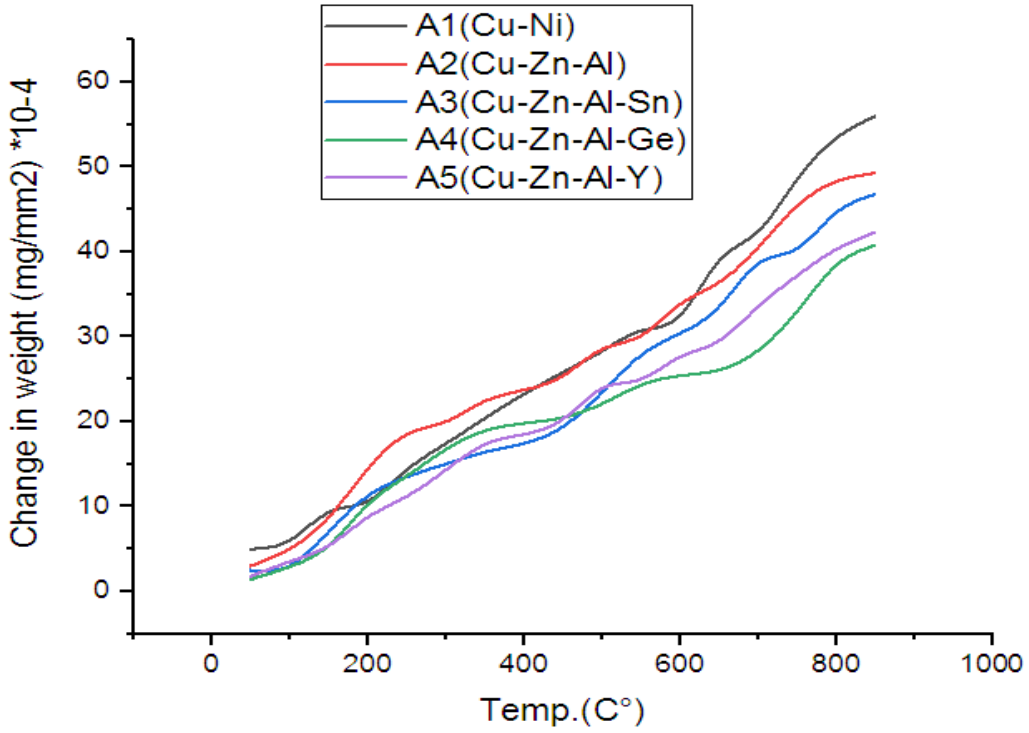

Figure (4.54): Effect of thermal stresses on oxide surface structure of alloys (A1, A2, A3,A4and A5), after sudden cooling down in water at different temperatures range (50, 100, 150, to 850^{o}C) at constant time (30 min.).

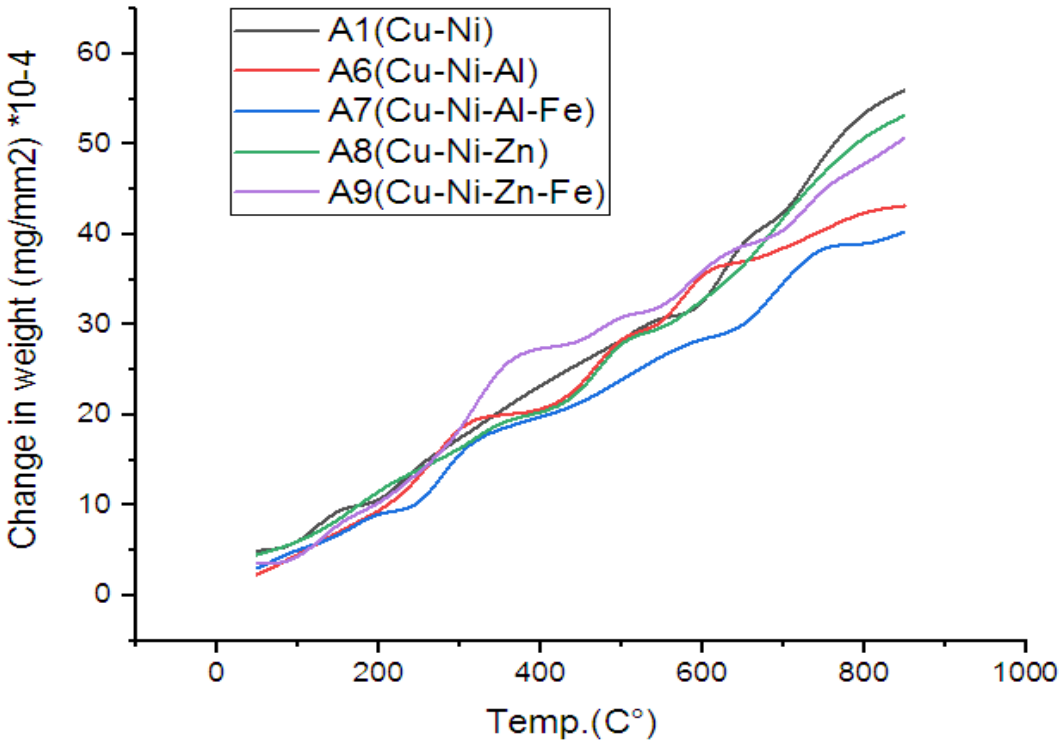

Figure (4.55): Effect of thermal stresses on oxide surface structure of alloys (A1, A6, A7,A8and A9), after sudden cooling down in water at different temperatures range (50, 100, 150, to 850^{o}C) at constant time (30 min.).

4.8Scanning Electron Microscope(SEM).

4.8.1 Scanning Electron Microscope for all Alloys after Simple-Corrosion Test.

Scanning electron microscope (SEM) has been employed to observe the corroded surfaces of alloys. The morphology of the A1 alloy (Cu-Ni) specimen is shown in Figure (4.56) shows, the surface of alloy appeared porous layer and corrosion products, due to breakdown of passivity and onset of pitting corrosion are of considerable practical significance in order

to determine the corrosion resistance of the material in aggressive environments, corrosion products are analyzed by EDS microanalyses shown in below Figure (4.56).

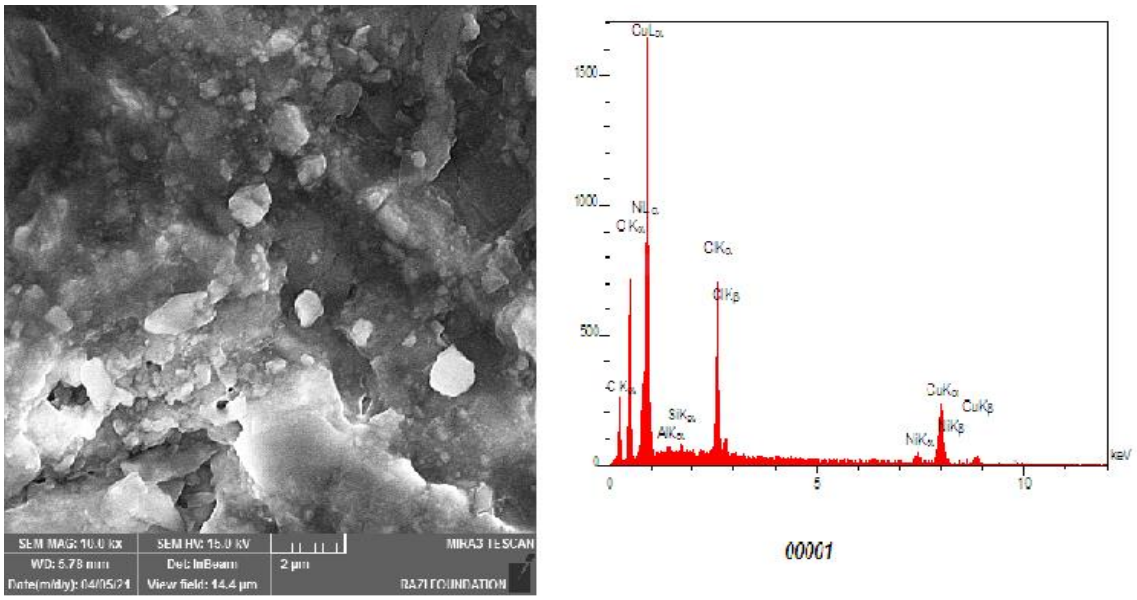

Figure (4.56): SEM image, EDS analysis for alloy A1 after simple immersion.

While, scanning electron microscope (SEM) has been employed to observe the corroded surfaces of free nickel alloys specimens(A2, A3, A4, and A5). Al, Sn, Ge, and Y addition, it is demonstrated that Sn,Ge, and Y elements could make corrosion products layer higher protective & strength the adhesion between the matrix and scale and inhibits zinc ions from coming down in aggressive environment during exposing to sea water test leading increase in corrosion resistance Figure (4.57) to Fig.(4.60).

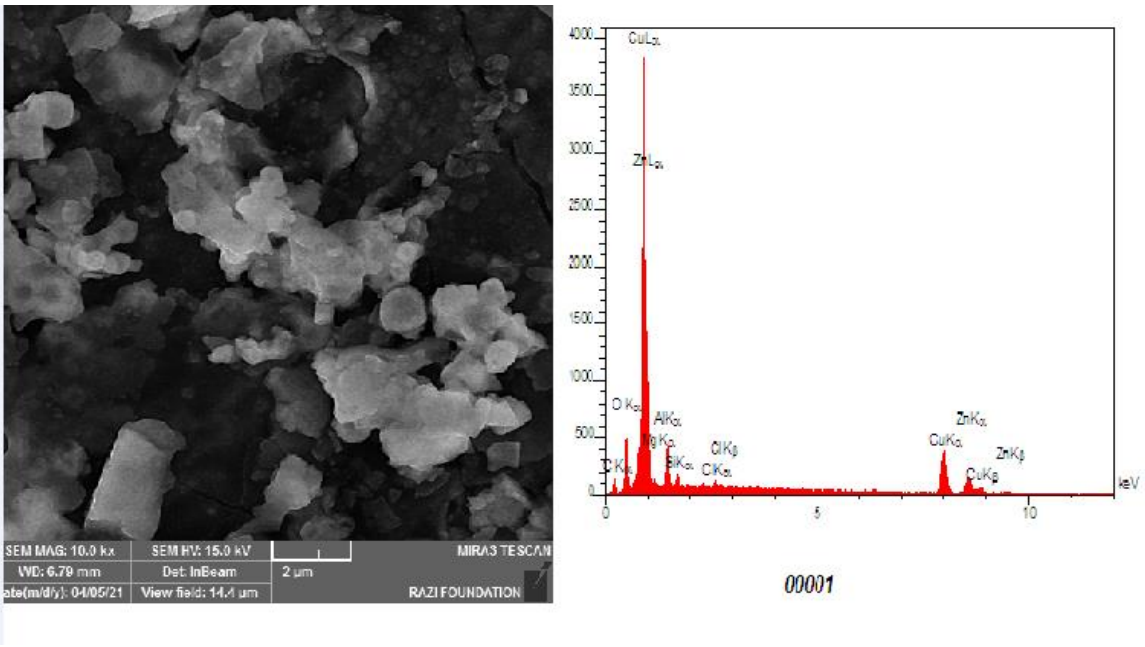

Figure (4.57): SEM image, EDS analysis for alloy A2 after simple immersion.

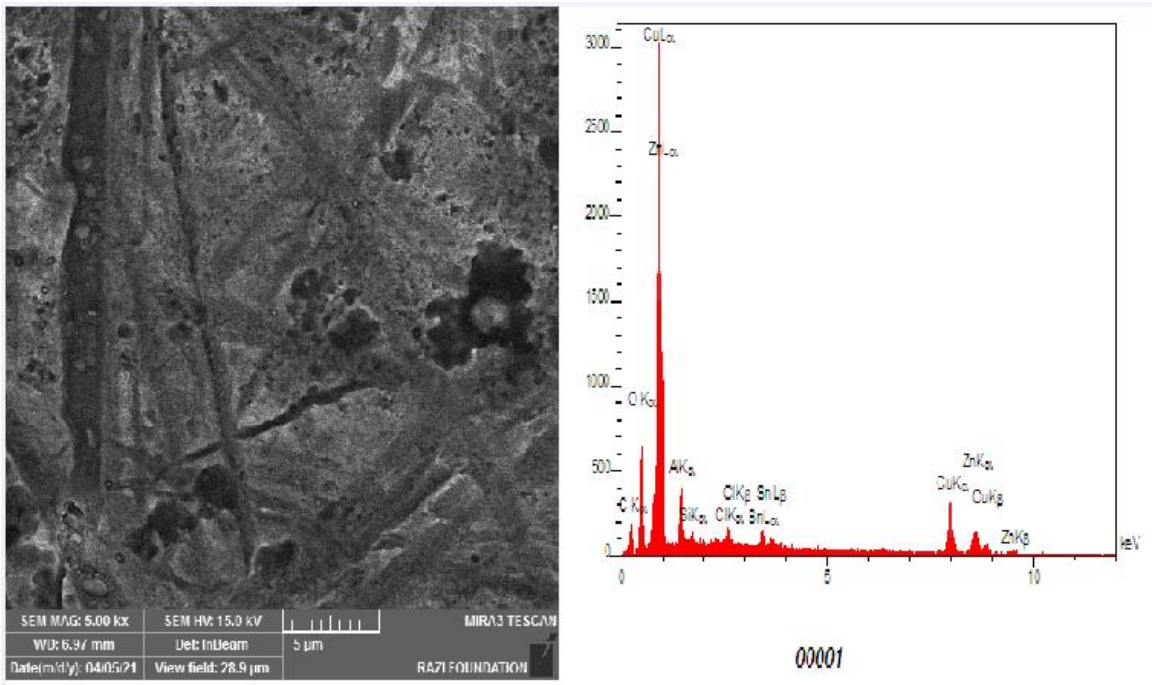

Figure (4.58): SEM image, EDS analysis for alloy A3 after simple immersion.

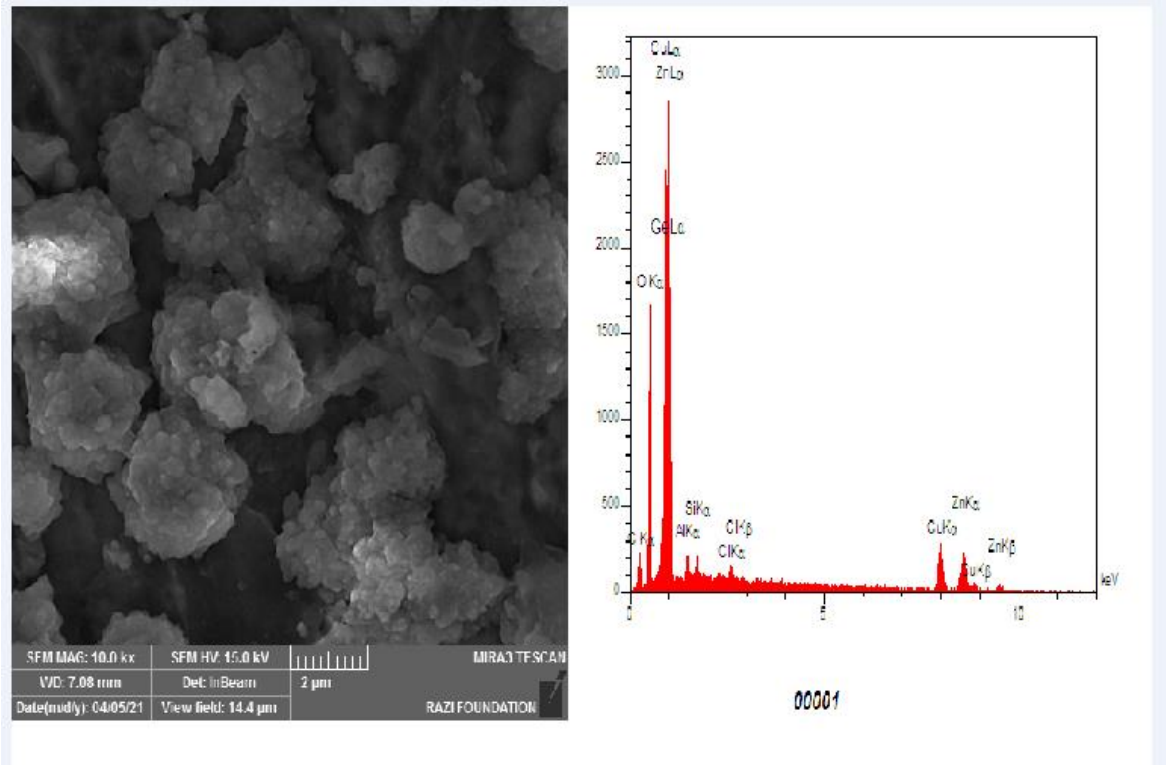

Figure (4.59): SEM image, EDS analysis for alloy A4 after simple immersion.

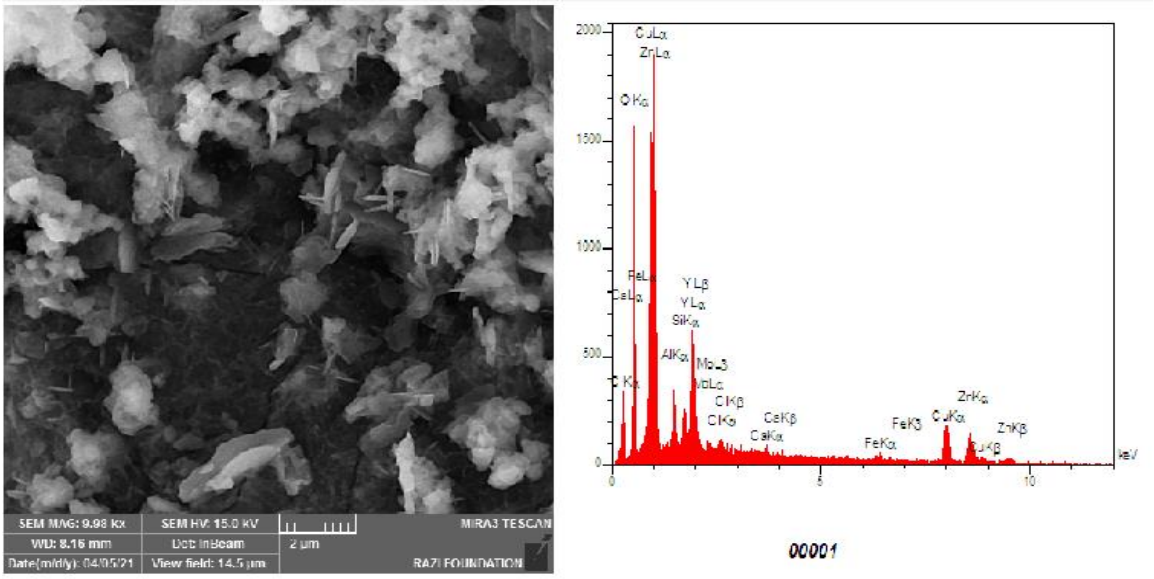

Figure (4.60): SEM image, EDS analysis for alloy A5 after simple immersion.

SEM and EDS observation has been done for alloys specimens A6& A7 after simple emersion test, showed in Figure (4.61) & Figure (4.62). The corrosion rate of copper alloy after addition of aluminum is lower than that of the copper alloy without aluminum. It can be determined that the addition of aluminum has a positive effect on the corrosion resistance of the alloy, this is due to perception of nickel- aluminum intermetallic compound Ni3Al, with a body centered cubic structure.

While, Figure (4.63) and Figure (4.64) observed SEM and EDS for alloys specimens A8& A9 after simple emersion test, It is evident that the films cover entire surface area and are made up of layer of rice grain like crystals and clusters of small grainy deposits. In addition, there are few patches of compact deposits in the film formed on Zn test containing alloys.

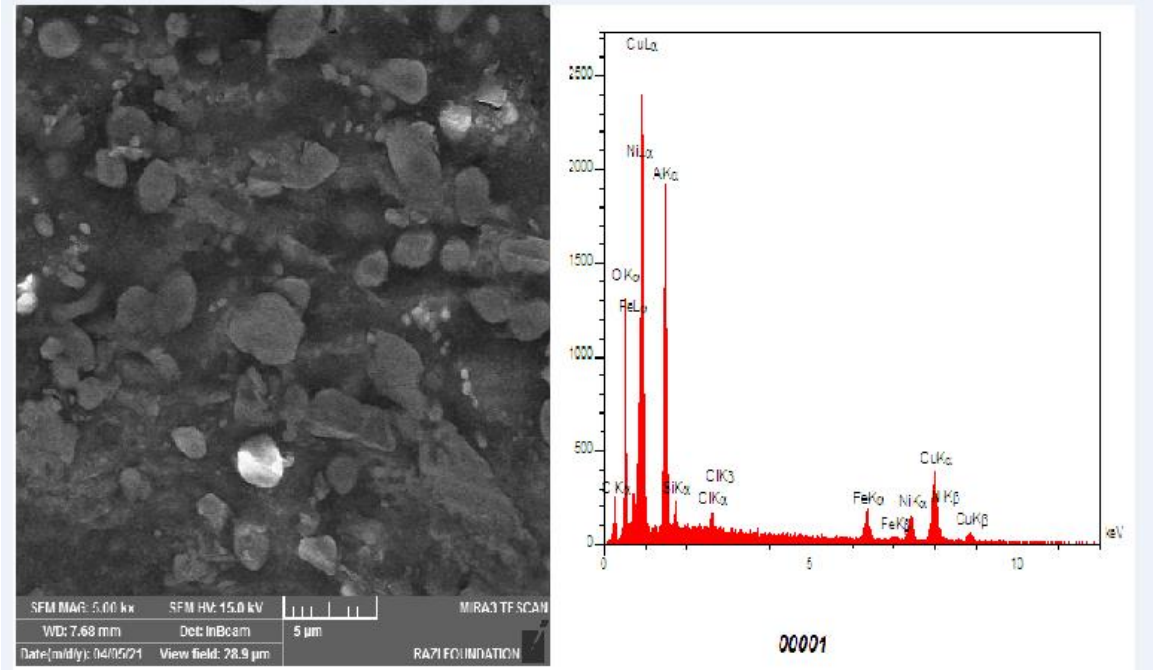

Figure (4.61): SEM image, EDS analysis for alloy A6 after simple immersion.

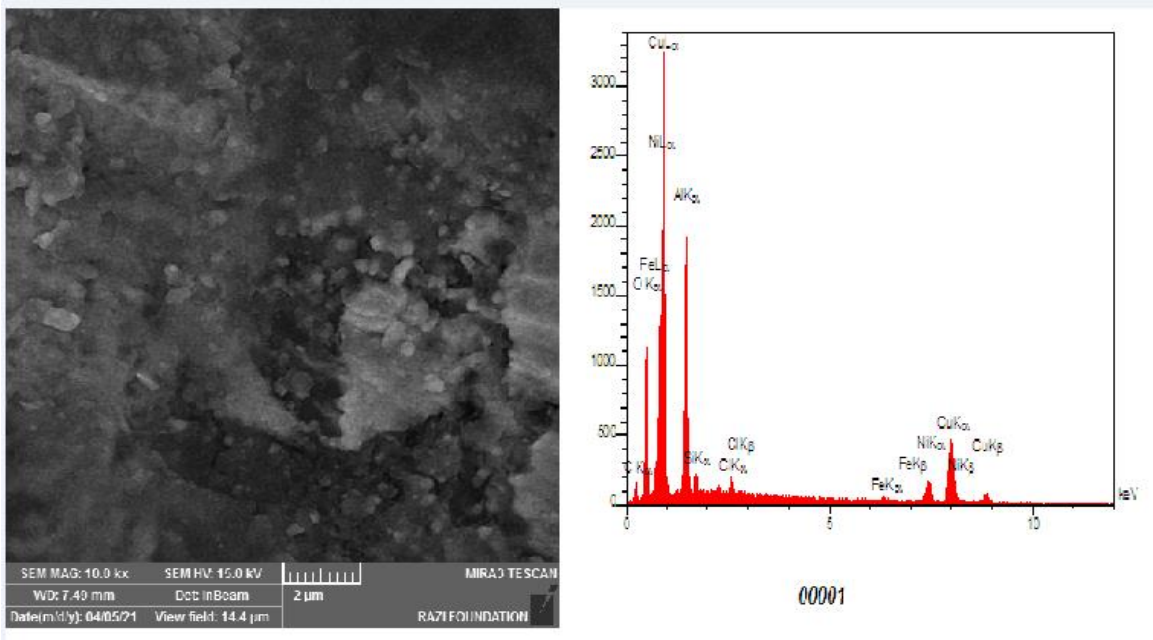

Figure (4.62): SEM image, EDS analysis for alloy A7 after simple immersion.

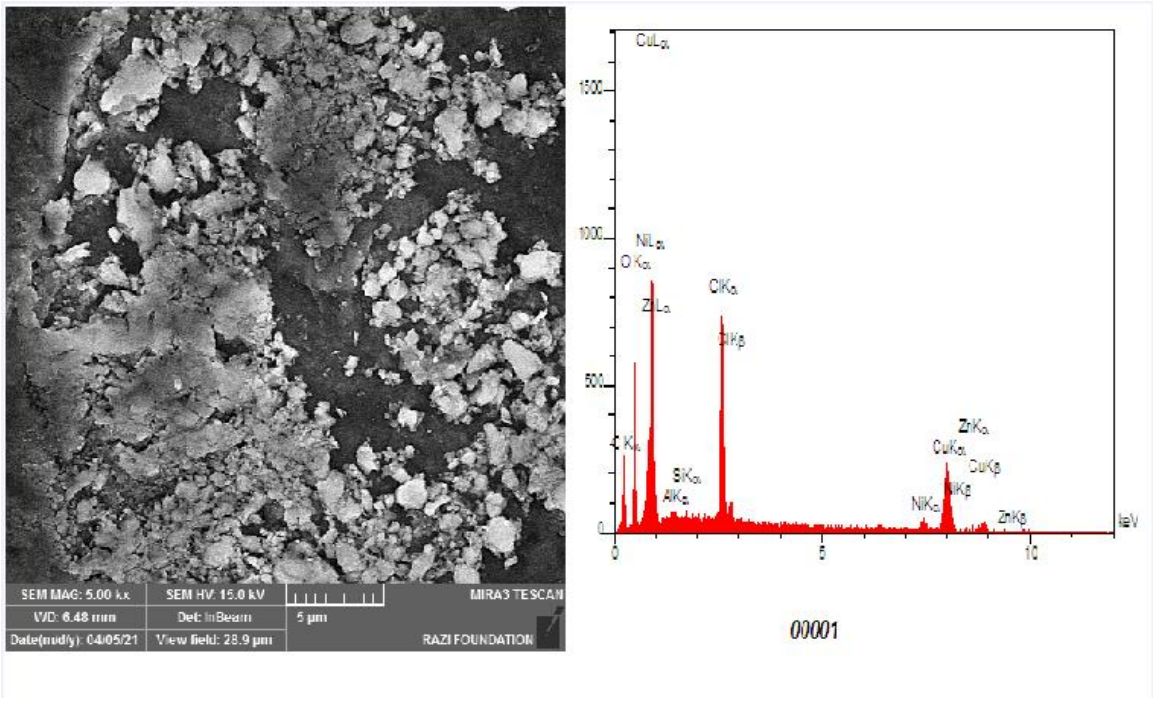

Figure (4.63): SEM image, EDS analysis for alloy A8 after simple immersion.

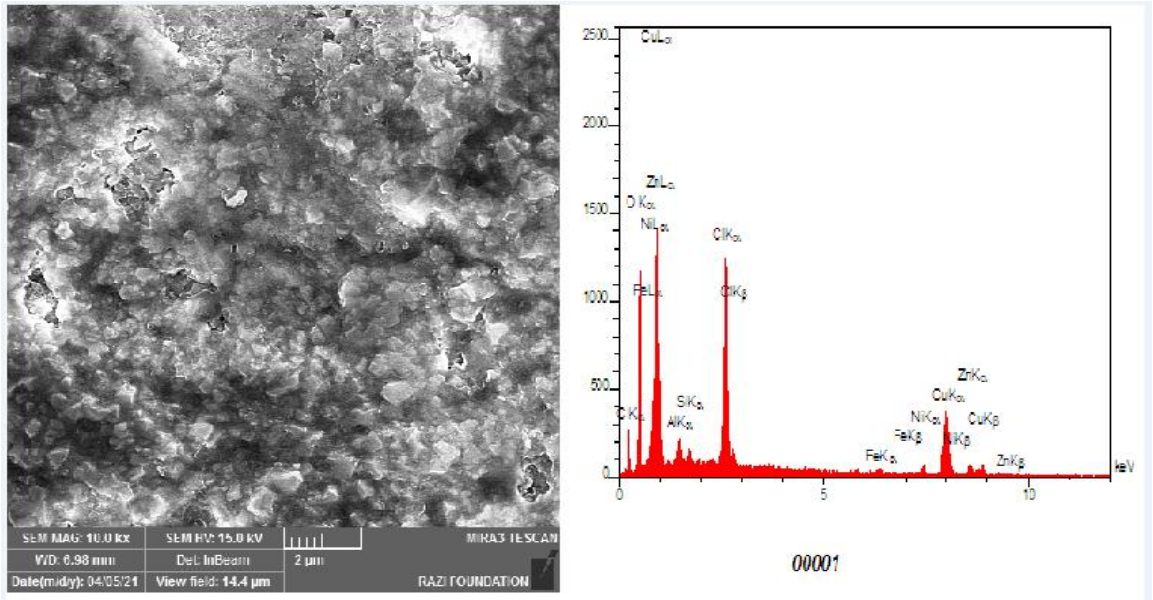

Figure (4.64): SEM image, EDS analysis for alloy A9 after simple immersion.

4.8.2 Scanning Electron Microscope for Alloys after Erosion-Corrosion Test.

Scanning electron microscope (SEM) has been employed to observe the corroded surfaces of alloys. The morphology of the all alloys specimens are shown in Figure (4.65) to Figure (4.73), the surface of alloy appeared corrosion products. The corrosion behaviors have obtained by the erosion-corrosion (salt solution) test have revealed the corrosion mechanism that chloride ions attacked the surface of alloy to enhance dissolubility, thus hindering the formation of protective films and leading to the corrosion process.

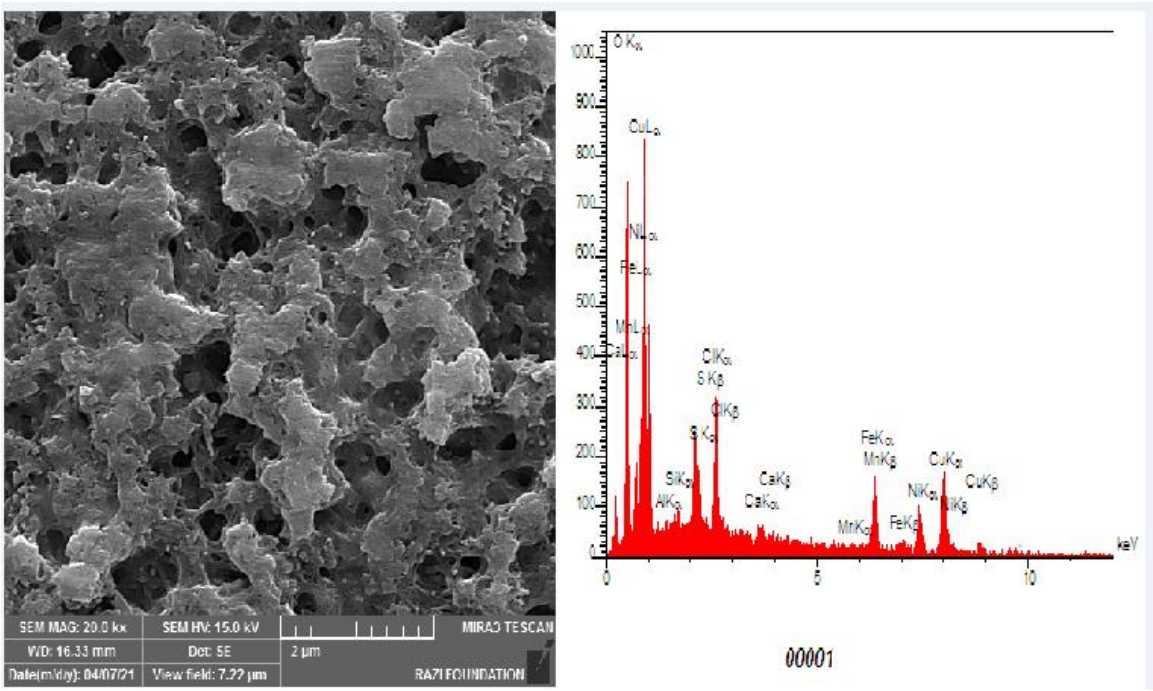

Figure (4.65): SEM image, EDS analysis for alloy A1 after erosion corrosion.

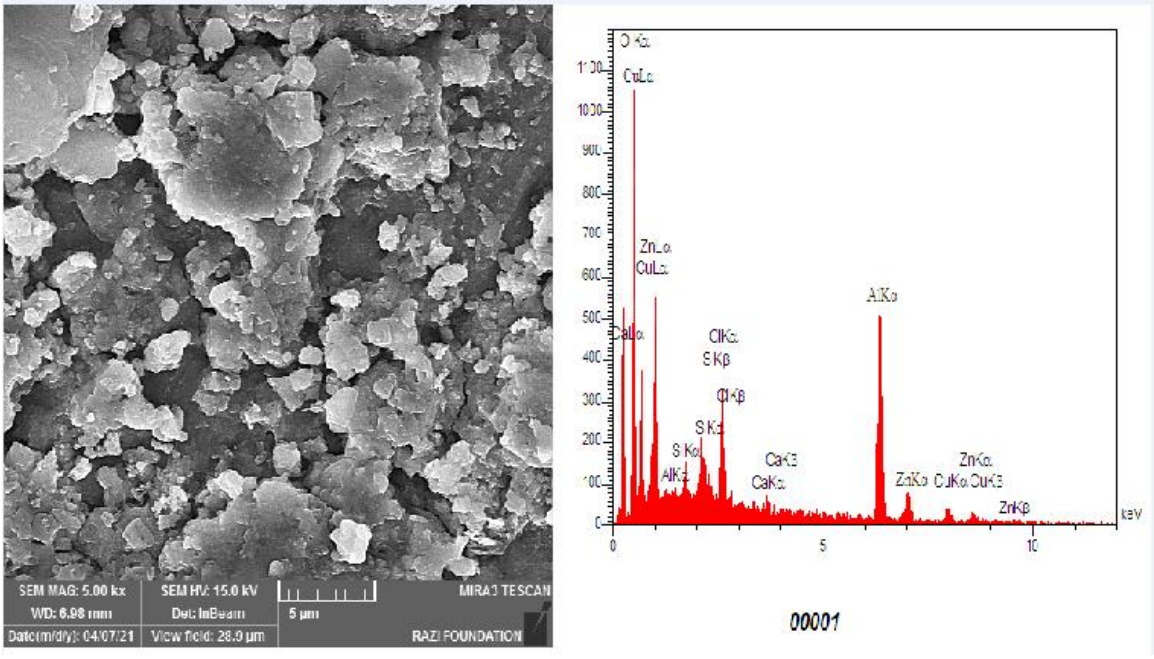

Figure (4.66): SEM image, EDS analysis for alloy A2 after erosion corrosion.

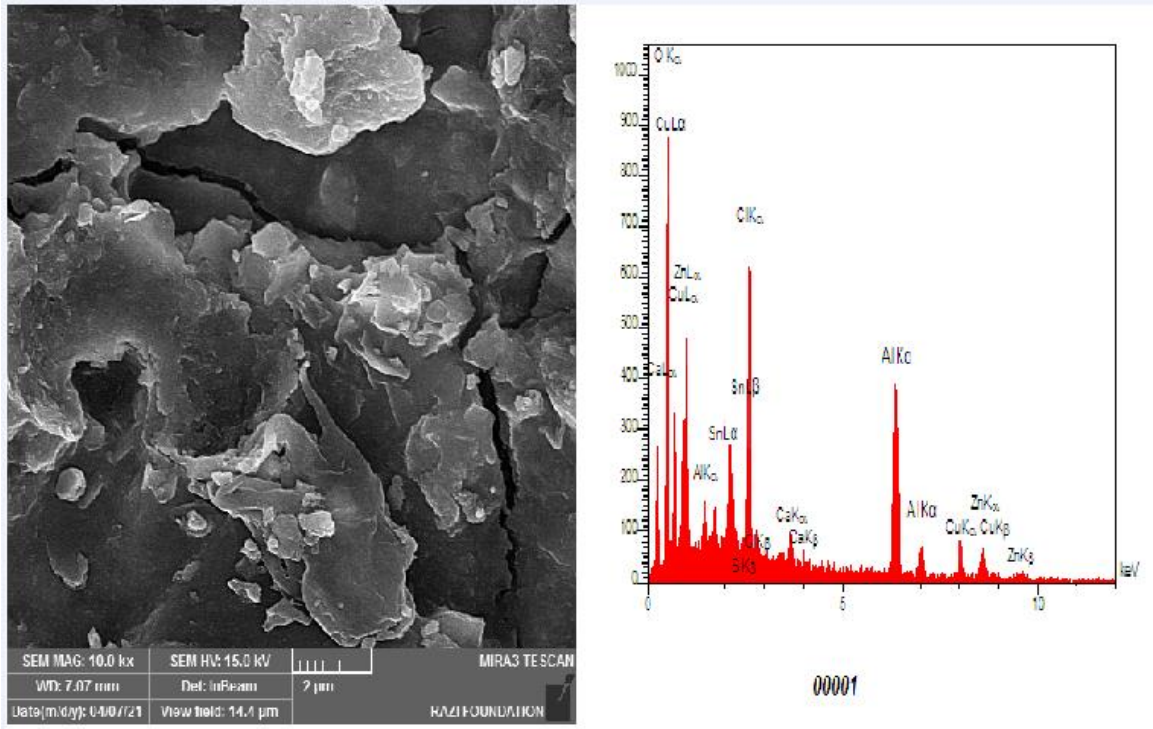

Figure (4.67): SEM image, EDS analysis for alloy A3 after erosion corrosion.

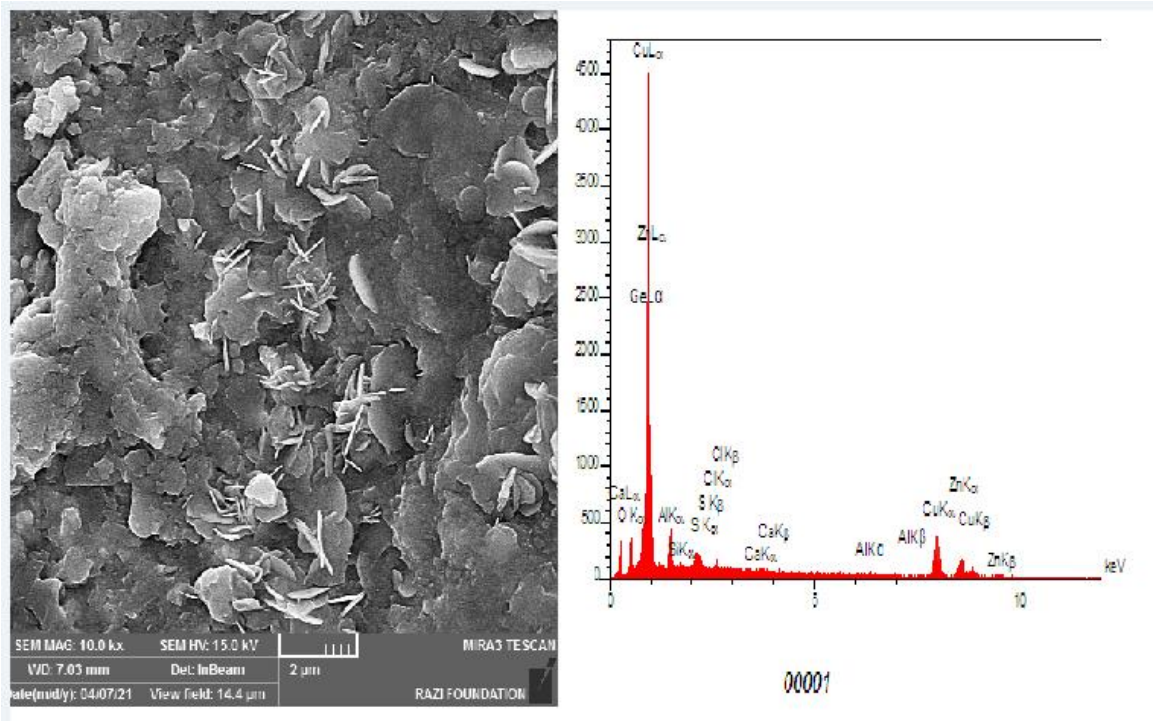

Figure (4.68): SEM image, EDS analysis for alloy A4 after erosion corrosion.

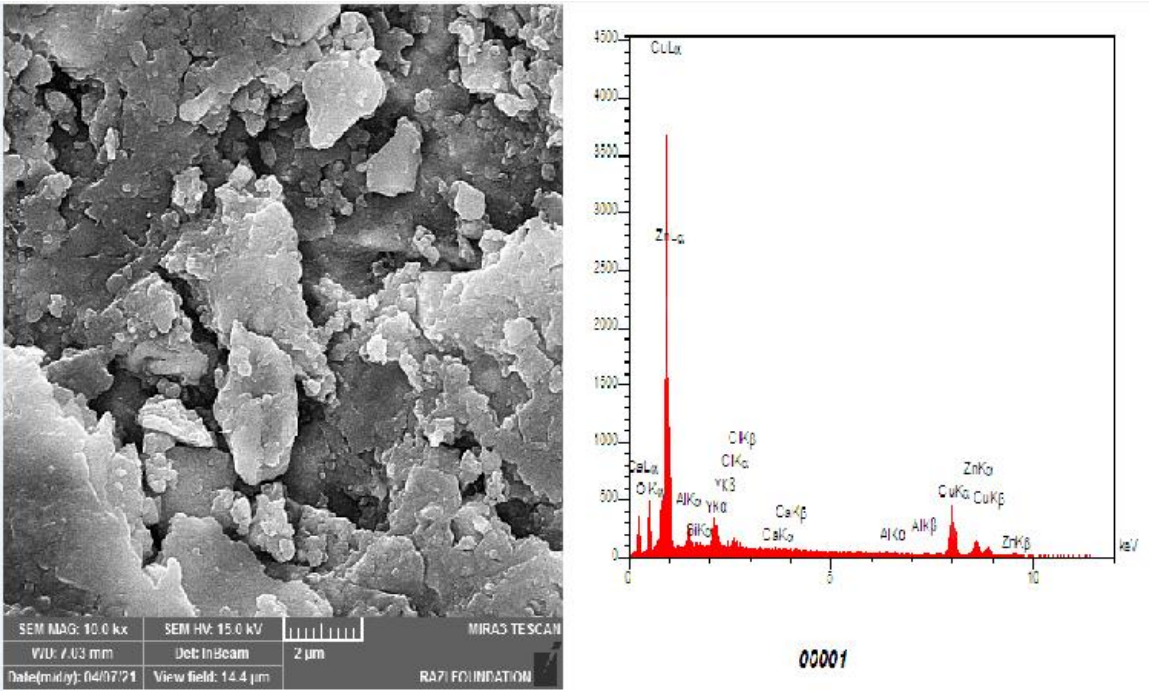

Figure (4.69): SEM image, EDS analysis for alloy A5 after erosion corrosion.

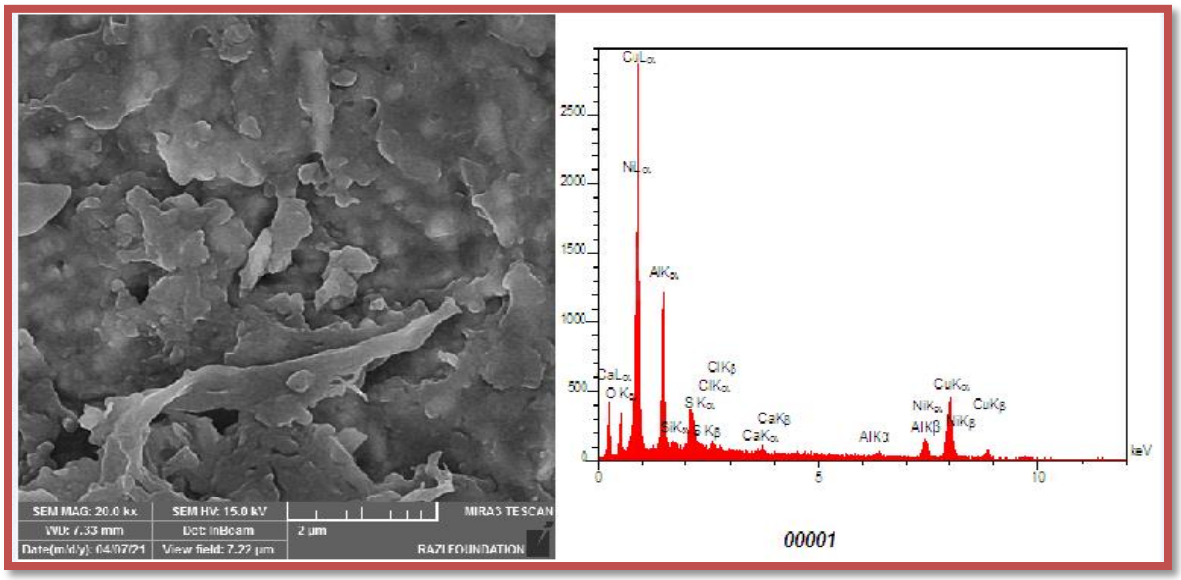

Figure (4.70): SEM image, EDS analysis for alloy A6 after erosion corrosion.

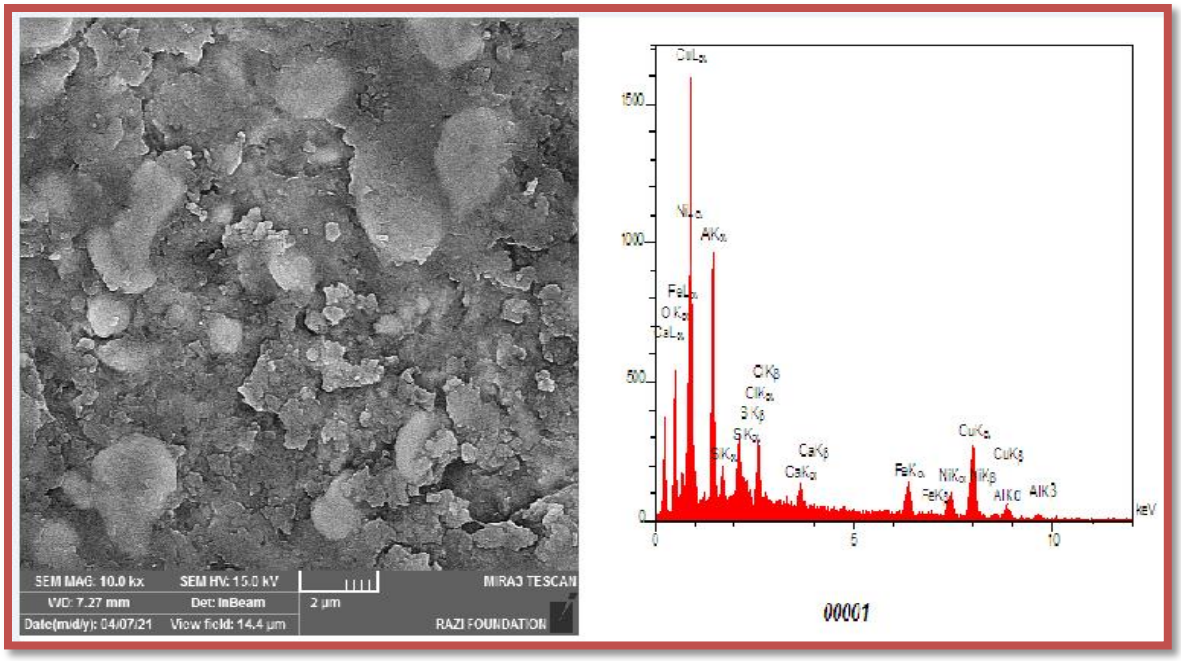

Figure (4.71): SEM image, EDS analysis for alloy A7 after erosion corrosion.

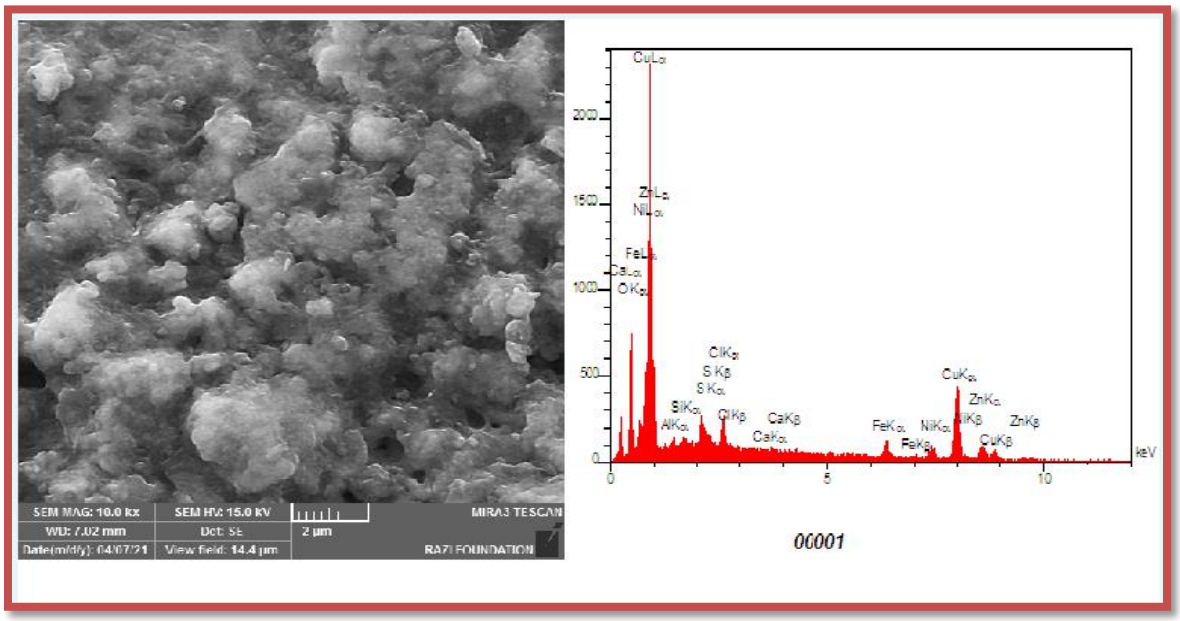

Figure (4.72): A .SEM image, B.EDS analysis for alloy A8after erosion corrosion.

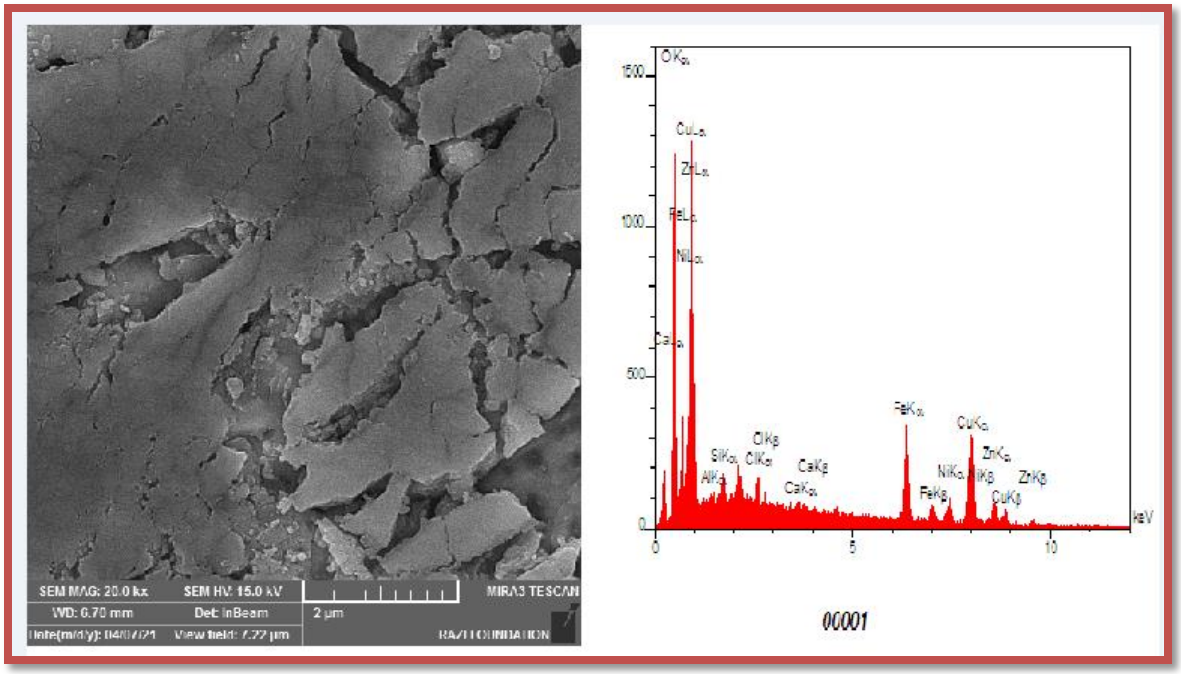

Figure (4.73): SEM image, EDS analysis for alloy A9 after erosion corrosion.

4.8.3 SEM Images for Alloys after Oxidation Test.

Scanning electron microscope (SEM) and EDS has been employed to observe the oxidized surfaces of alloys. The morphology of the A1(Cu-Ni) specimen is shown in Figure (4.74) shows, the surface of alloy appeared fractures in the oxide layer formed on the surface of alloy, this attributed that rate of oxidation increases with increase temperature and time which leads increasing the thickness of oxide which will become stratified, due to change in nature and composition of it, and this increase make oxide layer more exposing to fracture caused of existence high thermal stresses and much defects such as voids and cracks.

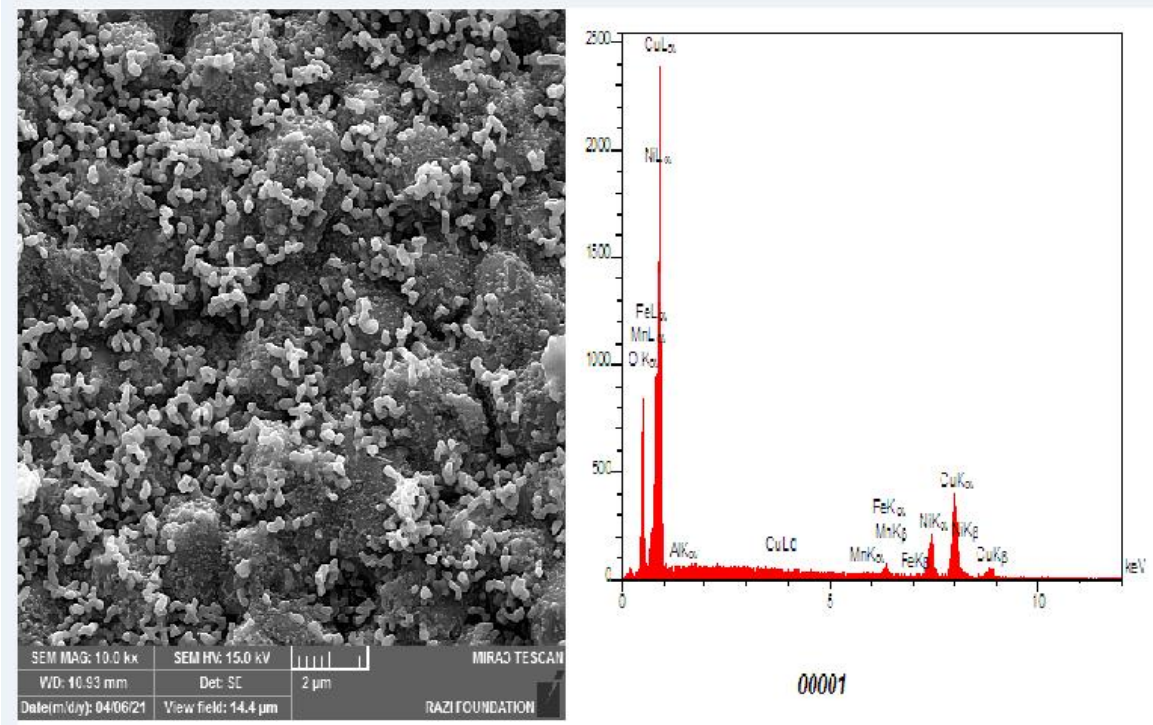

Figure (4.74): SEM image, EDS analysis for alloy A1 after Oxidation process.

While when Aluminum element has been added (A2) will decrease rate of oxidation, where the formed Al_2O_3 layer provides enough protective, but when tin, germanium, and yttrium are added will provide more protective to alloys(A3,A4,and A5), this attributed to fact that the germanium improves plasticity and adhesion of oxide layer with surface of alloy Figure (4.75) to Figure (4.78).

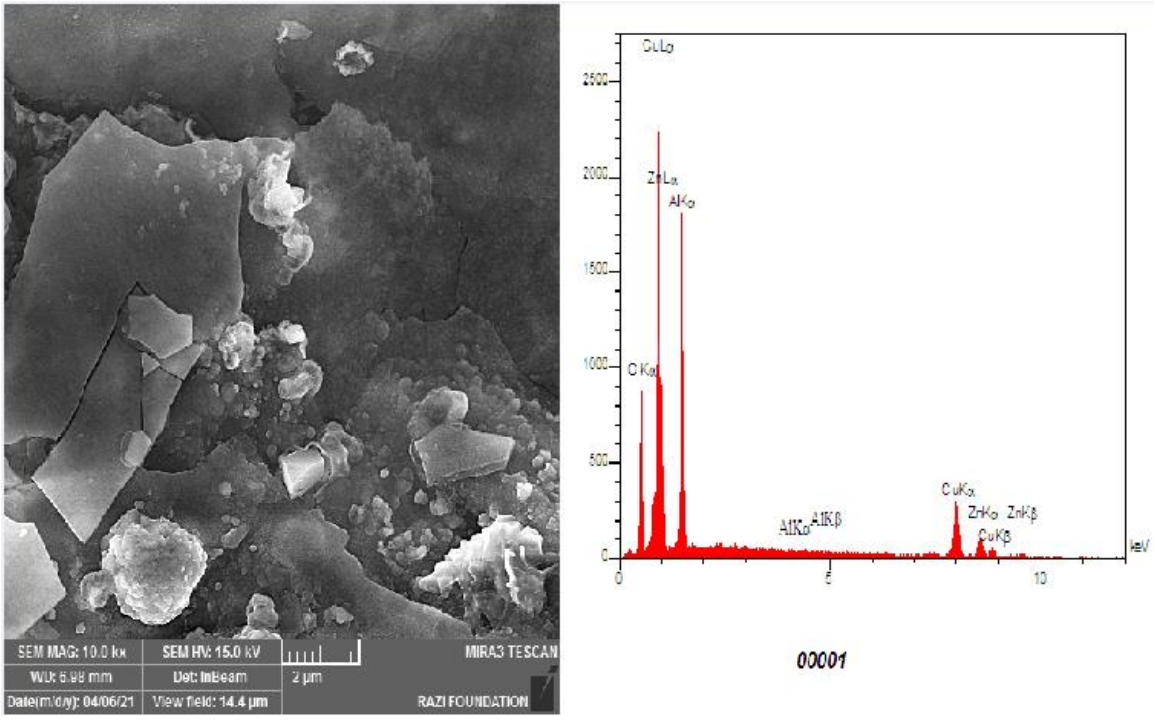

Figure (4.75): SEM image, EDS analysis for alloy A2 after Oxidation process.

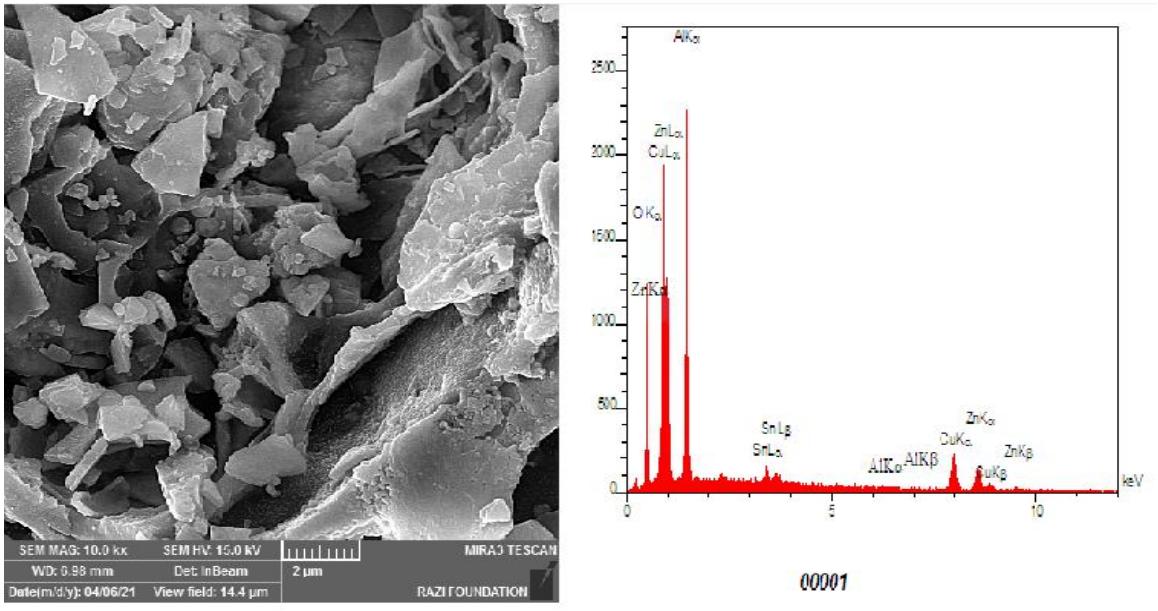

Figure (4.76): SEM image, EDS analysis for alloy A3 after Oxidation process.

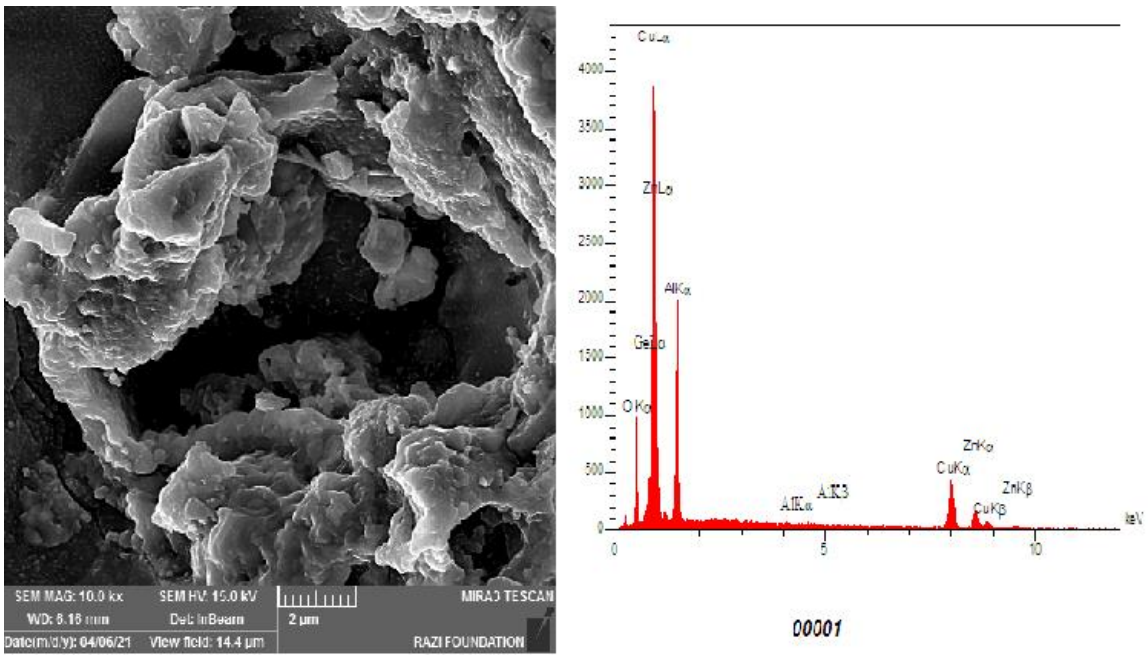

Figure (4.77): SEM image, EDS analysis for alloy A4 after Oxidation process.

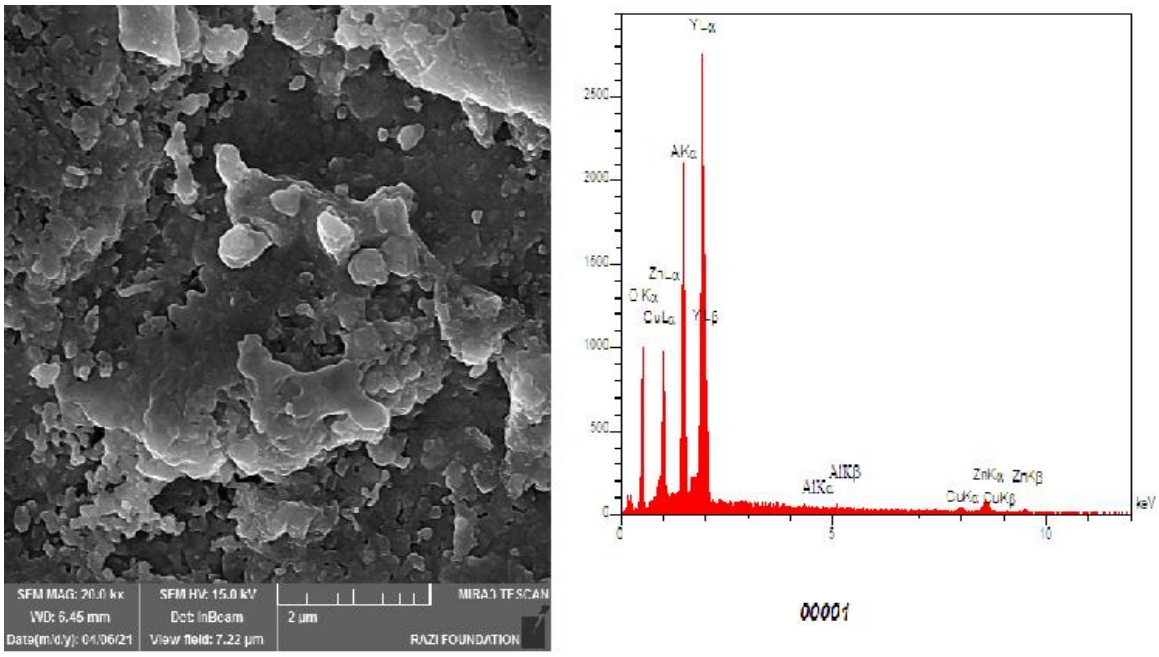

Figure (4.78): A .SEM image, B.EDS analysis for alloy A5 after Oxidation process.

SEM and EDS observation has been done for alloys specimens A6, A7, A7, and A8 after oxidation test, showed in Fig.(4.79) to fig.(4.82).Addition Al, Zn, and Fe will provide more protective to alloys, due to the effect of these elements in building the protective oxide layer and improving the adhesives of it.

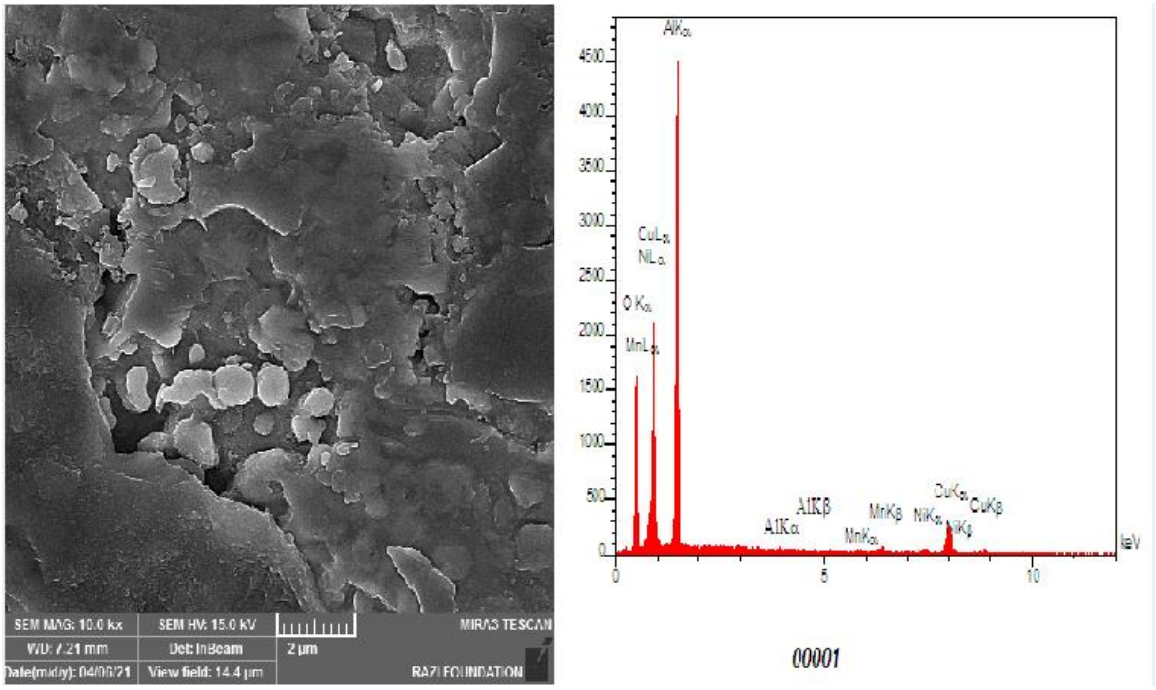

Figure (4.79): SEM image, EDS analysis for alloy A6 after Oxidation process.

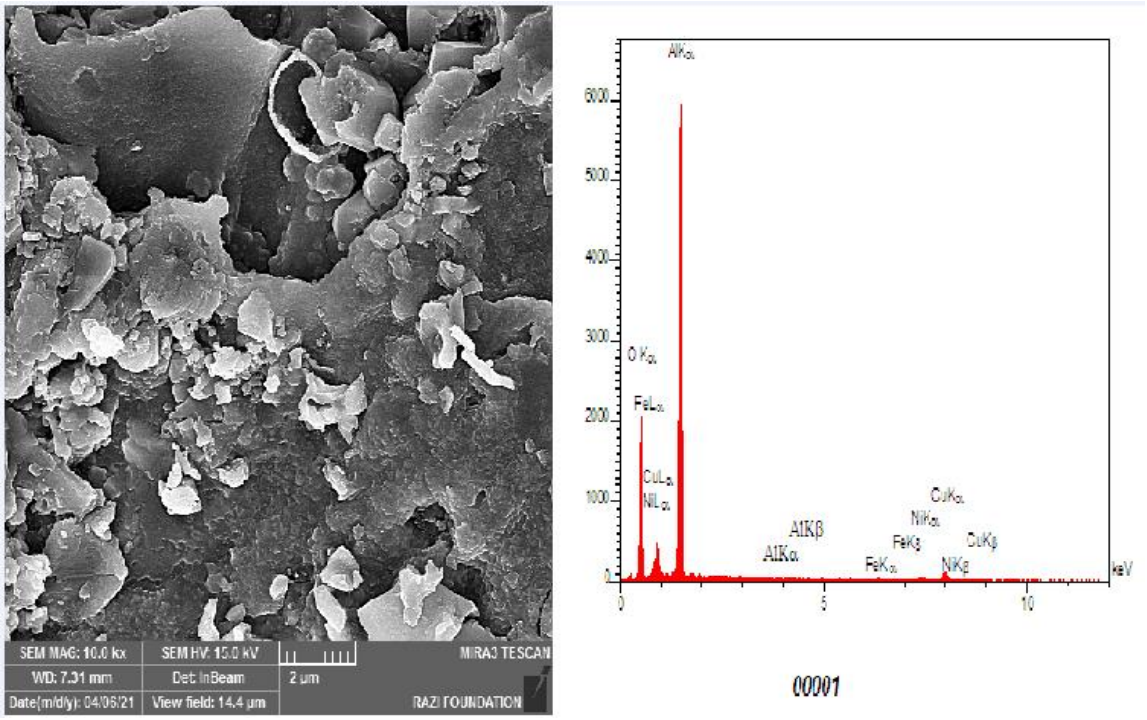

Figure (4.79): SEM image, EDS analysis for alloy A7 after Oxidation process.

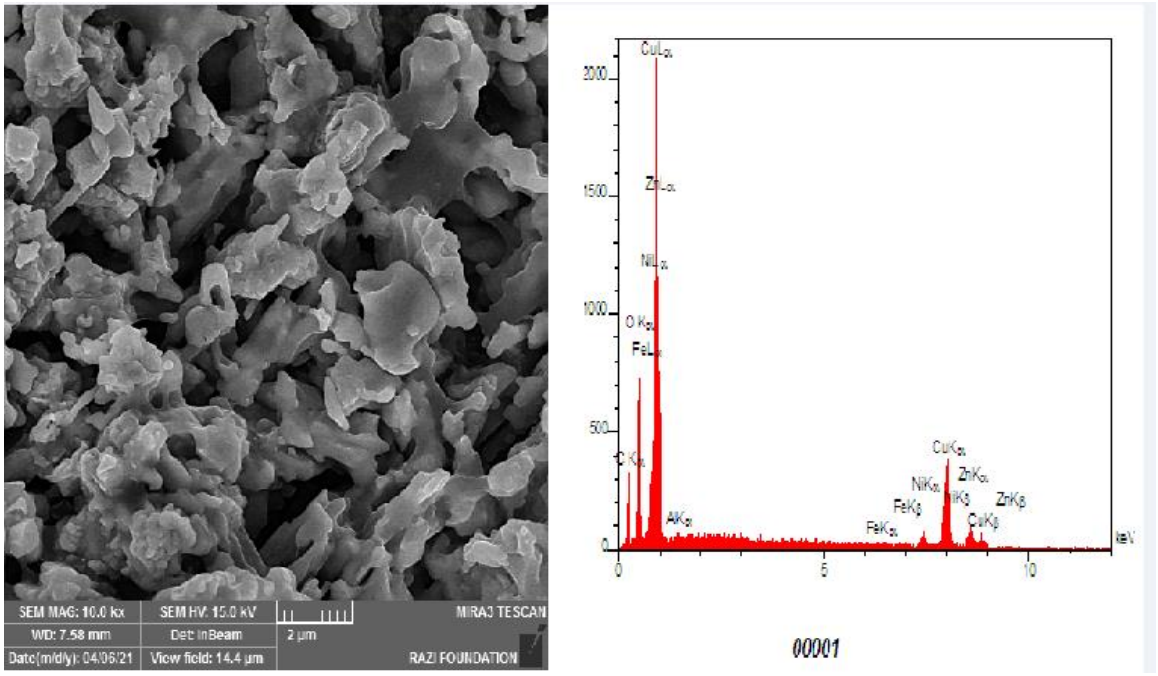

Figure (4.80): SEM image, EDS analysis for alloy A8 after Oxidation process.

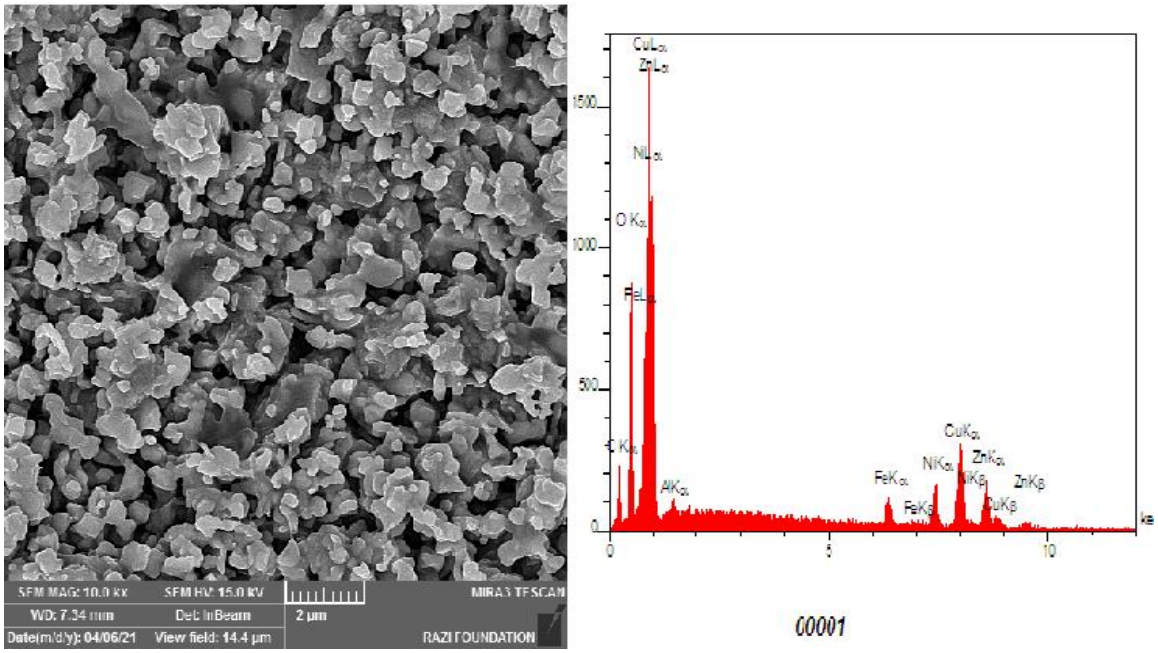

Figure (4.81): SEM image, EDS analysis for alloy A9 after Oxidation process.

Chapter Five
Optimization

5.1 Introduction

Particle swarm optimization has been a common heuristic methodology in the community of optimization, with numerous scholars investigating principles, problems, and algorithm implementations. No clear definition of exactly what is included in modern technical implementations has existed yet despite this consideration.. A standard here is intended to extend the original algorithm uncomplicated, while taking note of current advances that can be predicted to increase performance with standard measurements. The standard algorithm is designed both for use as a basis for testing performance of technological upgrades and for representing the PSO for the wider optimization community.

PSO is a heuristic Mehta method that Kennedy and Eberhart proposed initially. The program simulates the behavior of birds in search of a suitable site and flying together in multi-dimensional spaces, adapting their motions and distances for better searching. PSO is a genetic algorithm-like evolutionary computation approach (GA). Swars known as particles are randomly initialized and are then optimally searched by generations to update. PSO is called cognitive, and social, two methods. PSO has two techniques. The method imitates a particle that flies in the search area to optimize it globally. Each particle has its own speed and position that is altered in the beginning. Each particle must retain its best location known as the local best position and the best position known as the world's best among all the particles.

5.2 Representation of Solution

The particles s are makeup of real values (representing the values of the sample properties that be obtained by the laboratory tests) by using visual basic language. The size of a particles equal **N swarm** while first particle equal one that represent the **Density** properties, second particle equal one that represents the **Micro-Hardness** properties, third particle equal twenty eight that represents **Simple emersion corrosion** properties, fourth particle thirty one equal that represents the **Erosion Corrosion** ratio %, fifth particle equal thirteen that represents the **Open Circuit Potential (O.C.P)**, sixth particle equal one that represents the **Potentionstatic Polarization**, Seventh particle equal one that represents **Dry Sliding Wear**, eighth particle equal forty nine that represents **Cyclic oxidation,** ninth particle equal seventeen that represents **Thermal Shock** .

Features that used in Particle swarm optimization algorithm.

Density feature means the following:
F_1 = Drying density value at room temperature.

Micro-Hardness feature means the following:

F_2 = Vickers hardness value at load 500 g (10N) and dwelling time 10 s.

Simple emersion corrosion feature means the following:

F3= corrosion rate * 10^{-4} after 3 days.

F4= corrosion rate * 10^{-4} after 9 days.

F5= corrosion rate * 10^{-4} after 12 days.

F6= corrosion rate * 10^{-4} after 15 days.

F7= corrosion rate* 10^{-4} after 18 days.

F8= corrosion rate* 10^{-4} after 21 days.

F9= corrosion rate * 10^{-4} after 24 days.

F10= corrosion rate* 10^{-4} after 27 days.

F11= corrosion rate* 10^{-4} after 30 days.

F12= corrosion rate * 10^{-4} after 33 days.

F13= corrosion rate* 10^{-4} after 36 days.

F14= corrosion rate* 10^{-4} after 39 days.

F15= corrosion rate* 10^{-4} after 42 days.

F16= corrosion rate * 10^{-4} after 45 days.

F17= corrosion rate* 10^{-4} after 48 days.

F18= corrosion rate * 10^{-4} after 51 days.

F19= corrosion rate * 10^{-4} after 54 days.

F20= corrosion rate* 10^{-4} after 57 days.

F21= corrosion rate* 10^{-4} after 60 days.

F22= corrosion rate * 10^{-4} after 63 days.

F23= corrosion rate * 10^{-4} after 66 days.

F24= corrosion rate * 10^{-4} after 69 days.

F25= corrosion rate * 10^{-4} after 72 days.

F26= corrosion rate* 10^{-4} after 75 days.

F27= corrosion rate * 10^{-4} after 78 days.

F28= corrosion rate* 10^{-4} after 81 days.

F29= corrosion rate* 10^{-4} after 84 days.

F30= corrosion rate * 10^{-4} after 87 days.

Erosion /Corrosion Test feature means the following:

F31= Erosion Rate after 1 hour.

F32= Erosion Rate after 2 hour.

F33= Erosion Rate after 3 hour.

F34= Erosion Rate after 4 hour.

F35= Erosion Rate after 5 hour.

F36= Erosion Rate after 6 hour.

F37= Erosion Rate after 7 hour.

F38= Erosion Rate after 8 hour.

F39= Erosion Rate after 9 hour.

F40= Erosion Rate after 10 hour.

F41= Erosion Rate after 11 hour.

F42= Erosion Rate after 12 hour.

F43= Erosion Rate after 13 hour.

F44= Erosion Rate after 14 hour.

F45= Erosion Rate after 15 hour.

F46= Erosion Rate after 16 hour.

F47= Erosion Rate after 17 hour.

F48= Erosion Rate after 18 hour.

F49= Erosion Rate after 19 hour.

Open Circuit Potential (O.C.P) feature means the following:

F50= Open Circuit Potential after 5 minute.

F51= Open Circuit Potential after 10 minute.

F52= Open Circuit Potential after 15 minute.

F53= Open Circuit Potential after 20 minute.

F54= Open Circuit Potential after 25 minute.

F55= Open Circuit Potential after 30 minute.

F56= Open Circuit Potential after 35 minute.

F57= Open Circuit Potential after 40 minute.

F58= Open Circuit Potential after 45 minute.

F59= Open Circuit Potential after 50 minute.

F60= Open Circuit Potential after 55 minute.

Potentionstatic Polarization feature means the following:

F61= **Corrosion Rate (CR) mm/yr.**

Dry Sliding Wear feature means the following:

F62= Wear rate(m3/m)*10^{-4} under 10 N after 5 minute.

F63= Wear rate(m3/m)*10^{-4} under 10 N after 10 minute.

F64= Wear rate(m3/m)*10^{-4} under 10 N after 15 minute.

F65= Wear rate(m3/m)*10^{-4} under 10 N after 20 minute.

F66= Wear rate(m3/m)*10^{-4} under 10 N after 25 minute.

F67= Wear rate(m3/m)*10^{-4} under 10 N after 30 minute.

Cyclic oxidation at 450 c° feature means the following:

F68= Specific Weight Change *10^{-2} after 5 hour.

F69= Specific Weight Change*10^{-2} after 10 hour.

F70= Specific Weight Change*10^{-2}after 15 hour.

F71= Specific Weight Change *10^{-2}after 20 hour.

F72= Specific Weight Change *10^{-2}after 25 hour.

F73= Specific Weight Change*10^{-2} after 30 hour.

F74= Specific Weight Change*10^{-2} after 35 hour.

F75= Specific Weight Change*10^{-2} after 40 hour.

F76= Specific Weight Change *10^{-2}after 45 hour.

F77= Specific Weight Change *10^{-2}after 50 hour.

Cyclic oxidation at 550 c° feature means the following:

F78= Specific Weight Change*10^{-2} after 5 hour.

F79= Specific Weight Change *10^{-2}after 10 hour.

F80= Specific Weight Change *10^{-2}after 15 hour.

F81= Specific Weight Change*10^{-2} after 20 hour.

F82= Specific Weight Change *10^{-2}after 25 hour.

F83= Specific Weight Change*10^{-2} after 30 hour.

F84= Specific Weight Change*10^{-2} after 35 hour.

F85= Specific Weight Change*10^{-2} after 40 hour.

F86= Specific Weight Change*10^{-2} after 45 hour.

F87= Specific Weight Change*10^{-2} after 50 hour.

Cyclic oxidation at 650 c° feature means the following:

F88=Specific Weight Change *10^{-2}after 5 hour.

F89= Specific Weight Change *10^{-2}after 10 hour.

F90= Specific Weight Change*10^{-2} after 15 hour.

F91= Specific Weight Change *10^{-2}after 20 hour.

F92= Specific Weight Change *10^{-2}after 25 hour.

F93= Specific Weight Change *10^{-2}after 30 hour.

F94= Specific Weight Change*10^{-2} after 35 hour.

F95= Specific Weight Change *10^{-2}after 40 hour.

F96= Specific Weight Change *10^{-2}after 45 hour.

F97= Specific Weight Change *10^{-2}after 50 hour.

Cyclic oxidation at 750 c° feature means the following:

F98=Specific Weight Change*10^{-2} after 5 hour.

F99= Specific Weight Change*10^{-2} after 10 hour.

F100= Specific Weight Change*10^{-2} after 15 hour.

F101= Specific Weight Change after 20 hour.

F102= Specific Weight Change *10^{-2}after 25 hour.

F103= Specific Weight Change *10^{-2}after 30 hour.

F104= Specific Weight Change *10^{-2}after 35 hour.

F105= Specific Weight Change*10^{-2} after 40 hour.

F106= Specific Weight Change *10^{-2}after 45 hour.

F107= Specific Weight Change *10^{-2}after 50 hour.

Cyclic oxidation at 850 c° feature means the following:

F108=Specific Weight Change *10^{-2}after 5 hour.

F109= Specific Weight Change *10^{-2}after 10 hour.

F110= Specific Weight Change *10^{-2}after 15 hour.

F111= Specific Weight Change *10^{-2}after 20 hour.

F112= Specific Weight Change *10^{-2}after 25 hour.

F113= Specific Weight Change *10^{-2}after 30 hour.

F114= Specific Weight Change*10^{-2} after 35 hour.

F115= Specific Weight Change *10^{-2}after 40 hour.

F116= Specific Weight Change *10^{-2}after 45 hour.

F117= Specific Weight Change*10^{-2} after 50 hour.

Thermal Shock At Constant Time30 minutes Each Cycle (50oC) feature means the following:

F118= The change in weight (mg/mm^2) *10^{-4}at 50 c°.
F119= The change in weight (mg/mm^2) *10^{-4}at 100 c°.
F120= The change in weight (mg/mm^2) *10^{-4}at 150 c°.
F121= The change in weight (mg/mm^2) *10^{-4}at 200 c°.
F122= The change in weight (mg/mm^2) *10^{-4}at 250 c°.
F123= The change in weight (mg/mm^2) *10^{-4} at 300 c°.
F124= The change in weight (mg/mm^2) *10^{-4}at 350 c°.
F125= The change in weight (mg/mm^2) *10^{-4}at 400 c°.
F126= The change in weight (mg/mm^2) *10^{-4}at 450 c°.
F127= The change in weight (mg/mm^2) *10^{-4} at 500 c°.
F128= The change in weight (mg/mm^2) *10^{-4}at 550 c°.
F129= The change in weight (mg/mm^2) *10^{-4}at 600 c°.
F130= The change in weight (mg/mm^2) *10^{-4}at 650 c°.
F131= The change in weight (mg/mm^2) *10^{-4}at 700 c°.
F132= The change in weight (mg/mm^2) *10^{-4}at 750 c°.
F133= The change in weight (mg/mm^2) *10^{-4}at 800 c°.

The proportions of element in the alloys feature means the following:

F133= Copper Ratio %

F134= Nickel Ratio

F135=Zinc Ratio %

F136=Aluminum Ratio %

F137=Tin Ratio %

F138= Germanium Ratio %

F139=Yttrium ratio %

F140=Iron Ratio %

5.3 Implementation

The particle swarm operators are used in the particle swarm algorithm optimization procedure according to the flowchart given in **Fig.5.2**. It is not necessary to employ all of these operators in a particle swarm algorithm because each operates independently of the other, the choice or design of operators depends on the problem and the representation scheme employed.

If we have the following unconstrained question*:*

$f(X)$

$X^1 \leq X \leq X^u$

Since X^1 and X^u they represent the upper and lower limits of the X vector, respectively, the steps of the PSO algorithm can be implemented as follow:

1- Suppose that the size of the swarm (the number of particles in the swarm) is denoted by the symbol N, to reduce the number of evaluations of the target function required to find the solution, the size of the swarm must be small, and in this case finding the optimal solution takes longer, and the size of the swarm is usually between 20 And 30 particles as a compromise.

2- Generating the elementary population of X in the range [Xl, Xu] randomly such as X1, X2, …….., XN, then for the purpose of convenience the position of the particle j and its velocity in repetition i are represented Xj and Vj(i) respectively, Therefore, the particles generated at the beginning are denoted by X1(0), X2(0), …….., XN(0). If the vectors Xj(0), j= (1, 2,….., N) are called particles or particles coordinate vectors,

then the objective function corresponding to the particles is calculated as $f[X_1(0)]$, $f[X_2(0)]$, $f[X_N(0)]$.

3- Finding the velocity of the particles, since all the particles move to the optimum point using their velocity, and in the beginning the velocity of all the particles is zero and we set the repetition counter i=0.

4- In iteration i, we find the following two important and used parameters of the particle j:

a- Best local particle position.

b- Find the velocity of the particle j in repetition i as follows:

$$Vj(i)= Vj(i-1)+ c1r1[Pbest – Xj(i-1)] +c2r2[Gbest – Xj(i-1)] \quad , j=1, 2, \ldots,N \quad \ldots.(1)$$

As that:

Vj: Represents the particle's speed in iteration.

c1, c2: The acceleration coefficients usually take the value 2 .

r1, r2: They represent random values that lie within the range (0,1).

Pbest: It represents the best position for the current particle of the swarm.

Gbest :It represents the best particle position within the whole swarm.

We find the position or coordinate of the particle in the repetition in the following:

$$Xj(i)= Xj(i-1) + Vj(i) \quad , j=1,2,\ldots\ldots\ldots,N \quad \ldots\ldots\ldots\ldots\ldots\ldots.(2)$$

Then the objective function corresponding to the particles is calculated

$f[X_1(i)], f[X_2(i)], \ldots\ldots\ldots\ldots\ldots f[X_N(i)]$.

5- The convergence of the current solution is examined, and if the locations of all the particles are close to the same set of values, then this means that the convergence has occurred, but if the convergence criterion is not achieved, the fourth step is repeated by updating the iteration counter to be $i= i+1$ and calculating new values for Pb_{est} and G_{best}. The iterative process continues until all the particles approach the same optimal solution.

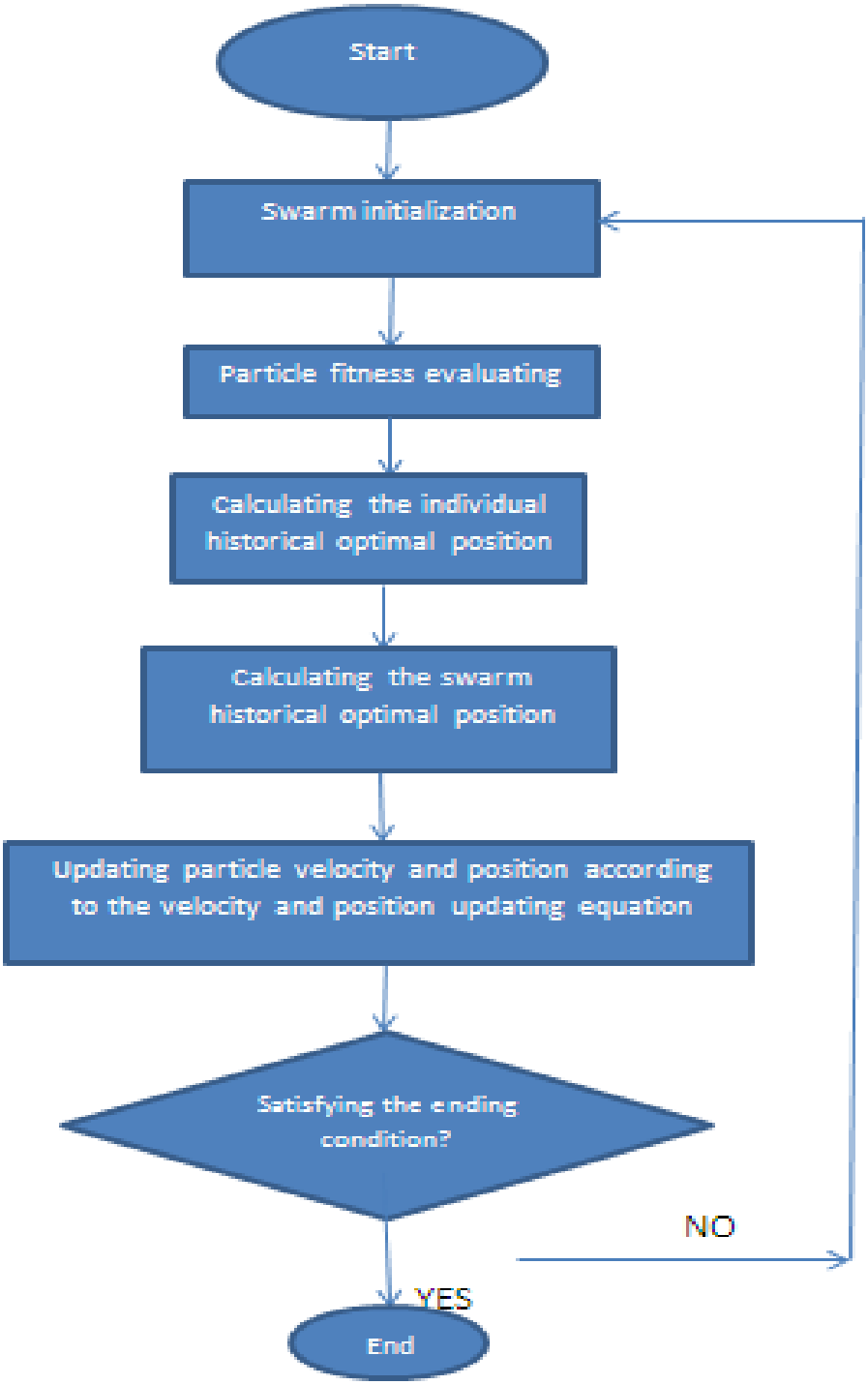

Figure (5.1): Flowchart of the particle swarm optimization algorithm

5.4 Results and Discussion

This study provides method to reach to the optimum sample using the Particle swarm optimization method, which is represented by the statistical parameters and genetic algorithms, where the use of data obtained from experiments to determine the optimum properties of samples (i.e. in this research eight of the properties of samples have been identified), accordingly, the database was built to describe samples is depending on their properties. Results showed Particle swarm optimization algorithm Figs.(5-3)-(5.17).

Step1 load the alloys database that contain the (**75**) alloys and (**147**) features (represented mechanical properties such as density test, hardness test , **Simple emersion corrosion** test, **Erosion Corrosion test, Open Circuit Potential (O.C.P)** test, **Potentionstatic Polarization test, Dry Sliding Wear test, Cyclic oxidation test,Thermal Shock test** with (**F1,F2,F3-F10,F11-F18,F19-F26 ……. and F147**) respectively.

Step 2 convert the values of above database to the values in the range [**0,1**].

Step 3 in this work, we apply the particle swarm optimization to find the optimal sample by using global optimization.

Particle swarm optimization algorithm is applied to find the best values of the final results of alloys features. Before this, we need to determine some of parameters related to PSO such as (Swarm size= 75 particles, Acceleration factoeor / alpha= 2, Acceleration factoeor / beta= 2, First number parameter

/E1 within [0,1]= 0.1, S number parameter /E2 within [0,1]= 0.7, Maximum iteration size =75, Iteria weight w_min. within[0,1]=0.3, Iteria weight w_max. within[0,1]=0.9.

Using Visual Basic, the algorithm steps described in the previous paragraph were implemented. The PSO algorithm was initialized with a set of random elements, and then searched for the best solution by updating these generations. In each iteration, each of the elements within the set is updated by following the optimal values of these elements. Which is represented by finding the value of P_{best} (the best position of the current particle in the swarm) and G_{best}(the best position of the particle within the whole swarm), and after finding the values, the elements adjust their speed and position according to the equation. The figures (5.2 to 5.17)show the results of implementing this algorithm.

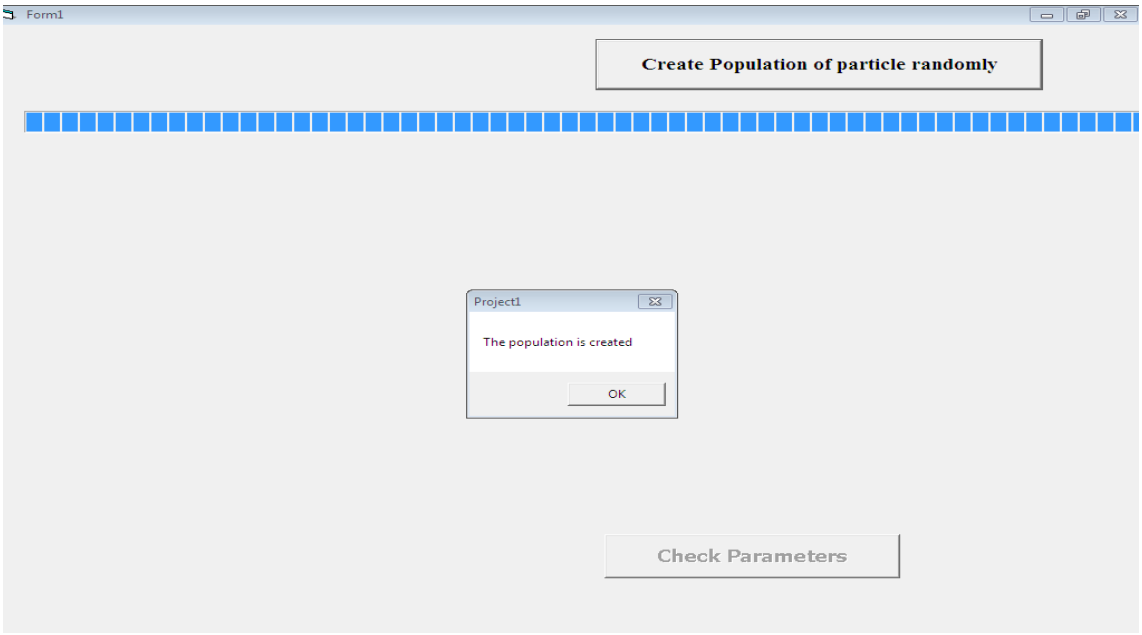

Figure (5.2): Load the samples database.

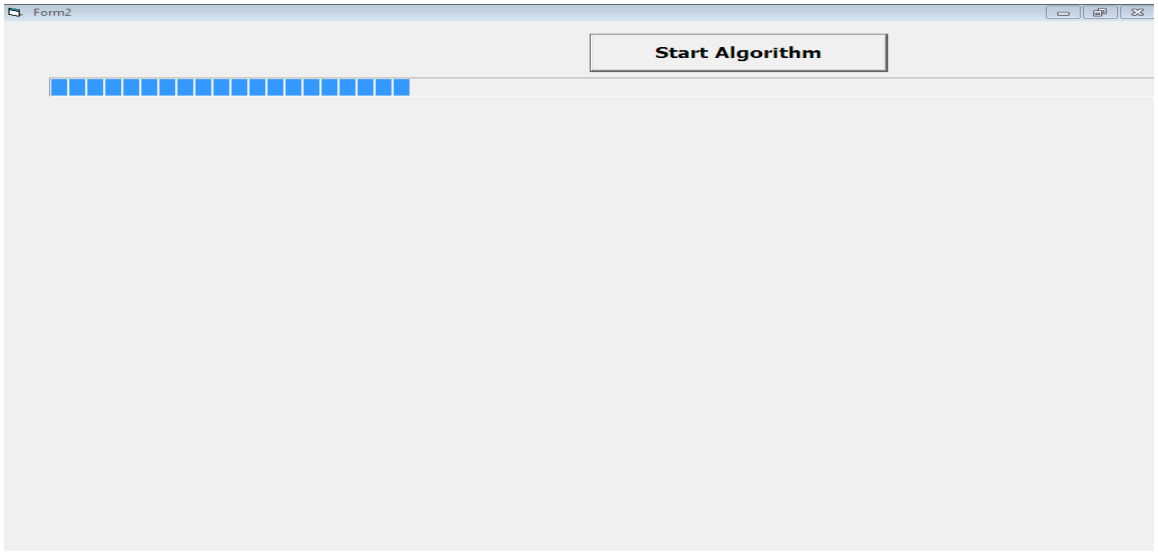

Figure (5.3): Transformation of alloys database.

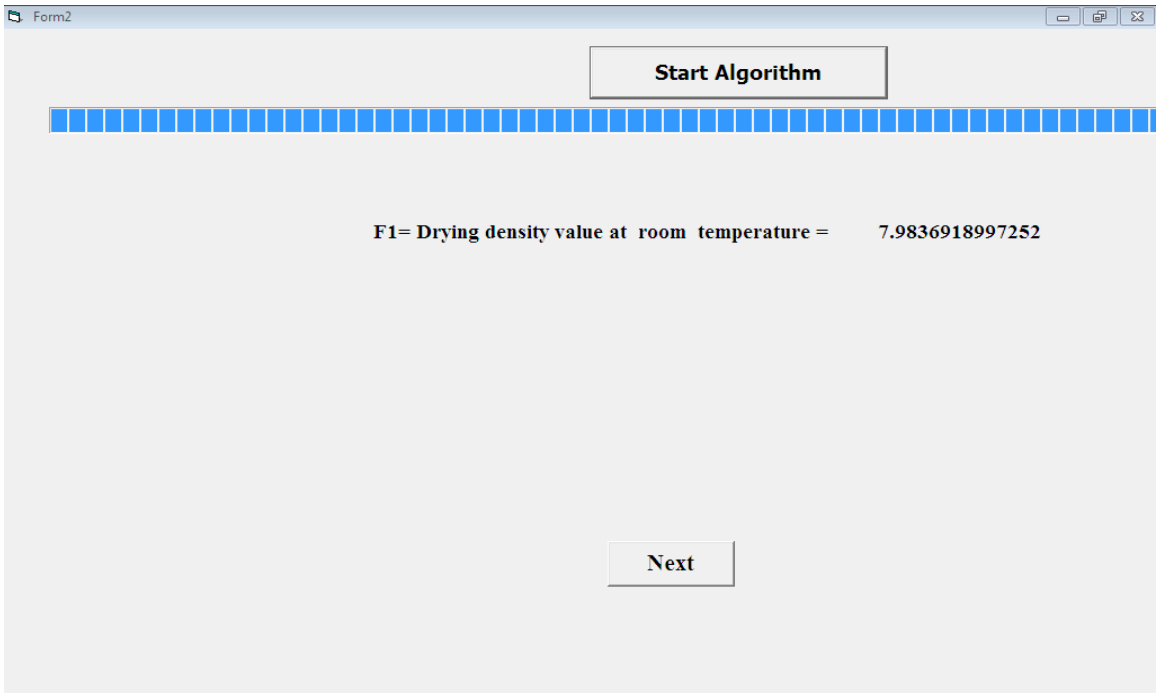

Figure (5.4): Results of PSO for density test.

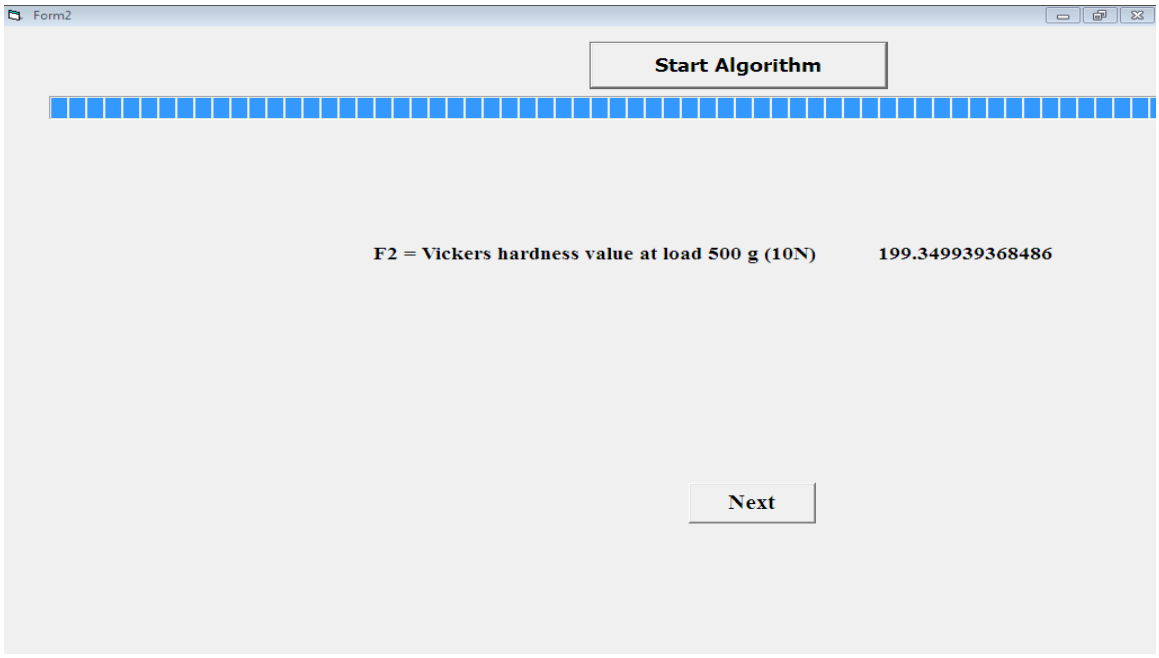

Figure (5.5): Results of PSO for Vickers hardness test

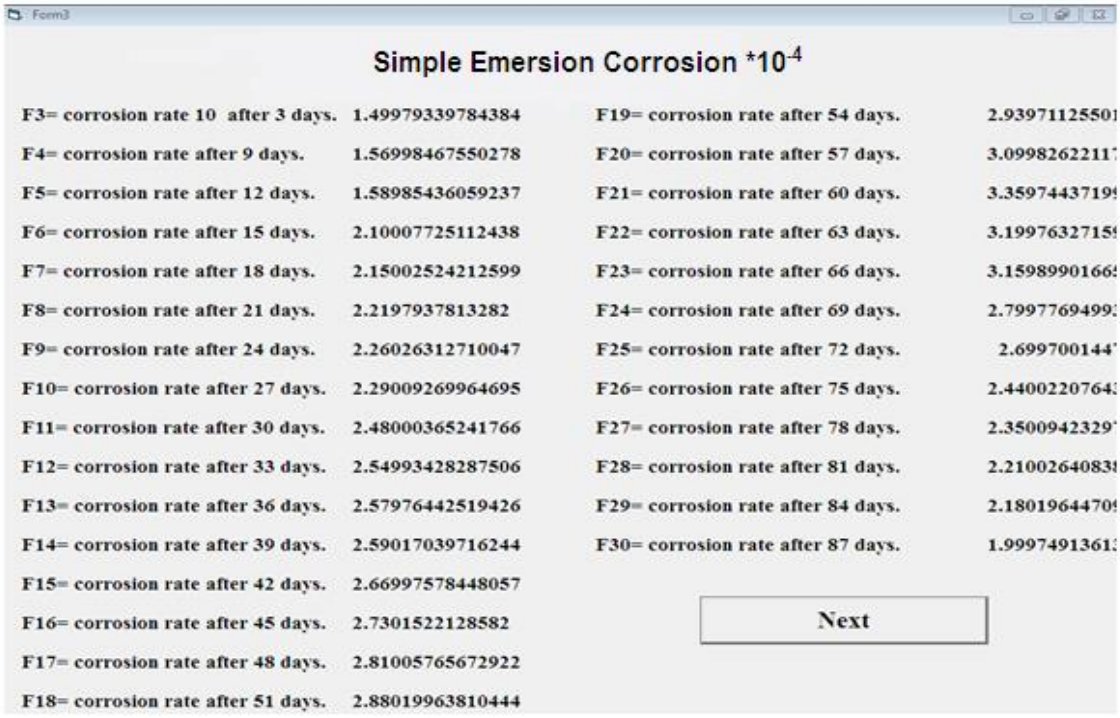

Figure (5.6): Results of PSO for simple emersion test

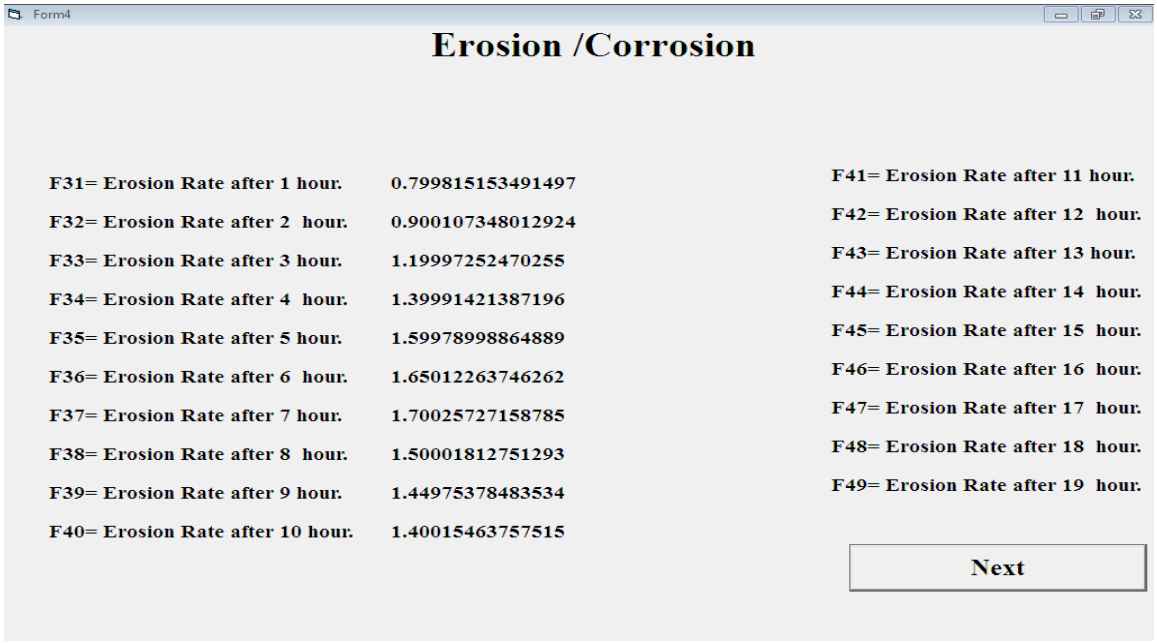

Figure (5.7):Results of PSO for erosion test

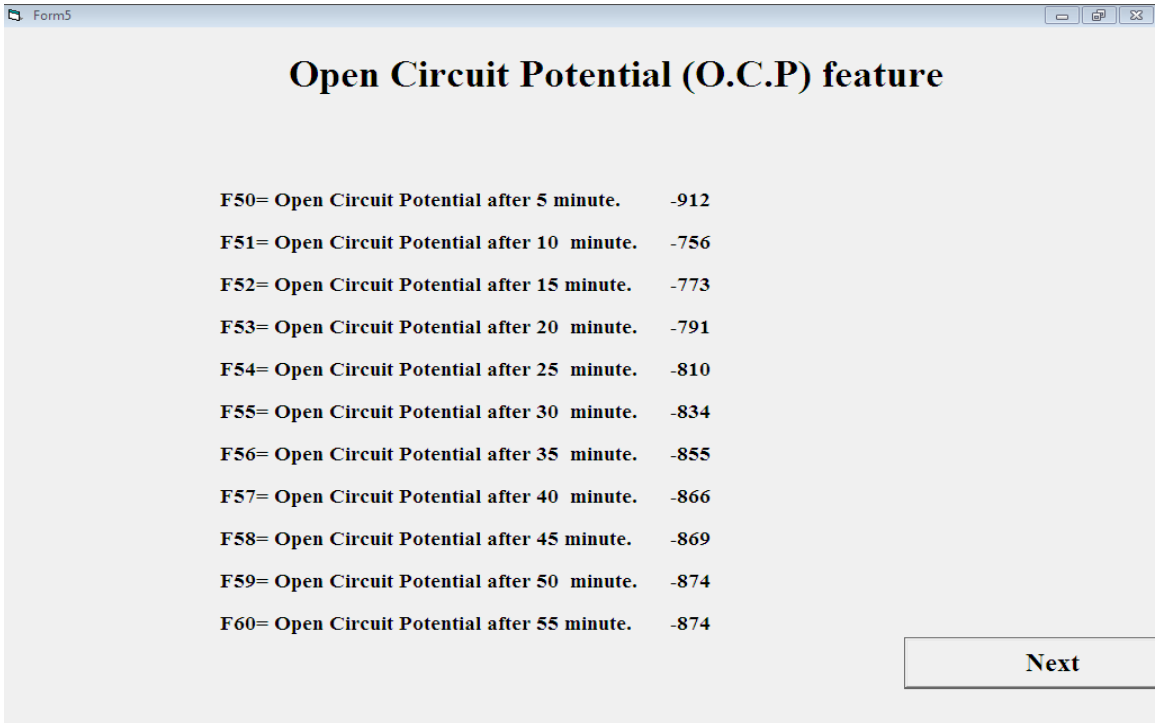

Figure (5.8): Results of PSO for open circut test

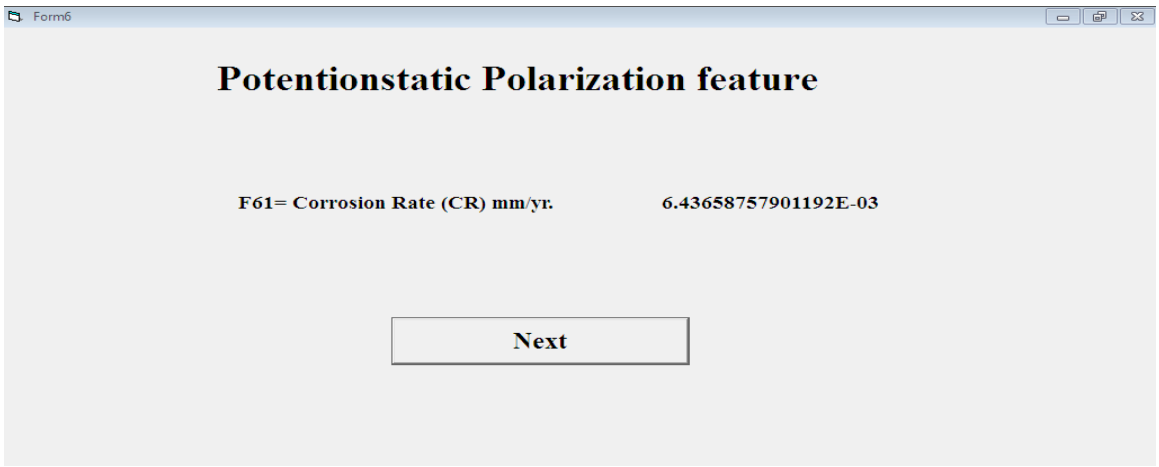

Figure (5.9): Results of PSO for Tafel polarization test

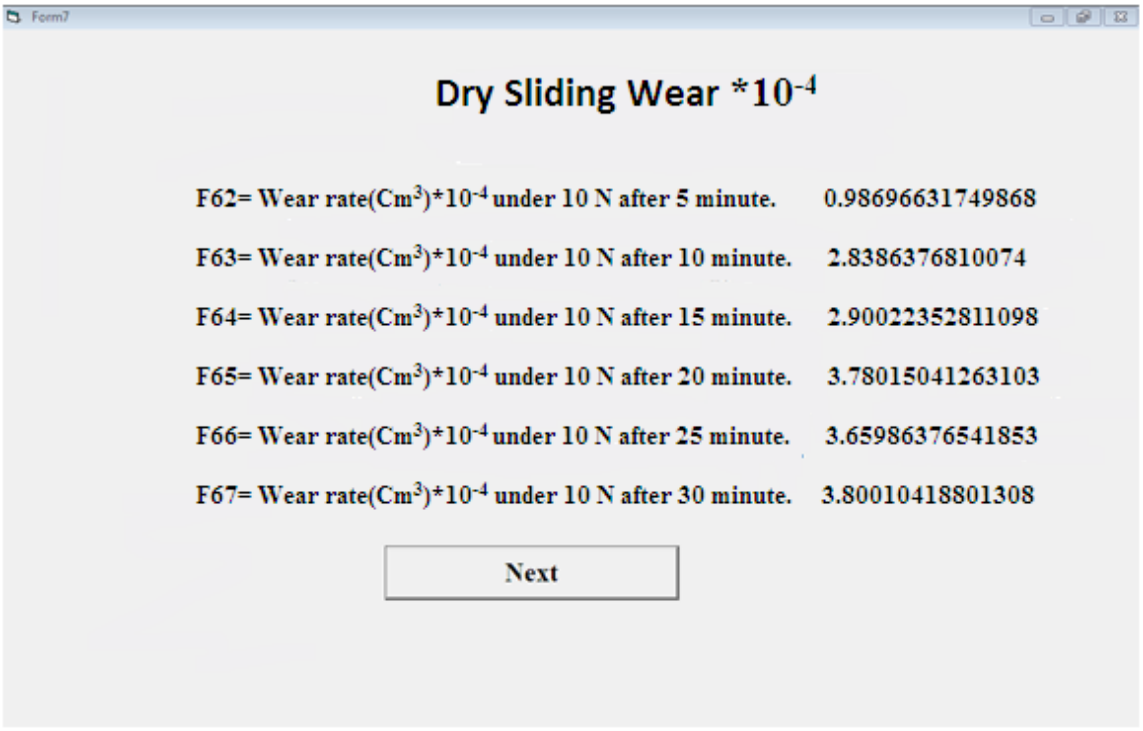

Figure (5.10): Results of PSO for Wear test

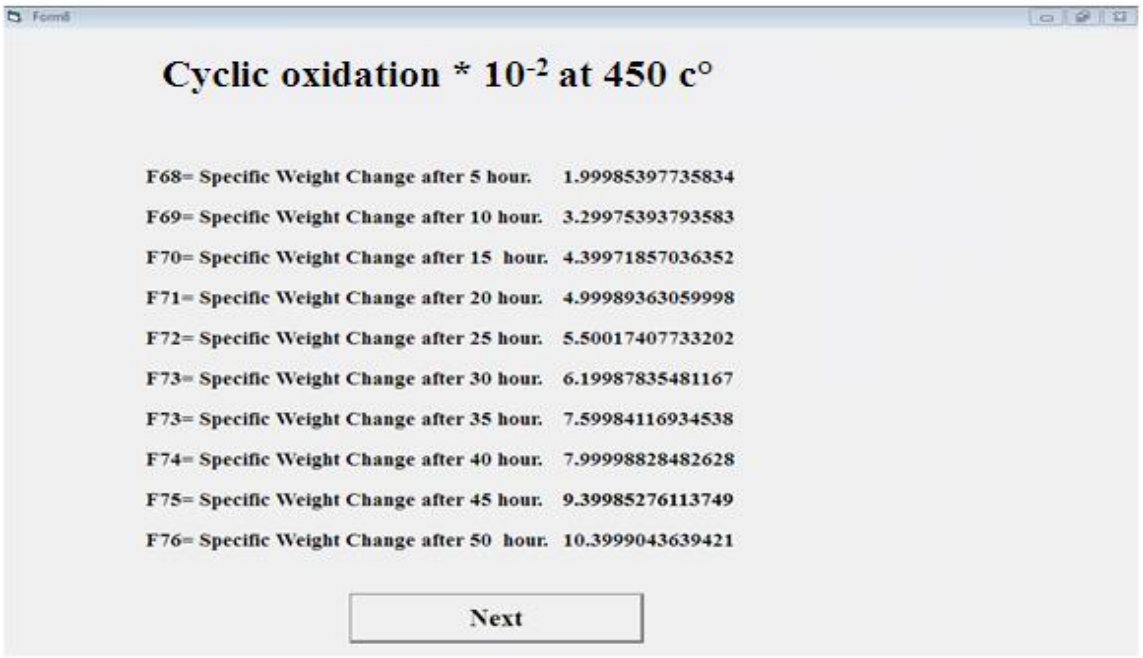

Figure (5.11): Results of PSO oxidation test

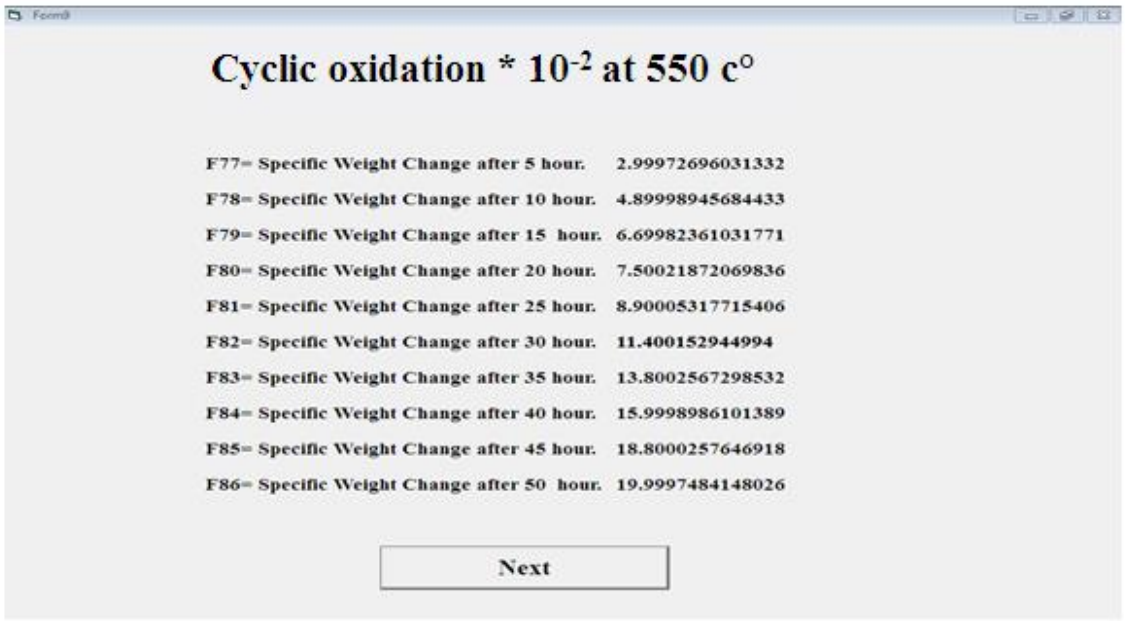

Figure (5.12): Results of PSO for oxidation test

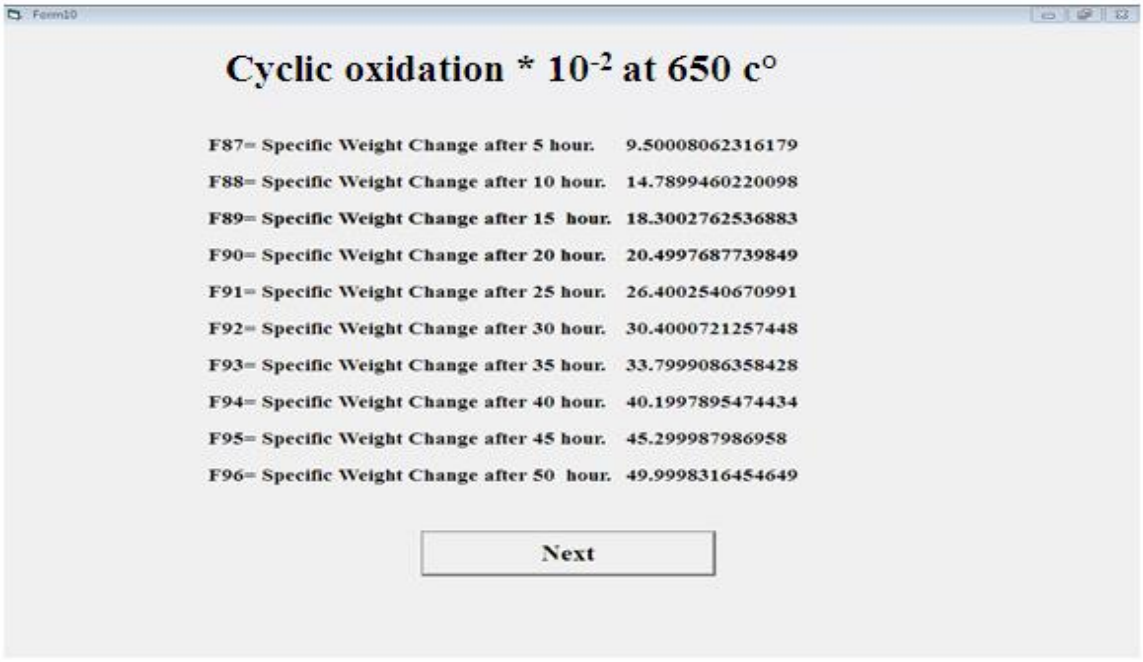

Figure (5.13): Results of PSO for oxidation test

Figure (5.14): Results of PSO for oxidation test

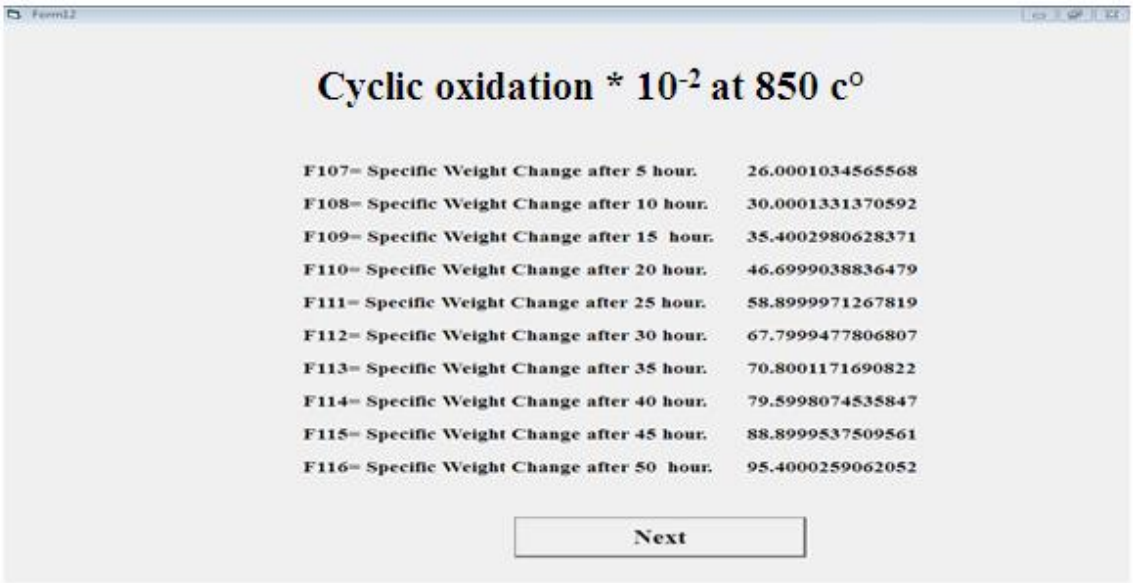

Fig.5.15 Results of PSO for oxidation test

Figure (5.16): Results of PSO for Thermal Shock test.

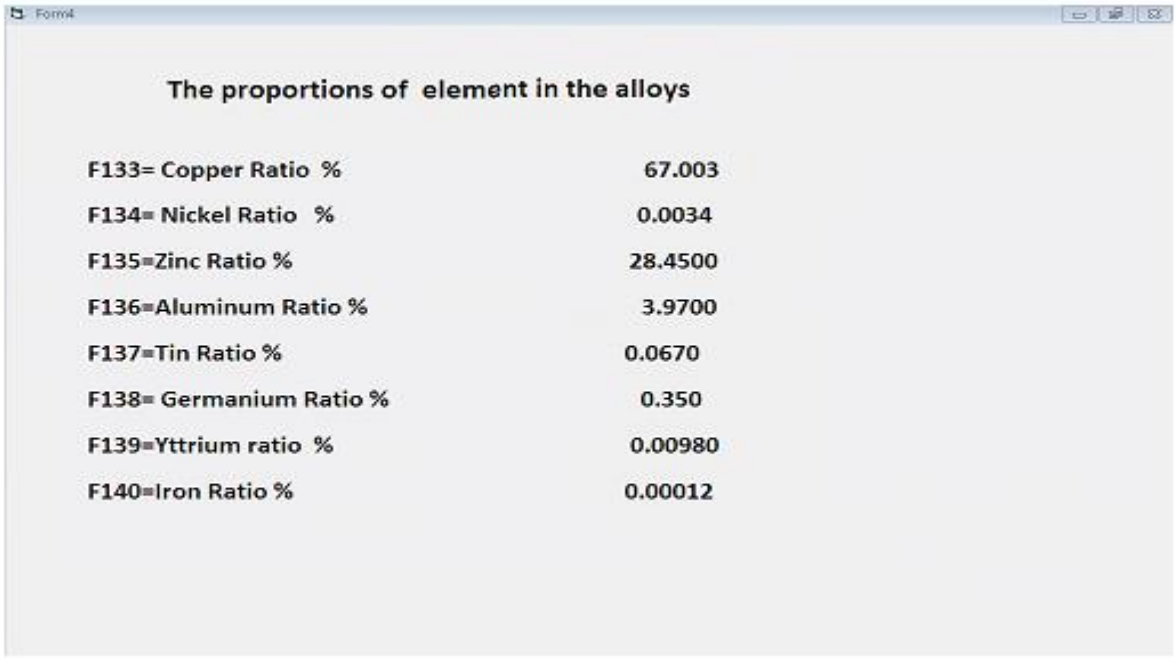

Figure (5.17): Results of PSO for the proportions of element in the alloys

Chapter Six

Conclusions & Recommendations

6.1 Conclusions

The based on the results obtained from the current work can be concluded:

1-The oxide of A1, base alloy (Cu-Ni) suffers the cracking and spalling with increase temperature .

2- When grain size is decreased, the oxidation rate will decrease because grain size is decreased.

3- The oxide of the growth generated on an alloy surface, except for a base alloy suffering from the deterioration could develop itself after oxidation and thermal shocks at high temperature.

4-The thin layer of oxides is more resistant than thick layer to the oxidation and thermal shocks.

5- The addition of a tin element (Sn) increases alloy hardness, slows the rate of oxidation and delays the beginning of the steady-state area. This is because of the alloy's increased resistance to selective liquidation and hardness.

6-Oxidation erosion-corrosion, sliding dry wear comes from added germanium element to strengthen the resistence against heat shocks (Ge). The improvement of oxide plasticity and adhesion is related to this.

10. The addition of yttrium and germanium to Alloy A1 is a qualitative leap in protecting the oxide layer from cracking and cracking when exposed to

thermal shock, whether at high or low temperatures, as well as increasing the alloy's resistance to corrosion and erosion.

8. The addition of elements such as aluminum, zinc and iron contributed to making the alloys mechanical, corrosive, microscopic and oxidative properties better compared to the base alloy due to the presence of a metal such as aluminum, which works to form a strong, adhesive protective layer that protects the alloy.

9.The particle swarm algorithm is given already the optimal solution of any problem by generation an integrated population individual as well as enabling to determine the properties with more accuracy and generality.

10.Through the optimization results that were obtained by using the particles swarm algorithm, the sample results are identical to the results of the A4 alloy.

6.2 Recommendation for Future Work

It is recommended that further research should be undertaken in the following points.

1- In order to record weight changes of alloy specimens, the oxidation tests must be monitored in detail. As a result, a micro-balance with a hook for weighing the specimens inside the furnace is required. Using ultrasonic or electromagnetic vibrations, solidify molten metal.

2- A set of oxidation tests can be used to assess oxidation resistance of alloys in various oxidized situations.

3-Another method can be used to prepare alloys instead of the casting process, such as powder metallurgy

4-Use a water purification plant used in electric power plants in Iraq.

5-Use another method of swarm algorithm techniques such as bee swarm or fish swarm algorithm to find the optimal solution.

6-It is possible to use a program other than Visual Basic to create the algorithm, such as Matlab, Minitab and Python.

References

1. AlSaffar, Kiffaya Abood, and Layla Muhsan Hasan Bdeir. "Recycling of aluminum beverage cans." Journal of Engineering and Development 12.3 (2008): 157-163.

2. ECD. "Working Party on Resource Productivity and Waste." Extended Producer Responsibility: Updated guidance ENV/EPOC/WPRPW (2015) 16/FINAL (2016).

3. Masindi, Vhahangwele, and Khathutshelo L. Muedi. "Environmental contamination by heavy metals." Heavy metals 10 (2018): 115-132.

4. Han, Kenneth N. "The Recovery of Metals from Secondary Sources A US Perspective Part III." Geosystem Engineering 5.3 (2002): 80-86.

5. Michel, James H., et al. "Development of copper alloys for seawater service from traditional application to state-of-the art engineering." CORROSION 2017. OnePetro, 2017.

6. Schleich, Wilhelm. "Typical failures of CuNi 90/10 seawater tubing systems and how to avoid them." (2004).

7. Edreis, Edreis, and A. Petrov. "Types of heat exchangers in industry, their advantages and disadvantages, and the study of their parameters." IOP Conference Series: Materials Science and Engineering. Vol. 963. No. 1. IOP Publishing, 2020.

8. Vasiliev, Leonard L. "Heat pipes in modern heat exchangers." Applied thermal engineering 25.1 (2005): 1-19.

9. Hesselgreaves, John E., Richard Law, and David Reay. Compact heat exchangers: selection, design and operation. Butterworth-Heinemann, 2016.

10. TEMA, 1999, Standards of TEMA, 8th ed., Tubular Exchanger Manufacturers Association,
New York.

11. Kakac, Sadik, Hongtan Liu, and Anchasa Pramuanjaroenkij. Heat exchangers: selection, rating, and thermal design. CRC press, 2002.

12. Martin, Holger. Heat exchangers. Routledge, 2018.

13. Florides, Georgios, and Soteris Kalogirou. "Ground heat exchangers—A review of systems, models and applications." Renewable energy 32.15 (2007): 2461-2478.

14. Shah, R. K., and D. P. Sekulic. "Heat exchangers." handbook of heat transfer 3 (1998).

15. Wilson, Arthur. The living rock: the story of metals since earliest times and their impact on developing civilization. Woodhead Publishing, 1994.

16. Wernick, Iddo K., and Nickolas J. Themelis. "Recycling metals for the environment." Annual Review of Energy and the Environment 23.1 (1998): 465-497.

17. Mauthoor, Sumayya, Romeela Mohee, and Prakash Kowlesser. "An assessment on the recycling opportunities of wastes emanating from scrap metal processing in Mauritius." Waste management 34.10 (2014): 1800-1805.

18. Sugiyama, S., T. Mera, and J. Yanagimoto. "Recycling of minute metal scraps by semisolid processing: Manufacturing of design materials." Transactions of Nonferrous Metals Society of China 20.9 (2010): 1567-1571.

19. Chapman PF, Roberts F. 1983. Metal Resources and Energy, p. 138. Boston: Butterworth.

20. Barney GO. 1980. The Global 2000 Report to the President of the United States. New York: Pergamon.

21. Hodges CA. 1995. Mineral resources, environmental issues, and land use. Science 268:1305–12.

22. Higgins, Raymond A. "Engineering Metallurgy: Part 1." Applied Physical Metallurgy, Edward Arnold, London (1993).

23. Crane, Fredrick Albert Andrew, James Anthony Charles, and Justin Furness. Selection and use of engineering materials. Elsevier, 1997.

24. Davis, Joseph R., ed. Copper and copper alloys. ASM international, 2001.

25. Sharma, Chandra P. Engineering materials: properties and applications of metals and alloys. PHI Learning Pvt. Ltd., 2003.

26. Schmidt, M. G. "Copper surfaces in the ICU reduced the relative risk of acquiring an infection while hospitalized." BMC Proceedings. Vol. 5. No. 6. BioMed Central, 2011.

27. Cottrell, Alan. An introduction to metallurgy. CRC Press, 2019.

28. Robert L. Thorp, China in the Early Bronze Age: Shang Civilization, University of Pennsylvania Press (2013).

29. Konečná, Radomila, and Stanislava Fintová. Copper and copper alloys: casting, classification and characteristic microstructures. Rijeka: InTech, 2012.

30. Schleich, Wilhelm. "Application of copper-nickel alloy UNS C70600 for seawater service." CORROSION 2005. OnePetro, 2005.

31. Vishwakarma, Vinita, et al. "Antibacterial copper–nickel bilayers and multilayer coatings by pulsed laser deposition on titanium." Biofouling 25.8 (2009): 705-710.

32. Ismail, Khaled M., Ahlam M. Fathi, and Waheed A. Badawy. "The influence of Ni content on the stability of copper—nickel alloys in alkaline sulphate solutions." Journal of applied electrochemistry 34.8 (2004): 823-831.

33.M Davies,. and P. J. B. Scott, Guide to the Use of Materials in Waters, NACE International 2003.

34. W. Schleich, and K. Steinkamp, Stainless Steel Conference 2003, Paper No: P0379, Maastricht .

35. G.W. Blunn, and E.B.G. Jones, "The Immobilisation of Copper by Marine Fouling Microorganisms, " INCRA Project No. 332A, January 1984.

36. Féron, Damien. Corrosion behaviour and protection of copper and aluminium alloys in seawater. Vol. 50. Elsevier, 2007.

37. Sastri, Vedula S. Green corrosion inhibitors: theory and practice. Vol. 10. John Wiley & Sons, 2012.

38. Kuźnicka, B. "Erosion–corrosion of heat exchanger tubes." Engineering Failure Analysis 16.7 (2009): 2382-2387.

39. Chen, J.L.; Li, Z.; Zhu, A.Y.; Luo, L.Y.; Liang, J. Corrosion behaviour of novel imitation-gold copper alloyn with rare earth in 3.5% NaCl solution. Mater. Des. 2012, 34, 618–623.

40. Rao, B.V.A.; Kumar, K.C. 5-(3-Aminophenyl)tetrazole—A new corrosion inhibitor for Cu-Ni (90/10) alloy in
seawater and sulphide containing seawater. Arab. J. Chem. 2017, 10, S2245–S2259.

41.Mousavi, M.; Baghgoli, T. Application of interaction energy in quantitative structure-inhibition relationship
study of some benzenethiol derivatives on copper corrosion. Corros. Sci. 2016, 105, 170–176.

42. North, R.F.; Pryor, M.J. The influence of corrosion product structure on the corrosion rate of Cu-Ni alloys. Corros. Sci. 1970, 10, 297–311.
Materials 2019, 12, 1869 13 of 15.

43. Kong, D.C.; Dong, C.F.; Zheng, Z.R.; Mao, F.X.; Xu, A.N.; Ni, X.Q.; Man, C.; Yao, J.A.; Xiao, K.; Li, X.G. Surface monitoring for pitting evolution into uniform corrosion on Cu-Ni-Zn ternary alloy in alkaline chloride solution: Ex-situ LCM and in-situ SECM. Appl. Surf. Sci. 2018, 440, 245–257.

44. Metikoš, M.H.; Babi´c, R.; Škugor, I.; Gruba˘cet, Z. Copper-nickel alloys modified with thin surface films: Corrosion behaviour in the presence of chloride ions. Corros. Sci. 2011, 53, 347–352.

45. Krätschmer, A.; Wallinder, I.O.; Leygraf, C. The evolution of outdoor copper patina. Corros. Sci. 2002, 44, 425–450.

46. Zhang, X.; Wallinder, I.O.; Leygraf, C. Mechanistic studies of corrosion product flaking on copper and copper-based alloys in marine environments. Corros. Sci. 2014, 85, 15–25.

47. Fuente, D.D.L.; Simancas, J.; Morcillo, M. Morphological study of 16-year patinas formed on copper in a wide range of atmospheric exposures. Corros. Sci. 2008, 50, 268–285.

48. Strandberg, H.; Johansson, L.G. Some aspects of the atmospheric corrosion of copper in the presence of sodium chloride. J. Electrochem. Soc. 1998, 145, 1093–1100.

49. Chen, Z.Y.; Persson, D.; Samie, F.; Zakipour, S.; Leygraf, C. E_ect of carbon dioxide on sodium chloride-induced atmospheric corrosion of copper. J. Electrochem. Soc. 2005, 152, B502–B511.

50. Xia, T.T.; Zeng, L.F.; Zhang, X.H.; Liu, J.; Zhang, W.L.; Liang, T.X.; Yang, B. Enhanced corrosion resistance of a Cu-10Ni alloy in a 3.5 wt% NaCl solution by means of ultrasonic surface rolling treatment. Surf. Coat. Tech. 2019, 363, 390–399.

51. D. G. Melton: Review of Five-Year Exposure Data for CuNi-Sheathed Steel Pilings. OTC, Houston-Texas, May 6-9(1991), pp 221-22.

52. Seawater Corrosion of 90/10 & 70/30 Copper-Nickel – Fourteen-year exposures K. D. Efird & D. B. Anderson Materials Performance, 37-40, Nov. 1975 (INCO).

53. Proc. 5th International Congress on Marine Corrosion & Fouling, Barcelona, May 1980 (YIA).

54. TAIWADE, Ravindra V., et al. "Corrosion Engineering Corrosion Engineering 78, 2005." ISIJ international 53.1 (2013): 102-109.

55. De Sanchez, S. R., and D. J. Schiffrin. "The use of high speed rotating disc electrodes for the study of erosion-corrosion of copper base alloys in sea water." Corrosion Science 28.2 (1988): 141-151.

56. Féron, Damien. Corrosion behaviour and protection of copper and aluminium alloys in seawater. Vol. 50. Elsevier, 2007.

57. McGuinness, Terence, and A. Thiruvengadam. "Cavitation Erosion—Corrosion Modeling." Erosion, Wear, and Interfaces with Corrosion. ASTM International, 1974.

58. Czichos, Horst, and Tetsuya Saito. Springer handbook of materials measurement methods. Ed. Leslie Smith. Vol. 978. Berlin: Springer, 2006.

59. Stott, F. H. "High-temperature sliding wear of metals." Tribology International 35.8 (2002): 489-495.

60. Rynio, C., et al. "The evolution of tribolayers during high temperature sliding wear." Wear 315.1-2 (2014): 1-10.

61. Birks, Neil, Gerald H. Meier, and Frederick S. Pettit. Introduction to the high temperature oxidation of metals. Cambridge university press, 2006.

62. Mohammed, Newal, Ali Hubi Haleem, and Jaleel Kareem Ahmed. "Oxidation of Ni–Al Electrodeposited Composite Coating of Inconel 600 Alloys." journal of kerbala university 4.3 (2008): 129-140.

63. Sequeira, César AC. High temperature corrosion: fundamentals and engineering. John Wiley & Sons, 2019.

64. Al-Sultani, Kadhim F. "Oxidation Studies On 209 T1 and 213 T11 Alloys With Inhibition Corrosion By Using MgO." Journal of Petroleum Research and Studies 2.3 (2011): 153-168.

65. Fry, A., S. Osgerby, and M. Wright. "Oxidation of alloys in steam environments-a review." (2002).

66. Rajabi, Zahra, and Hamid Doostmohammadi. "Effect of addition of tin on the microstructure and machinability of α-brass." Materials Science and Technology 34.10 (2018): 1218-1227.

67. HALLEM, ALIH, and ISRAA NAYYEF KADHIM. "Improving Oxidation Behavior of (Alpha-Beta)(Cu-Zn40) Brass by Aluminum Addition."

68. Vander Voort, George F., ed. Metallography and microstructures. Asm International, 2004.

69. Moosa, Ahmad Ali, Muna Khedeir Abbas, and Mr Rajab Mohammed. "Improving Oxidation Resistance of Stainless Steel (AISI 316L) by Pack Cementation." Engineering and Technology Journal 25.7 (2007).

70. Nebot, Vicent J., et al. "Molecular Hydrogels from Bolaform Amino Acid Derivatives: A Structure–Properties Study Based on the Thermodynamics of Gel Solubilization." Chemistry–A European Journal 18.13 (2012): 4063-4072.

71. Birks, Neil, Gerald H. Meier, and Frederick S. Pettit. Introduction to the high temperature oxidation of metals. Cambridge university press, 2006.

72. Rapp, Robert A. "The high temperature oxidation of metals forming cation-diffusing scales." Metallurgical Transactions. A, Physical Metallurgy and Materials Science 15.5 (1984): 765-782.

73. Sequeira, César AC. High temperature corrosion: fundamentals and engineering. John Wiley & Sons, 2019.

74. Birks, Neil, Gerald H. Meier, and Frederick S. Pettit. Introduction to the high temperature oxidation of metals. Cambridge university press, 2006.

75. Xu, Chunhua, and Wei Gao. "Pilling-Bedworth ratio for oxidation of alloys." Material Research Innovations 3.4 (2000): 231-235.

76. Cottrell, Alan. An introduction to metallurgy. CRC Press, 2019.

77Pedeferri, Pietro, and Marco Ormellese. Corrosion science and engineering. Italy: Springer, 2018.

78. TAIWADE, Ravindra V., et al. "Corrosion Engineering Corrosion Engineering 78, 2005." ISIJ international 53.1 (2013): 102-109.

79. Michalska-Domańska, Marta, et al. "Fabrication of high quality anodic aluminum oxide (AAO) on low purity aluminum—A comparative study with the AAO produced on high purity aluminum." Electrochimica Acta 105 (2013): 424-432.

80. Pettit, Fred. "Hot corrosion of metals and alloys." Oxidation of Metals 76.1 (2011): 1-21.

81. Mattox, D.M. and Rigney, D.A., 1986. Adhesion processes in the technological applications. Materials Science and Engineering, 83(2), pp.189- 195.

82. Blaas, H., 1981. Methods of determination of strength of scale adhesion. Wire World Int., 23(6), pp.133-139.

83. Evans, H.E. and Lobb, R.C., 1984. Conditions for the initiation of oxide-scale cracking and spallation. Corrosion Science, 24(3), pp.209-222

84. Whittle, D.P. and Stringer, J., 1980. Improvements in high temperature oxidation resistance by additions of reactive elements or oxide dispersions. Philosophical Transactions of the Royal Society of London. Series A, Mathematical and Physical Sciences, 295(1413), pp.309-329.

85. Revie, R.W., 2008. Corrosion and corrosion control: an introduction to corrosion science and engineering. John Wiley & Sons.

86. Delaunay, D., Huntz, A.M. and Lacombe, P., 1980. Mechanical stresses developed in high temperature resistant alloys during isothermal and cyclic oxidation treatments: the influence of yttrium additions on oxide scale adherence. Corrosion Science, 20(10), pp.1109-1117.

87. Whittle, D.P. and Stringer, J., 1980. Improvements in high temperature oxidation resistance by additions of reactive elements or oxide dispersions. Philosophical Transactions of the Royal Society of London. Series A, Mathematical and Physical Sciences, 295(1413), pp.309-329.

88. Revie, R.W., 2008. Corrosion and corrosion control: an introduction to corrosion science and engineering. John Wiley & Sons.

89. Kennedy, J., and R. Eberhart. "Ieee, Particle swarm optimization." 1995 Ieee International Conference on Neural Networks Proceedings, Vols 1-61995. 1948.

90. De Moura Meneses, Anderson Alvarenga, Marcelo Dornellas Machado, and Roberto Schirru. "Particle swarm optimization applied to the nuclear reload problem of a pressurized water reactor." Progress in Nuclear Energy 51.2 (2009): 319-326.

91. Sarkar, Sunita, Arindam Roy, and Bipul Shyam Purkayastha. "Application of particle swarm optimization in data clustering: A survey." International Journal of Computer Applications 65.25 (2013).

92. Eberhart, Russell, and James Kennedy. "A new optimizer using particle swarm theory." MHS'95. Proceedings of the Sixth International Symposium on Micro Machine and Human Science. Ieee, 1995.

93. Clerc, Maurice, and James Kennedy. "The particle swarm-explosion, stability, and convergence in a multidimensional complex space." IEEE transactions on Evolutionary Computation 6.1 (2002): 58-73.

94. Shi, Y., and R. C. Eberhart. "Proceedings of the 2001 Congress on Evolutionary Computation." Particle swarm optimization: developments, applications, and resources (2001).

95. dos Santos Coelho, Leandro, and Viviana Cocco Mariani. "Particle swarm optimization with quasi-Newton local search for solving economic dispatch problem." 2006 IEEE International Conference on Systems, Man and Cybernetics. Vol. 4. IEEE, 2006.

96. Han, Kuk-Hyun, and Jong-Hwan Kim. "Quantum-inspired evolutionary algorithm for a class of combinatorial optimization." IEEE transactions on evolutionary computation 6.6 (2002): 580-593.

97. Srisukkham, Worawut, et al. "Intelligent leukaemia diagnosis with bare-bones PSO based feature optimization." Applied soft computing 56 (2017): 405-419.

98. Zhu, Hanhong, et al. "Particle Swarm Optimization (PSO) for the constrained portfolio optimization problem." Expert Systems with Applications 38.8 (2011): 10161-10169.

99. Azimifar, A., and S. Payan. "Enhancement of heat transfer of confined enclosures with free convection using blocks with PSO algorithm." Applied Thermal Engineering 101 (2016): 79-91.

100. Mohee, Romeela, and Ackmez Mudhoo. "Analysis of the physical properties of an in-vessel composting matrix." Powder Technology 155.1 (2005): 92-99.

101. Sharma, Pawan, and T. S. Bhatti. "A review on electrochemical double-layer capacitors." Energy conversion and management 51.12 (2010): 2901-2912.

102. Noguera, Ana Lisbeth Galindo, et al. "Optimum design of a hybrid diesel-ORC/photovoltaic system using PSO: Case study for the city of Cujubim, Brazil." Energy 142 (2018): 33-45.

103. Mabrouk, M. T., A. Kheiri, and M. Feidt. "A systematic procedure to optimize integrated solar combined cycle power plants (ISCCs)." Applied Thermal Engineering 136 (2018): 97-107.

104. Ajdad, H., et al. "Particle swarm optimization algorithm for optical-geometric optimization of linear fresnel solar concentrators." Renewable energy 130 (2019): 992-1001.

105. Farahmand, A., S. Payan, and SM Hosseini Sarvari. "Geometric optimization of radiative enclosures using PSO algorithm." International journal of thermal sciences 60 (2012): 61-69.

106. Padhye, Nikhil, Kalyanmoy Deb, and Pulkit Mittal. "Boundary handling approaches in particle swarm optimization." Proceedings of Seventh International Conference on Bio-Inspired Computing: Theories and Applications (BIC-TA 2012). Springer, India, 2013.

107. Al-Deen J.H, (1998), Effect the addition of (Ge, Te, and Al) to (70/30) brass alloy for improvement erosion-corrosion resistance.

108. Gaoyong, L. I. N., et al. "Influence of rare earth elements on corrosion behavior of Al-brass in marine water." Journal of Rare Earths 29.7 (2011): 638-644.

109. Atiyah, Ali H. Haleem Alaa Abdulhasan, and Nawal Mohammed. "Improvement of Anti-Oxidation Properties of Alpha Brass Alloy By Aluminum Addition."

110. Badawy, W. A., M. M. El-Rabiei, and H. Nady. "Synergistic effects of alloying elements in Cu-ternary alloys in chloride solutions." Electrochimica Acta 120 (2014): 39-45.

111. Yang, Ran, "Effect of Al element on the microstructure and properties of Cu-Ni-Fe-Mn Alloys." Materials 11.9 (2018): 1777.

112. Shi, J. M., et al. "Corrosion behaviors of pure copper and Cu-Ni-Zn alloy in NaCl solution and artificial salt water." IOP Conference Series: Materials Science and Engineering. Vol. 292. No. 1. IOP Publishing, 2018.

113. Tandon, Vipin, Awanikumar P. Patil, and Ankur Bansod. "Effect of Zn addition on corrosion resistance of Cu-10Ni alloy in clean and sulphide contaminated seawater." Canadian Metallurgical Quarterly 57.2 (2018): 194-200.

114. Poli, Riccardo, James Kennedy, and Tim Blackwell. "Particle swarm optimization." Swarm intelligence 1.1 (2007): 33-57.

115. Wang, Dongshu, Dapei Tan, and Lei Liu. "Particle swarm optimization algorithm: an overview." Soft Computing 22.2 (2018): 387-408.

116. Alam, Mahamad Nabab. "Particle swarm optimization: Algorithm and its codes in matlab." ResearchGate 8 (2016): 1-10.

117. je, Ovat Friday, and Anyandi Adie Josephat. "The particle swarm optimization (PSO) algorithm application–A review." Global Journal of Engineering and Technology Advances 3.3 (2020): 001-006.

118. Hayder J. Karim, Kadhim F. Al-Sultani and Ekbal M. Saeed, Improving Corrosion Resistance and Mechanical Properties of (60% Cu /40% Zn) Alloy, March- April 2020,ISSN: 0193-4120 Page No. 13024 -13034.

119. Yang, Ran, et al. "Effect of Al element on the microstructure and properties of Cu-Ni-Fe-Mn Alloys." Materials 11.9 (2018): 1777.

120.M indivan, H., H. Çimenoğlu, and E. S. Kayali. "Microstructures and wear properties of brass synchroniser rings." Wear 254.5-6 (2003): 532-537.

121. Huang, X. C., et al. "Correlation between the wear resistance of Cu-Ni alloy and its electron work function." Philosophical Magazine 95.34 (2015): 3896-3909.

122. Karpagavalli, R. and Balasubramaniam, R., 2007. Development of novel brasses to resist dezincification. Corrosion science, 49(3), pp.963-979.

123. Metikoš-Huković, M., et al. "Copper–nickel alloys modified with thin surface films: corrosion behaviour in the presence of chloride ions." Corrosion science 53.1 (2011): 347-352

124.Awad NK, Ashour EA, Fouda AS, et al. Effect of alloying elements on the electrochemical behaviour of Cu-Ni-Zn ternary system in sulphide-polluted saltwater. Appl Surf Sci. 2014;307:621–630.

125. Badawy, W. A., M. M. El-Rabiei, and H. Nady. "Synergistic effects of alloying elements in Cu-ternary alloys in chloride solutions." Electrochimica Acta 120 (2014): 39-45.

126. Nady, H., M. M. El-Rabiei, and G. M. Abd El-Hafez. "Electrochemical Stability of Cu–10Al–10Zn, Cu–10Al–10Ni, and Cu–10Ni–10Zn Ternary Alloys in Simulated Physiological Solutions." Journal of Bio-and Tribo-Corrosion 2.4 (2016): 1-12.

127. W.A. Badawy, M.M. El-Rabiee, N.H. Hilal, H. Nady, Effect of nickel content on theelectrochemical behavior of Cu–Al–Ni alloys in chloride free neutral solutions,Electrochim. Acta 56 (2010) 913–918.

128. J.A. Wharton, R.C. Barik, G. Kear, R.J.K. Wood, K.R. Stokes, F.C. Walsh, The corro-sion of nickel–aluminium bronze in seawater, Corros. Sci. 47 (2005) 3336–3367.

128. R. Procaccini, D.J. Schiffrin, Oxygen reduction on Cu-Zn alloys, J. Appl. Elec-trochem. 39 (2009) 177–184.

129. B. Chen, C. Liang, D. Fu, D. Ren, Corrosion behavior of Cu and the Cu–Zn–Al shapememory alloy in simulated uterine fluid, Contraception 72 (2005) 221–224.

130. Hussein, R.M. and Abd, O.I., 2014. Influence of Al and Ti additions on microstructure and mechanical properties of leaded brass alloys. Indian Journal of Materials Science, 2014.

131. Chen, Jianyu, et al. "Enhanced oxidation-resistant Cu–Ni core–shell nanowires: controllable one-pot synthesis and solution processing to transparent flexible heaters." *Nanoscale* 7.40 (2015): 16874-16879.

132. Rizk, Mohamed R., and Muhammad G. Abd El-Moghny. "Controlled galvanic decoration boosting catalysis: Enhanced glycerol electro-oxidation at Cu/Ni modified macroporous films." International Journal of Hydrogen Energy 46.1 (2021): 645-655.

Appendices

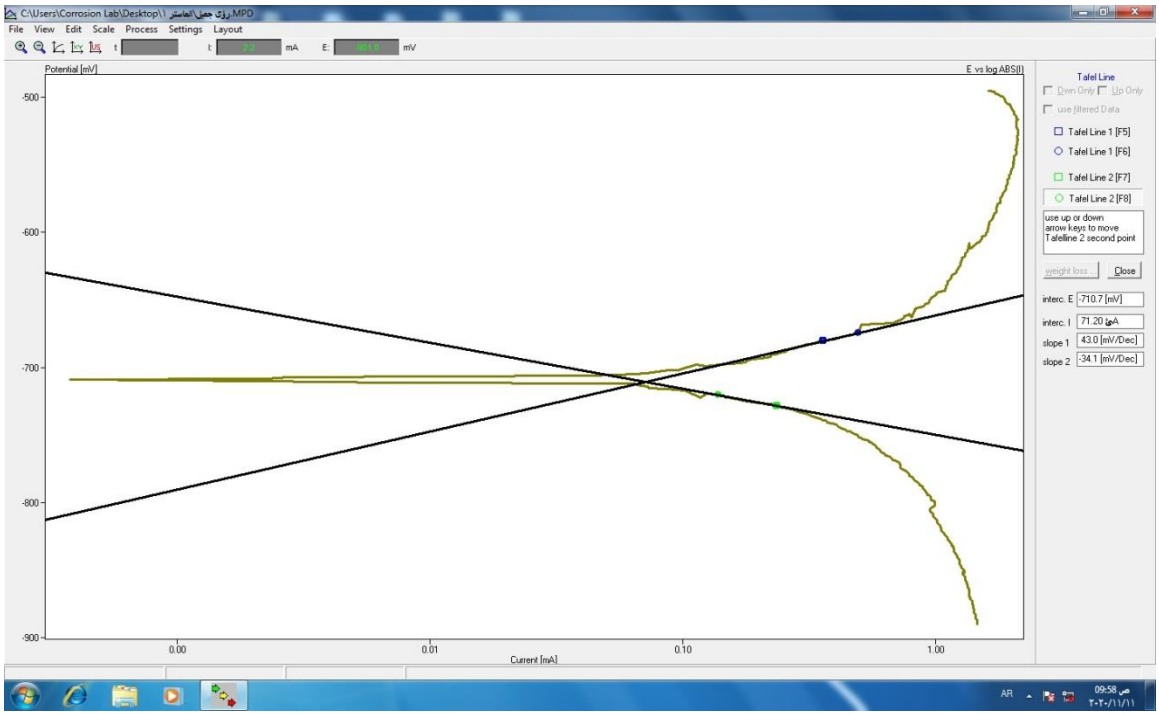

Fig. (1): Polarization Curve for A1, Base Alloy (*Cu-Ni*) in Salt Solution

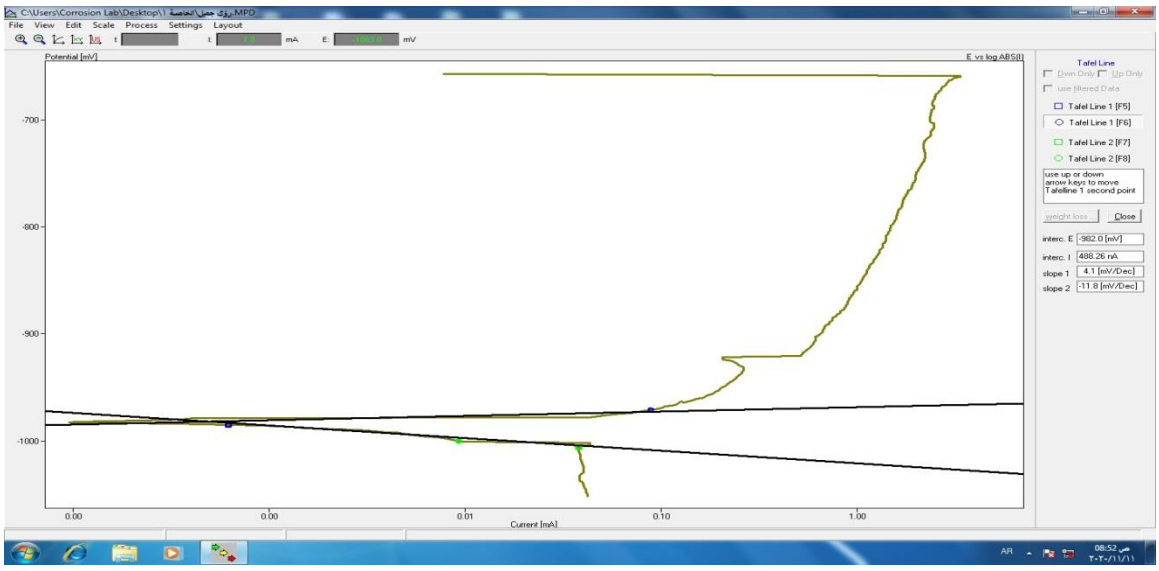

Fig. (2): Polarization Curve for A2 in Salt Solution

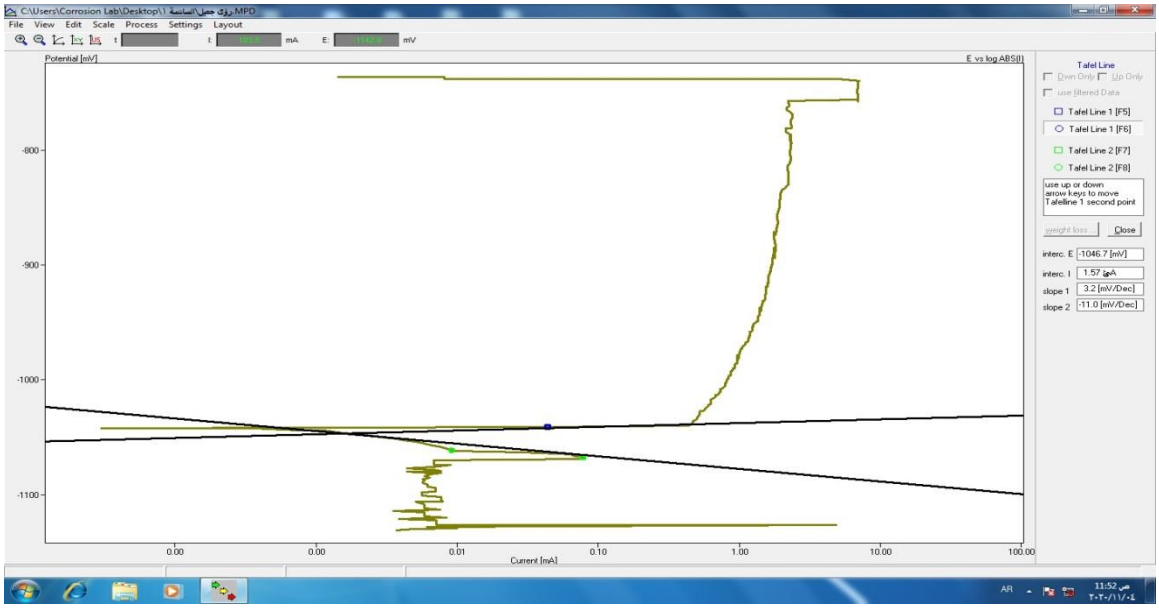

Fig. (3): Polarization Curve for A3 in Salt Solution

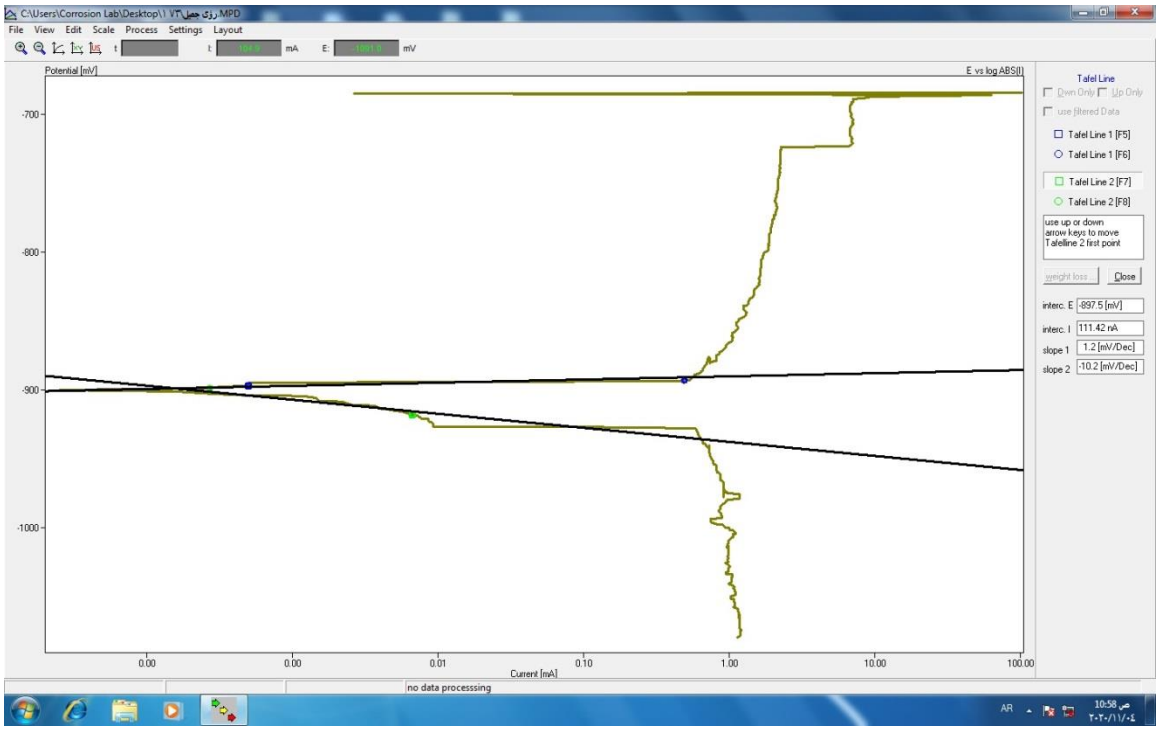

Fig. (4): Polarization Curve for A4 in Salt Solution.

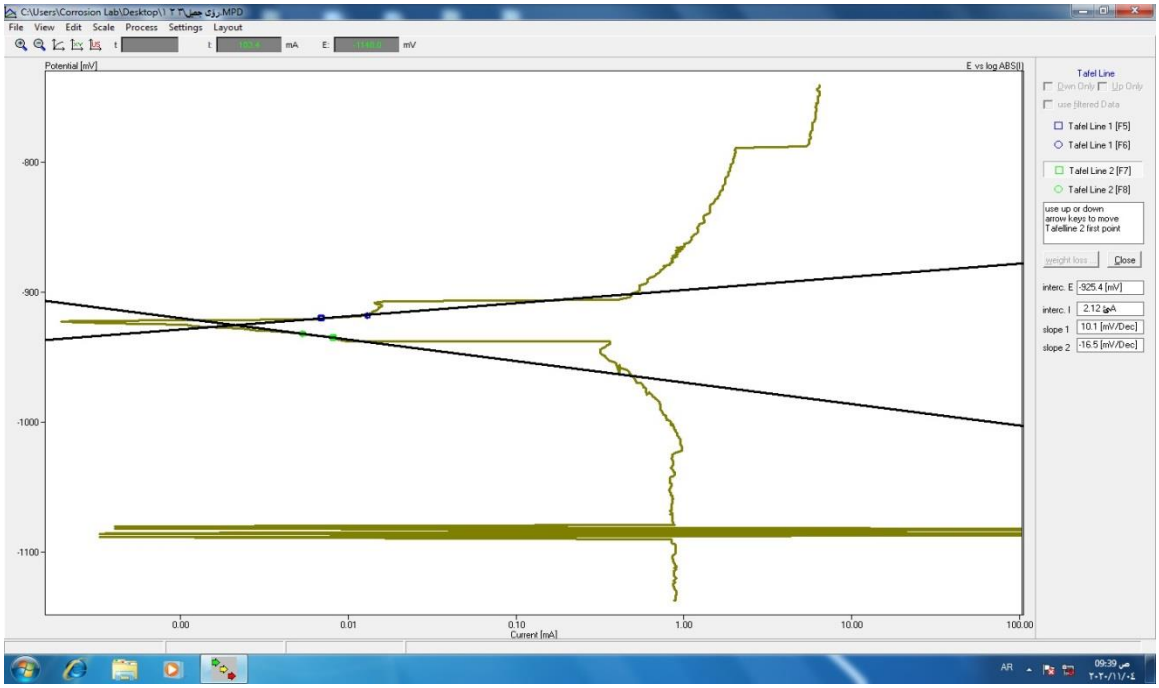

Fig. (5): Polarization Curve for A5 in Salt Solution.

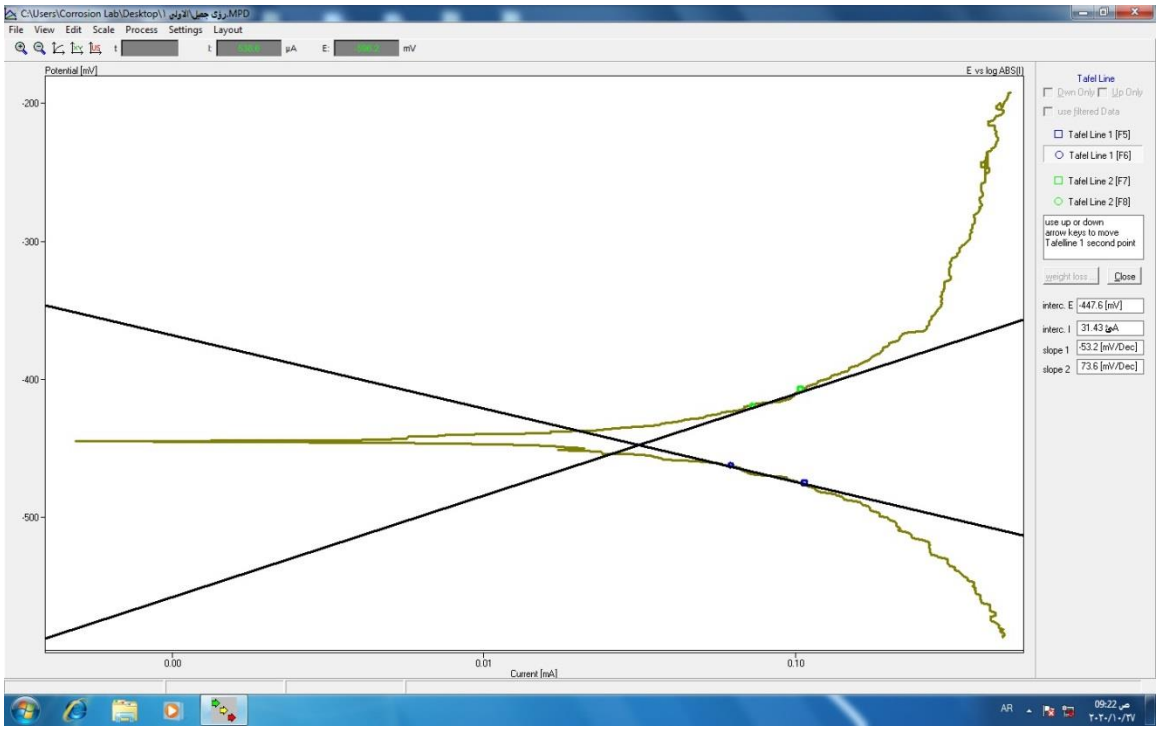

Fig. (6): Polarization Curve for A6 in Salt Solution.

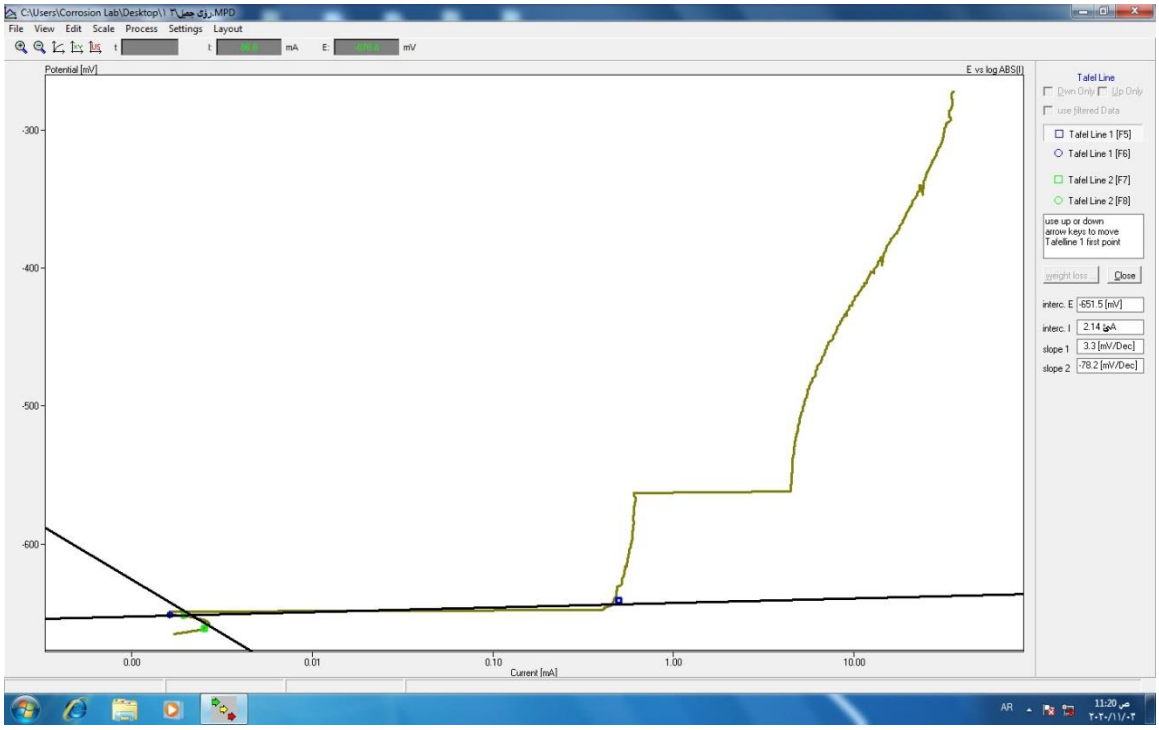

Fig. (7): Polarization Curve for A7 in Salt Solution.

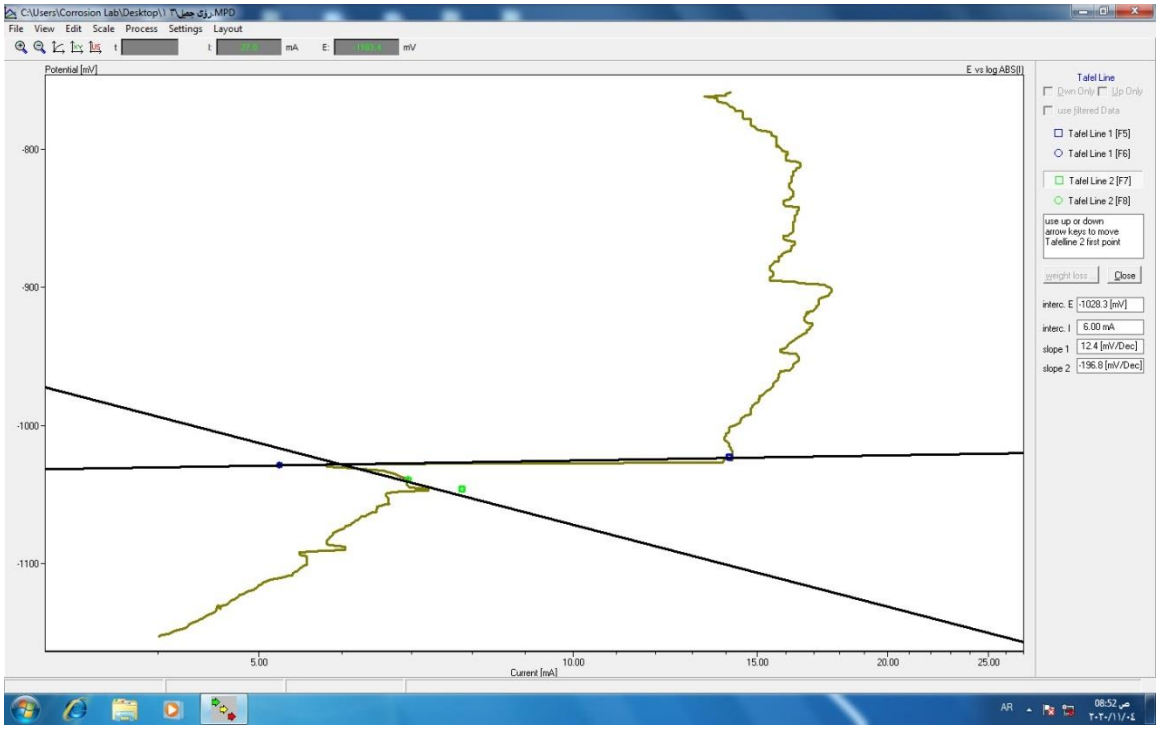

Fig.(8): Polarization Curve for A8in Salt Solution.

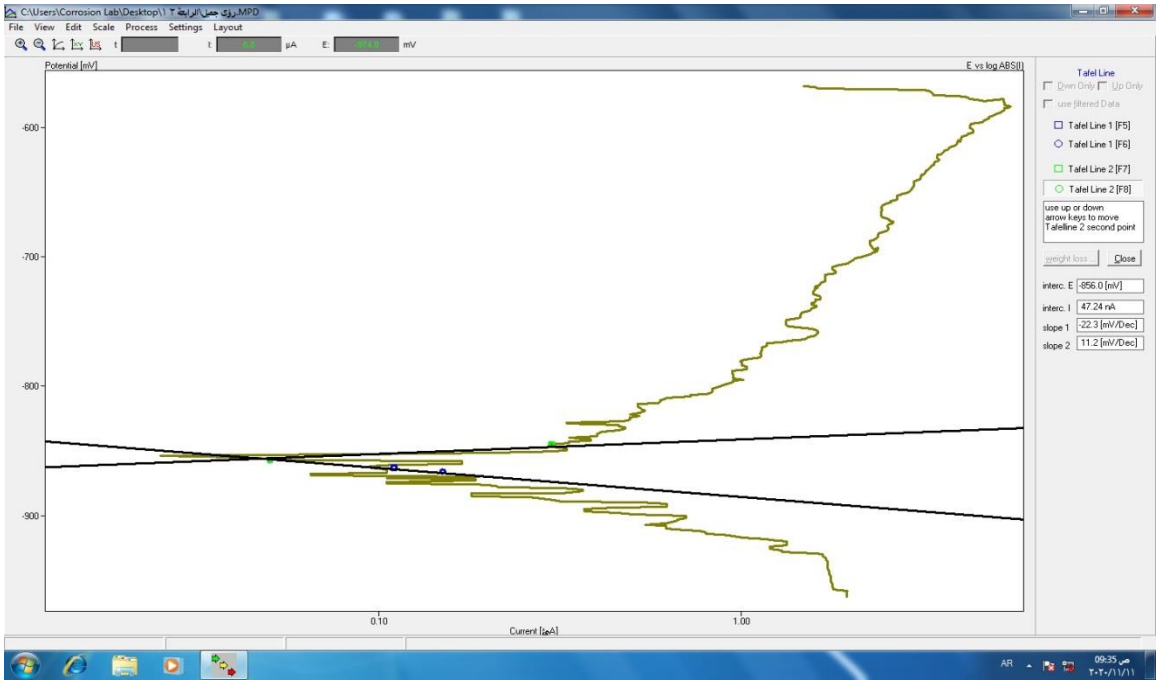

Fig. (8): Polarization Curve for A8in Salt Solution.

Customer Name: Bashar Abbas Jalil

Customer Address: NO.9, St 57,Qods Blvd, Dolat Abad, Shahre Rey

Sample Name: -5-Cu-Ni

Client Reference Number: Laboratory Environmental Conditions: Temperature : 25°c Moisture: 30% Attachments:

Test was performed under the scope of ISO/IEC17025 standard. Sampling was done by the customer.

Date Of Issue:

Order No: 5-26230

Revision No.: 0

Sample(s) Received at: 2019/12/24

Date of Financial Verifying: 2019/12/29

Date of Test: 2019/12/30

Page: 1 of 2

Spectrochemical Analysis

According to: **BS EN 15079-15**

Instrument: ARL ☐ WAS ☒ PMI ☐ OXFORD ☐

Prepration: Cutting & Grinding ☒ Surface Grinding ☐ Re-Melting & Grinding ☐

The weight percent of measured elements:

Zn	Mg	Sn	P	Mn	Fe	Ni	Si	C	Al	S
0.08	0.03	< 0.01	0.02	0.36	1.50	9.72	< 0.005	Trace	Trace	None
Ge	Y	Cu								
Trace	< 0.01	88.29								

Notes

– The weight percent (wt%) of "Cu" has been calculated from subtraction of measured element's weight percent out of 100.

Mohamad Rasoul Molfarazi

For Information Only

M. Jaferian

Customer Name: Bashar Abbas Jalil

Customer Address: NO.9, St 57,Qods Blvd, Dolat Abad, Shahre Rey

Sample Name: -3-Cu-Zn-Al

Client Reference Number: Laboratory Environmental Conditions: Temperature : 25°c Moisture: 30% Attachments:

Test was performed under the scope of ISO/IEC17025 standard. Sampling was done by the customer.

Date Of Issue:

Order No: 3-26230
Revision No.: 0
Sample(s) Received at: 2019/12/24
Date of Financial Verifying: 2019/12/29
Date of Test: 2019/12/30
Page: 1 of 2

Spectrochemical Analysis

According to: **BS EN 15079-15**
Instrument: ARL ☐ WAS ☒ PMI ☐ OXFORD ☐
Prepration: Cutting & Grinding ☒ Surface Grinding ☐ Re-Melting & Grinding ☐

The weight percent of measured elements:

Zn	Mg	Sn	P	Mn	Fe	Ni	Si	C	Al	S
27.4	0.05	< 0.01	< 0.003	0.04	0.12	0.01	<0.05	Trace	3.05	None
Ge	Y	Cu								
Trace	< 0.01	69.33								

Notes

- The weight percent (wt%) of "Cu" has been calculated from subtraction of measured element's weight percent out of 100.

Mohammad Rasoul Mollarazi

For Information Only

N. Jaferian

Customer Name: Bashar Abbas Jalil

Customer Address: NO.9, St 57,Qods Blvd, Dolat Abad, Shahre Rey

Sample Name: -4-Cu-Zn-Al_Y

Client Reference Number: Laboratory Environmental Conditions: Temperature : 25°c Moisture: 30% Attachments:

Test was performed under the scope of ISO/IEC17025 standard. Sampling was done by the customer.

Date Of Issue:

Order No: 4-26230
Revision No.: 0
Sample(s) Received at: 2019/12/24
Date of Financial Verifying: 2019/12/29
Date of Test: 2019/12/30
Page: 1 of 2

Spectrochemical Analysis

According to: **BS EN 15079-15**
Instrument: ARL ☐ WAS ☒ PMI ☐ OXFORD ☐
Prepration: Cutting & Grinding ☒ Surface Grinding ☐ Re-Melting & Grinding ☐

The weight percent of measured elements:

Zn	Mg	Sn	P	Mn	Fe	Ni	Si	C	Al	S
28.7	0.05	< 0.01	< 0.003	0.04	0.17	< 0.005	0.02	Trace	3.50	0.005
Ge	Y	Cu								
Trace	0.23	67.28								

Notes

- The weight percent (wt%) of "Cu" has been calculated from subtraction of measured element's weight percent out of 100.

Mohammad Rasoul Mollarazi

For Information Only

N. Jaferian

Customer Name: Bashar Abbas Jalil

Customer Address: NO.9, St 57,Qods Blvd, Dolat Abad, Shahre Rey

Sample Name: -1-Cu-Zn-Al-Sn

Client Reference Number: Laboratory Environmental Conditions: Temperature : 25°c Moisture: 30% Attachments:

Test was performed under the scope of ISO/IEC17025 standard. Sampling was done by the customer.

Date Of Issue:

Order No: 1-26230
Revision No.: 0
Sample(s) Received at: 2019/12/24
Date of Financial Verifying: 2019/12/29
Date of Test: 2019/12/30
Page: 1 of 2

Spectrochemical Analysis

According to: **BS EN 15079-15**
Instrument: ARL ☐ WAS ☒ PMI ☐ OXFORD ☐
Prepration: Cutting & Grinding ☒ Surface Grinding ☐ Re-Melting & Grinding ☐

The weight percent of measured elements:

Zn	Mg	Sn	P	Mn	Fe	Ni	Si	C	Al	S
27.94	0.05	2.67	0.019	0.03	0.17	< 0.005	0.01	Trace	3.10	None
Ge	Y	Cu								
Trace	< 0.01	66.01								

Notes

- The weight percent (wt%) of "Cu" has been calculated from subtraction of measured element's weight percent out of 100.

Mohammad Rasoul Mollarazi

For Information Only

N. Jaferian

Customer Name: Bashar Abbas Jalil

Customer Address: NO.9, St 57,Qods Blvd, Dolat Abad, Shahre Rey

Sample Name: -2-Ge-Cu-Zn-Al

Client Reference Number: Laboratory Environmental Conditions: Temperature : 25°c Moisture: 30% Attachments:

Test was performed under the scope of ISO/IEC17025 standard. Sampling was done by the customer.

Date Of Issue:

Order No: 2-26230
Revision No.: 0
Sample(s) Received at: 2019/12/24
Date of Financial Verifying: 2019/12/29
Date of Test: 2019/12/30
Page: 1 of 2

Spectrochemical Analysis

According to: **BS EN 15079-15**
Instrument: ARL ☐ WAS ☒ PMI ☐ OXFORD ☐
Prepration: Cutting & Grinding ☒ Surface Grinding ☐ Re-Melting & Grinding ☐

The weight percent of measured elements:

Zn	Mg	Sn	P	Mn	Fe	Ni	Si	C	Al	S
29.21	0.05	< 0.01	< 0.003	0.03	0.30	< 0.005	0.02	Trace	3.60	None
Ge	Y	Cu								
0.3	< 0.01	66.46								

Notes

- The weight percent (wt%) of "Cu" has been calculated from subtraction of measured element's weight percent out of 100.

Mohammad Rasoul Mollarazi

For Information Only

N. Jaferian

Customer Name: Bashar Abbas Jalil

Customer Address: NO.9, St 57,Qods Blvd, Dolat Abad, Shahre Rey

Sample Name: -5-Cu-Ni

Client Reference Number: Laboratory Environmental Conditions: Temperature : 25°c Moisture: 30% Attachments:

Test was performed under the scope of ISO/IEC17025 standard. Sampling was done by the customer.

Date Of Issue:

Order No: 5-26230

Revision No.: 0

Sample(s) Received at: 2019/12/24

Date of Financial Verifying: 2019/12/29

Date of Test: 2019/12/30

Page: 1 of 2

Spectrochemical Analysis

According to: **BS EN 15079-15**

Instrument: ARL ☐ WAS ☒ PMI ☐ OXFORD ☐

Prepration: Cutting & Grinding ☒ Surface Grinding ☐ Re-Melting & Grinding ☐

The weight percent of measured elements:

Zn	Mg	Sn	P	Mn	Fe	Ni	Si	C	Al	S
0.08	0.03	< 0.01	0.02	0.36	1.50	9.72	< 0.005	Trace	Trace	None
Ge	Y	Cu								
Trace	< 0.01	88.29								

Notes

- The weight percent (wt%) of "Cu" has been calculated from subtraction of measured element's weight percent out of 100.

Mohamma d Rasoul Mollara z i

For Information Only

N. Jaferian

Customer Name: Bashar Abbas Jalil

Customer Address: NO.9, St 57,Qods Blvd, Dolat Abad, Shahre Rey

Sample Name: 6-Cu-Ni-Al

Client Reference Number: Laboratory Environmental Conditions: Temperature : 25°c Moisture: 30% Attachments:

Test was performed under the scope of ISO/IEC17025 standard. Sampling was done by the customer.

Date Of Issue:

Order No: 5-26230

Revision No.: 0

Sample(s) Received at: 2019/12/24

Date of Financial Verifying: 2019/12/29

Date of Test: 2019/12/30

Page: 1 of 2

Spectrochemical Analysis

According to: **BS EN 15079-15**

Instrument: ARL ☐ WAS ☒ PMI ☐ OXFORD ☐

Prepration: Cutting & Grinding ☒ Surface Grinding ☐ Re-Melting & Grinding ☐

The weight percent of measured elements:

Zn	Mg	Sn	P	Mn	Fe	Ni	Si	C	Al	S
0.04	0.03	< 0.01	0.07	0.32	1.2	8.21	< 0.005	Trace	10.66	None
Ge	Y	Cu								
Trace	< 0.01	79.44								

Notes

- The weight percent (wt%) of "Cu" has been calculated from subtraction of measured element's weight percent out of 100.

Mohamma d Rasoul Mollara z i

For Information Only

N. Jaferian

Customer Name: Bashar Abbas Jalil

Customer Address: NO.9, St 57,Qods Blvd, Dolat Abad, Shahre Rey

Sample Name: 7-Cu-Ni-Al-Fe

Client Reference Number: Laboratory Environmental Conditions: Temperature : 25°c Moisture: 30% Attachments:

Test was performed under the scope of ISO/IEC17025 standard. Sampling was done by the customer.

Date Of Issue:

Order No: 5-26230
Revision No.: 0
Sample(s) Received at: 2019/12/24
Date of Financial Verifying: 2019/12/29
Date of Test: 2019/12/30
Page: 1 of 2

Spectrochemical Analysis

According to: **BS EN 15079-15**
Instrument: ARL ☐ WAS ☒ PMI ☐ OXFORD ☐
Prepration: Cutting & Grinding ☒ Surface Grinding ☐ Re-Melting & Grinding ☐

The weight percent of measured elements:

Zn	Mg	Sn	P	Mn	Fe	Ni	Si	C	Al	S
0.08	0.03	< 0.01	0.005	0.3	2.336	8.34	< 0.005	Trace	10.58	None
Ge	Y	Cu								
Trace	< 0.01	78.38								

Notes

- The weight percent (wt%) of "Cu" has been calculated from subtraction of measured element's weight percent out of 100.

Mohammad Rasoul Mollarazi

For Information Only

N. Jaferian

Customer Name: Bashar Abbas Jalil

Customer Address: NO.9, St 57,Qods Blvd, Dolat Abad, Shahre Rey

Sample Name: 8-Cu-Ni-Zn

Client Reference Number: Laboratory Environmental Conditions: Temperature : 25°c Moisture: 30% Attachments:

Test was performed under the scope of ISO/IEC17025 standard. Sampling was done by the customer.

Date Of Issue:

Order No: 5-26230
Revision No.: 0
Sample(s) Received at: 2019/12/24
Date of Financial Verifying: 2019/12/29
Date of Test: 2019/12/30
Page: 1 of 2

Spectrochemical Analysis

According to: **BS EN 15079-15**
Instrument: ARL ☐ WAS ☒ PMI ☐ OXFORD ☐
Prepration: Cutting & Grinding ☒ Surface Grinding ☐ Re-Melting & Grinding ☐

The weight percent of measured elements:

Zn	Mg	Sn	P	Mn	Fe	Ni	Si	C	Al	S
9.55	0.08	< 0.01	0.02	0.2	1.33	8.53	< 0.005	Trace	Trace	None
Ge	Y	Cu								
Trace	< 0.01	80.26								

Notes

- The weight percent (wt%) of "Cu" has been calculated from subtraction of measured element's weight percent out of 100.

Mohammad Rasoul Mollarazi

For Information Only

N. Jaferian

Customer Name	Bashar Abbas Jalil		**Date Of Issue:**
Customer Address:	NO.9, St 57,Qods Blvd, Dolat Abad, Shahre Rey		Order No: 5-26230
			Revision No.: 0
Sample Name:	9-Cu-Ni-Zn-Fe		Sample(s) Received at: 2019/12/24
			Date of Financial Verifying: 2019/12/29
Client Reference Number:	Laboratory Environmental Conditions:	Temperature : 25°c Moisture: 30% Attachments:	Date of Test: 2019/12/30
Test was performed under the scope of ISO/IEC17025 standard.		Sampling was done by the customer.	Page: 1 of 2

Spectrochemical Analysis

According to: **BS EN 15079-15**
Instrument: ARL ☐ WAS ☒ PMI ☐ OXFORD ☐
Prepration: Cutting & Grinding ☒ Surface Grinding ☐ Re-Melting & Grinding ☐

The weight percent of measured elements:

Zn	Mg	Sn	P	Mn	Fe	Ni	Si	C	Al	S
10.12	0.03	< 0.01	0.04	0.24	2.5	8.28	< 0.005	Trace	Trace	None
Ge	Y	Cu								
Trace	< 0.01	78.76								

Notes

- The weight percent (wt%) of "Cu" has been calculated from subtraction of measured element's weight percent out of 100.

Mohamad Rasoul Mollaraz

For Information Only

M. Jaferian

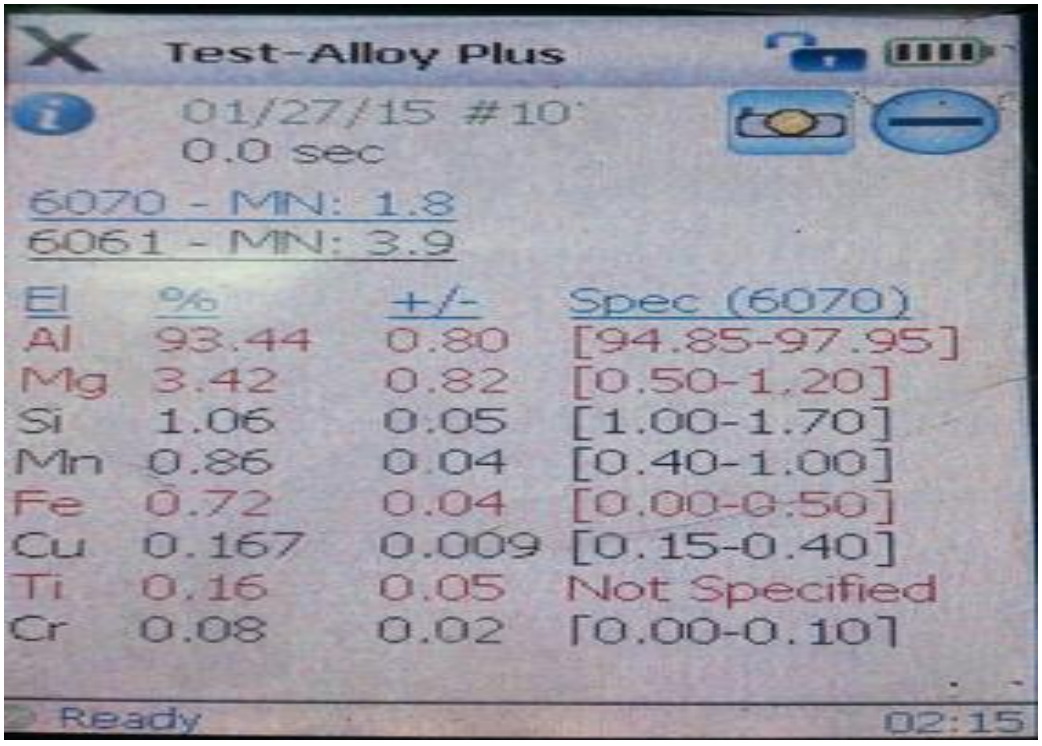

Customer Name: Mohamed Abaas

Customer Address: NO.9, St 57,Qods Blvd, Dolat Abad, Shahre Rey

Sample Name: 11-Cu

Client Reference Number: Laboratory Environmental Conditions: Temperature : 25°c Moisture: 30% Attachments:

Test was performed under the scope of ISO/IEC17025 standard. Sampling was done by the customer.

Date Of Issue:

Order No: 5-26230

Revision No.: 0

Sample(s) Received at: 2019/12/24

Date of Financial Verifying: 2019/12/29

Date of Test: 2019/12/30

Page: 1 of 2

Spectrochemical Analysis

According to: **BS EN 15079-15**

Instrument: ARL ☐ WAS ☒ PMI ☐ OXFORD ☐

Prepration: Cutting & Grinding ☒ Surface Grinding ☐ Re-Melting & Grinding ☐

The weight percent of measured elements:

Zn	Mg	Sn	P	Mn	Fe	Ni	Si	C	Al	S
1.33	None	< 0.01	< 0.003	Trace	0.56	0.43	Trace	Trace	1.21	0.03
Ge	Y	Cu								
None	None	96.5								

Notes

- The weight percent (wt%) of "Cu" has been calculated from subtraction of measured element's weight percent out of 100.

Mohamm d RaSou l Molfaraz i

For Information Only

N. Jaferian

Customer Name: Mohmed Abbas

Customer Address: NO.9, St 57,Qods Blvd, Dolat Abad, Shahre Rey

Sample Name: 10-Fe

Client Reference Number: Laboratory Environmental Conditions: Temperature : 25°c Moisture: 30% Attachments:

Test was performed under the scope of ISO/IEC17025 standard. Sampling was done by the customer.

Date Of Issue:

Order No: 5-26230

Revision No.: 0

Sample(s) Received at: 2019/12/24

Date of Financial Verifying: 2019/12/29

Date of Test: 2019/12/30

Page: 1 of 2

Spectrochemical Analysis

According to: **BS EN 15079-15**

Instrument: ARL ☐ WAS ☒ PMI ☐ OXFORD ☐

Prepration: Cutting & Grinding ☒ Surface Grinding ☐ Re-Melting & Grinding ☐

The weight percent of measured elements:

Zn	Mg	Sn	P	Mn	Fe	Ni	Si	C	Al	S
None	1.55	< 0.01	0.35	0.8	95.61	Trace	0.60	0.27	Trace	0.46
Ge	Y	Cu								
None	None	0.35								

Notes

- The weight percent (wt%) of "Cu" has been calculated from subtraction of measured element's weight percent out of 100.

Mohamm d RaSou l Molfaraz i

For Information Only

N. Jaferian

گزارش آزمون

Azma Powder
Shargh Lab.

نام آزمون : آنالیز شیمیایی | شماره درخواست : ۶۴۹۸/۰۱۲۵ | روش انجام آزمون : آنالیز با دستگاه XRF

نام مشتری : آقای زمانی | تاریخ دریافت نمونه: ۹۸/۰۸/۰۲ | تاریخ انجام آزمون : ۲ الی ۹۸/۰۸/۰۹

کد مشتری : کد ۶ | کد آزمایشگاه : ۶۴۹۸/۰۱۲۵ | تاریخ صدور نتیجه: ۹۸/۰۸/۱۱

شرایط محیطی : دما ۲۵ درجه سانتیگراد و رطوبت ۳۱ درصد

این آزمون به وسیله دستگاه X-ray fluorescence مدل PW1410 (شرکت سازنده Philips) انجام شده است.

نتایج آزمون:

نام اکسید	درصد وزنی	محدوده اطمینان
Si	0.052	± 0.005
Fe	0.334	± 0.005
Mn	0.021	± 0.005
Mg	0.010	± 0.005
Sn	0.006	± 0.005
Co	0.003	± 0.005
Sb	0.006	± 0.005
Al	0.124	± 0.05
Bi	0.004	± 0.005
Na	38.628	± 0.05
Cl	59.621	± 0.05
Total Percent	100.0	

شرایط اندازه گیری و نتیجه آزمون

توضیحات :

انجام دهنده آزمون:
تاریخ و امضاء: ۹۸/۰۸/۱۱

مدیر فنی آزمایشگاه
تاریخ و امضاء: ۹۸/۰۸/۱۱

- نمونه‌گیری توسط ☐آزمایشگاه ☒ مشتری انجام شده است.
- نتایج فقط برای نمونه‌های ارسالی معتبر است
- این گزارش آزمون در حوزه گواهینامه ISO/IEC 17025 از نظام تایید صلاحیت ایران (NACI) این مجموعه: ☐می‌باشد ☒نمی‌باشد.
- عدم قطعیت نتایج آزمون در سطح اطمینان، بزرگتر یا مساوی ۹۵٪ هستند.
- گزارش نتایج آزمون نباید بدون اجازه کتبی آزمایشگاه تولید شود مگر اینکه کامل باشد.
- آزمون‌های که توسط پیمانکار انجام شده است نام پیمانکار در قسمت توضیحات آورده شده است
- نمونه ها پس از انجام آنالیز حداکثر به مدت سه ماه در آزمایشگاه نگهداری می شود و پس از این مدت آزمایشگاه مسئولیتی برای نگهداری آنها ندارد. لذا هر گونه شکایت نسبت به نتایج آزمون حداکثر تا سه ماه پس از تاریخ انجام آنالیز قابل پیگیری می باشد

آدرس مشتری: مشهد، دانشگاه فردوسی مشهد

آدرس آزمایشگاه: مشهد، خیابان خواجه ربیع، آیت اله عبادی ۷۲، پلاک ۹۵۸ | تلفن: ۰۵۱-۳۷۳۹۳۳۰۶ | فکس: ۰۵۱-۳۷۳۹۳۳۰۶
کد پستی: ۹۱۹۳۹۹۵۴۶۶ | پست الکترونیک:

الملخص

إعادة التدوير هو العامل الأكثر أهمية في ضمان استمرار تقدم معظم العناصر المعدنية والتطور ، لا سيما إعادة تدوير كل من النحاس والالمنيوم والحديد. في الآونة الأخيرة ، كانت إعادة تدوير الألمنيوم والنحاس والحديد محور معظم الأبحاث حيث يوجد طلب متزايد على استخدام الصناعة الخضراء و ذلك للحد من الانبعاثات في البيئة. يمكن تحويل الألومنيوم المعاد تدويره والنحاس والحديد إلى أشكال مختلفة لاستخدامها في أغراض مختلفة ، مثل استخدامها في تحضير السبائك المستخدمة في انابيب المبادل الحراري.

السبيكة الرئيسية المستخدمة في هذا البحث هي سبيكة (90٪ نحاس -10٪ نيكل) المستخدمة في محطة توليد الكهرباء (محطة جنوب بغداد). حيث تم تحضير نوعين من السبائك: أولاً إزالة النيكل من سبيكة الاساس بصورة نهائية حيث تم استبداله بعناصر أخرى. هذه السبائك هي:

A2 (69.33٪ Cu + 27.4٪ Zn + 3.05٪ Al) ،A3 (66.01٪ Cu-27.94٪ Zn-3.10٪ Al-2.67٪ Sn) ،A4 (66.46٪ Cu-29.21٪ Zn-3.60٪ Al -0.3٪ Ge) و A5 (6.28٪ Cu-28.7٪ Zn-3.50٪ Al-0.23٪ Y).

ثانيًا ، السبائك التي تم تقليل نسبة النيكل فيها من سبيكة الاساس واستبدال النيكل بعناصر أخرى. هذه السبائك هي:

A6 (79.44٪ Cu-8.21٪ Ni-10.66٪ Al) ،A7 (78.38٪ Cu-8.34٪ Ni-10.58٪ Al-2.33٪ Fe) ،A8 (80.26٪ Cu-8.53٪ Ni-9.55٪ Zn و A9 (78.76 ٪8.28- ٪ نحاس نيكل 10.12٪ زنك -2.6٪ حديد).

تم استخدام السباكة بالقوالب المعدنية التقليدية والمعالجة الحرارية ، وتم إجراء الصب بطريقة تضمن تجانس الدقائق لتحسين الخواص ، وقد تم إجراء عدد من الاختبارات ، بما في ذلك اختبار الأكسدة والصدمة الحرارية في درجات حرارة عالية (RT، 250C° ، 350C° ، 450C° ، 550C° ، 650C° ، 750C° و 850C°). بالإضافة إلى اختبار الصلادة والبلى الميكانيكي والتآكل بالتعرية والغمر البسيط واختبار التافل.

السبيكة ذات الخصائص الأفضل بين السبائك الخالية من النيكل هي (A4) والسبائك ذات الخصائص الأفضل بين السبائك التي تم تقليل نسبة النيكل فيها هي (A7).

أظهرت النتائج تفوقًا ملحوظًا لسبائك النيكل الحرة في اختبارات مختلفة ، أي أن تحسين مقاومة التآكل في محلول الملح (اختبار الغمر البسيط) ، على سبيل المثال ، أدى انخفاض معدل التآكل في السبيكة (A4) ، مقارنةً بالسبيكة الأساسية (A1) ، لتصل إلى (27.30٪). بينما انخفض معدل تآكل السبيكة المحتوية على النيكل مقارنة بالسبيكة القاعدية ، بلغ معدل تآكل السبيكة (53.8 (A7٪.

من ناحية أخرى ، أدى تقليل الكثافة الحالية للسبائك (A4) و (A5) مقارنة بالسبيكة الأساسية (A1) إلى تحسين الوصول إلى الترتيب (96.5٪) و (99.92٪) على التوالي ، مع التحسن في نسبة الانخفاض في كثافة تيار السبيكة (A7) مقارنة بالسبيكة القاعدية (A1) بلغت (99.99٪).

في اختبار الأكسدة ، كان التحسن في مقاومة الاكسدة لـ A4 عند 850 درجة مئوية 17.07٪ ، بينما التحسن في مقاومة الاكسدة لـ (A7) عند 850 درجة مئوية كان 23.21٪.

بينما كان التحسن في سبائك الخالية من النيكل والسبائك الحاوية على النيكل أثناء الاختبارات الميكانيكية ، على سبيل المثال زيادة صلابة السبائك A4 و A7 مقارنة بسبيكة الاساس (A1) بترتيب (89.2٪) و (97.98٪) على التوالي ، بالإضافة إلى ذلك التحسن فيى مقاومة التأكل بالتعرية بلغ (89.28٪) و (92.85٪) على التوالي. إلى جانب التحسن في مقاومة البلى عند (الحمل 20 نيوتن والسرعة 250 دورة في الدقيقة) بلغ (57.2٪) و (70.15٪) على التوالي.

يتم استخدام مفهوم الامثلية للعثور على أفضل عينة من حيث الخصائص من خلال التعامل مع مفهوم خوارزميات سرب الجسيمات . تم تصميم البرنامج بالاعتماد على 75 عينة بالعتماد على نتائج 9 عينات مختبرية . لقد استخدم مبدأ الاختيار كدالة لصلاحية أفضل لأن العلاقة بين هذا المقياس والسلطة هي علاقة عكسية. بعد ذلك ، كانت العينات المثلى الناتجة عن PSO تقارب خصائص العينة (Cu-Ni-Al-Ge) A4.

وزارة التـــعليم الـــعالي والبـحث الـعلمي
جـــــامعة بـــــابل/كـــلية هـندسة المواد
قســـــــم هـــــندسة المـــــــعادن

توصيف الاكسدة والتأكل لسبائك ذات اساس نحاس والمستخدمة في المبادلات الحرارية

اطروحة

مقدمة الى قسم هندسة المعادن في كلية هندسة المواد /جامعة بابل وهي من متطلبات نيل درجة الدكتوراه فلسفة في هندسة المواد /المعادن

من قبل

رؤى جميل عباس فرهود

بكالوريوس هندسة مواد (2013)

ماجستير هندسة معادن(2016)

بأشراف

أ . د اقبال محمد سعيد **أ. د حيدر عبد حسن الجبوري**

2022م 1443هـ